

**Multifunctional polymeric nanoparticles for RNA delivery:
from carrier design to cancer immunotherapy**

Bo Lou

2018

The printing of this thesis was partially financially supported by: Utrecht Institute for Pharmaceutical Sciences (UIPS), Utrecht, the Netherlands.



Universiteit Utrecht

UIPS *Utrecht Institute for
Pharmaceutical Sciences*

The research in this thesis was performed at the Department of Pharmaceutics, Utrecht Institute for Pharmaceutical Sciences (UIPS), Utrecht University, the Netherlands.

ISBN: 978-90-393-7034-6

Cover: "mRNA bullet" by Bo/Off Page

Layout and printing production: Off Page, Amsterdam

© Bo Lou, 2018.

All rights reserved. No parts of this thesis may be reproduced, stored in a retrieval system or transmitted in any form or by any means without prior permission in writing of the author.

**Multifunctional polymeric nanoparticles for RNA delivery:
from carrier design to cancer immunotherapy**

**Multifunctionele polymere nanodeeltjes voor afgifte van RNA:
van formulering tot immunotherapie van kanker**

(met een samenvatting in het Nederlands)

Proefschrift

ter verkrijging van de graad van doctor aan de Universiteit Utrecht op gezag van
de rector magnificus, prof.dr.H.R.B.M. Kummeling, ingevolge het besluit van het college voor
promoties in het openbaar te verdedigen op
maandag 10 september 2018 des middags te 2.30 uur

door

Bo Lou

geboren op 13 januari 1989
te Henan, China

Promotor: Prof. dr. ir. W. E. Hennink

Copromotor: Dr. E. Mastrobattista

This thesis was (partly) accomplished with financial support from China Scholarship Council.

| Table of Contents

Chapter 1	General introduction	7
Chapter 2	Small nanosized poly(vinyl benzyl trimethylammonium chloride) based polyplexes for siRNA delivery	25
Chapter 3	RGD-decorated cholesterol stabilized polyplexes for targeted siRNA delivery to Glioblastoma cells	47
Chapter 4	Post-PEGylated and crosslinked polymeric ssRNA nanocomplexes as adjuvants targeting lymph nodes with increased cytolytic T cell inducing properties	83
Chapter 5	Modular core-shell polymeric nanoparticles mimicking viral structures for vaccination	115
Chapter 6	mRNA polyplexes with post-conjugated GALA peptides efficiently target, transfect and activate antigen presenting cells	155
Chapter 7	Summary and Perspectives	189
Appendix	Nederlandse Samenvatting	205
	Acknowledgements	211
	List of publications	214
	Curriculum Vitae	216

CHAPTER

General introduction

1

| RNA therapeutics

Around the 30 years ago, the concept that nucleic acids can be used as drug has been proven when Wolff *et al.* demonstrated that direct injection of messenger RNA (mRNA) or DNA into the skeletal muscle of mice led to the expression of the encoded protein in the injected muscle [1]. At the time, RNA was thought to be a poor choice as therapeutic agent as it is less stable compared with DNA, and the field focused on technologies based on DNA [2]. In the last fifteen years, however, RNA-based therapeutics, such as small-interfering RNA (siRNAs), microRNAs (miRNAs), antisense oligonucleotides (ASOs), synthetic messenger RNAs (mRNAs) and CRISPR–Cas9, have witnessed an explosion of interest in both academia and industry [3]. RNA-based drugs target gene and RNA levels rather than proteins, thus there is a great promise to greatly extend the domain of druggable targets beyond what can be achieved with small molecules and biologics [4]. Conceptually, RNA-based drugs can be divided into two groups. The first type is those whose specific activity is mediated by an antisense mechanism [5], namely by recognizing a complementary sequence on mRNA. Those can be used to inhibit gene expression (siRNAs, miRNA), alter splicing to produce functional proteins (ASOs) or edit mutated DNA (CRISPR–Cas). The other type is coding RNAs (mRNA) that can be used for transient *in vivo* transcription to replace mutated proteins or produce new proteins without the risk of genomic alteration (Fig.1) [4,6].

With the advance of next-generation sequencing technology and new chemistries, RNA-based therapeutics are poised to become new therapeutic paradigms for treatment of diseases, ranging from cancer to viral infections (e.g. influenza, HIV, Zika) to neurological diseases (e.g. Parkinson, Alzheimer) [7]. In 2017, two antisense oligonucleotides (ASOs) drugs that alter mRNA splicing of genes were approved by U.S. Food and Drug Administration for Duchenne muscular dystrophy (Exondys 51) [8] and spinal muscular atrophy (Spinraza) [9], and more siRNA drugs are now reaching the clinical finish line [10]. Moreover, mRNA-based drugs, especially mRNA vaccines, have emerged as promising alternatives to conventional vaccine approaches and are developing rapidly. A large body of preclinical data has accumulated over the past several years, and multiple human clinical trials have been initiated [11]. For example, based on strong pre-clinical results of tumor associated antigen (TAA) or neo-antigen (neo-Ag) mRNA personalized vaccines either in naked form or as liposomal formulation, BioNTech RNA Pharmaceuticals (Mainz, Germany) initiated three clinical trials for treatment of melanoma and breast cancer [12,13]. Likewise, RNA biotech companies, such as Moderna Therapeutics (Cambridge, MA, USA) and CureVac (Tübingen, Germany) initiated clinical trials with mRNA vaccines against infectious diseases (Rabies [14], Zika [15], influenza virus [16]) based on intramuscular injection of mRNA encoding for a viral antigen.

| Barriers for RNA therapeutics delivery

Even though with all the enthusiastic upside surrounding the potential of RNA-based therapeutics, turning RNAs into drugs still need to overcome three major (extra- and intracellular) barriers: (i) the poor pharmacological properties of RNA due to degradation by

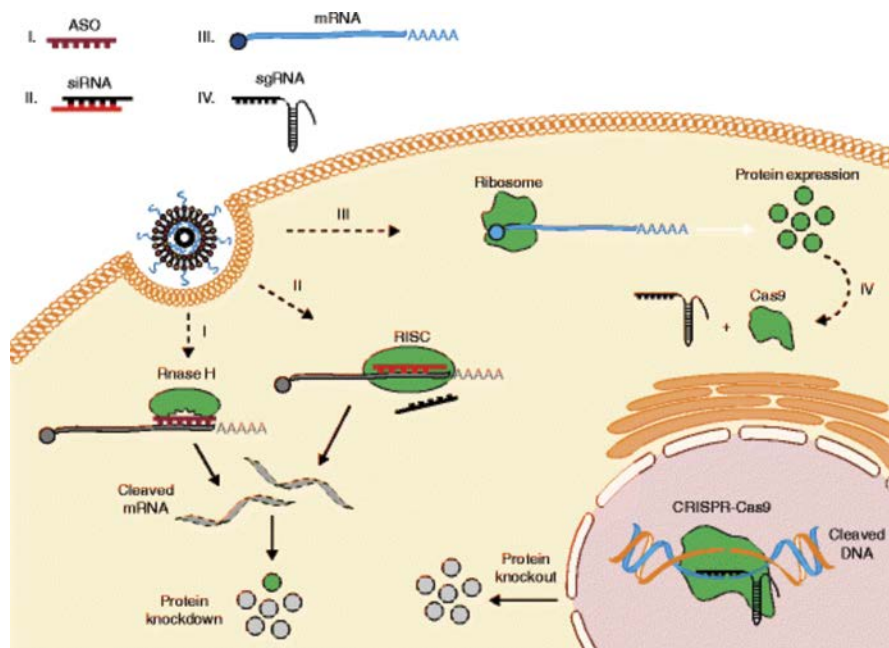


Fig. 1. RNA-based drug mechanisms. Once delivered into the cells, RNA macromolecules can utilize diverse intracellular mechanisms to control gene and protein expression. (I) Hybridization of antisense oligonucleotides (ASOs) to a target mRNA can result in specific inhibition of gene expression by induction of RNase H endonuclease activity, which cleaves the mRNA–ASO heteroduplex. (II) Short interfering RNA (siRNA) is recognized by the RNA-induced silencing complex (RISC), which guided by an antisense strand of the siRNA, specifically binds and cleaves target mRNA. (III) *In vitro* transcribed mRNA utilizes the protein synthesis machinery of host cells to translate the encoded genetic information into a protein. Ribosome subunits are recruited to mRNA together with a cap and poly(A)-binding proteins, forming a translation initiation complex. (IV) In the CRISPR–Cas9 system, co-delivery of a single guide RNA (sgRNA) together with the mRNA encoding the Cas9 DNA endonuclease allows site-specific cleavage of double-stranded DNA, leading to the knockout of a target gene and its product. CRISPR, clustered regularly interspaced short palindromic repeats. Reproduced with permission [6].

RNases that are present in all body fluids, (ii) the activation of extracellular and intracellular innate immune responses, and (iii) the delivery of charged nucleic acid across hydrophobic cell membranes into the cytosol or nucleus where they need to act [17].

The new RNA chemistries have vastly improved the stability of RNA therapeutics, reduced unintended off-target effects and maximized on-target pharmacological activities. For example, chemical modifications of the native 2'-hydroxyl (OH) of the ribose with 2'-fluoro (F) as well as introduction of phosphothioate linkages protect siRNAs against nuclease digestion to earn a prolonged half-life in serum [18]. Further, modifications of nucleosides with 5'-methylcytidine nucleotide decrease the innate immune activation and increase translation efficiency of mRNA [19]. The combining modification of the oligonucleotide backbone, sugars, bases and the phosphate groups can solve the first and second problem and have significantly improved

the potency and pharmacological properties of RNA drugs [20]. In fact, most of therapeutic siRNAs in clinical trials today contain 2'-F/O-Me modifications [21,22].

Of all these barriers, delivering RNA through lipid bilayers into cells has remained as the major problem for the widespread development of RNA therapeutics [3]. Most RNA-based therapeutics are highly negatively charged, large macromolecules with a molecular weight that roughly ranges from several to thousands kilo Dalton. As a consequence, these RNA-based molecules have no ability to cross cellular membranes (with the exception of some ASOs) as well as endosomal membranes to reach the cytoplasm. Against this background, an efficient delivery system is required to exploit the therapeutic potential of RNA based drugs to finally result in clinical applications. Different strategies have been developed to tackle these most difficult twin hurdles, such as physical delivery methods (gene gun, electroporation), viral and non-viral vectors [6]. However, the physical methods have limitations of increased cell death and restricted access to target cells or tissue, and viral vectors might induce severe and unwanted immune reactions and also have restricted packaging capacity. Recently, the RNA research field has benefited from the use of non-viral vectors, especially lipid or polymer-based nanoparticles as potent and versatile delivery vehicles [11].

| Non-viral RNA delivery system

Broadly speaking, the non-viral RNA delivery platforms can be divided into three different categories: naked RNA, RNA-ligand conjugates and lipid or polymer-based nanoparticles. Interestingly, some of the current clinical trials utilize naked chemically modified RNA (Fig. 2a), including siRNA [23], ASOs [24,25] and mRNA [26]. Importantly, local delivery of naked RNAs can reduce the risk of RNA degradation and systemic immune activation compared to that associated with systemic delivery. Another more conceptually straightforward and chemically well-defined means of delivery is to directly conjugate a bioactive ligand to the RNA, which will allow it to enter the cell of interest (Fig. 2b). Different ligands have been conjugated with RNA in recent years, such as cholesterol [27], vitamin E [28], antibodies [29] and cell penetrating peptides [30]. The most clinically advanced construct is trivalent N-acetylgalactosamine-siRNA (GalNAc-siRNA), which is typically dosed subcutaneously and has shown an ability to rapidly enter the systemic circulation and target the asialoglycoprotein receptor on hepatocytes in the liver [31]. A recent clinical study to treat hypercholesterolemia has shown impressive results. Around 80–95% knockdown lasting for as long as 3–6 months after a single injection without significant safety concerns in thousands of patients was observed [32]. This suggests that GalNAc-RNA platform as a whole will be adaptable for developing drugs against multiple liver targets [7]. Nevertheless, therapeutic gene knock in other organ than the liver is still an area that needs to be actively developed.

The most studied delivery methods of RNA therapeutics are to encapsulate them into nanoparticles that are based on cationic lipids (Fig. 2c) or polymers (Fig. 2d), which physically protect nucleic acids from enzymatic degradation and aid in cellular uptake and endosomal escape. The majority of the initial clinical development of RNA therapeutics has been focused

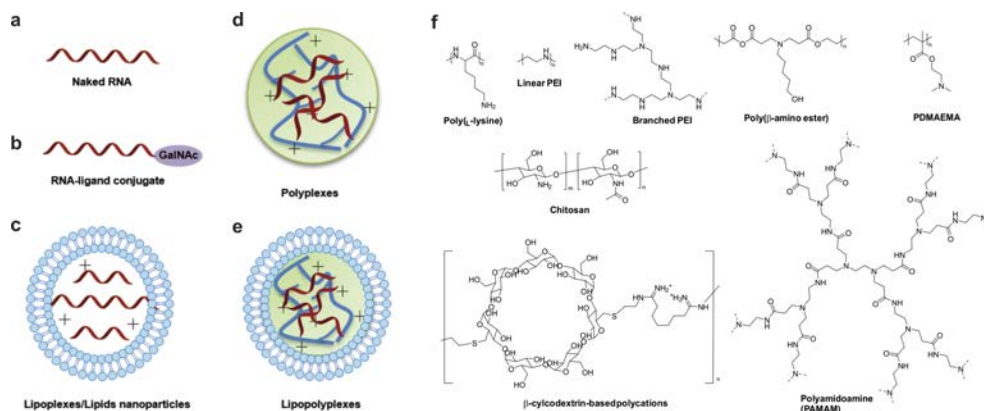


Fig. 2. Commonly used delivery formulations and cationic polymers for RNA-based drugs. (a) naked RNA; (b) RNA conjugates; (c) cationic RNA lipoplexes or lipids nanoparticles; (d) RNA polyplexes; (e) RNA lipoplexes; (f) chemical structures of commonly used cationic polymers.

on developing lipid nanoparticles (LNP) to introduce siRNAs or mRNA into hepatocytes, since the liver is a major filtering organ that traps RNA nanoparticles. In contrast to traditional DOTAP (1,2-dioleoyl-3-trimethylammonium-propane)-based formulations that carry a positive zeta potential at neutral pH, ionizable LNP only exhibited a positive surface charge in the acidic environment of the endosome to help endosomal escape and subsequent release of the encapsulated payload in the cytosol [33]. However, treatment of chronic diseases with RNA requires repeated LNP RNA administration, which can be associated with toxicity [34].

An alternative way for RNA delivery is using hybrid nanoparticles which are composed of lipids and polymers, named as lipopolyplexes (Fig. 2e). This method integrates several potential advantages of its components, thus providing more flexibility when compared with nonhybrid systems for the delivery of RNA therapeutics [35]. Generally, RNA is first mixed with a cationic polymer, for example protamine or poly(β -amino esters) as core to facilitate endosomal escape, after which a shell of lipids decorated with targeting ligands or a stealth polymer (such as poly(ethylene glycol) (PEG)) is coated on the core to enhance the nanoparticle stability, circulation kinetics and cell specificity [36,37]. In particular, lipopolyplexes have a great potential to efficiently deliver mRNA into dendritic cells (DCs) for cancer treatment [38–42].

Synthetic polymers, are also frequently applied for RNA delivery due to their high degree of chemical flexibility and the possibility to be tuned to integrate various functionalities to overcome specific biological barriers [43]. For instance, cationic polymers can electrostatically condense negatively charged RNA into nanoparticles, namely polyplexes (Fig. 2d). The size of polyplexes ranges from 6 nm (average hydrodynamic diameter of single polymer-complexed siRNA molecules [44]) to several hundreds of nanometers (containing multiple copies of the nucleic acid). Typical examples of cationic polymers used for polyplex formation are shown in Fig. 2f. Cationic polymers, like polyethyleneimine (PEI), with effective RNA transfection both *in vitro* and *in vivo* is mostly ascribed to the protonation of amines under acid environment

that resulted in endosomal rupture, so called ‘proton-sponge’ effect [45,46]. Nowadays, a new generation of biodegradable polymers has been synthesized specially for aid the RNA delivery. Most biodegradable polymers are environmental sensitive, meaning that the polyplexes start to disintegrate and release the RNA cargo by employing a change of pH, reductive gradient, and enzyme concentration at different target sites. To further increase the polyplexes stability in the extracellular environment, versatile methods have been studied, including surface coating with non-charged, hydrophilic polymers such as PEG [47,48], reversible cross-linking of polyplexes [49,50], incorporating hydrophobic components [51,52] and using of quaternary amines [53,54]. The ability of modifying polyplexes with multiple functional groups, like targeting ligands and endosomal escape peptides with versatile chemistry tools (e.g. strain-promoted azide–alkyne cycloaddition [55], thiol-yne click reaction [56]), confers that polymeric systems have a great potential in RNA therapeutics delivery.

| Cancer immunotherapy

Cancer immunotherapy is a strategy that harnesses the body’s immune system to kill cancerous cells, leading to tumor shrinkage and to improve clinical outcomes in patients [57]. In recent years, this field has boomed with the development of many different classes of agents aimed at enhancing immune responses against tumors. These include cytokines [58], immune checkpoint inhibitors [59], adoptive T cell therapies [60], and numerous vaccination strategies [61]. Recent clinical success on chimeric antigen receptor T (CAR-T) cell therapies, collecting and engineering patients’ own immune T cells to treat B-cell precursor acute lymphoblastic leukaemia, has led two CAR-T cell therapies to get approved by the U.S. Food and Drug Administration (FDA) in 2017 [62].

| Cancer vaccines

To harness the immune system to treat cancer, one needs to develop approaches to neutralize tumor-promoting inflammation, to modify the tumor microenvironment that regulates T cell activity, and to broaden the T cell repertoire by vaccination [63–65]. The aimed mechanism of cancer immunotherapy is to activate the adaptive immune system by both humoral and cellular immune response against tumor cells. Especially, the elicitation of tumor specific cytotoxic CD8 positive cells (CTLs) cells is critical for immunotherapy [61]. Among others, cancer vaccines are designed to fulfill this purpose. Compared to other therapies, cancer vaccines are relatively safe and specific compared to e.g. classical chemotherapy. Besides, it also offers the potential to avoid drug resistance and obtain durable treatment responses due to immunological memory [66]. For the viral-associated cancers, prophylactic cancer vaccines, that seek to prevent or eliminate cancers before they become established, have been developed [67]. For example, the successful development of prophylactic cancer vaccines targeting two cancer-causing viruses, the hepatitis B virus (HBV) and the human papillomavirus (HPV), has demonstrated conclusively that prophylactic immunization is a successful strategy [65]. However, around 85% of cancer types are not caused by viruses, and therefore are mainly treated with therapeutic cancer vaccines.

With an increasing number of identified tumor associated antigens and neoantigens [13], much effort has been directed to the use of tumor antigen based vaccines for active immunization against growing tumors [61]. In general, there are four main categories of cancer vaccines: (1) protein/peptide-based vaccines, (2) cellular vaccines, including tumor cell and immune cell vaccines, (3) viral vector vaccines, and (4) nucleic acid vaccines, including DNA and RNA vaccines.

Protein/peptide-based vaccines

The first reports of plasmid DNA (pDNA) and mRNA vaccines appeared around the same time (1992 and 1993, respectively) [68,69], however, owing to concerns associated with mRNA instability, high innate immunogenicity, difficult to manufacture and expensive, the field pursued DNA-based and protein/peptide-based vaccine approaches since then [70,71]. Protein/peptide vaccines using tumor associated recombinant/purified proteins or synthetic peptides containing T or B cell epitopes as target tumor antigen have been extensively investigated in clinical study due to their good safety profiles and ease of quality control [72,73]. However, due to the poor immunogenicity of protein and peptides, additional adjuvants are necessary to induce a more potent immune response. Adjuvants can activate innate immune cells, promote cell-mediated transport of antigens to lymphoid tissues. For example, emulsion adjuvant AS03 and MF59[®] [74], toll like receptors (TLR) 7/8 agonist [75,76] have been used in clinical trials together with protein/peptide vaccines. Among them single chain RNA (ssRNA) which can activate TLR7/8 have also been studied and are now under clinical assessment [77]. Mixtures of protein/peptide-based vaccines and adjuvants have shown poor anti-tumor efficacy in clinical trials, which has been ascribed to inefficient co-delivery of antigen and adjuvants to draining lymph nodes (dLNs), and subsequent immunological tolerance and CTL fratricide [78]. Recently, various polymeric nanoparticle platforms have been studied for the co-delivery of antigen and adjuvants to dLNs for improved T cell immunity [79].

mRNA cancer vaccines

In recent ten years, major technological innovation and research investments have enabled mRNA to become a promising therapeutic tool in the fields of vaccine development and protein replacement therapy. The use of mRNA for vaccination purposes has several beneficial features over subunit protein, killed and live attenuated viruses, as well as DNA-based vaccines. Firstly, there is a safety benefit, since mRNA has the minimal vector enabling transient protein expression and does not harbor the risk of insertional mutagenesis or permanent genomic alteration. Additionally, mRNA is degraded by normal cellular processes and no acquired anti-vector immunity exists [80]. Secondly, there is a better efficiency. Similar to DNA, mRNA vaccines lack MHC haplotype restriction, unlike peptide vaccination strategies. Thirdly, mRNA vaccines have the potential for rapid, relatively inexpensive and scalable manufacturing [11]. Finally, intrinsic costimulatory and inflammatory triggers in addition to the provision of the antigenic information, makes mRNA an all-in-one molecule that does not need additional adjuvants [81].

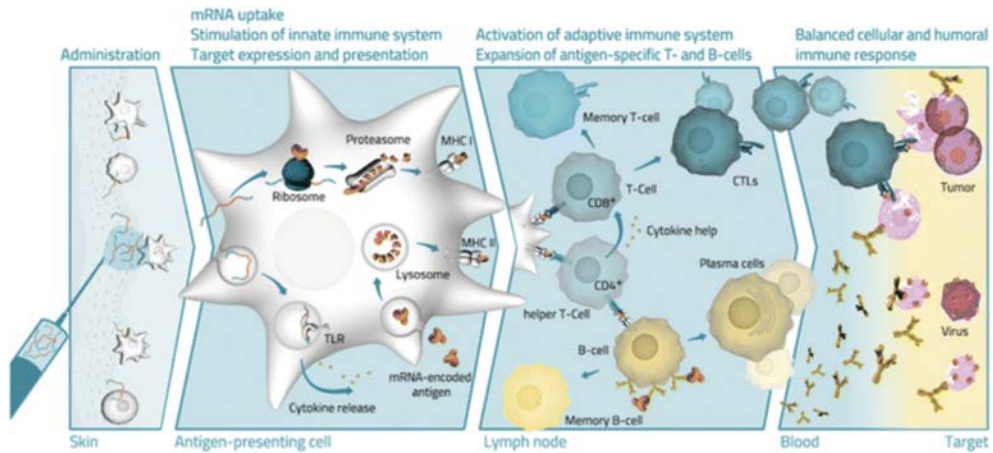


Fig. 3. Schematic overview of injected mRNA vaccines. A balanced cellular and humoral immune response after vaccination with mRNA vaccines. After intradermal or subcutaneous application of an mRNA vaccine, antigen-presenting cells (APCs) taken up antigen-coding mRNA to express a protein and at same time are activated by recognition with Toll-like receptors (TLRs). The activated APCs then present peptides derived from the endogenously expressed antigens on MHC-I or MHC-II, respectively, which leads to an efficient priming of the adaptive immune system, the expansion of antigen-specific T and B cells, and a balanced cellular and humoral immune response. Reproduced with permission [82].

All these features make mRNA vaccine the most promising alternative to conventional vaccine approaches, and numerous clinical studies to treat cancer are ongoing.

Induction of T-cell immunity is a multi-faceted process comprising antigen acquisition, antigen processing and presentation, as well as immune stimulation (Fig. 3). While direct injection of mRNA vaccines is simple and cost-effective, the clinical benefit in cancer patients was modest and mostly noted as prolonged survival and/or improved quality of life. The RActive[®] mRNA vaccine from CureVac AG failed in a phase IIb trial regarding survival benefit of patients with metastatic prostate cancer is one typical example (Company annual report). A suboptimal vaccine delivery platform and an immunosuppressive cancer microenvironment are the major causes for the poor clinical outcome [83]. To modify the tumor microenvironment, in a number of mRNA vaccine clinical trials, immune checkpoints inhibitors (PD1/PD-L1), which release brake on the T cells to kill tumor cells, are co-administered [59,84]. At present, the outcome of these studies has not yet published. The effectiveness of mRNA vaccines is critically dependent on making the antigen(s) of interest available to professional antigen-presenting cells, particularly dendritic cells (DCs). The present methods to achieve this is loading mRNA into DCs *ex vivo*, followed by re-infusion of the transfected cells into patients [58]. Most clinical trials are based on this method, but this form of cell therapy is rather expensive, time-consuming and labor-intensive. Therefore, an exquisite delivery platform which could efficiently deliver mRNA into DCs, aid to mRNA endosomal escape, and at same time promote T cell immunity *in vivo* is the ultimate objective in the delivery field and will undoubtedly accelerate the progress in mRNA cancer vaccines development.

| Aim of the thesis and outline

The lack of safe and efficient gene delivery system limits the efforts to develop new RNA drugs to combat various diseases including genetic disorders, viral infections and cancer. Even though substantial success has been made with polymeric vectors, their applications has been restricted by the inefficient *in vivo* delivery of RNA therapeutics. With the recent technological advances and better understanding of the fundamental biological mechanisms for different diseases, development of multifunctional polymeric delivery platforms that will efficiently transport RNA therapeutics to the target site, are becoming the critical step for clinical translation. In this thesis, we have investigated different newly synthesized polymers for siRNA and mRNA delivery. With employing copper-free click chemistry, we were able to design and build multifunctional polymeric delivery system to fulfill different applications. The delivery target was from tumor cells with siRNA gene silencing to antigen presenting cells (DCs) for mRNA cancer vaccines.

In **Chapter 2**, a series of novel polymers containing quaternized amines and a hydrophobic benzyl groups as backbones and synthesized by reversible addition-fragmentation chain transfer (RAFT) polymerization were evaluated to deliver siRNA to human ovarian adenocarcinoma cells. **Chapter 3** provides a new method to introduce hydrophobic groups, in this case cholesterol, to a RAFT synthesized cationic polymer. This polymeric delivery system was designed to locally deliver therapeutic siRNA to malignant brain tumor for down-regulation of key mediator for tumor cells invading and proliferation. We expected that cholesterol introduction will enhance the stability of siRNA polyplexes. The preformed polyplexes were subsequently post-modified with PEG-cRGD to shield the surface charge and target glioblastoma cells. The transfection efficiency and cellular uptake of siRNA polyplexes were tested *in vitro* using U87R cell lines. In addition, a pilot *in vivo* study in healthy, non-tumor bearing C57BL/6 mice was carried out to investigate the safety of this delivery system.

As potent adjuvants are highly demanded for most protein and peptide-based vaccine candidates in clinical development, a novel ssRNA nanocomplex adjuvant formulation was developed in **Chapter 4**. Similar as chapter 3, the preformed PolyU polyplexes were post-PEGylated via copper-free click chemistry and crosslinked with disulphide bonds to increase the particle stability. The post-PEGylation kinetics was studied by zeta potential measurements and fluorescence correlation spectroscopy. The generated ssRNA adjuvant was proved to efficiently target and mature DCs in lymph nodes and the adjuvant effect of the immunostimulatory ssRNA adjuvant were tested *in vivo* by co-injection of soluble ovalbumin (OVA) as a model antigen. In **Chapter 5**, a modular core (RNA)-shell (antigen) polymeric reductive nanoparticle formulation mimicking viral structures as cancer vaccine was constructed using a cationic polymer as building block. A water-soluble polymer with mannose side groups was also decorated on the surface of the particles to target DCs. We anticipated that codelivery of an adjuvant (ssRNA, which is a ligand for Toll-like receptor 7 (TLR7) and TLR8) and an antigen in structural organization mimicking viruses, will promote the cytotoxic T cell immunity. The stability of the nanoparticles was evaluated with dynamic light scattering (under reducing and non-reducing conditions) and the immunogenicity of these vaccines was evaluated both

in vitro and *in vivo*. Lastly, to move into the direction from a protein to a mRNA vaccine, in **Chapter 6**, different membrane active peptides that potentially can promote DCs endosomal escape of polyplexes were screened and tested to improve the antigen mRNA translation and presentation. The mRNA transfection and presentation mechanism and the underlying cellular trafficking pathway were also investigated. **Chapter 7** summarizes the results, and possible optimization and perspectives of mRNA vaccines are discussed.

| References

1. J. a Wolff, R.W. Malone, P. Williams, W. Chong, G. Acsadi, a Jani, P.L. Felgner, Direct gene transfer into mouse muscle in vivo., *Science*. 247 (1990) 1465–8.
2. U. Sahin, K. Karikó, Ö. Türeci, mRNA-based therapeutics — developing a new class of drugs, *Nat. Rev. Drug Discov.* 13 (2014) 759–780.
3. S.F. Dowdy, Overcoming cellular barriers for RNA therapeutics, *Nat. Biotechnol.* 35 (2017) 222–229.
4. J. Lieberman, Tapping the RNA world for therapeutics, *Nat. Struct. Mol. Biol.* 25 (2018) 357–364.
5. S.A. Gorski, J. Vogel, J.A. Doudna, RNA-based recognition and targeting: Sowing the seeds of specificity, *Nat. Rev. Mol. Cell Biol.* 18 (2017) 215–228.
6. J.C. Kaczmarek, P.S. Kowalski, D.G. Anderson, Advances in the delivery of RNA therapeutics: From concept to clinical reality, *Genome Med.* 9 (2017).
7. J.C. Kaczmarek, P.S. Kowalski, D.G. Anderson, Advances in the delivery of RNA therapeutics: From concept to clinical reality, *Genome Med.* 9 (2017) 60.
8. S. Cirak, V. Arechavala-Gomez, M. Guglieri, L. Feng, S. Torelli, K. Anthony, S. Abbs, M.E. Garralda, J. Bourke, D.J. Wells, G. Dickson, M.J. Wood, S.D. Wilton, V. Straub, R. Kole, S.B. Shrewsbury, C. Sewry, J.E. Morgan, K. Bushby, F. Muntoni, Exon skipping and dystrophin restoration in patients with Duchenne muscular dystrophy after systemic phosphorodiamidate morpholino oligomer treatment: an open-label, phase 2, dose-escalation study, *Lancet*. 378 (2011) 595–605.
9. R.S. Finkel, E. Mercuri, B.T. Darras, A.M. Connolly, N.L. Kuntz, J. Kirschner, C.A. Chiriboga, K. Saito, L. Servais, E. Tizzano, H. Topaloglu, M. Tulinius, J. Montes, A.M. Glanzman, K. Bishop, Z.J. Zhong, S. Gheuens, C.F. Bennett, E. Schneider, W. Farwell, D.C. De Vivo, Nusinersen versus Sham Control in Infantile-Onset Spinal Muscular Atrophy, *N. Engl. J. Med.* 377 (2017) 1723–1732.
10. The commercial tipping point, *Nat. Biotechnol.* 35 (2017) 181–181.
11. N. Pardi, M.J. Hogan, F.W. Porter, D. Weissman, mRNA vaccines — a new era in vaccinology, *Nat. Rev. Drug Discov.* 17 (2018) 261–279.
12. L.M. Kranz, M. Diken, H. Haas, S. Kreiter, C. Loquai, K.C. Reuter, M. Meng, D. Fritz, F. Vascotto, H. Hefesha, C. Grunwitz, M. Vormehr, Y. Hüsemann, A. Selmi, A.N. Kuhn, J. Buck, E. Derhovanessian, R. Rae, S. Attig, J. Diekmann, R.A. Jabulowsky, S. Heesch, J. Hassel, P. Langguth, S. Grabbe, C. Huber, Ö. Türeci, U. Sahin, Systemic RNA delivery to dendritic cells exploits antiviral defence for cancer immunotherapy, *Nature*. 534 (2016) 396–401.
13. U. Sahin, Ö. Türeci, Personalized vaccines for cancer immunotherapy, *Science*. 359 (2018) 1355–1360.
14. M. Alberer, U. Gnad-Vogt, H.S. Hong, K.T. Mehr, L. Backert, G. Finak, R. Gottardo, M.A. Bica, A. Garofano, S.D. Koch, M. Fotin-Mleczek, I. Hoerr, R. Clemens, F. von Sonnenburg, Safety and immunogenicity of a mRNA rabies vaccine in healthy adults: an open-label, non-randomised, prospective, first-in-human phase 1 clinical trial, *Lancet*. 390 (2017) 1511–1520.
15. J.M. Richner, S. Himansu, K.A. Dowd, S.L. Butler, V. Salazar, J.M. Fox, J.G. Julander, W.W. Tang, S. Shresta, T.C. Pierson, G. Ciaramella, M.S. Diamond, Modified mRNA Vaccines Protect against Zika Virus Infection, *Cell*. 168 (2017) 1114–1125.e10.
16. K. Bahl, J.J. Senn, O. Yuzhakov, A. Bulychev, L.A. Brito, K.J. Hassett, M.E. Laska, M. Smith, Ö. Almarsson, J. Thompson, A. (Mick) Ribeiro, M. Watson, T. Zaks, G. Ciaramella, Preclinical and Clinical Demonstration of Immunogenicity by mRNA Vaccines against H10N8 and H7N9 Influenza Viruses, *Mol. Ther.* 25 (2017) 1316–1327.

17. H. Yin, R.L. Kanasty, A.A. Eltoukhy, A.J. Vegas, J.R. Dorkin, D.G. Anderson, Non-viral vectors for gene-based therapy, *Nat. Rev. Genet.* 15 (2014) 541–555.
18. D. V Morrissey, J.A. Lockridge, L. Shaw, K. Blanchard, K. Jensen, W. Breen, K. Hartsough, L. Machermer, S. Radka, V. Jadhav, N. Vaish, S. Zinnen, C. Vargeese, K. Bowman, C.S. Shaffer, L.B. Jeffs, A. Judge, I. MacLachlan, B. Polisky, Potent and persistent in vivo anti-HBV activity of chemically modified siRNAs, *Nat. Biotechnol.* 23 (2005) 1002–1007.
19. K. Karikó, M. Buckstein, H. Ni, D. Weissman, Suppression of RNA recognition by Toll-like receptors: The impact of nucleoside modification and the evolutionary origin of RNA, *Immunity.* 23 (2005) 165–175.
20. A. Khvorova, J.K. Watts, The chemical evolution of oligonucleotide therapies of clinical utility, *Nat. Biotechnol.* 35 (2017) 238–248.
21. R.L. Juliano, The delivery of therapeutic oligonucleotides, *Nucleic Acids Res.* 44 (2016) 6518–6548.
22. G.R. Rettig, M.A. Behlke, Progress toward in vivo use of siRNAs-II, *Mol. Ther.* 20 (2012) 483–512.
23. T. Golan, E.Z. Khvalevsky, A. Hubert, R.M. Gabai, N. Hen, A. Segal, A. Domb, G. Harari, E. Ben David, S. Raskin, Y. Goldes, E. Goldin, R. Eliakim, M. Lahav, Y. Kopleman, A. Dancour, A. Shemi, E. Galun, RNAi therapy targeting KRAS in combination with chemotherapy for locally advanced pancreatic cancer patients., *Oncotarget.* 6 (2015) 24560–70.
24. L.A. Becker, B. Huang, G. Bieri, R. Ma, D.A. Knowles, P. Jafar-Nejad, J. Messing, H.J. Kim, A. Soriano, G. Auburger, S.M. Pulst, J.P. Taylor, F. Rigo, A.D. Gitler, Therapeutic reduction of ataxin-2 extends lifespan and reduces pathology in TDP-43 mice, *Nature.* 544 (2017) 367–371.
25. D.R. Scoles, P. Meera, M.D. Schneider, S. Paul, W. Dansithong, K.P. Figueroa, G. Hung, F. Rigo, C.F. Bennett, T.S. Otis, S.M. Pulst, Antisense oligonucleotide therapy for spinocerebellar ataxia type 2, *Nature.* 544 (2017) 362–366.
26. U. Sahin, E. Derhovanessian, M. Miller, B.P. Kloke, P. Simon, M. Löwer, V. Bukur, A.D. Tadmor, U. Luxemburger, B. Schrörs, T. Omokoko, M. Vormehr, C. Albrecht, A. Paruzynski, A.N. Kuhn, J. Buck, S. Heesch, K.H. Schreeb, F. Müller, I. Ortseifer, I. Vogler, E. Godehardt, S. Attig, R. Rae, A. Breitzkreuz, C. Tolliver, M. Suchan, G. Martic, A. Hohberger, P. Sorn, J. Diekmann, J. Ciesla, O. Waksman, A.K. Brück, M. Witt, M. Zillgen, A. Rothermel, B. Kasemann, D. Langer, S. Bolte, M. Diken, S. Kreiter, R. Nemecek, C. Gebhardt, S. Grabbe, C. Höller, J. Utikal, C. Huber, C. Loquai, Ö. Türeci, Personalized RNA mutanome vaccines mobilize poly-specific therapeutic immunity against cancer, *Nature.* 547 (2017) 222–226.
27. C. Lorenz, P. Hadwiger, M. John, H.-P. Vornlocher, C. Unverzagt, Steroid and lipid conjugates of siRNAs to enhance cellular uptake and gene silencing in liver cells, *Bioorg. Med. Chem. Lett.* 14 (2004) 4975–4977.
28. K. Nishina, T. Unno, Y. Uno, T. Kubodera, T. Kanouchi, H. Mizusawa, T. Yokota, Efficient in vivo delivery of siRNA to the liver by conjugation of α -tocopherol, *Mol. Ther.* 16 (2008) 734–740.
29. T.L. Cuellar, D. Barnes, C. Nelson, J. Tanguay, S.-F. Yu, X. Wen, S.J. Scales, J. Gesch, D. Davis, A. van Brabant Smith, D. Leake, R. Vandlen, C.W. Siebel, Systematic evaluation of antibody-mediated siRNA delivery using an industrial platform of THIOMAB–siRNA conjugates, *Nucleic Acids Res.* 43 (2015) 1189–1203.
30. L. Pärnaste, P. Arukuusk, K. Langel, T. Tenson, Ü. Langel, The Formation of Nanoparticles between Small Interfering RNA and Amphiphathic Cell-Penetrating Peptides, *Mol. Ther. - Nucleic Acids.* 7 (2017) 1–10.
31. J.K. Nair, J.L.S. Willoughby, A. Chan, K. Charisse, M.R. Alam, Q. Wang, M. Hoekstra, P. Kandasamy, A. V. Kelin, S. Milstein, N. Taneja, J. Oshea, S. Shaikh, L. Zhang, R.J. Van Der Sluis, M.E. Jung, A. Akinc, R.

- Hutabarat, S. Kuchimanchi, K. Fitzgerald, T. Zimmermann, T.J.C. Van Berkel, M.A. Maier, K.G. Rajeev, M. Manoharan, Multivalent N -acetylgalactosamine-conjugated siRNA localizes in hepatocytes and elicits robust RNAi-mediated gene silencing, *J. Am. Chem. Soc.* 136 (2014) 16958–16961.
32. K. Fitzgerald, S. White, A. Borodovsky, B.R. Bettencourt, A. Strahs, V. Clausen, P. Wijngaard, J.D. Horton, J. Taubel, A. Brooks, C. Fernando, R.S. Kauffman, D. Kallend, A. Vaishnav, A. Simon, A Highly Durable RNAi Therapeutic Inhibitor of PCSK9, *N. Engl. J. Med.* 376 (2017) 41–51.
 33. S. Rietwyk, D. Peer, Next-Generation Lipids in RNA Interference Therapeutics, *ACS Nano.* 11 (2017) 7572–7586.
 34. R.L. Juliano, The delivery of therapeutic oligonucleotides, *Nucleic Acids Res.* 44 (2016) 6518–6548.
 35. S. Guan, J. Rosenecker, Nanotechnologies in delivery of mRNA therapeutics using nonviral vector-based delivery systems, *Gene Ther.* 24 (2017) 133–143.
 36. F. Perche, T. Benvegna, M. Berchel, L. Lebegue, C. Pichon, P.-A. Jaffrès, P. Midoux, Enhancement of dendritic cells transfection in vivo and of vaccination against B16F10 melanoma with mannosylated histidylated lipopolyplexes loaded with tumor antigen messenger RNA, *Nanomedicine Nanotechnology, Biol. Med.* 7 (2011) 445–453.
 37. K. Kusumoto, H. Akita, T. Ishitsuka, Y. Matsumoto, T. Nomoto, R. Furukawa, A. El-Sayed, H. Hatakeyama, K. Kajimoto, Y. Yamada, K. Kataoka, H. Harashima, Lipid envelope-type nanoparticle incorporating a multifunctional peptide for systemic siRNA delivery to the pulmonary endothelium, *ACS Nano.* 7 (2013) 7534–7541.
 38. M. Mockey, E. Bourseau, V. Chandrashekhar, A. Chaudhuri, S. Lafosse, E. Le Cam, V.F.J. Quesniaux, B. Ryffel, C. Pichon, P. Midoux, mRNA-based cancer vaccine: Prevention of B16 melanoma progression and metastasis by systemic injection of MART1 mRNA histidylated lipopolyplexes, *Cancer Gene Ther.* 14 (2007) 802–814.
 39. S. Persano, M.L. Guevara, Z. Li, J. Mai, M. Ferrari, P.P. Pompa, H. Shen, Lipopolyplex potentiates anti-tumor immunity of mRNA-based vaccination, *Biomaterials.* 125 (2017) 81–89.
 40. C. Pichon, P. Midoux, Mannosylated and histidylated LPR technology for vaccination with tumor antigen mRNA., *Methods Mol. Biol.* 969 (2013) 247–274.
 41. A. Le Moignic, V. Malard, T. Benvegna, L. Lemiègre, M. Berchel, P.-A. Jaffrès, C. Baillou, M. Delost, R. Macedo, J. Rochefort, G. Lescaille, C. Pichon, F.M. Lemoine, P. Midoux, V. Mateo, Preclinical evaluation of mRNA trimannosylated lipopolyplexes as therapeutic cancer vaccines targeting dendritic cells, *J. Control. Release.* 278 (2018) 110–121.
 42. X. Su, J. Fricke, D.G. Kavanagh, D.J. Irvine, In vitro and in vivo mRNA delivery using lipid-enveloped pH-responsive polymer nanoparticles, *Mol. Pharm.* 8 (2011) 774–787.
 43. U. Lachelt, E. Wagner, *Nucleic Acid Therapeutics Using Polyplexes: A Journey of 50 Years (and Beyond)*, *Chem. Rev.* 115 (2015) 11043–11078.
 44. D.W. Pack, A.S. Hoffman, S. Pun, P.S. Stayton, Design and development of polymers for gene delivery, *Nat. Rev. Drug Discov.* 4 (2005) 581–593.
 45. J. Behr, The proton sponge: a trick to enter cells the viruses did not exploit, *Int. J. Chem.* 2 (1997) 34–36.
 46. O. Boussif, F. Lezoualc'h, M.A. Zanta, M.D. Mergny, D. Scherman, B. Demeneix, J.P. Behr, A versatile vector for gene and oligonucleotide transfer into cells in culture and in vivo: polyethylenimine., *Proc. Natl. Acad. Sci. U. S. A.* 92 (1995) 7297–301.
 47. J.S. Suk, Q. Xu, N. Kim, J. Hanes, L.M. Ensign, PEGylation as a strategy for improving nanoparticle-based drug and gene delivery, *Adv. Drug Deliv. Rev.* 99 (2016) 28–51.

48. S. Üzgün, G. Nica, C. Pfeifer, M. Bosinco, K. Michaelis, J.-F. Lutz, M. Schneider, J. Rosenecker, C. Rudolph, PEGylation Improves Nanoparticle Formation and Transfection Efficiency of Messenger RNA, *Pharm. Res.* 28 (2011) 2223–2232.
49. D.J. Lee, E. Kessel, T. Lehto, X. Liu, N. Yoshinaga, K. Padari, Y.C. Chen, S. Kempter, S. Uchida, J.O. Rädler, M. Pooga, M.T. Sheu, K. Kataoka, E. Wagner, Systemic Delivery of Folate-PEG siRNA Lipopolyplexes with Enhanced Intracellular Stability for in Vivo Gene Silencing in Leukemia, *Bioconjug. Chem.* 28 (2017) 2393–2409.
50. L. Novo, E.V.B. Van Gaal, E. Mastrobattista, C.F. Van Nostrum, W.E. Hennink, Decationized crosslinked polyplexes for redox-triggered gene delivery, *J. Control. Release.* 169 (2013) 246–256.
51. Y. Oe, R.J. Christie, M. Naito, S.A. Low, S. Fukushima, K. Toh, Y. Miura, Y. Matsumoto, N. Nishiyama, K. Miyata, K. Kataoka, Actively-targeted polyion complex micelles stabilized by cholesterol and disulfide cross-linking for systemic delivery of siRNA to solid tumors, *Biomaterials.* 35 (2014) 7887–7895.
52. C. Cheng, A.J. Convertine, P.S. Stayton, J.D. Bryers, Multifunctional triblock copolymers for intracellular messenger RNA delivery, *Biomaterials.* 33 (2012) 6868–6876.
53. B. Lou, N. Beztsinna, G. Mountrichas, J.B. van den Dikkenberg, S. Pispas, W.E. Hennink, Small nanosized poly(vinyl benzyl trimethylammonium chloride) based polyplexes for siRNA delivery, *Int. J. Pharm.* 525 (2017) 388–396.
54. E. Amar-Lewis, A. Azagury, R. Chintakunta, R. Goldbart, T. Traitel, J. Prestwood, D. Landesman-Milo, D. Peer, J. Kost, Quaternized starch-based carrier for siRNA delivery: From cellular uptake to gene silencing, *J. Control. Release.* 185 (2014) 109–120.
55. J. Dommerholt, O. van Rooijen, A. Borrmann, C.F. Guerra, F.M. Bickelhaupt, F.L. van Delft, Highly accelerated inverse electron-demand cycloaddition of electron-deficient azides with aliphatic cyclooctynes, *Nat. Commun.* 5 (2014) 5378.
56. S.S. Zalesskiy, N.S. Shlapakov, V.P. Ananikov, Visible light mediated metal-free thiol–yne click reaction, *Chem. Sci.* 7 (2016) 6740–6745.
57. P.N. Kelly, The Cancer Immunotherapy Revolution., *Science.* 359 (2018) 1344–1345.
58. T.A. Waldmann, Cytokines in Cancer Immunotherapy, *Cold Spring Harb. Perspect. Biol.* (2017) a028472.
59. A. Ribas, J.D. Wolchok, Cancer immunotherapy using checkpoint blockade., *Science.* 359 (2018) 1350–1355.
60. J.N. Brudno, J.N. Kochenderfer, Chimeric antigen receptor T-cell therapies for lymphoma, *Nat. Rev. Clin. Oncol.* 15 (2017) 31–46.
61. L.H. Butterfield, Cancer vaccines., *BMJ.* 350 (2015) h988.
62. S.S. Neelapu, S. Tummala, P. Kebriaei, W. Wierda, C. Gutierrez, F.L. Locke, K. V. Komanduri, Y. Lin, N. Jain, N. Daver, J. Westin, A.M. Gulbis, M.E. Loghin, J.F. de Groot, S. Adkins, S.E. Davis, K. Rezvani, P. Hwu, E.J. Shpall, Chimeric antigen receptor T-cell therapy — assessment and management of toxicities, *Nat. Rev. Clin. Oncol.* 15 (2017) 47–62.
63. M.A. Oberli, A.M. Reichmuth, J.R. Dorkin, M.J. Mitchell, O.S. Fenton, A. Jaklenec, D.G. Anderson, R. Langer, D. Blankschtein, Lipid Nanoparticle Assisted mRNA Delivery for Potent Cancer Immunotherapy, *Nano Lett.* 17 (2017) 1326–1335.
64. A.K. Palucka, L.M. Coussens, The Basis of Oncoimmunology, *Cell.* 164 (2016) 1233–1247.
65. L.M. Coussens, L. Zitvogel, A.K. Palucka, Neutralizing Tumor-Promoting Chronic Inflammation: A Magic Bullet?, *Science.* 339 (2013) 286–291.
66. M.A. McNamara, S.K. Nair, E.K. Holl, RNA-Based Vaccines in Cancer Immunotherapy, *J. Immunol. Res.* 2015 (2015) 1–9.

67. B.A. Scott, E. Mark Yarchoan, E.M. Jaffee, Prophylactic Vaccines for Nonviral Cancers, *Annu. Rev. Cancer Biol.* 2 (2018) 195–211.
68. D. Tang, M. DeVit, S.A. Johnston, Genetic immunization is a simple method for eliciting an immune response, *Nature.* 356 (1992) 152–154.
69. F. Martinon, S. Krishnan, G. Lenzen, R. Magné, E. Gomard, J. -G Guillet, J. -P Lévy, P. Meulien, Induction of virus-specific cytotoxic T lymphocytes in vivo by liposome-entrapped mRNA, *Eur. J. Immunol.* 23 (1993) 1719–1722.
70. C. Grunwitz, L.M. Kranz, mRNA cancer vaccines—messages that prevail, in: *Curr. Top. Microbiol. Immunol.*, Springer, Cham, 2017: pp. 145–164.
71. J.J. Suschak, J.A. Williams, C.S. Schmaljohn, Advancements in DNA vaccine vectors, non-mechanical delivery methods, and molecular adjuvants to increase immunogenicity, *Hum. Vaccin. Immunother.* 13 (2017) 1–12.
72. R. Arens, T. van Hall, S.H. van der Burg, F. Ossendorp, C.J.M. Melief, Prospects of combinatorial synthetic peptide vaccine-based immunotherapy against cancer, *Semin. Immunol.* 25 (2013) 182–190.
73. G.G. Kenter, M.J.P. Welters, A.R.P.M. Valentijn, M.J.G. Lowik, D.M.A. Berends-van der Meer, A.P.G. Vloon, F. Essahsah, L.M. Fathors, R. Offringa, J.W. Drijfhout, A.R. Wafelman, J. Oostendorp, G.J. Fleuren, S.H. van der Burg, C.J.M. Melief, Vaccination against HPV-16 Oncoproteins for Vulvar Intraepithelial Neoplasia, *N. Engl. J. Med.* 361 (2009) 1838–1847.
74. N.P.H. Knudsen, A. Olsen, C. Buonsanti, F. Follmann, Y. Zhang, R.N. Coler, C.B. Fox, A. Meinke, U. D'Oro, D. Casini, A. Bonci, R. Billeskov, E. De Gregorio, R. Rappuoli, A.M. Harandi, P. Andersen, E.M. Agger, Different human vaccine adjuvants promote distinct antigen-independent immunological signatures tailored to different pathogens., *Sci. Rep.* 6 (2016) 19570.
75. L. Nuhn, N. Vanparijs, A. De Beuckelaer, L. Lybaert, G. Verstraete, K. Deswarte, S. Lienenklaus, N.M. Shukla, A.C.D. Salyer, B.N. Lambrecht, J. Grooten, S.A. David, S. De Koker, B.G. De Geest, pH-degradable imidazoquinoline-ligated nanogels for lymph node-focused immune activation, *Proc. Natl. Acad. Sci.* 113 (2016) 8098–8103.
76. G.M. Lynn, R. Laga, P.A. Darrah, A.S. Ishizuka, A.J. Balaci, A.E. Dulcey, M. Pechar, R. Pola, M.Y. Gerner, A. Yamamoto, C.R. Buechler, K.M. Quinn, M.G. Smelkinson, O. Vanek, R. Cawood, T. Hills, O. Vasalatiy, K. Kastemüller, J.R. Francica, L. Stutts, J.K. Tom, K.A. Ryu, A.P. Esser-Kahn, T. Etrych, K.D. Fisher, L.W. Seymour, R.A. Seder, In vivo characterization of the physicochemical properties of polymer-linked TLR agonists that enhance vaccine immunogenicity., *Nat. Biotechnol.* 33 (2015) 1201–1210.
77. R. Heidenreich, E. Jasny, A. Kowalczyk, J. Lutz, J. Probst, P. Baumhof, B. Scheel, S. Voss, K.J. Kallen, M. Fotin-Mlecsek, A novel RNA-based adjuvant combines strong immunostimulatory capacities with a favorable safety profile, *Int. J. Cancer.* 137 (2015) 372–384.
78. C.J.M. Melief, S.H. Van Der Burg, Immunotherapy of established (pre) malignant disease by synthetic long peptide vaccines, *Nat. Rev. Cancer.* 8 (2008) 351–360.
79. T.J. Moyer, A.C. Zmolek, D.J. Irvine, Beyond antigens and adjuvants: formulating future vaccines, *J. Clin. Invest.* 126 (2016) 799–808.
80. K. Hollevoet, P.J. Declerck, State of play and clinical prospects of antibody gene transfer, *J. Transl. Med.* 15 (2017) 131.
81. M. Diken, L.M. Kranz, S. Kreiter, U. Sahin, mRNA: A Versatile Molecule for Cancer Vaccines, *Curr. Issues Mol. Biol.* 22 (2017) 113–128.
82. S. Rauch, J. Lutz, A. Kowalczyk, T. Schlake, R. Heidenreich, RNAActive® technology: Generation and testing of stable and immunogenic mRNA vaccines, in: *Methods Mol. Biol.*, Humana Press, New York, NY, 2017: pp. 89–107.
83. C.J.M. Melief, T. Van Hall, R. Arens, F. Ossendorp, S.H. Van Der Burg, Therapeutic cancer vaccines, *J. Clin. Invest.* 125 (2015) 3401–3412.

84. S.H. Van Der Burg, R. Arens, F. Ossendorp, T. Van Hall, C.J.M. Melief, Vaccines for established cancer: Overcoming the challenges posed by immune evasion, *Nat. Rev. Cancer.* 16 (2016) 219–233.

CHAPTER

2

Small nanosized poly(vinyl benzyl trimethylammonium chloride) based polyplexes for siRNA delivery

Bo Lou¹, Nataliia Beztsinna¹, Grigoris Mountrichas²,
Joep B. van den Dikkenberg¹, Stergios Pispas², Wim E. Hennink^{1,*}

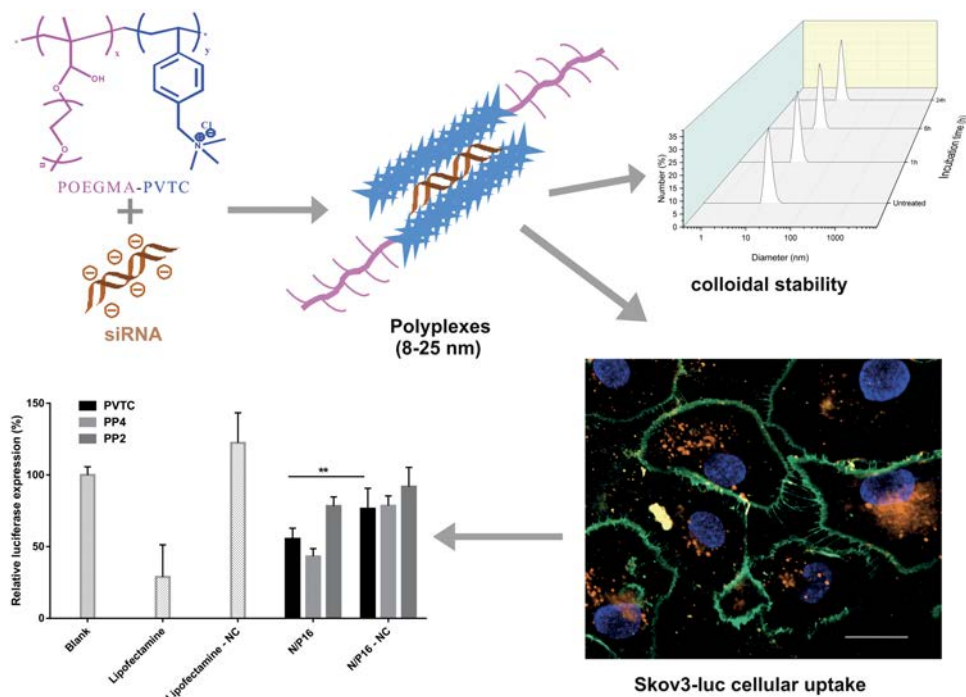
¹Department of Pharmaceutical Sciences, Utrecht Institute for
Pharmaceutical Sciences, Utrecht University,
Universiteitsweg 99, 3584 CG, Utrecht, The Netherlands.

²Theoretical and Physical Chemistry Institute, National Hellenic Research
Foundation, 48 Vass. Constantinou Ave., 11635 Athens, Greece.

| Abstract

The success of siRNA gene therapy requires the availability of safe and efficient delivery systems. In the present study, we investigated poly(vinyl benzyl trimethylammonium chloride) (PVTC) and its block copolymer with poly(oligo(ethyleneglycol) methacrylate) (POEGMA) as delivery vector for siRNA. Small polyplexes ranging from 8 to 25 nm in diameter were formed in aqueous solution by spontaneous self-assembly of both the homopolymer and block copolymer with siRNA and the formed particles were stable at physiological ionic strength. It was shown that when human ovarian adenocarcinoma cells were transfected, siRNA polyplexes based on PVTC (40 kDa) and PVTC-POEGMA-4 (PP4, 34 kDa) efficiently induced luciferase gene silencing to the same extent as the formulation based on a commercial lipid (Lipofectamine®) (~ 80%), and showed higher gene silencing than the linear polyethylenimine formulation linear polyethylenimine (~ 35%). Importantly, the POEGMA block polymers displayed a significantly lower cytotoxicity as compared to L-pEI. siRNA polyplexes based on the block polymers displayed high cellular uptake resulting in ~50% silencing of luciferase expression also in the presence of serum. These results demonstrate that PVTC-based polymers are promising siRNA delivery vectors.

Graphical abstract



| Introduction

In the past 15 years, RNA interference opened exciting therapeutic possibilities and large investments have been made for its use to treat various diseases, including viral infections and cancer [1,2]. siRNA, a short double stranded oligonucleotide with 21-23 base pairs, is a highly water-soluble polyanion (Mw around 13 kDa), which is rapidly degraded by nucleases in the extracellular environment [3]. Moreover, siRNAs are unable to spontaneously pass cellular membranes as both the oligonucleotide and cellular membrane are negatively charged. Since RNA interference has to occur in the cytoplasm, it is crucial for siRNA to be presented in the cytosol for exerting its pharmacological activity. Therefore, safe and highly efficient siRNA delivery systems, which protect these nucleic acid based drugs from enzymatic degradation and assist in overcoming the delivery barriers are required.

Polymer-based non-viral vectors, especially cationic polymers, have been widely studied for siRNA delivery both *in vitro* and *in vivo*. These polymeric delivery systems are known to have several advantages such as safety, easy large-scale production, and absence of immune side effects as compared to viral vectors. Cationic polymers form nano-sized complexes with negatively charged siRNAs and these complexes can be, depending on their biophysical properties such as size and charge, internalized by living cells. A great variety of both natural and (semi) synthetic cationic polymers have been investigated for nucleic acid delivery, including poly(L-Lysine) [4,5], poly(ethylene imine) [6,7], PDMAEMA [8,9], poly(amido amine)s [10], cationic cyclodextrins [11] and chitosan [12]. The gene binding capacities and the transfection abilities of these and other polymers have been summarized in a number of review papers [13–15]. However, one major obstacle for the translation of non-viral gene delivery systems into clinical application is their colloidal stability. Cationic polyplexes tend to aggregate/dissociate in the presence of proteins and other polyanions in blood and other biological fluids, which leads to premature nucleic acid release [16,17]. A commonly used approach to tackle the poor colloidal stability of the first generation polyplexes is their surface modification with a neutral and hydrophilic polymer [e.g., poly(ethylene glycol) (PEG)] that shields their charge and reduces nonspecific interactions [18–21]. However, several studies have shown that PEGylated polyplexes still exhibited undesirable release of siRNA payloads and displayed poor pharmacokinetics in animal models [22–25]. To increase the colloidal stability of PEGylated polyplexes, several sophisticated methods have been developed including reversible cross-linking for spatio-temporal release [26,27] and hydrophobic interactions [5,28,29]. Apart from this, several studies have indicated that the simple conversion of primary into quaternary amines or the use of polymers already containing quaternary amine groups could enhance the polymer-siRNA binding strength and lead to the particles that are more colloiddally stable in physiological fluids. [17,30–34].

Recently, a novel polymer, poly(vinyl benzyl trimethyl-ammonium chloride) (PVTC) containing permanently quaternized amines and a hydrophobic benzyl groups as backbone, was synthesized by RAFT polymerization [35]. This study showed that this quaternized polymer formed complexes with plasmid DNA with a size ranging of 80-300 nm and with a good particle stability even in the presence of 300 mM sodium chloride. It is expected that these PVTC-based

polymers could also form stable particles with siRNA and ensure its successful intracellular delivery. In this study, we characterized the physicochemical properties of polyplexes formed with the homopolymer PVTC and block copolymers POEGMA-PVTC and evaluated the ability of these polyplexes to deliver siRNA into the cells.

| Materials and Methods

Materials

The double-stranded anti-luc siRNA-1(D-002050-01) which specifically targets firefly luciferase (used against mRNA from pGL3; sense strand: 5' - CUU ACG CUG AGU ACU UCGA - 3'), siGLO Red(DY-547) Transfection Indicator (D-001630-02) and Non-target siRNA-1(D-001810-01) were obtained from Dharmacon Bioscience (Lafayette, USA). The homopolymer poly(vinyl benzyl trimethyl-ammonium chloride) (referred as PVTC) and two different poly[oligo(ethylene glycol) methacrylate]-b-poly(vinyl benzyl trimethylammonium chloride) block copolymers (referred as PP2 and PP4) were synthesized by RAFT polymerization as described previously [35]. Their molecular characteristics are shown in the Table 1. Linear polyethylenimine (L-pEI, Mw 25,000) was obtained from Polysciences and Lipofectamine 2000 was from Thermo Fisher Scientific (Etten-Leur, The Netherlands).

Agarose multi-purpose was purchased from Roche Molecular Biochemicals (Mannheim, Germany). 6× DNA Loading Dye was purchased from Fermentas (St. Leon-Roth, Germany). SYBR Safe DNAGel stain, Opti-MEM, DMEM medium and dialyzed fetal bovine serum (FBS) were purchased from Life Technologies (Breda, The Netherlands). Skov3-luc (human ovarian carcinoma cell line stably expressing firefly luciferase) cells were obtained from CellBioLabs (San Diego, USA). Luciferase assay kit was purchased from Promega (Leiden, The Netherlands). All other chemicals, reagents and media were obtained from Sigma-Aldrich (Zwijndrecht, The Netherlands).

Preparation and characterization of polymer/siRNA polyplexes

Polymer/siRNA polyplexes of nitrogen/phosphate (N/P) ratios from 0.5 to 16 were prepared by adding 400 μ L of polymer solution (varying concentrations in 10 mM HEPES buffer, pH 7.4) to 200 μ L of siRNA (40 μ g/mL in 10 mM HEPES buffer, pH 7.4), followed by vortexing for 5 s and incubating at room temperature for 30 min. Particle sizes were measured with dynamic

Table 1. Characteristics of the PVTC-based homo- and block copolymers used in this study.

code	name	M_n (g.mol ⁻¹)	PVTC M_n (g.mol ⁻¹)	POEGMA M_n (g.mol ⁻¹)	PVTC % (w/w)	M_w/M_n
PVTC	PVTC-40k	39,600	39,600		100	1.28
PP2	PVTC- POEGMA-2	22,400	4,200	18,200	19	1.21
PP4	PVTC- POEGMA-4	33,600	15,400	18,200	46	1.24

light scattering (DLS) using an ALV CGS-3 system (Malvern Instruments, Malvern, U.K.) equipped with a JDS Uniphase 22 mW He – Ne laser operating at 632.8 nm, an optical fiber-based detector, and a digital LV/LSE-5003 correlator with temperature controller set at 25 °C. The zeta-potential of the polyplexes was measured at 25 °C using a Malvern Zetasizer Nano-Z (Malvern Instruments, Malvern, U.K.).

Gel retardation assay

Polyplexes prepared at different N/P ratios were made by adding 5 μ L of polymer solution (varying concentration 14-2400 μ g/mL in 10 mM HEPES, pH 7.4) to 5 μ L of siRNA solution (40 μ g/mL in 10 mM HEPES, pH 7.4), followed by vortexing for 5 s and the dispersions were incubated for 30 min at room temperature. For release studies with heparin, the sample prepared at N/P of 8 was mixed with of 5 μ L heparin sodium salt (varying concentration 75-900 μ g/mL). Next, 1 μ L of sodium chloride (1.54 M) was added to get a final salt concentration of 150 mM, and the samples were incubated for 10 min at room temperature [36]. After the addition of 3 μ L of 6 \times loading buffer (Fermentas), the mixture was loaded into a 2% agarose gel containing GelGreen (Biotium) in a tris-acetate-EDTA (TAE) buffer and the gel was developed at 100 V for 30 min. Next, the gel was analyzed by a Gel Doc XR+ system (BioRad Laboratories Inc., Hercules, CA) with Image Labsoftware.

Transmission Electron Microscopy (TEM)

Transmission Electron Microscopy (TEM) was carried out using a FEI Tecnai T10 microscope from FEI company (Eindhoven, Netherland). Twenty microliters of polyplexes dispersion at 20 μ g/mL siRNA in 10 mM HEPES, pH 7.4, was placed on a carbon-coated copper grid. The samples were stained with 2% uranyl acetate. Scale bars were added with a help of ImageJ software.

Cell culture

Skov3-luc cells which stably express firefly luciferase, were cultured in DMEM (4.5 g/L glucose) supplemented with 10% FBS (Sigma-Aldrich). Cells were maintained at 37°C in a 5% CO₂ and humidified air atmosphere.

In vitro luciferase gene silencing efficiency assay

Skov3-luc cells were plated in 96-well plates (7 \times 10³ cells/well) cultured in full medium for at least 24 h until 60-70% cell confluence was reached. The cells were then washed with PBS buffer and subsequently incubated in medium with or without 10% serum. Next, the siRNA polyplexes (anti-luciferase or negative control) of varying N/P ratios were prepared as described in section 2.2 (10 mM HEPES buffer, pH 7.4) and added to the cells (siRNA concentration was 100 or 200 nM) and incubated for 4 h at 37°C in a 5% CO₂-containing atmosphere. The cells were washed with PBS, replaced with fresh full medium and further incubated for 44 h. The transfection experiments were done in triplicate. A transfection formulation with L-pEI prepared at an

optimal N/P ratio of 10/1 or with Lipofectamine 2000 (1.5 μ L +1 μ g siRNA), were applied as positive controls. The cells treated with PBS were used as negative control. The luciferase protein expression was analyzed using luciferase reporter gene assay (Promega). Briefly, after 44 h, the cells were washed with 100 μ L cold PBS and lysed with 50 μ L lysis buffer. Next, 20 μ L cell lysate was mixed with 50 μ L luciferase assay reagent (Promega) with a microinjector, and after 2 s, luminescence was measured for 10 s using a FLUOstar OPTIMA microplate, equipped with a luminescence light guide (BMG LabTech, Germany). Polyplexes based on the commercially available transfection agents L-PEI and Lipofectamine 2000 were used as positive controls. The gene silencing results were corrected for cytotoxicity, and the results are expressed as relative luciferase expression compared to untreated cells [37].

Cell viability assay

The cytotoxicity of the different polymers or the siRNA polyplexes was determined by the AlamarBlue assay (Invitrogen). In brief, Skov3-luc cells were incubated with polymer solutions (concentrations ranging from 2 to 100 μ g/mL) or siRNA polyplexes (concentrations ranging from 100 to 200 nM siRNA, at N/P ratio of 8 or 16) for 4 h in the absence or presence of serum, and subsequently the medium was replaced by fresh full medium. After 40 h, the medium was removed and the cells were washed twice with PBS buffer and incubated with freshly made 100 μ L 1 \times Alamar Blue-DMEM medium (i.e. 10-fold diluted AlamarBlue in DMEM full medium) for 4 h. Thereafter, 80 μ L of medium from the different wells (including 1 \times AlamarBlue-DMEM medium as a blank) were transferred into a 96-well plate and the UV optical density (OD) was measured using a plate reader (Spectrostar, BMG, Germany) at 570 nm and 630 nm, respectively. Cell viability was calculated as follows:

$$\text{Cell viability (\%)} = (\text{OD}_{\text{sample}} - \text{OD}_0) / (\text{OD}_{\text{control}} - \text{OD}_0) \times 100,$$

where $\text{OD}_{\text{sample}}$, $\text{OD}_{\text{control}}$, and OD_0 are the OD values of the medium of transfected cells, the medium of untreated cells, and 1 \times AlamarBlue-DMEM medium, respectively. The value for untreated cells was taken as 100% cell viability.

Cellular uptake of polyplexes

Skov3-luc cells were seeded into a 96-well plate (10,000 cells/well) and incubated for 24 h with the growth medium, DY-547 labeled siRNA was used to prepare polyplexes. Next, the cells were incubated with the polyplexes (final siRNA concentration was 100 nM, N/P ratio of 16) for 4 h at 37°C with or without serum. The cells were then washed twice with ice-cold PBS. To quench the fluorescence of polyplexes associated with the cell membrane, the cells were incubated with 0.4% trypan blue-containing PBS for 5 min and washed with PBS [38]. After trypsinization, the cells were collected and suspended in PBS. Cellular uptake of siRNA polyplexes was examined by a flow cytometry with a help of Canto II (BD, USA).

Confocal laser scanning microscopy studies

Skov3-luc cells were seeded into 96-well μ Clear[®] black plates (7000 cells/ well) and incubated for 24 h. Then, the medium was replaced with fresh medium with or without serum. Polyplexes with DY-547 labeled siRNA (final siRNA concentration was 100 nM) were added and the cells were subsequently incubated for another 2 or 4 h at 37 °C. Before the observation, the medium was replaced with fresh full medium containing Hoechst33342 and Wheat Germ Agglutinin-Oregon Green[®] conjugate (Molecular probes, Oregon, USA) for staining the nuclei and cell membranes, respectively (incubation at 37 °C for 5 min). After washing with PBS, the cells were fixed with 2% formaldehyde (w/v) (diluted from Pierce[™] 16% formaldehyde (w/v) with PBS). CLSM images were recorded using Yokogawa CV7000S imager (Yokogawa group, Tokyo, Japan) equipped with a 60x water immersion objective at excitation wavelength of 405, 488 and 561 nm for Hoechst33342, Oregon Green[®] 488 and DY-547, respectively.

Statistical Analysis

p Values were determined by Student's test with two-tailed distribution performed with the software GraphPad Prism 5 (GraphPad Software Inc., La Jolla, California). *p* Values <0.05 were considered as statistically significant.

| Results and Discussion

Physicochemical characteristics of polymer/siRNA polyplexes

Three cationic PVTC-based polymers were used to study their ability to condense siRNA into nano-sized polyplexes, namely one homopolymer PVTC and two block copolymers composed of PVTC and POEGMA (PP2 and PP4). The polymer chemical structures are shown in Figure 1. Compared to plasmid DNA (several kilo bp), siRNA only consists of two short annealed oligonucleotides of 20–23 bp, and thus has less electrostatic interactions with polycations. As a result, it is more difficult for cationic polymers to condense siRNA and form stable particles with this nucleic acid based drug [7,39].

The binding ability of PVTC-based polymers with siRNA was evaluated by a gel retardation assay. Figure 2 shows that all polymers exhibited good siRNA binding at N/P ratio of 4 and above, where complete siRNA retardation was observed. Studies have shown that competition between biologically polyanionic molecules (such as proteins and polysaccharides) and cationic polyplexes may occur under physiological conditions. This may cause the release of siRNA from the polyplexes and also can result in shorter circulation kinetics of the nucleic acid and lower transfection efficiency [40–42]. The strongly negatively charged polysaccharide heparin was added to the siRNA polyplexes at increasing concentrations to investigate the particle stability (Figure 2). In this case, polyplexes prepared at N/P ratio of 8 was used for this study as it was shown in Figure 2 that the polymer already could fully complex the siRNA at N/P ratio of 8, also sodium chloride (final concentration was 150 mM) was added to polyplexes to mimic physiological ionic strength during the addition of heparin. We found that siRNA

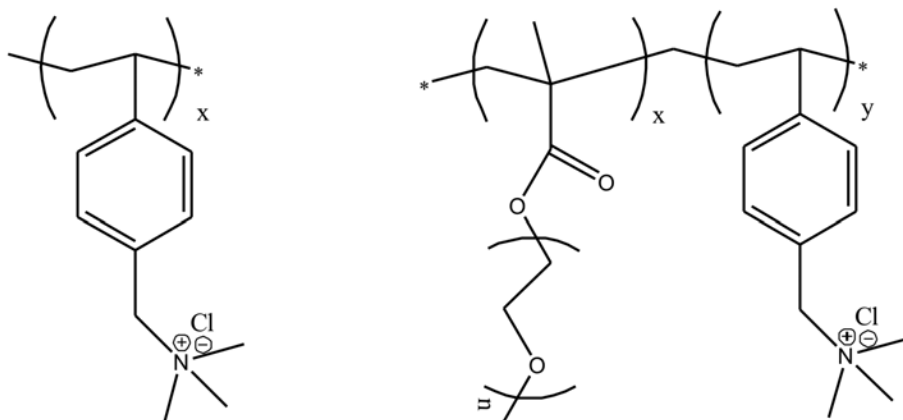


Fig. 1. Structures of poly(vinyl benzyl trimethyl ammonium chloride) (left, PVTC $x=224$) and poly[oligo(ethylene glycol) methacrylate]- b -poly(vinyl benzyl trimethyl ammonium chloride) block copolymer (right, PP2 $x=38$ and $y=24$, PP4 $x=38$ and $y=87$).

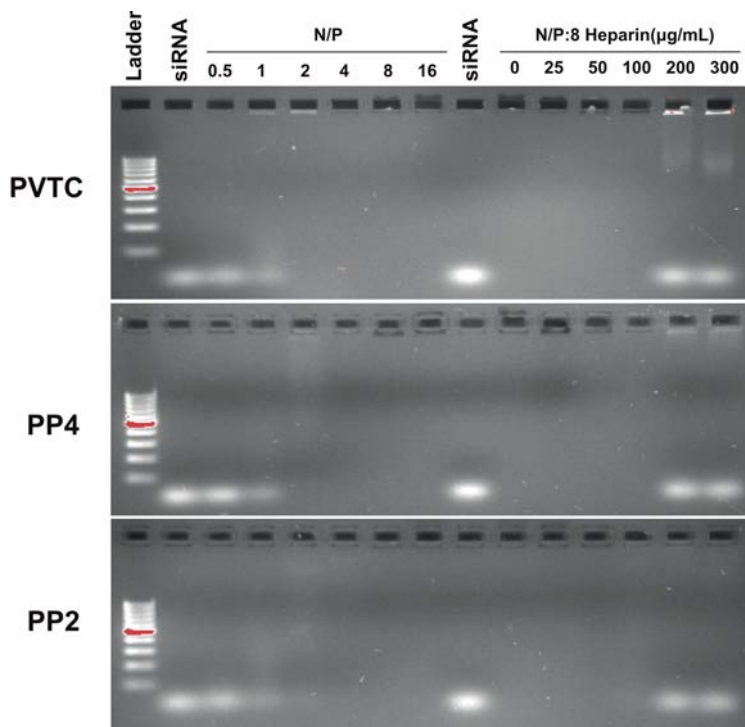


Fig. 2. Agarose gel retardation assay of the PVTC/siRNA (up), PP4/siRNA (middle) and PP2/siRNA (bottom) polyplexes at different N/P ratios. To study heparin induced polyplex destabilization, siRNA polyplexes of N/P 8 were incubated with heparin (different concentrations) for 10 mins in 10 mM HEPES buffer (pH 7.4, containing 150 mM NaCl).

polyplexes based on all three polymers at N/P ratio of 8 still complexed siRNA strongly at heparin concentration up to 100 $\mu\text{g}/\text{mL}$. At a heparin concentration of 200 $\mu\text{g}/\text{mL}$ and higher, siRNA was completely released from PP4/PP2 polyplexes, whereas only part of siRNA released from the PVTC/siRNA polyplexes. This heparin competition study demonstrates that strong electrostatic interactions occur between the quaternary amine groups of the polymers and the phosphate groups of siRNA, which is accordance with previous studies [34,37].

To further study the siRNA complexation ability of the different polymers, DLS and zeta-potential measurements were carried out with siRNA polyplexes. As shown in Table 2, all three polymers were able to bind to siRNA to yield positively charged polyplexes with an average diameter smaller than 25 nm ($\text{PDI} < 0.3$). The PVTC polymer, having the longest polycation segment, formed polyplexes with siRNA of around 20 nm, which was close to the size visualized by TEM (Figure S1). Interestingly, the PP4 and PP2 polymers with shorter polycation chains formed particles of smaller diameter, 14 nm and 9 nm, respectively. The smaller size of PP2 and PP4 polyplexes compared to PVTC polyplexes at same N/P ratio could be explained by the presence of PEG chain, similar results also have been observed in previous studies [28,43]. Such small nanosized siRNA polyplexes (10-20 nm) were also found in previous studies of polyplexes based a block copolymer of poly(ethylene glycol)-b-poly(L-lysine) (PEG-LL) [24,44–46]. siRNA polyplexes with diameter around 10 nm were considered as monomolecular assembly of oppositely charged siRNA and PLL, i.e., a particle composed of a single siRNA molecule coated with PLL-PEG via electrostatic interactions. We hypothesize that the polymers used in this study had similar assembling behavior as PEG-PLL, where each polyplex particle contained one molecule of siRNA.

With increase of N/P ratio, because of the excess of cationic amines, all three polyplexes showed slightly increase of surface charges (Figure S2). At N/P ratio of 16, the zeta potential of siRNA polyplexes prepared by homopolymer PVTC was the highest (27.6 mV), whereas the PP4 and PP2 siRNA polyplexes have lower zeta potential (19.7 and 9.2 mV, respectively) which can be attributed to the shielding effect of the neutral and hydrophilic POEGMA moieties [19,47,48].

An effective siRNA delivery system should retain its colloidal stability under physiological conditions. Therefore, we investigated the stability of the polyplexes (N/P = 16) in 140 mM NaCl/10 mM HEPES buffer (Figure S3). DLS measurements showed that the size of the three

Table 2. Size and zeta potential of siRNA polyplexes^a

Polyplexes	Size (nm) \pm S.D.	Zeta potential (mV) \pm S.D.	PDI
PVTC	19 \pm 2	27.6 \pm 1.4	0.24
PP4	14 \pm 1	19.7 \pm 2.1	0.20
PP2	9 \pm 1	9.2 \pm 3.2	0.27

^a Prepared at N/P = 16 and a siRNA concentration of 10 $\mu\text{g}/\text{mL}$ in 10 mM Hepes buffer, pH 7.4.

different polyplexes remained constant after incubation in this buffer for 24 h, which can be ascribed to electrostatic repulsion between the nanoparticles due to their relatively high zeta potential for the PVTC/siRNA polyplexes and steric stabilization of the particles due to the POEGMA blocks of the PP4/siRNA and PP2/siRNA polyplexes.

In vitro cytocompatibility and gene silencing activity of the polyplexes

The cytotoxicity of the PVTC-based polymers was assessed in the human ovarian adenocarcinoma cell line (Skov3-luc) in the absence of serum using AlamarBlue assay (Figure 3). In this experiment, L-pEI was used as control polycation. L-pEI was significantly more cytotoxic than the PVTC-based polymer at a polymer concentration of 15 $\mu\text{g/mL}$ and above. The 50% inhibitory concentration (IC_{50}) for the homopolymer was two times higher than that of PEI (Table S1). It is known that the cytotoxicity of polycations is a function resulting from the polyamine nature (i.e., primary, secondary, tertiary, and quaternary amino groups) rather than its charge density [49,50]. Previous studies have shown that although polymers with quaternary amine groups have a higher charge density, they exhibited lower toxicity compared to tertiary polyamines due to their lower cell membrane disruptive activity [32,33,51]. The IC_{50} values of PP4 and PP2 polymers were substantially higher compared to the PVTC homopolymer (92 $\mu\text{g/mL}$ vs 32 $\mu\text{g/mL}$), which may be due to the hydrophilic blocks (POEGMA) but also because of the shorter amine blocks [52]. For the cell transfection experiments we used a maximum polymer concentration of 15.6 $\mu\text{g/mL}$, which is far below their IC_{50} values.

The luciferase gene silencing (RNAi) activities of the siRNA polyplexes in Skov3-luc cells were examined as a function of the N/P ratio and siRNA concentration both in the absence

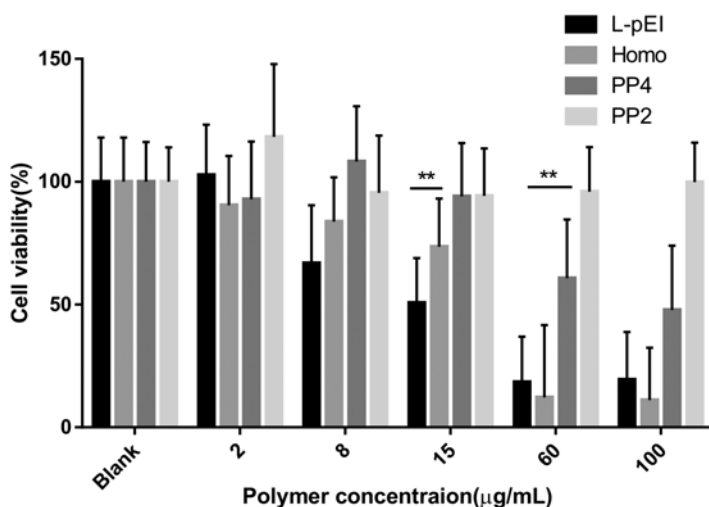


Fig. 3. Viability of Skov3-luc cells after incubation with polymers or L-pEI in serum free medium for 4 hours at 37°C. All values are given as the mean \pm SD (n=3). Representative results from one of the three experiments are shown. **p < 0.01.

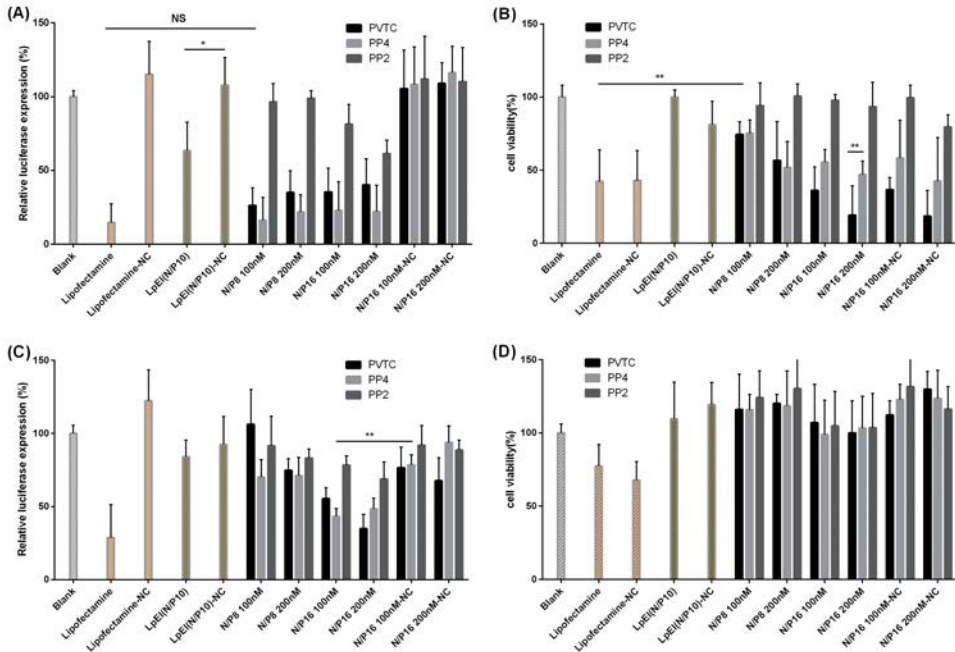


Fig. 4. Luciferase gene expression after incubation of Skov3-luc cells with siRNA polyplexes in the absence (A) or presence (C) of serum. Cell viability was measured by AlamarBlue assay after incubation of Skov3-luc cells with siRNA complexes in the absence (B) or presence (D) of serum. siRNA concentration was 100 or 200 nM. NC: Negative control siRNA. Representative results from one of the three experiments are shown. All values are given as the mean \pm SD (n=3). *p<0.05, **p < 0.01, ***p<0.001.

(Figure 4A) and presence of serum (Figure 4C). At N/P 8 and siRNA concentration of 100 nM, PVTC and PP4 polyplexes showed a knock down of around 80% of luciferase expression, which was comparable to the efficiency of the lipofectamine formulation and significantly higher than that of the L-PEI/siRNA polyplexes (~ 35%), as shown in Figure 4A. On the other hand, PP2/siRNA showed negligible gene silencing activity at N/P ratio of 8. Incubation of the cells with the three polyplexes prepared at N/P ratio of 16 resulted in similar gene silencing effects as observed for polyplexes of N/P of 8. Additionally, increasing the polyplexes dose to 200 nM siRNA did not increase the knock down efficiency. However, increasing the N/P ratio to 16 and the dose of the polyplexes to 200 nM siRNA, led to a drop in cell viability, which can be explained by the higher concentrations of polymer to which the cells were exposed (Figure 4B). It should be noted that at N/P of 8 the cytotoxicity of polyplexes was mild (~ 80% cell viability), being even lower than that of the lipofectamine formulation (~ 45% cell viability). The higher cell viability of PEGylated PP4/PP2 polymers compared to PVTC at higher N/P ratio and siRNA dose demonstrates that the POEGMA corona could effectively reduce the cytotoxicity by shielding the surface charge of polyplexes. Moreover, comparison of the silencing effects between anti-luciferase siRNA and negative control siRNA polyplexes (N/P 16, Figure 4A)

supports the fact that the reduced luminescence observed for the polyplex formulations was due to the specific inhibition of luciferase expression and not because of their cytotoxicity.

The transfection activity of the polyplexes was also investigated in medium with serum (Figure 4C). Figure 4C shows that at N/P 8 and a siRNA dose of 200 nM, the luciferase knock down efficiency was substantially decreased to 20-30%. At N/P 16 and siRNA dose of 200 nM the PVTC and PP4 based polyplexes led to about 60 and 50% gene silencing, respectively, which was slightly lower than in the absence of serum (70% and 75 % respectively). The reduction in transfection activity of the polyplexes in the presence of serum might be explained by the adsorption of negatively charged serum proteins onto the polyplexes surface resulting in polyplexes destabilization and/or reduced cellular uptake due to the polyplexes charge reversal [53,54]. The cell viability was maintained close to 100% for all polyplex formulations, and the cytotoxicity of lipofectamine formulation was reduced as compared to the serum-free conditions (Figure 4D).

Cellular uptake of siRNA polyplexes studied by flow cytometry and CLSM

The cellular uptake of DY-547 labeled siRNA polyplexes by Skov-3-luc cells was studied using flow cytometry and confocal laser scanning microscopy (CLSM). Figure 5 presents the percentage of DY-547 positive cells as well as mean fluorescence intensity (MFI) of the cell population upon incubation with different formulations in the absence or presence of serum. As shown in Figure 5A&B, the polyplexes based on PP4 and PP2 showed lower cellular uptake compared to PVTC/siRNA polyplexes, presumably due to the lower zeta potential as a result of the POEGMA corona. Moreover, the PP4, PVTC and lipofectamine formulations showed much higher cell uptake than the polyplexes based on L-pEI and PP2. Additionally, a higher cellular uptake was observed when the cells were incubated with PVTC and PP4 based polyplexes in the presence of serum (Figure 5D), which might be caused by the positive charge of the PVTC/siRNA (27.6 mV) and PP4/siRNA polyplexes (19.7 mV). For positively charged particles the presence of serum in the incubation medium has shown to increase their cellular uptake [38,55,56]. In contrast, the cellular uptake level of DY547-siRNA for PP2 and L-pEI polyplexes was negligible in the presence of serum, most likely due to the low stability of the complexes (Figure 5A&B). Therefore, the high gene silencing activities of the PVTC/siRNA and PP4/siRNA complexes can be ascribed to their high cellular uptake.

Examination of polyplexes uptake by Skov-3-luc cells with confocal laser scanning microscopy confirmed the flow cytometric analysis (Figure 6). As expected, PP2/siRNA complexes showed the lowest degree of cell internalization. The PP4/siRNA polyplexes displayed time-dependent uptake in both serum-free and serum-containing media. Moreover, the serum proteins had an obvious influence on the uptake profile of PP4/siRNA as the subcellular localization of labelled siRNA significantly differed for the studied conditions (with or without serum). The more diffused cytosolic signal from the cells incubated with the polyplexes in presence of serum might indicate higher degree of siRNA release from the polyplexes after cellular internalization. Interestingly, the uptake profile of PVTC/siRNA polyplexes was also highly

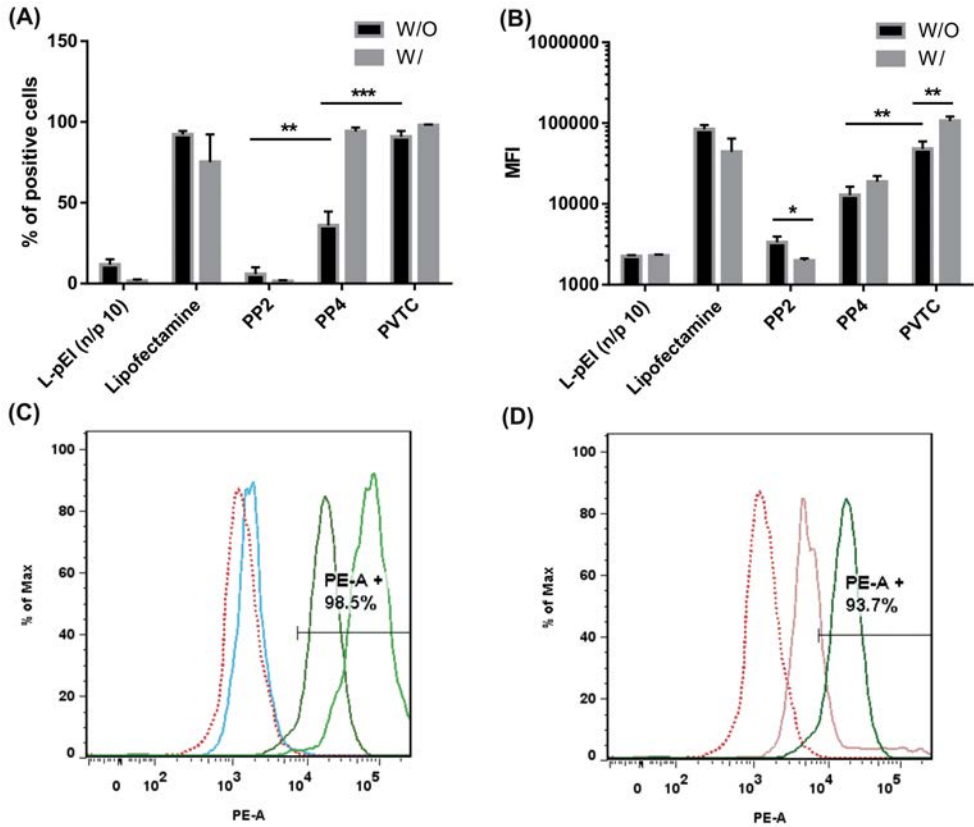


Fig. 5. Cellular uptake of DY-547 labeled siRNA polyplexes (N/P=16) by Skov3-luc cells in the absence (W/O) or presence (W/) of serum; L-pEI 25kDa and lipofectamine based formulations were used as controls. (A) Percentage of the DY-547 positive cells. (B) Mean fluorescence intensity of the cell population. Data represent the means \pm SD (n = 3). * $p < 0.05$, ** $p < 0.01$, *** $p < 0.001$. (C) Fluorescence histogram of Skov3-luc cells incubated with the different polyplexes in the presence of serum: untreated cells (red dots), PP2/siRNA (blue), PP4/siRNA (dark-green) and PVTC/siRNA (green). (D) Fluorescence histogram of Skov3-luc cells with PP4/siRNA polyplexes in the absence (pink) or presence (dark green) of serum; untreated cells were used as a blank (red dots).

affected by the presence of serum. In serum-free medium PVTC/siRNA polyplexes displayed a more diffusive cytosolic signal in contrast to round micrometer-sized vesicles localized in the perinuclear space observed for cells in a serum-containing medium.

Taken together, the PVTC-based polymers are capable of silencing luciferase expression both in the absence and presence of serum. The PP4 polymer is the most promising candidate since it formed small polyplexes (~ 14 nm) and displayed lower cytotoxicity with good gene silencing knock down efficiency in the presence of serum (Figure 4). It has been demonstrated in many studies that the particle size plays an important role for the cellular uptake and subsequent trafficking of polyplexes [57–60]. For siRNA or DNA delivery systems, endosomal escape is

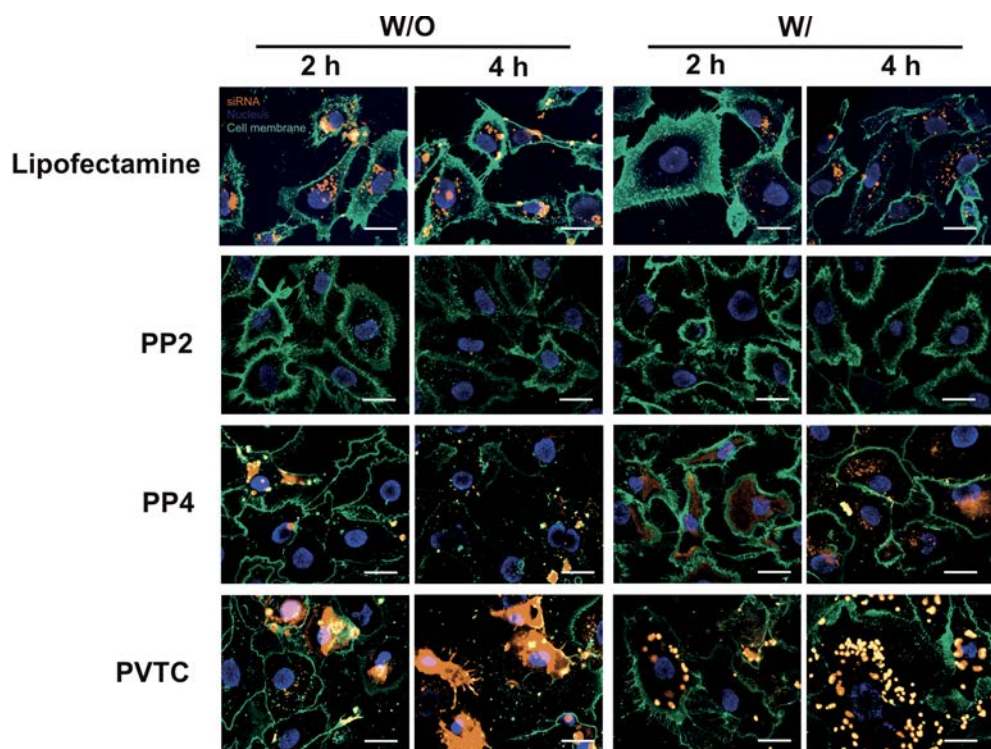


Fig. 6. Confocal microscopy images of Skov-3-luc cells after 4 h incubation with different polyplexes in the absence (Left, W/O) and presence (Right, W/) of serum. All images are overlays of the fluorescent signals from DY547-siRNA (orange), cell membrane Wheat Germ Agglutinin-Alexa Fluor® 488 (green), and cell nucleus Hoechst33342 (blue). Bars indicate 20 μm .

considered to be a major bottleneck in the transfection process. Generally, siRNA polyplexes with a size of 80–200 nm are internalized by clathrin-mediated endocytosis, and those particles would accumulate in the late endosomes associated with oligonucleotide degradation [1,14]. Recent studies have shown that small-sized particles (< 50 nm) are preferentially internalized by caveolin-mediated endocytosis to end up in 50 nm sized caveolae, this pathway is known to avoid vesicle fusion with lysosomes and subsequent siRNA degradation [60–62]. The PVTC-based polymers in this study complexed siRNA to particles with sizes less than 25 nm (Table 2). Therefore, we expect that these particles are internalized by cells through caveolin-mediated endocytosis, avoiding endolysosomal uptake pathways which might explain why PVTC-based polyplexes possessed such high gene silencing efficiencies. Nevertheless, a detailed investigation to prove this assumption will be a subject of future studies.

| Conclusions

In this study, we evaluated a series of PVTC-based polymers that are capable of delivering intact siRNA intracellularly resulting in gene silencing. The quaternary amine groups of PVTC

enable the polymer to form colloidally stable, small nano-sized particles (< 25 nm) with siRNA. Polyplexes based on PP4 block copolymer with a hydrophilic and uncharged POEGMA moiety exhibit excellent gene silencing efficiency without compromising the cell viability both in the presence and the absence of serum proteins. The results presented in this paper demonstrate that the PP4/siRNA polyplexes formulations are attractive candidates for siRNA therapy by means of I.V. administration, as they are large enough to escape rapid renal clearance (~10 nm cutoff) but small enough to penetrate into the tissues, e.g. solid tumors.

| Acknowledgments

The research was partially supported by China Scholarship Council.

References

1. K. a Whitehead, R. Langer, D.G. Anderson, Knocking down barriers: advances in siRNA delivery., *Nat. Rev. Drug Discov.* 8 (2009) 129–138.
2. R. Kole, A.R. Krainer, S. Altman, RNA therapeutics: Beyond RNA interference and antisense oligonucleotides, *Nat. Rev. Drug Discov.* 11 (2012) 125–140.
3. R.W. Carthew, E.J. Sontheimer, Origins and Mechanisms of miRNAs and siRNAs, *Cell.* 136 (2009) 642–655.
4. W. Zauner, M. Ogris, E. Wagner, Polylysine-based transfection systems utilizing receptor-mediated delivery, *Adv. Drug Deliv. Rev.* 30 (1998) 97–113.
5. Y. Oe, R.J. Christie, M. Naito, S.A. Low, S. Fukushima, K. Toh, Y. Miura, Y. Matsumoto, N. Nishiyama, K. Miyata, K. Kataoka, Actively-targeted polyion complex micelles stabilized by cholesterol and disulfide cross-linking for systemic delivery of siRNA to solid tumors, *Biomaterials.* 35 (2014) 7887–7895.
6. O. Boussif, F. Lezoualc'h, M.A. Zanta, M.D. Mergny, D. Scherman, B. Demeneix, J.P. Behr, A versatile vector for gene and oligonucleotide transfer into cells in culture and in vivo: polyethylenimine., *Proc. Natl. Acad. Sci. U. S. A.* 92 (1995) 7297–301.
7. S. Liu, W. Huang, M.J. Jin, B. Fan, G.M. Xia, Z.G. Gao, Inhibition of murine breast cancer growth and metastasis by survivin-targeted siRNA using disulfide cross-linked linear PEI, *Eur. J. Pharm. Sci.* 82 (2016) 171–182.
8. J.Y. Cherng, P. van de Wetering, H. Talsma, D.J. Crommelin, W.E. Hennink, Effect of size and serum proteins on transfection efficiency of poly ((2-dimethylamino)ethyl methacrylate)-plasmid nanoparticles., *Pharm. Res.* 13 (1996) 1038–42.
9. P. Van De Wetering, E.E. Moret, N.M.E. Schuurmans-nieuwenbroek, M.J. Van Steenbergen, W.E. Hennink, Structure-Activity Relationships of Water-Soluble Cationic Methacrylate / Methacrylamide Polymers for Nonviral Gene Delivery, *Bioconjug. Chem.* 10 (1999) 589–597.
10. C. Lin, C.-J. Blaauboer, M.M. Timoneda, M.C. Lok, M. van Steenbergen, W.E. Hennink, Z. Zhong, J. Feijen, J.F.J. Engbersen, Bioreducible poly(amido amine)s with oligoamine side chains: synthesis, characterization, and structural effects on gene delivery., *J. Control. Release.* 126 (2008) 166–174.
11. M.E. Davis, J.E. Zuckerman, C.H.J. Choi, D. Seligson, A. Tolcher, C.A. Alabi, Y. Yen, J.D. Heidel, A. Ribas, Evidence of RNAi in humans from systemically administered siRNA via targeted nanoparticles, *Nature.* 464 (2010) 1067–1070.
12. V.R. Sinha, R. Kumria, Polysaccharides in colon-specific drug delivery, *Int. J. Pharm.* 224 (2001) 19–38.
13. S.Y. Wong, J.M. Pelet, D. Putnam, Polymer systems for gene delivery-Past, present, and future, *Prog. Polym. Sci.* 32 (2007) 799–837.
14. U. Lachelt, E. Wagner, *Nucleic Acid Therapeutics Using Polyplexes: A Journey of 50 Years (and Beyond)*, *Chem. Rev.* 115 (2015) 11043–11078.
15. J. Chen, Z. Guo, H. Tian, X. Chen, Production and clinical development of nanoparticles for gene delivery., *Mol. Ther. Methods Clin. Dev.* 3 (2016) 16023.
16. P.R. Dash, M.L. Read, L.B. Barrett, M.A. Wolfert, L.W. Seymour, Factors affecting blood clearance and in vivo distribution of polyelectrolyte complexes for gene delivery, *Gene Ther.* 6 (1999) 643–650.
17. C. Arigita, N.J. Zuidam, D.J.A. Crommelin, W.E. Hennink, Association and dissociation characteristics of polymer/DNA complexes used for gene delivery, *Pharm. Res.* 16 (1999) 1534–1541.
18. M. Ogris, S. Brunner, S. Schüller, R. Kircheis, E. Wagner, PEGylated DNA/transferrin-PEI complexes: reduced interaction with blood components, extended circulation in blood

- and potential for systemic gene delivery, *Gene Ther.* 6 (1999) 595–605.
19. B. Zoetebier, A. Sohrabi, B. Lou, M.A. Hempenius, W.E. Hennink, G.J. Vancso, PEG stabilized DNA – poly(ferrocenylsilane) polyplexes for gene delivery, *Chem. Commun.* 52 (2016) 7707–7710.
 20. J.S. Suk, Q. Xu, N. Kim, J. Hanes, L.M. Ensign, PEGylation as a strategy for improving nanoparticle-based drug and gene delivery, *Adv. Drug Deliv. Rev.* 99 (2016) 28–51.
 21. R. Kircheis, T. Blessing, S. Brunner, L. Wightman, E. Wagner, Tumor targeting with surface-shielded ligand-polycation DNA complexes, *J. Control. Release.* 72 (2001) 165–170.
 22. H.J. Kim, T. Ishii, M. Zheng, S. Watanabe, K. Toh, Y. Matsumoto, N. Nishiyama, K. Miyata, K. Kataoka, Multifunctional polyion complex micelle featuring enhanced stability, targetability, and endosome escapability for systemic siRNA delivery to subcutaneous model of lung cancer, *Drug Deliv. Transl. Res.* 4 (2014) 50–60.
 23. A. Malek, O. Merkel, L. Fink, F. Czubayko, T. Kissel, A. Aigner, In vivo pharmacokinetics, tissue distribution and underlying mechanisms of various PEI(-PEG)/siRNA complexes, *Toxicol. Appl. Pharmacol.* 236 (2009) 97–108.
 24. R.J. Christie, Y. Matsumoto, K. Miyata, T. Nomoto, S. Fukushima, K. Osada, J. Halnaut, F. Pittella, H.J. Kim, N. Nishiyama, K. Kataoka, Targeted polymeric micelles for siRNA treatment of experimental cancer by intravenous injection, *ACS Nano.* 6 (2012) 5174–5189.
 25. H.K. de Wolf, C.J. Snel, F.J. Verbaan, R.M. Schiffelers, W.E. Hennink, G. Storm, Effect of cationic carriers on the pharmacokinetics and tumor localization of nucleic acids after intravenous administration, *Int. J. Pharm.* 331 (2007) 167–175.
 26. L. Novo, K.M. Takeda, T. Petteta, G.R. Dakwar, J.B. Van Den Dikkenberg, K. Remaut, K. Braeckmans, C.F. Van Nostrum, E. Mastrobattista, W.E. Hennink, Targeted decationized polyplexes for siRNA delivery, *Mol. Pharm.* 12 (2015) 150–161.
 27. C. Lin, Z. Zhong, M.C. Lok, X. Jiang, W.E. Hennink, J. Feijen, J.F.J. Engbersen, Linear poly(amido amine)s with secondary and tertiary amino groups and variable amounts of disulfide linkages: synthesis and in vitro gene transfer properties., *J. Control. Release.* 116 (2006) 130–137.
 28. H.J. Kim, M. Oba, F. Pittella, T. Nomoto, H. Cabral, Y. Matsumoto, K. Miyata, N. Nishiyama, K. Kataoka, PEG-detachable cationic polyaspartamide derivatives bearing stearoyl moieties for systemic siRNA delivery toward subcutaneous BxPC3 pancreatic tumor, *J. Drug Target.* 20 (2012) 33–42.
 29. C.E. Nelson, J.R. Kintzing, A. Hanna, J.M. Shannon, M.K. Gupta, C.L. Duvall, Balancing cationic and hydrophobic content of PEGylated siRNA polyplexes enhances endosome escape, stability, blood circulation time, and bioactivity in vivo, *ACS Nano.* 7 (2013) 8870–8880.
 30. E. Amar-Lewis, A. Azagury, R. Chintakunta, R. Goldbart, T. Traitel, J. Prestwood, D. Landesman-Milo, D. Peer, J. Kost, Quaternized starch-based carrier for siRNA delivery: From cellular uptake to gene silencing, *J. Control. Release.* 185 (2014) 109–120.
 31. S.A. Engelberth, N. Hempel, M. Bergkvist, Chemically Modified Dendritic Starch: A Novel Nanomaterial for siRNA Delivery, *Bioconjug. Chem.* 26 (2015) 1766–1774.
 32. A. Tamura, M. Oishi, Y. Nagasaki, Efficient siRNA delivery based on PEGylated and partially quaternized polyamine nanogels: Enhanced gene silencing activity by the cooperative effect of tertiary and quaternary amino groups in the core, *J. Control. Release.* 146 (2010) 378–387.
 33. M.L. Patil, M. Zhang, S. Betigeri, O. Taratula, H. He, T. Minko, Surface-modified and internally cationic polyamidoamine dendrimers for efficient siRNA delivery, *Bioconjug. Chem.* 19 (2008) 1396–1403.

34. F. Delisavva, G. Mountrichas, S. Pispas, Quaternized Poly[3,5-bis(dimethylaminomethylene)hydroxystyrene]/DNA Complexes: Structure Formation as a Function of Solution Ionic Strength, *J. Phys. Chem. B.* 117 (2013) 7790–7796.
35. E. Haladjova, G. Mountrichas, S. Pispas, S. Rangelov, Poly(vinyl benzyl trimethylammonium chloride) Homo and Block Copolymers Complexation with DNA, *J. Phys. Chem. B.* 120 (2016) 2586–2595.
36. Lutz Nuhn, Size-Dependent Knockdown Potential of siRNA- Loaded Cationic Nanohydrogel Particles, *Biomacromolecules.* 0033 (2014) 4111–4121.
37. A.K. Varkouhi, G. Mountrichas, R.M. Schiffelers, T. Lammers, G. Storm, S. Pispas, W.E. Hennink, Polyplexes based on cationic polymers with strong nucleic acid binding properties, *Eur. J. Pharm. Sci.* 45 (2012) 459–466.
38. R.J. Naik, P. Chandra, A. Mann, M. Ganguli, Exogenous and cell surface glycosaminoglycans alter DNA delivery efficiency of arginine and lysine homopeptides in distinctly different ways, *J. Biol. Chem.* 286 (2011) 18982–18993.
39. C. Scholz, E. Wagner, Therapeutic plasmid DNA versus siRNA delivery: Common and different tasks for synthetic carriers, *J. Control. Release.* 161 (2012) 554–565.
40. A. Sato, S.W. Choi, M. Hirai, A. Yamayoshi, R. Moriyama, T. Yamano, M. Takagi, A. Kano, A. Shimamoto, A. Maruyama, Polymer brush-stabilized polyplex for a siRNA carrier with long circulatory half-life, *J. Control. Release.* 122 (2007) 209–216.
41. G.R. Dakwar, E. Zagato, J. Delanghe, S. Hobel, A. Aigner, H. Denys, K. Braeckmans, W. Ceelen, S.C. De Smedt, K. Remaut, Colloidal stability of nano-sized particles in the peritoneal fluid: Towards optimizing drug delivery systems for intraperitoneal therapy, *Acta Biomater.* 10 (2014) 2965–2975.
42. S. Mao, M. Neu, O. Germershaus, O. Merkel, J. Sitterberg, U. Bakowsky, T. Kissel, Influence of polyethylene glycol chain length on the physicochemical and biological properties of poly(ethylene imine)-graft-poly(ethylene glycol) block copolymer/SiRNA polyplexes, *Bioconjug. Chem.* 17 (2006) 1209–1218.
43. S. Lin, F. Du, Y. Wang, S. Ji, D. Liang, L. Yu, Z. Li, An Acid-Labile Block Copolymer of PDMAEMA and PEG as Potential Carrier for Intelligent Gene Delivery Systems An Acid-Labile Block Copolymer of PDMAEMA and PEG as Potential Carrier for Intelligent Gene Delivery Systems, (2008) 109–115.
44. K. Hayashi, H. Chaya, S. Fukushima, S. Watanabe, H. Takemoto, K. Osada, N. Nishiyama, K. Miyata, K. Kataoka, Influence of RNA Strand Rigidity on Polyion Complex Formation with Block Cationomers, *Macromol. Rapid Commun.* 37 (2016) 486–493.
45. S. Florinas, M. Liu, R. Fleming, L. Van Vlerken-Ysla, J. Ayriess, R. Gilbreth, N. Dimasi, C. Gao, H. Wu, Z.-Q. Xu, S. Chen, A. Dirisala, K. Kataoka, H. Cabral, R.J. Christie, A Nanoparticle Platform To Evaluate Bioconjugation and Receptor-Mediated Cell Uptake Using Cross-Linked Polyion Complex Micelles Bearing Antibody Fragments, *Biomacromolecules.* 17 (2016) 1818–1833.
46. J. Derouchey, C. Schmidt, G.F. Walker, C. Koch, C. Plank, E. Wagner, J.O. Rädler, Monomolecular Assembly of siRNA and Poly(ethylene glycol)-Peptide Copolymers, *Biomacromolecules.* 9 (2008) 724–732.
47. F.J. Verbaan, C. Oussoren, C.J. Snel, D.J. a Crommelin, W.E. Hennink, G. Storm, Steric stabilization of poly(2-(dimethylamino)ethyl methacrylate)-based polyplexes mediates prolonged circulation and tumor targeting in mice., *J. Gene Med.* 6 (2004) 64–75.
48. S. Uezguen, O. Akdemir, G. Hasenpusch, C. Maucksch, M.M. Golas, B. Sander, H. Stark, R. Imker, J.-F. Lutz, C. Rudolph, Characterization of Tailor-Made Copolymers of Oligo(ethylene glycol) Methyl Ether Methacrylate and N,N-Dimethylaminoethyl Methacrylate as Nonviral Gene Transfer Agents: Influence of Macromolecular Structure on Gene

- Vector Particle Properties and Transfect, *Biomacromolecules*. 11 (2010) 39–50.
49. D. Fischer, Y. Li, B. Ahlemeyer, J. Krieglstein, T. Kissel, In vitro cytotoxicity testing of polycations: influence of polymer structure on cell viability and hemolysis, *Biomaterials*. 24 (2003) 1121–31.
 50. K. Kim, W.C.W. Chen, Y. Heo, Y. Wang, Polycations and their biomedical applications, *Prog. Polym. Sci.* 60 (2016) 18–50.
 51. J.H. Lee, Y.B. Lim, J.S. Choi, Y. Lee, T. Il Kim, H.J. Kim, J.K. Yoon, K. Kim, J.S. Park, Polyplexes Assembled with Internally Quaternized PAMAM-OH Dendrimer and Plasmid DNA Have a Neutral Surface and Gene Delivery Potency, *Bioconjug. Chem.* 14 (2003) 1214–1221.
 52. D. Fischer, T. Bieber, Y.X. Li, H.P. Elsasser, T. Kissel, A novel non-viral vector for DNA delivery based on low molecular weight, branched polyethylenimine: Effect of molecular weight on transfection efficiency and cytotoxicity, *Pharm. Res.* 16 (1999) 1273–1279.
 53. M.A. Gosselin, W. Guo, R.J. Lee, Efficient Gene Transfer Using Reversibly Cross-Linked Low Molecular Weight Polyethylenimine, *Bioconjug. Chem.* 12 (2001) 989–994.
 54. H.K. De Wolf, J. Luten, C.J. Snel, C. Oussoren, W.E. Hennink, G. Storm, In vivo tumor transfection mediated by polyplexes based on biodegradable poly(DMAEA)-phosphazene, *J. Control. Release*. 109 (2005) 275–287.
 55. G.R. Dakwar, K. Braeckmans, J. Demeester, W. Ceelen, S.C. De Smedt, K. Remaut, Disregarded Effect of Biological Fluids in siRNA Delivery: Human Ascites Fluid Severely Restricts Cellular Uptake of Nanoparticles, *ACS Appl. Mater. Interfaces*. 7 (2015) 24322–24329.
 56. Q. Yin, Y. Gao, Z. Zhang, P. Zhang, Y. Li, Bioreducible poly (β -amino esters)/shRNA complex nanoparticles for efficient RNA delivery, *J. Control. Release*. 151 (2011) 35–44.
 57. A. Albanese, P.S. Tang, W.C.W. Chan, The Effect of Nanoparticle Size, Shape, and Surface Chemistry on Biological Systems, *Annu. Rev. Biomed. Eng.* 14 (2012) 1–16.
 58. H. Cabral, Y. Matsumoto, K. Mizuno, Q. Chen, M. Murakami, M. Kimura, Y. Terada, M.R. Kano, K. Miyazono, M. Uesaka, N. Nishiyama, K. Kataoka, Accumulation of sub-100 nm polymeric micelles in poorly permeable tumours depends on size, *Nat. Nanotechnol.* 6 (2011) 815–823.
 59. W. Jiang, B.Y.S. Kim, J.T. Rutka, W.C.W. Chan, Nanoparticle-mediated cellular response is size-dependent, *Nat. Nanotechnol.* 3 (2008) 145–50.
 60. L. Nuhn, S. Tomcin, K. Miyata, V. Mailänder, K. Landfester, K. Kataoka, R. Zentel, Size-dependent knockdown potential of siRNA-loaded cationic nanohydrogel particles, *Biomacromolecules*. 15 (2014) 4111–4121.
 61. J. Harris, D. Werling, M. Koss, P. Monaghan, G. Taylor, C.J. Howard, Expression of caveolin by bovine lymphocytes and antigen-presenting cells, *Immunology*. 105 (2002) 190–195.
 62. G. Sahay, D.Y. Alakhova, A. V. Kabanov, Endocytosis of nanomedicines, *J. Control. Release*. 145 (2010) 182–195.

| Supplementary information

2

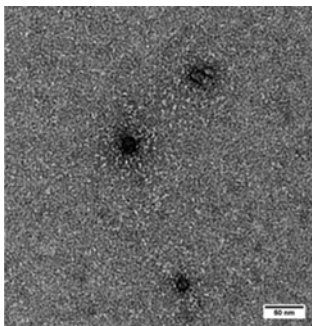


Fig. S1. TEM images of PVTC/siRNA polyplexes prepared at N/P = 16. Bar indicated 50 nm.

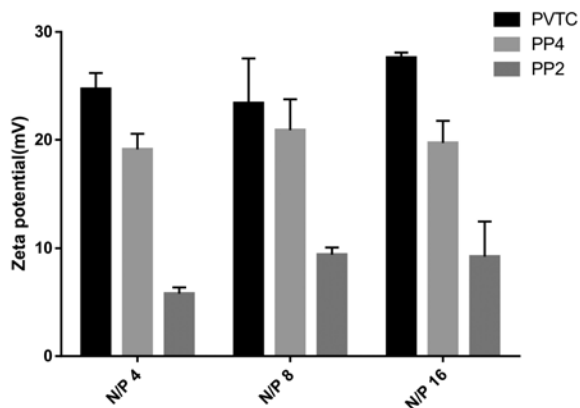


Fig. S2. Zeta potential of polymer/siRNA polyplexes as a function of the N/P (mol/mol ratio) as measured by DLS with a siRNA concentration of 10 $\mu\text{g}/\text{mL}$ in 10 mM HEPES buffer, pH 7.4.

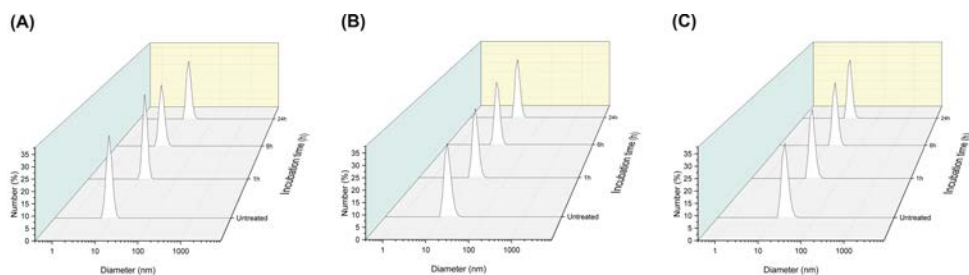


Fig. S3. Number-based DLS histograms of polyplexes at N/P of 16, PP2/siRNA (A), PP4/siRNA(B), PVTC/siRNA(C).

Table S1. IC₅₀ of the polymers incubated with Skov-3_luc cells in the absence of serum

Polymer	IC ₅₀ ^a (µg/mL)	IC ₅₀ based on cationic part (µg/mL)
L-pEI	15	15
PVTC	32	32
PP4	92	42
PP2	n.d.	n.d.

^aIC₅₀ is defined as the polymer concentration with 50% cell survival. n.d. means not detected.

CHAPTER

3

RGD-decorated cholesterol stabilized polyplexes for targeted siRNA delivery to Glioblastoma cells

Bo Lou^{1*}, Kate Connor^{2*}, Kieron Sweeney^{2,3}, Ian Miller²,
Alice O'Farrell², Eduardo Ruiz-Hernandez⁴, David Murray²,
Garry P. Duffy⁵, Alan Wolf⁶, Enrico Mastrobattista¹,
Wim E. Hennink¹ and Annette T. Byrne^{2**}

¹Department of Pharmaceutical Sciences, Utrecht Institute for
Pharmaceutical Sciences, Utrecht University,
Universiteitsweg 99, 3584 CG, Utrecht, The Netherlands

²Department of Physiology and Medical Physics, Royal College of Surgeons
in Ireland, York Street, Dublin 2

³Department of Neurosurgery, Beaumont hospital, Dublin

⁴School of Pharmacy and Pharmaceutical Sciences, Trinity College Dublin

⁵Anatomy, School of Medicine, College of Medicine Nursing and Health
Sciences, National University of Ireland, Galway, Ireland

⁶UCD School of *Veterinary* Medicine, Belfield, Dublin, Ireland

*Equal Contribution

**Corresponding author

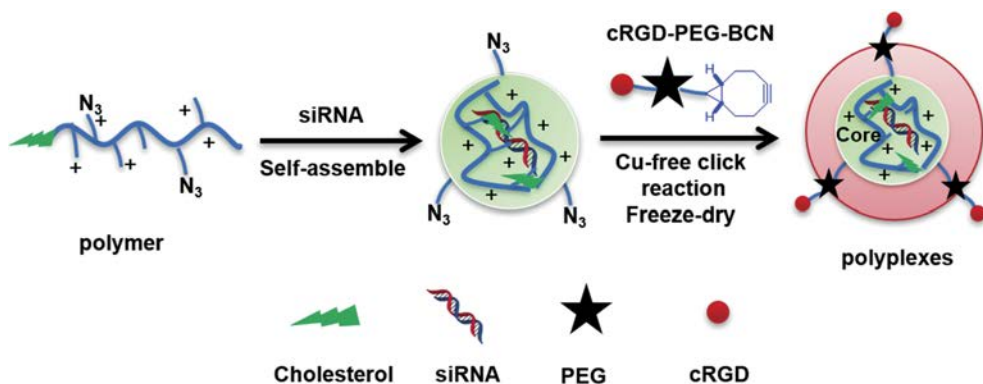
Submitted for publication

| Abstract

The development of an effective and safe treatment for glioblastoma (GBM) represents a significant challenge in oncology today. Down-regulation of key mediators of cell signal transduction by RNA interference is considered a promising treatment strategy but requires efficient, intracellular delivery of siRNA into GBM tumor cells. Here we describe novel polymeric siRNA nanocarriers functionalized with cRGD peptide that mediate targeted and efficient reporter gene silencing in U87R invasive human GBM cells. The polymer was synthesized *via* RAFT copolymerization of N-(2-hydroxypropyl)-methacrylamide (HPMA) and N-acryloxysuccinimide (NAS), followed by post-polymerization modification with cholesterol for stabilization, cationic amines for siRNA complexation and azides for copper-free click chemistry. The novel resultant cationic polymer harboring a terminal cholesterol group, self-assembled with siRNA to yield nanosized polyplexes (~ 40 nm) with good colloidal stability at physiological ionic strength. Post-modification of the preformed polyplexes with PEG-cRGD end-functionalized with bicyclo[6.1.0]nonyne (BCN) group resulted in enhanced cell uptake and increased luciferase gene silencing in U87R cells, compared to polyplexes lacking RGD targeting groups. Toxicity studies in C57BL/6 mice showed that the PEG-cRGD polyplex system is well-tolerated *in vivo* when delivered either locally or parenterally.

3

Graphical abstract



| Introduction

GBM is the most common malignant brain tumor in adults and is an incurable disease characterized by rapid tumour growth, neovascularization and aggressive invasion throughout the brain [1]. The standard of care (SOC) for GBM is maximal safe surgical resection followed by radiation therapy with concomitant and adjuvant Temozolamide (TMZ) delivered via the established “Stupp protocol” [2]. Notwithstanding, patients diagnosed with GBM have a devastatingly low median life expectancy of less than 2 years, with SOC treatment remaining largely palliative. There is therefore an urgent need for new therapeutic modalities.

RNA interference (RNAi) is an established therapeutic approach based on the delivery of small interfering RNAs (siRNAs) into target cells to induce sequence-specific gene silencing. While RNAi has significant potential as a therapeutic strategy in oncology [3,4] the therapeutic utility of ‘unpackaged’ siRNAs is limited due to their intrinsic instability and poor delivery into target tissues. Moreover, delivery in the setting of GBM is further limited by the poor penetration of drugs into the tumor due to the presence of the blood brain and blood tumour barriers. Targeting of integrins has been demonstrated to be a rational approach to circumvent these delivery and penetration issues. These proteins are key mediators in GBM cell growth, invasion and angiogenesis with $\alpha_v\beta_3$ and $\alpha_v\beta_5$ integrin family receptors further overexpressed on the endothelial cells of tumor vessels. Arg-Gly-Asp motifs (RDG) binds to these integrins and thus allows selective targeting. To date, several studies have demonstrated the utility of an RGD based targeting strategy in the GBM setting [5].

To effectively implement RNAi as a strategy in the treatment of GBM, an effective biodegradable delivery system is essential. To this end, a number of cationic polymers have been employed for siRNA delivery, including poly(ethylene imine), [6] poly(L-Lysine), [7] poly(amino amine)s [8], and N-(2-hydroxypropyl)-methacrylamide (HPMA)-based cationic polymers [9–11]. Moreover, Poly(N-(2-hydroxypropyl)-methacrylamide) (pHPMA) has been approved for clinical use following demonstration of a favourable safety profile [12,13]. A pHPMA derivative- p(HPMA-DMAE) has further been studied for gene delivery in ovarian cancers having the advantage of intrinsic degradable properties [14] and low cytotoxicity [15]. However, an inherent problem with positively-charged siRNA polyplexes is the tendency to aggregate or dissociate upon interaction with serum proteins, leading to premature siRNA release *in vitro* [16–18]. Currently, PEGylation of gene delivery carriers is the typical approach to improve stability and pharmacokinetic profiles [19]. The most common strategy involves the direct introduction of PEG into the synthetic polymer chains as diblock or graft copolymer. However, the presence of PEG during complexation directly influences the nucleic acid complexation and condensation capacity as well as size and morphology of formed nanoparticles, due to the anti-compaction force from PEG steric repulsion [20–22]. One alternative strategy involves post-PEGylation of the desired polyplexes, with several studies showing that this method can increase stability *in vivo* [23,24]. However, the presence of a PEG corona covering the surface of polyplexes also has drawbacks; it inhibits cellular uptake and endosomal escape of the siRNA complexes, potentially leading to a substantial decrease in the gene silencing efficiency [25].

One method to resolve this (PEG) dilemma is the linking of PEG to the siRNA complexes *via* disulfide bonds, enabling PEG detachment from the siRNA complex in response to changes in environmental redox potential [26,27]. To further increase the stability of PEGylated siRNA polyplexes, additional sophisticated approaches have been explored including disulfide crosslinking [28], quaternary amines [29,30] and hydrophobic interactions [20,27,31]. In particular, hydrophobic moieties, eg cholesterol, can assist the spontaneous assembly of polyplexes through hydrophobic interactions in aqueous solutions, rendering polyplexes more resistant to dissociation, eventually leading to a long longer circulation times *in vivo* [7,32].

To circumvent the many challenges discussed above, we have designed and implemented a novel polymeric siRNA nanocarrier functionalized with cRGD peptide to facilitate GBM cellular uptake. The nanocarrier supports efficient delivery of RNAi to GBM cells, and mediates efficient reporter gene silencing in a targeted manner. Herein, we describe the synthesis, characterization and utility of ω -cholesteryl p(HPMA-r-NAS) polymers containing the reactive group NAS using RAFT polymerization. Cholesterol conjugation was performed by heating the polymer in the presence of a cholesterol-modified radical initiator, to form a stable group at the ω chain-end. After polymerization, the NAS groups of the polymer were modified with reducible azide groups containing disulfide bonds. HPMA groups were further derivatized with a cationic group (N,N'-dimethyl-aminoethanol, DMAE) coupled to the secondary hydroxyl group of HPMA *via* a hydrolysable carbonate ester. The resulting polymers formed small siRNA polyplexes through both polycation electrostatic interaction and siRNA and hydrophobic interaction *via* cholesterol. Subsequently, these polyplexes were post-modified with PEG-cRGD modified with bicyclo[6.1.0]nonyne (BCN) using copper-free click chemistry to shield surface charge and enable ligand-mediated cell binding and uptake. *In vitro* experiments showed enhanced cellular uptake of PEG-cRGD modified polyplexes, which in turn resulted in improved transfection efficiency as compared to non-PEGylated particles. *In vivo* rodent toxicity studies showed that the newly developed particles were well-tolerated when delivered either locally or parenterally.

| Materials and methods

Materials

N-(2-hydroxypropyl) methacrylamide (HPMA) [33], 2-(dimethylamino)ethyl ¹H-imidazole-1-carboxylate (DMAE-CI) [14], and imidazole-1-sulfonyl azide hydrochloride [34] were synthesized as previously described. Azobis(isobutyronitrile) (AIBN), 4,4'-azobis (N,N'-cyanopentanoic acid) (V501), cholesterol, dicyclohexylcarbodiimide (DCC), 4-(dimethylamino)pyridine (DMAP) and all other reagents and solvents used in the synthesis were obtained from Sigma-Aldrich and were used without further purification. 2,5-Dioxopyrrolidin-1-yl 4-(((1R,8S,9s)-bicyclo[6.1.0] non-4-yn-9-ylmethoxy)carbonyl)amino)butanoate (BCN, SX-A1036) was purchased from Synaffix BV (Oss, The Netherlands). cRGD-azide was provided by ChinaPeptides Co.,Ltd. (Shanghai, China). Agarose multi-purpose was purchased from Roche Molecular Biochemicals (Mannheim, Germany). 6 \times DNA Loading Dye was purchased

from Fermentas (St. Leon-Roth, Germany). SYBR Safe DNA gel stain, Lipofectamine 2000, DEME/F12 medium, Opti-MEM, G418 and heat inactivated fetal bovine serum (HI-FBS) were purchased from Life Technologies (Breda, The Netherlands). Luc2 siRNA targeted for luc2 luciferase, scrambled siRNA (siCon) and a Cy5-labeled Luc2 siRNA were obtained from Dharmacon, Inc. (Eindhoven, The Netherlands). The sequence of the sense strand of the Luc2 siRNA is 5'-GGACGAGGACGAGCACUUCUU-3', and the antisense strand sequence is 3'-UUCCUGCUCCUGCUCGUGAAG-5'. The Cy5 fluorophore within the Cy5-labeled Luc2 siRNA was conjugated to the 3' terminus of the anti-sense strand.

Synthesis of monomers

Synthesis of cholesteryl V501 derivative (C-V₅₀₁-C)

The procedure as shown in Figure 1a was used to synthesize C-V₅₀₁-C. DCC (4.85 g, 23.5 mmol) was dissolved in dry DCM (100 mL) and stirred in an ice-water bath under an argon atmosphere. Next, V501 (3.00 g, 10 mmol) and DMAP (0.29 g, 2.35 mmol) were added and the mixture was stirred for 5 mins followed by the addition of cholesterol (8.25 g, 21.3 mmol). After 4 h, the ice-water bath was removed, and the solution was kept at room temperature for 16 h and then filtered to remove the solids. DCM was removed under reduced pressure, and the crude product was dissolved in DCM and purified by silica gel chromatography with DCM as eluent yielding C-V₅₀₁-C as a white solid in 45% overall yield (4.80 g, R_f = 0.47). The monomer was characterized by ATR-IR and ¹H NMR (400 MHz, CDCl₃) (Figure S1).

Synthesis of 2-((2-azidoethyl) disulfanyl) ethan-1-amine hydrochloride (AEDA)

The synthesis procedures were similar as previously published with slight modifications (Scheme S1) [34]. Typically, cystamine dihydrochloride salt (3.22 g, 14.3 mmol), K₂CO₃ (6.00 g, 43.4 mmol) and CuSO₄·5H₂O (35.73 mg, 143.1 μmol) were dissolved in methanol (60 mL). Imidazole-1-sulfonyl azide hydrochloride (3.00 g, 14.3 mmol) was added to the suspension and the mixture was stirred at room temperature for 12 h. Next, the mixture was concentrated by evaporation of the solvent under reduced pressure, diluted with H₂O (180 mL), and extracted with DCM (3×120 mL). The combined organic layers were dried (MgSO₄), filtered and concentrated. Silica gel flash chromatography gave yellow waxy solids (DCM/MeOH/NH₄OH, 50:2:1-80:20:1), the yield was 0.80 g (32%, R_f = 0.5). The monomer was characterized by ATR-IR and NMR δ ¹H NMR (400 MHz, DMSO-d₆) (Figure S3).

Polymer synthesis

Synthesis of BCN-PEG and BCN-PEG-cRGD

NH₂-PEG₅₀₀₀-COOH (100 mg, 0.02 mmol, 1 equiv), and cyclooctyne-NHS (BCN-NHS; 9.0 mg, 0.024 mmol, 1.2 equiv) and triethylamine (8.5 μL, 0.06 mmol, 3 equiv) were dissolved in 1.3 mL DMSO, the reaction mixture was stirred at room temperature overnight. The final product was precipitated in cold ether twice, then dissolved in milliQ water, followed by dialysis against water (MWCO: 3000, Merck Millipore, Germany) for two days. After filtration and freeze-

drying, the BCN-PEG-COOH (BCN-PEG) was obtained as a white powder (90 mg, 85.7%). ¹H NMR (400 MHz, DMSO): δ = 7.05(s, 1H; OC(=O)NH), 7.05(s, 1H; C=ONH), 4.52 (t, 2H; PEG-OH), 4.00 (d, 2H; BCN-CH₂-O(=O)), 3.66 (t, 2H; PEG-CH₂), 3.48 (bs, 440H; PEG), 3.04 (s, 2H; OCONHCH₂), 2.90 (s, 2H; C=ONHCH₂), 2.0-2.21 (m, 4H; CH₂C(=O)NH₂, alkane), 1.99 (m, 2H; NHCH₂CH₂), 1.69-1.41 (m, 6H; alkane), 1.54-1.13 (m, 1H; alkane), 0.80-0.71 (m, 2H; alkane).

To a solution of NH₂-PEG₆₀₀₀-NH₂ (300 mg, 0.05 mmol) in DMSO (1.5 mL), cyclooctyne-NHS (BCN-NHS; 75.3 mg, 0.2 mmol, 4 equiv) and trimethylamine (41.8 μL, 0.3 mmol, 6 equiv) were added. The solution was subsequently stirred for 16 hours at room temperature. Next, the solution was dropped into cold ether twice to precipitate the formed product. The precipitate was subsequently dissolved in 10 ml water and dialyzed against water using a membrane with a molecular weight cut off of 3000 for two days. After filtration and freeze drying, BCN-PEG-BCN was obtained as a white powder (270 mg, 85.7%). Then, BCN-PEG-BCN (41.6 mg, 6.41 μmol) was dissolved in 1 mL dry DMSO, followed by the addition of cyclic RGD-azide (4.0 mg, 6.41 μmol), the obtained solution was stirred for 16 hours at room temperature. Next, 10 mL water was added and the product was obtained after freeze drying. Subsequently, the product was dissolved in 5 mL water and dialyzed against water for two days using a membrane with a molecular weight cut off of 3000. The product was obtained in a yield of 90%. The amount of cRGD conjugated to BCN-PEG-BCN was determined using ¹H NMR analysis based on the peak intensity ratio of phenyl protons of the cRGD peptide (7.0-7.2 ppm) to ethylene protons of PEG (-CH₂-CH₂-, 3.4-3.6 ppm) (Figure S6). The product was analyzed by SEC (Figure S7) and the shift of the PEG peak to a slightly shorter retention time proved that a product with higher molecular weight was obtained and thus showed the successful conjugation of cRGD and BCN-PEG. It should be noted that the applied procedure resulted in the formation of a statistical mixture of BCN-PEG-cRGD, cRGD-PEG-cRGD and unreacted BCN-PEG-BCN.

Synthesis of *p*(HPMA-*r*-NAS) (*pHN*) by RAFT polymerization

p(HPMA-*r*-NAS) was synthesized by reversible addition fragmentation chain transfer (RAFT) copolymerization as previously published[35]. Briefly, 4-cyano-4-[(dodecylsulfanylthiocarbonyl)-sulfanyl] pentanoic acid (CDTPA) was used as chain transfer agent (CTA), and AIBN as initiator (I). The polymer was synthesized using monomers (HPMA/NAS) to chain transfer agent and initiator ratio (monomers/CTA/I) of 100/1/0.1 (mol/mol/mol) and feed ratio HPMA/NAS of 70/30 (mol/mol). 1,3,5-Trioxane was added as internal NMR standard with a final concentration of 0.1 M. After purging the solution with argon for half an hour, the polymerization was carried at 70 °C for 9 h in dry DMF under argon, using a final monomer concentration of 1.0 M. After polymerization, the conversion of the monomers was analyzed by ¹H NMR spectroscopy by dilution a sample of the reaction mixture 10 times with DMSO-d₆. The synthesized polymer was precipitated into a mixture of anhydrous acetone and diethyl ether (50/50, v/v). The procedure was repeated for three times and the product was dried in vacuo prior to ¹H NMR and GPC analysis (yield: 60%). The theoretical molecular weight was calculated as follows: $M_n(\text{theory}) = [\text{monomer}]/[\text{CTA}] \times (\text{conversion}_{(\text{HPMA})} \times M_w(\text{HPMA}) \times 0.7 +$

conversion_(NAS) × Mw_(NAS) × 0.3) + Mw_{CTA}, the ratio of [monomer]/[CTA] was 100. ¹H NMR (400 MHz, DMSO-d₆); δppm; 0.95–1.52 (backbone-CH₃, CH₃CH(OH)), 1.55–2.41 (backbone CH₂, backbone-CH), 3.00–3.33 (CH₂NH), 3.5 (NHS-CH₂), 3.90 (CHOH) (Figure 2).

Radical Cross-Coupling of pHN with C-V₅₀₁-C (C-pHN)

The reaction process was based on previously published methods.[36] p(HPMA-r-NAS) (400 mg, 40.5 μmol, calculated based on the M_n(theory)= 9800 g/mol) and C-V501-C (1238 mg, 1217 μmol) were dissolved in 4 mL dry DMF, and the solution purged with argon for 30 minutes. Subsequently, the flask was put into the preheated oil bath (70 °C) and incubated for 4 h. A control polymer without cholesterol modification was synthesized as follows: p(HPMA-r-NAS) (100 mg, 10.1 μmol, calculated based on the M_n(theory)= 9800g/mol) and AIBN (50 mg, 304 μmol) were dissolved in 1 mL dry DMF and heated at 70 °C for 4 hours under an argon atmosphere. The product was precipitated two times in a mixture of anhydrous acetone and diethyl ether (50/50, v/v), dried in vacuo prior to ¹H NMR and GPC analysis (yield: 65%).

Synthesis of Cholesteryl p(HPMA-DMAE-r-AEDA) (C-pHDA)

The cholesteryl copolymer (C-pHN, 300 mg) (0.56 mmol of NAS, 1.44 mmol of HPMA) was dissolved in 3 mL dry DMSO and flushed with argon for 30 min. Next, 72 mg (0.40 mmol) of 2-((2-azidoethyl) disulfanyl) ethan-1-amine hydrochloride (AEDA) was added to this solution under argon purge. Then, 340 mg (3.36 mmol) of triethylamine was injected into the reaction vessel and the solution was stirred at 35 °C. After 48 h, 84 mg (1.2 mmol) of d,l-amino-2-propanol was injected into the reaction mixture and the solution was stirred for 16 hours at room temperature. The modified polymer was precipitated twice into a mixture of anhydrous acetone and diethyl ether (50/50) and dried in vacuo to get the white colored product C-pHNA (yield: 63%). The resulting polymer was then dissolved in 2 mL dry DMSO. DMAE-CI (3.4 g, 14.4 mmol) was added and the solution was flushed with argon. After 72 hours of reaction at room temperature, the solution was diluted with 20 ml of 5 mM ammonium acetate buffer (pH 5) and purified with same buffer by ultrafiltration for 24 h using a membrane with MWCO of 3000. The resulting polymer solution was filtered with 0.2 mm filter and the polymer was obtained after freeze drying (yield 94.7 mg).

Characterization of polymer

The copolymer composition of the different polymers was determined by ¹H NMR analysis performed with a Gemini 400 MHz spectrometer (Varian Associates Inc., NMR Instruments, Palo Alto, CA). The polymers were dissolved in D₂O or DMSO-d₆. The molecular weights and molecular weight distributions of the synthesized copolymers pHN and C-pHN were determined by gel permeation chromatography (GPC) [37]. For the polymer C-pHNA and C-pHDA, the molecular weights and molecular weight distributions were determined by GPC using a Viscotek-GPC max (Viscotek, Oss, The Netherlands) light scattering (λ = 670 nm, right (90°) and low (7°) angle)/viscosimetric detection system, using a ultrahydrogel 2000, 7.8 × 300

mm column in series with a ultrahydrogel 6.0 × 40 mm guard column (Waters) and 0.3 M NaAc, pH 4.4, 30% acetonitrile as eluent [38]. The flow rate was 0.6 mL/min and the run time was 50 min. PolyCAL™ PEO standard ($M_n=24$ kDa, PDI=1.01, Malvern) was used for calibration.

Preparation and characterization of polymer/siRNA polyplexes

siRNA polyplex preparation

siRNA duplexes for target genes were purchased from IDT (Coralville, IA, USA). The siRNA polyplexes preparation process consisted of 3 consecutive steps: complexation, pegylation, and lyophilization. Briefly, for complexation, four volumes of polymer and one volume of nucleic acid both dissolved in 10 mM NaOAc buffer, pH 5, at the desired N/P ratio, were mixed by vortexing with a final siRNA concentration of 50 µg/mL. For pegylation, BCN-PEG (BCN-PEG-COOH) or BCN-PEG-cRGD as added to the polyplexes at the amount of PEG equivalent to 60 mol% of azide of the polymer used for preparing polyplexes and left to react for 2 h at room temperature. For freeze-drying of the polyplexes, sucrose was added to the polyplex formulation to a final concentration of 5% before snap-freezing in liquid nitrogen. Frozen samples were freeze dried overnight using an Alpha 1–2 LD plus freeze dryer (Marin Christ, Osterode, Germany).

Particle size and zeta-potential measurements

Particle sizes of the polyplexes (10 µg/mL siRNA concentration) were measured with dynamic light scattering (DLS) using an ALV CGS-3 system (Malvern Instruments, Malvern, U.K.) equipped with a JDS Uniphase 22 mW He–Ne laser operating at 632.8 nm, an optical fiber-based detector, and a digital LV/LSE-5003 correlator at 25°C. The zeta-potential of the polyplexes was measured at 25 °C using a Malvern Zetasizer Nano-Z (Malvern Instruments, Malvern, U.K.) in 10 mM HEPES buffer. To detach PEG from C-pHDA/siRNA polyplexes, the polyplexes were incubated with 10 mM DTT at room temperature before measurement.

Gel retardation assay

Polyplexes prepared at different N/P ratios were made by adding 5 µL of polymer solution (concentrations varying between 14–2400 µg/mL in 10 mM HEPES, pH 7.4) to 5 µL of siRNA solution (40 µg/mL in 10 mM HEPES, pH 7.4), followed by vortexing for 5 s and the dispersions were incubated for 30 min at room temperature. For release studies with heparin, the sample prepared at an N/P of 8 (10 µL) was mixed with of 5 µL heparin sodium salt (concentrations varying between 75–900 µg/mL). Next, 1 µL of sodium chloride (1.54 M) was added to get a final salt concentration of 150 mM, and the samples were incubated for 10 min at room temperature [39]. Next, the gel was analyzed by a Gel Doc XR+ system (BioRad Laboratories Inc., Hercules, CA) with Image Labsoftware.

Transmission Electron Microscopy (TEM)

Transmission electron microscopy (TEM) was carried out on a FEI Tecnai T10 microscope from FEI company (Eindhoven, The Netherlands). Twenty microliters of polyplex dispersion of

50 µg/mL siRNA in 10 mM HEPES, pH 7.4, was placed on a carbon-coated copper grid and left to dry. The samples were stained with 2% uranyl acetate. Scale bars were added with a help of ImageJ software.

In vitro cytotoxicity and cell transfection study

Human glioblastoma cells (line U87R-GFP; gift from Peter Forsyth, Moffitt Cancer Center, FL, USA) modified with luciferase were cultured in Dulbecco's Modified Eagles Medium (DMEM) F12 supplemented with 10% fetal bovine serum and 200 µg/ml G418 as previously described [40]. Cells were seeded at a density of 10,000 cells per well in 96 well plate 24 hours prior to polyplex addition. Cells were cultured in (10% HI FBS,) before transfection, the medium was removed and replaced with opti-MEM or culture medium containing 10% FBS. siRNA polyplexes were then added to each well at a final siRNA concentration of 100 and 200 nM. Lipofectamine 2000 (Invitrogen, Karlsruhe, Germany) (Lipo) was used as positive control (100 nM siRNA, Lipo/siRNA volume/weight ratio of 3/1), and formulations containing scrambled siRNA and PBS treated cells were used as negative controls. After 4 h incubation, the medium was replaced with culture medium containing 10% FBS.

To determine cytotoxicity of the polyplexes the Alamar Blue cell viability assay (Invitrogen, Karlsruhe, Germany) was carried out. 44 h hours following transfection, the cell medium was replaced with medium containing Alamar Blue (50 nM) and incubated for 4 h. Next, 80 µL of medium from each well was then transferred into a flat-bottom 96-well plate. The relative cell metabolic activity was calculated by normalizing the absorbance at 570 nm (reference wavelength of 630 nm) with the absorbance of PBS-treated cells.

Luciferase cellular expression was measured 48 h after transfection. Cells were washed with 100 µL cold PBS and lysed with 100 µL lysis buffer. Subsequently, 50 µL luciferase assay reagent (Promega) was added to 20 µL cell lysate using a microinjector, and luminescence measured after 2 seconds using a white microplate, using an FLUOstar OPTIMA equipped with a luminescence light guide (BMG LabTech, Germany). To normalize for transfection efficiency, the GFP intensity was also measured. The relative luciferase activity in each well was obtained by dividing the luminescence intensity by the corresponding GFP fluorescent intensity. This activity was then normalized against the PBS-treated control samples [41].

Cellular uptake of polyplexes studied by Flow cytometry

U87R-GFP-Luc2 cells were seeded into a 96-well plate (30,000 cells/well) and incubated with polyplexes prepared as described above using Cy5 labelled siRNA (final siRNA concentration was 100 nM, N/P ratio of 8) for 4 h at 37 °C in medium with serum incomplete sentence). For the cRGD competition study, the cells were first treated for 1 h with 200 nM cRGD before addition of polyplexes. Cells were then washed twice with ice-cold PBS. To quench the fluorescence of polyplexes associated with the cell membrane, the cells were incubated with 0.4% trypan blue-containing PBS for 5 min and washed with PBS.[42] Following trypsinization cells were collected and suspended in PBS. Cellular uptake of siRNA polyplexes was then examined through flow cytometry with help of Canto II (BD, USA).

Confocal laser scanning microscopy studies

U87R-GFP-Luc2 cells were seeded into 96-well μ Clear[®] black plates (20,000 cells/ well) and incubated for 24 h in full medium. Polyplexes with Cy5 labeled siRNA (final siRNA concentration was 100 nM, N/P ratio of 8), were added and the cells were subsequently incubated for another 4 h at 37 °C. For the cRGD competition study, the cells were first incubated with 200 nM cRGD for 1 h before adding the polyplexes. Prior to imaging, the medium was replaced with fresh full medium containing Hoechst33342 and LysoTracker Red (Molecular probes, Oregon, USA) for staining the nuclei and lysosomes (incubation at 37 °C for 20 min). After washing with PBS, CLSM images were recorded using Yokogawa CV7000S imager (Yokogawa group, Tokyo, Japan) equipped with a 60x water immersion objective at excitation wavelength of 405, 488, 561 and 646 nm for Hoechst33342, GFP, LysoTracker Red and siRNA-Cy5, respectively.

3

In vivo toxicity studies

All *in vivo* studies were performed at the Royal College of Surgeons in Ireland with experimental protocols approved by the RCSI Animal Research Ethics Committee (AREC). All work was further performed according to national regulations under Health Products Regulatory Authority HPRA license number AE19127/P033 and the NIH Guide for Care and Use of Laboratory Animals. Animals (Adult, female, C57BL/6 mice) were bred in the RCSI facility and maintained in individually ventilated cages in a specific pathogen free environment throughout the study. Mice were housed in groups of 5 and maintained on a 12-hour light/dark cycle, with free access to standard rodent chow and water. PEG-cRGD polyplexes containing scrambled siRNA (PP-siRNA) were prepared at N/P 8 according to the above procedure (IDT Scrambled anti-sense: UCA CAA GGG AGA GAA AGA GAG GAA GGA; Sense: CUU CCU CUC UUU CUC UCC CUU GUG A). Mice were randomized into four groups and treated polyplexes were administered either systemically *via* IV injection or locally *via* intracranial injection.

Mice received either: a) intravenous PP-siRNA as a direct injection into the lateral tail-vein (IV; 3 injections a week for 2 weeks; 10 mg siRNA, 100 μ l volume), b) intravenous vehicle (PBS; 3 injections a week for 2 weeks; 100 μ l volume), c) intracranial PP-siRNA (IC Stereotaxic injection; 2 injections 7 days apart; 10 mg siRNA, 10 μ l volume) or d) intracranial vehicle (PBS; IC Stereotaxic injection; 2 injections 7 days apart, 10 μ l volume). To perform intracranial administration, animals were maintained under anesthesia of 1.5% isoflurane/1LO₂ and placed in a stereotaxic frame. The bregma was located and a burr hole made 2mm to the right. Polyplexes were administered 2mm below the surface using a Hamilton syringe. Mice were scored daily during the treatment period followed then by regular monitoring (weight measured 3 times a week; daily observation) for changes in weight, behavior or emergence of adverse neurological effects. Three weeks following treatment end mice were euthanized and tissue collected for full veterinary pathological analysis.

Statistical analysis

p Values were determined by Student's test with two-tailed distribution performed with the software GraphPad Prism 5 (GraphPad Software Inc. La Jolla, California). p Values <0.05 were considered as statistically significant.

| Results and discussion

Synthesis and characterization of random copolymers

A random copolymer poly (HPMA-*r*-NAS) (pHN) was synthesized by RAFT polymerization, as shown in Figure 1b, through a procedure described previously [35]. Due to the significantly different reactivity ratios of HPMA ($r_{\text{HPMA}} = 0.29$) and NAS ($r_{\text{NAS}} = 1.99$), RAFT copolymerization of those two monomers could lead to the compositional drift during polymerization. Interestingly, Moraes et al. found that RAFT polymerization of HPMA and NAS in DMF at a specific feed ratio of 30 mol% NAS resulted in a minimal compositional drift [35]. Therefore, pHN was synthesized using this feed ratio at a total monomer concentration of 1 M (Figure 1b). The monomer

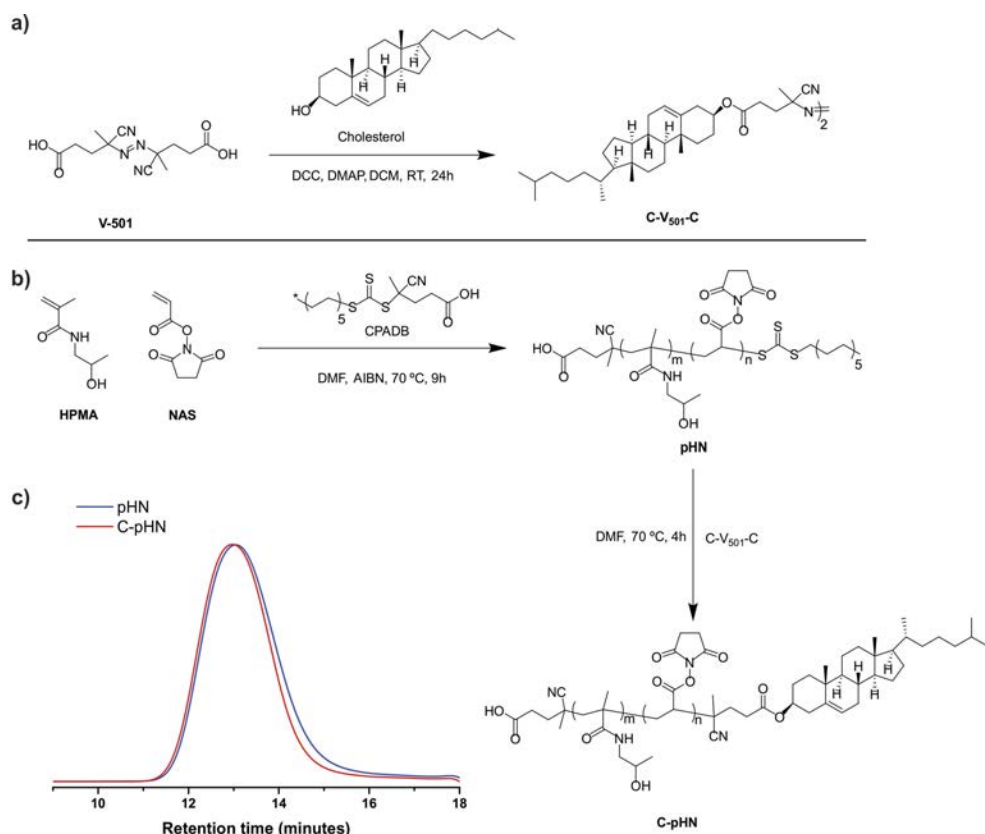


Fig. 1. a) Synthesis of cholesteryl V501 derivative (C-V₅₀₁-C); b) Synthesis of cholesteryl p(HPMA-*r*-NAS) (C-pHN); c) GPC traces of pHN (blue) and C-pHN (red).

3

conversions were determined using the ratio of the vinyl peak of the monomers (5.61 ppm for HPMA and 6.31 ppm for NAS) to the methylene peak (5.07 ppm) of internal standard 1,3,5-trioxane. ^1H NMR analysis showed that after a reaction time of 9 hours the conversions of HPMA and NAS were 64 and 57 %, respectively. After purification, the copolymer composition was also determined by ^1H NMR spectroscopy. The molar ratio of HPMA/NAS in the copolymer was calculated by comparing the integrals at 3.65 ppm (methine protons of HPMA) and at 2.79 ppm (methylene protons of NAS), with a result of 28% mol of NAS in the copolymer (Figure 2). The is in excellent agreement with the value of NAS composition (29%) as determined by the conversion of the monomers, which suggests the NAS groups were not hydrolyzed during the polymerization and precipitation processes. GPC analysis showed that the obtained pHN had a number average molecular weight of 15,800 g/mol, with a relatively low polydispersity index (PDI) of 1.43 (Figure 1c, Table 1), which is similar to the results from literature (PDI = 1.37) [35]. The deviation of the molecular weight from theoretical molecular weight ($M_n = 9800$ g/mol) calculated on the basis of the monomer conversion is attributed to the fact that calibration was done with PEG standards.

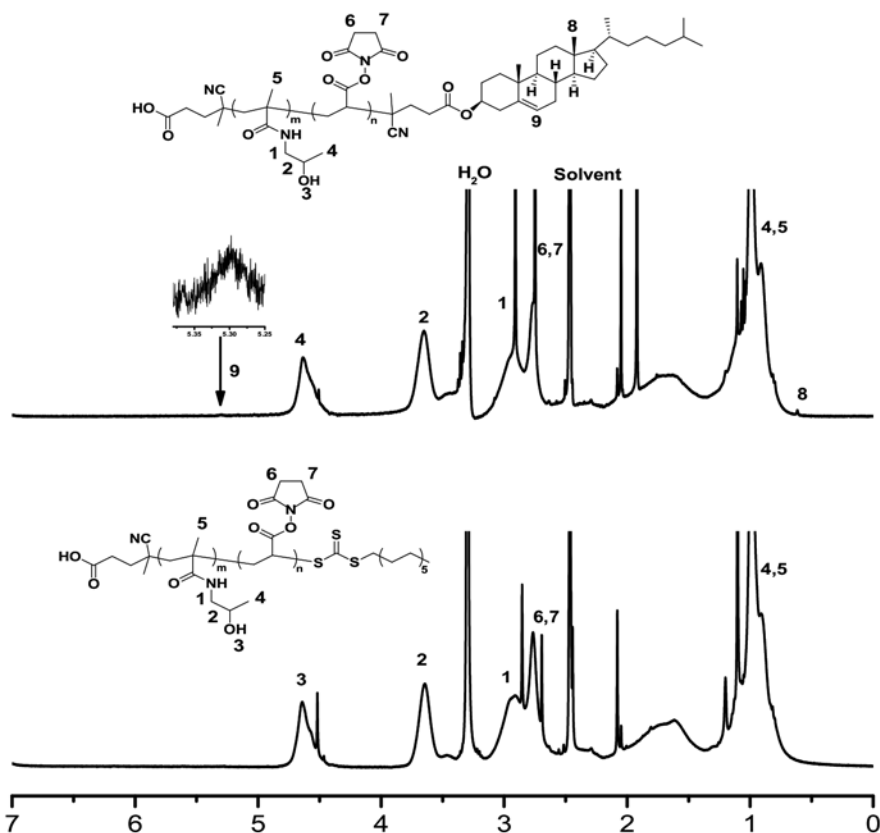
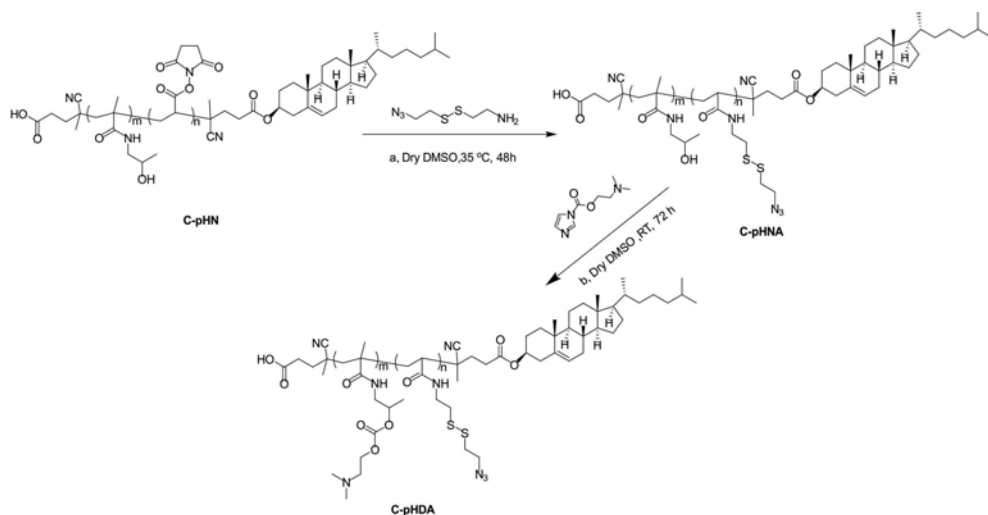


Fig. 2. ^1H NMR ($\text{DMSO-}D_6$) spectra of pHN (under) and C-pHN (upper).



Scheme 1. Post-polymerization modification of cholesteryl p(HPMA-r-NAS)

The chain transfer agent (CTA) used for the polymerization typically yields a dithioester or trithioester group at the ω -end of the polymer chain, which is available for further post-polymerization functionalization [43,44]. A radical cross-coupling reaction[36] between the trithiocarbonate chain end and a cholesterol modified azo-initiator was used to introduce a cholesterol moiety at the ω -end of pHN (Figure 1b). The cholesterol modified initiator was synthesized using DCC-mediated esterification of the hydroxyl group of cholesterol and carboxylic acid of V501, yielding C-V₅₀₁-C in 45 % yield (Figure 1a). ¹H NMR spectrum (Figure S1a) shows the disappearance of the signal at 3.51 ppm (assigned to the methine protons of cholesterol) and appearance of new signal at 4.60 ppm (assigned to the methine protons of C-V₅₀₁-C) suggests the formation of an ester bond between cholesterol and V501. The ester bond formation was further verified by the ATR-FTIR with its absorbance at wavenumber of 1743 cm⁻¹ (Figure S1b). Radical cross-coupling of pHN and C-V₅₀₁-C was performed at 70 °C in DMF for 4 h (Figure 1b). ¹H NMR analysis of the obtained polymer confirmed incorporation of the cholesterol moiety as evident by the appearance of peaks at 0.61 ppm (methyl protons of cholesterol) and 5.30 ppm (methylene protons of cholesterol) in the NMR spectrum (Figure 2). NMR analysis further showed that around 60% of pHN chains had a cholesterol terminus. The GPC chromatogram of pHN and C-pHN showed that there was no significant change in the molecular weight distribution (Figure 1c) and polydispersity index (Table 1), and the decrease of the UV absorbance (90%) (Figure S2) at 309 nm (thiocarbonylthio chromophore)[43] demonstrates again successful cross-coupling of cholesterol to the polymer. The resulting polymer C-pHN contained 27 mol% of NAS (calculated from NMR) demonstrated that these reactive esters were not hydrolyzed, due to possible presences of traces of water, during cholesterol modification and are therefore available for further post-polymerization modification.

The cholesteryl poly(HPMA-*r*-NAS) (C-pHN) copolymer was subsequently modified with 2-((2-azidoethyl) disulfanyl) ethan-1-amine hydrochloride (ADAE) to introduce azide groups which can be exploited for conjugation of compounds with bicyclo[6.1.0]nonyne (BCN) groups (using copper free click chemistry - Scheme 1) [45]. ADAE was synthesized *via* conversion of one of the cystamine amines into azide, according to a previous study (Scheme S1) [34]. ¹H NMR analysis and the absorbance at wavenumber of 2300 cm⁻¹ in ATR-IR spectrum showed the success of azide formation (Figure S3). C-pHN was first reacted with ADAE, followed by an excess of 1-amino-propan-2-ol to quench remaining unreacted NAS units (Scheme 1a). ¹H NMR analysis of the obtained azide polymer (C-pHNA) (the decreased integral of 2.79 ppm) confirmed the reaction between NAS and ADAE (Figure S4). The C-pHNA containing 20 mol% of ADAE meaning that the conjugation efficiency was 88% (Table 1). The C-pHNA polymer was further modified with 2-(dimethylamino) ethyl -imidazole-1-carboxylate (DMAE-CI), coupled *via* a carbonate ester bond, to get the final polymer C-pHDA (Scheme 1b). As shown in Figure 3, the decrease in intensity of the methine proton of the HPMA peak at 3.7 ppm and the appearance of peak at 2.3 ppm (the methyl groups of DMAE) demonstrates that 75% of the OH groups of HPMA had reacted with DMAE groups. SEC analysis of the copolymer before and after DMAE modification showed monomodal distribution with a relative narrow distribution (PDI <1.4) (Figure S5).

Formation of C-pHDA polyplexes and *in vitro* siRNA delivery

The effect of introducing cholesterol moieties in the polymer on the formation of siRNA polyplexes and gene delivery properties were studied. Agarose gel electrophoresis and dynamic light scattering techniques were employed to study the interaction of polymers with siRNA. A representative gel electrophoretic pattern is shown in Figure 4a. siRNA was mixed with

Table1. Characteristics of synthesized random copolymers

Polymers	Abbreviation	HPMA (% mol) ^a	NAS (% mol)	HPMA-DMAE (%mol)	ADAE (%mol)	M _n (g/mol)	M _w /M _n
P(HPMA- <i>r</i> -NAS)	pHN	72 (64%) ^b	28 (60%) ^b	0	0	15,800 ^c	1.43
P(HPMA- <i>r</i> -NAS)- Cholesteryl	C-pHN	73	27	0	0	17,700 ^c	1.40
P(HPMA- <i>r</i> -ADAE)- Cholesteryl	C-pHNA	80	0	0	20 (88%) ^b	24,700 ^d	1.20
P(HPMA-DMAE- <i>r</i> -ADAE)- Cholesteryl	C-pHDA	19	0	61 (75%) ^b	20	34,100 ^d	1.30
Control polymer P(HPMA-DMAE- <i>r</i> -ADAE)	pHDA	18	0	59	23	25,600 ^d	1.33

^a Copolymer composition as determined by ¹H NMR analysis; ^b Conversion of each step (percentage) calculated from ¹H NMR; ^c Determined by GPC; ^d GPC viscotek analysis.

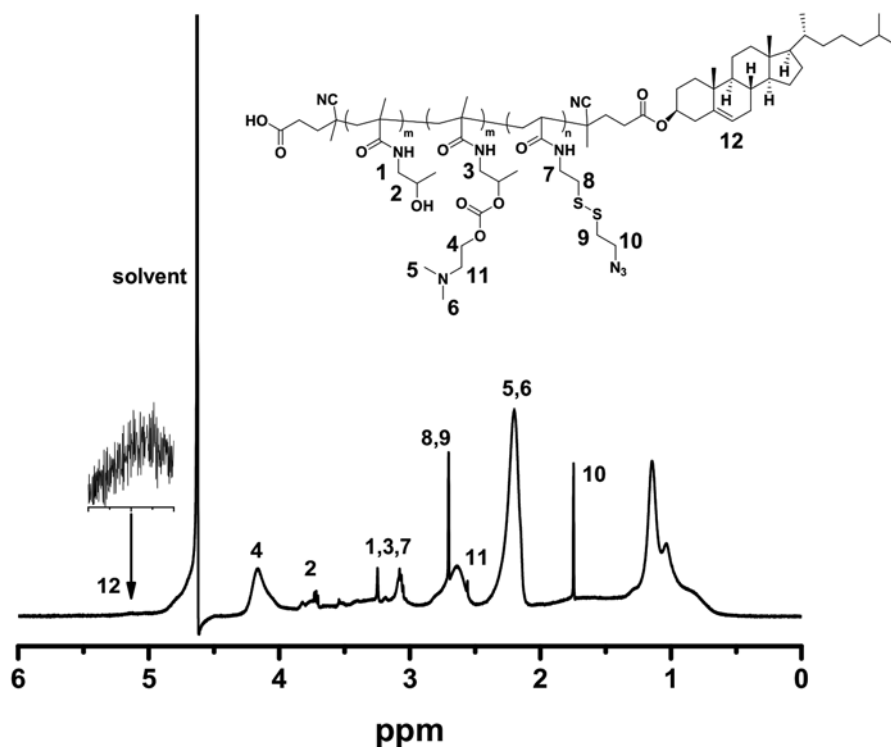


Fig. 3. ^1H NMR (D_2O) spectrum of C-pHDA.

polymer with (C-pHDA) or without (pHDA) cholesterol moiety (Table 1), at varying molar ratio of amine in the polymer to phosphate in siRNA (N/P ratio) from 0.5 to 12. Complete siRNA complexation (absence of free siRNA bands in the gel) for pHDA was achieved at N/P ratio of 4 and above, whereas for C-pHDA this was achieved at N/P 3. These data indicate that there was no hindering of the complexation of siRNA following introduction of cholesterol on the ω -end of pHDA. This is consistent with results previously obtained, in which cholesterol was introduced into PAsp(DET)-PEG copolymer [32,46]. Table S1 reports the size and zeta potential of C-pHDA polyplexes prepared at varying N/P ratios. At N/P ratio 2, the average size of polyplexes was largest (319 nm) and with a near neutral charge (5 mV), which implies it is close to the charge neutralization point between c-pHDA and siRNA, consistent with the gel retardation results. The particle size and scattering light intensity (SLI) decreased with increasing N/P ratios in the range of 2-12, together with the increased polydispersity (PDI) of the polyplexes. Thus, an N/P ratio of 8 was selected for further evaluation, at which C-pHDA form particles of 37 nm and with an acceptable PDI (<0.35). The effect of cholesterol on polyplex stability at increasing ionic strength was also evaluated (Figure 4b). After incubation with 150 mM NaCl (physiological ionic strength) in 10 mM HEPES buffer for half an hour, the size of pHDA/siRNA

polyplexes increased from 90 to 350 nm, which is normal for cationic polyplexes without PEG shielding [47]. In contrast, the size of C-pHDA/siRNA polyplexes only slightly increased from 37 to 60 nm, demonstrating that the hydrophobic interaction between the cholesterol moieties could significantly enhanced the stability of the C-pHDA siRNA polyplexes.

The effect of the presence of cholesterol in the polyplexes on siRNA transfection efficiency was evaluated in the invasive U87R-GFP-Luc2 GBM cell line, which co-expresses green fluorescence protein (GFP) and luciferase (Luc) from a bicistronic transcript. To exclude the influence of serum, the polyplexes were incubated with the cells OPTI-MEM medium without serum, which favors stability of unshielded, cationic polyplexes and lipoplexes made

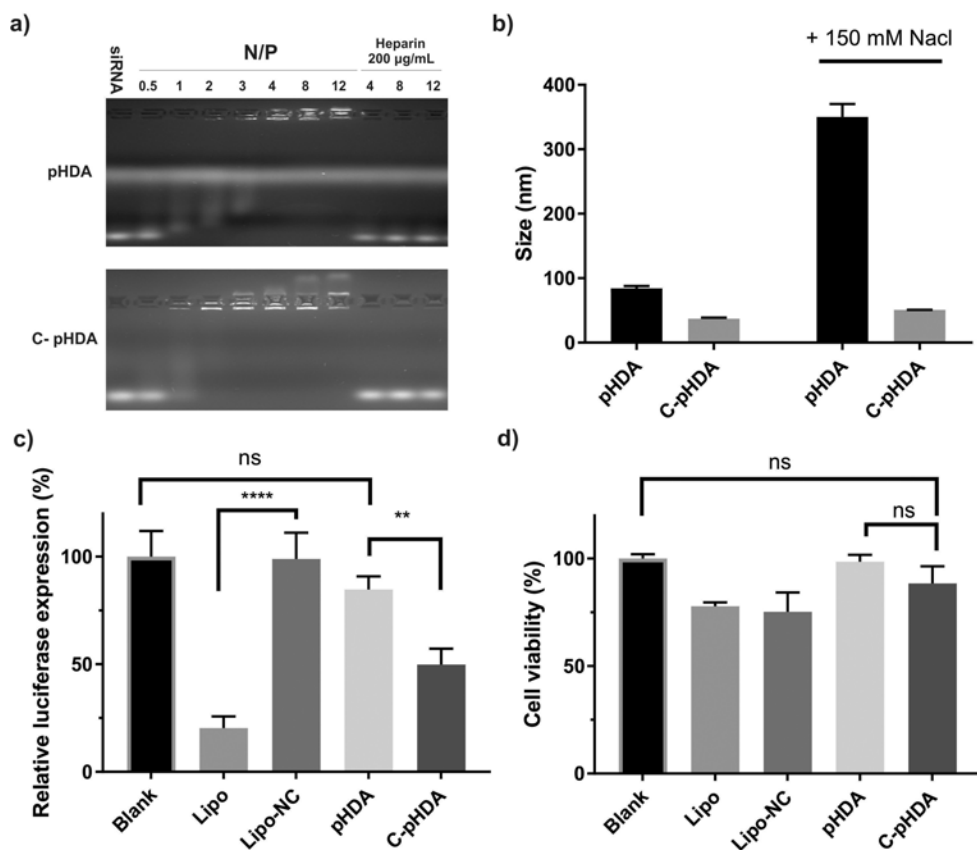


Fig. 4. (a) Agarose gel retardation assay of the polymer/siRNA polyplexes at different N/P ratios. To study heparin induced polyplex destabilization, siRNA polyplexes were incubated with heparin (200 µg/mL) for 10 mins in 10 mM HEPES buffer (pH 7.4, containing 150 mM NaCl); (b) particle size of siRNA polyplexes at concentration of 10 µg/ml, N/P molar ratio of 8, before and after 150 mM NaCl for 0.5 h; Transfection efficiency (c) and cytotoxicity (d) of siRNA polyplexes at N/P ratio of 8 with a final siRNA concentration of 100 nM. **** $p < 0.0001$, ** $p < 0.01$, ns: no significantly difference. Blank: untreated cells. NC: Negative control siRNA. Representative results from one of three experiments are shown. All values are given as the mean \pm SD (n=3).

with commercial agent Lipofectamine 2000 (Lipo). At an N/P 8, C-pHDA polyplexes containing anti-luciferase siRNA potently silenced around 50% of the expression of luciferase, which was significantly higher than observed for the polyplexes based on pHDA (10% silencing) (Figure 4c). The improved gene silencing efficacy of c-PHDA polyplexes compared to pHDA polyplexes is likely caused by the smaller size (37 vs 90 nm) and higher surface charge (25 vs 16 mV) of the polyplexes, as the size and zeta potential of polyplexes strongly influence the transfection efficiency [48]. Moreover, polyplexes prepared by pHDA and C-pHDA showed minimal cytotoxicity to U87R cells (Figure 4d). These data again demonstrate that p(HPMA-DMAE) has an excellent cytocompatibility, in agreement with a previous study using different cell lines [49]. In conclusion, the introduction of cholesterol into the polymer enhanced stability of formed siRNA polyplexes and lead to smaller particle size and higher gene silencing efficacy.

Effect of post-PEGylation of C-pHDA polyplexes with PEG-cRGD on cellular uptake and transfection efficiency

To shield the positive surface charges of C-pHDA-siRNA polyplexes, post-PEGylation *via* copper free click chemistry was applied. Cyclic RGD (cRGD) was coupled to the distal end of PEG to enable binding to integrin receptors overexpressed on angiogenic blood vessels and tumors, including human GBM cells [50–52]. BCN-PEG-cRGD was synthesized according to scheme S2 and characterized by ¹H NMR spectroscopy (Figure S6&7) and SEC analysis (Figure S8). Post-PEGylation was carried out by adding BCN-PEG (BCN-PEG-COOH) or BCN-PEG-cRGD to preformed C-pHDA polyplexes, followed by freeze-drying which results in an acceleration of the click reaction [53]. For lyophilization, 5% sucrose was added as lyoprotectant. As shown in Table 1, after PEGylation, the size of C-pHDA polyplexes increased from 37 to 56 nm, with decrease of surface charge (25 to 9.4 mV). It is important to note that the PEGylation process did not lead to detectable siRNA release, as characterized by gel electrophoresis before and after lyophilization (Figure S9). Therefore, the decrease of the surface charge is due its shielding by the grafted PEG chains. No changes in PDI were detected after lyophilization, demonstrating that the freeze-drying procedure did not cause aggregation of the particles. The PEG-cRGD post-modified siRNA polyplexes resulted in similar size (50 nm), as confirmed by TEM (Figure S10). Further, the observation that the PDI did not change indicates that the presence of BCN-PEG-BCN in BCN-PEG-cRGD (see section Experimental Procedures, Synthesis of BCN-PEG-

Table 2. Size and zeta potential of siRNA/C-pHDA polyplexes^a

Polyplexes	Size (nm)	Zeta potential (mV)	PDI
no PEGylation	37 ± 1	25.0 ± 2.1	0.34
PEG	56 ± 2	9.4 ± 1.2	0.36
PEG-cRGD	50 ± 3	8.7 ± 0.2	0.35

^a Prepared at N/P = 8 and after lyophilization resuspended at a siRNA concentration of 10 µg/mL in 10 mM HEPES buffer, pH 7.4. Data are presented as mean ± SD (n=3).

cRGD) did not cause significant inter-polyplex crosslinking, likely because the formulations were prepared at relative low particle concentration (siRNA was 50 $\mu\text{g}/\text{mL}$). In addition, zeta potential of polyplexes was measured to confirm detachment of PEG. Following incubation of the polyplexes with DTT, the zeta potential increased from 9.4 to around 20 mV, close to the zeta potential of non-PEGylated polyplexes (25 mV) (Figure S11). This demonstrates that a significant fraction of PEG was detached.

To verify the siRNA biological delivery effects of PEG (-cRGD) post-modification on c-pHDA polyplexes, *in vitro* transfection activity and cytotoxicity were investigated. U87R-GFP-Luc2 cells were transfected with anti-luc siRNA formulations in the presence and absence of serum. U87R-GFP-Luc2 was chosen as a target cell line due to their overexpression of integrins on their cellular surface [54], and are thus appropriate for assessing the cRGD targeting effect on cellular uptake and transfection. As shown in Figure 5a, when the cells were incubated with formulations in the absence of serum, non-PEGylated and PEG-cRGD modified polyplexes showed high gene knock down efficacy (>70%), which is comparable to the positive control lipofectamine. PEG-cRGD polyplexes prepared with scrambled siRNA did not silence luciferase expression. Importantly, PEGylated polyplexes without RGD targeting ligand showed no gene silencing, presumably due to limited cellular uptake. In the presence of serum, only PEG-cRGD polyplexes showed significant luciferase silencing (40%). The low gene silencing activity of C-pHDA siRNA polyplexes in the presence of serum is most likely explained by a substantial decrease in cellular uptake (Figure S12), presumably due to the interaction of serum proteins with cationic charged polyplexes that can lead to the premature release of siRNA. Alternatively,

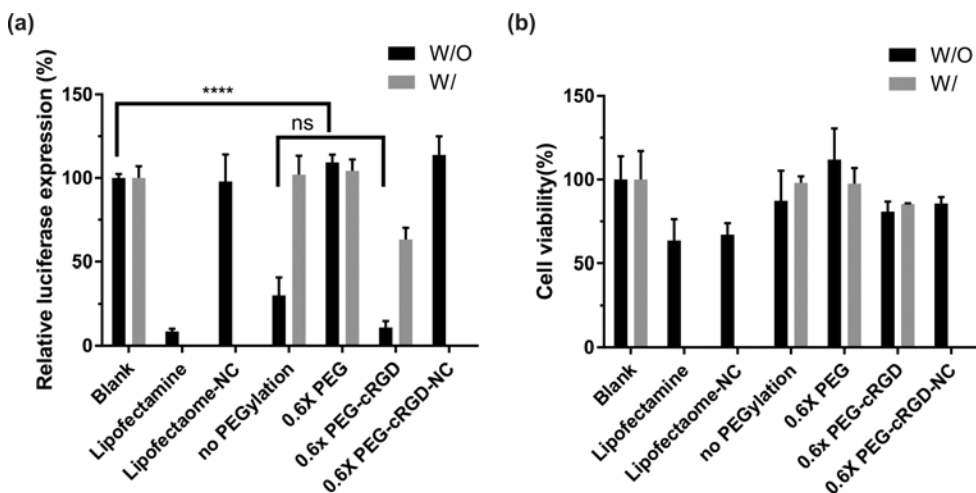


Fig. 5. Luciferase gene expression (a) and cytotoxicity (b) of different functionalized C-pHDA/siRNA polyplexes following transfection into U87R-GFP-Luc2 in the absence or presence of serum. Final siRNA concentration was 200 nM. Blank: untreated cells. NC: Negative control scramble siRNA. W/O: in the absence of serum; W/: in the presence of serum. Representative results from one of the three experiments are shown. Values are given as the mean \pm SD (n=3).

the absorbance of serum proteins can change the surface charge of particles leading to a reduced interaction with cell membranes. The results presented in Figure S12c demonstrate that more siRNA was co-localized with late endosome/lysosome when transfected in the presence of serum (in comparison with transfection without serum) indicating that serum proteins could possibly change the endocytosis pathway of C-pHDA siRNA polyplexes. Again, the AlamarBlue assay showed limited cytotoxicity for the formulations tested (Figure 5b).

To determine whether differences in gene silencing efficiencies of various polyplex formulations could be attributed to differences in cellular uptake, both flow cytometry (Figure 6a) and confocal fluorescence microscopy studies (Figure 6b and Figure S13) were performed in the presence of serum. As shown in Figure 6a, after PEGylation, the level of cellular uptake of fluorescently-labelled siRNA was substantially decreased compared to non-PEGylated formulations, potentially explaining why PEGylated formulations without RGD decoration were

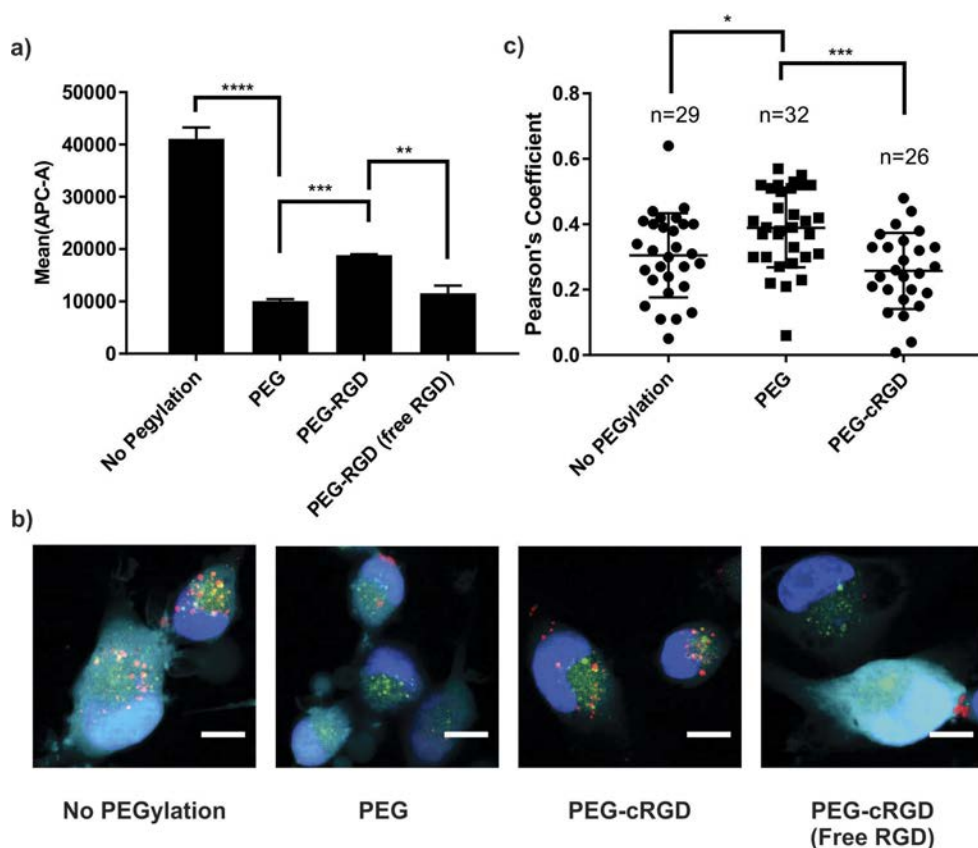


Fig. 6. Cellular uptake of Cy5 labeled C-pHDA/siRNA polyplexes (N/P=8) by U87R-GFP-Luc2 cells in the presence of serum after 4 h incubation at 37 °C measured by flow cytometry (a) and confocal microscopy (b); all images are overlays of the fluorescent signals from Cy5-siRNA (red), Lysosome Red (green), GFP (cyan) and cell nucleus Hoechst33342 (blue); (c) Quantification of Cy5-labeled siRNA co-localization with LysoTracker Red in the U87R-GFP-Luc2 cells.

not successful in silencing luciferase expression (Figure 5a). The uptake efficiency of siRNA was augmented two-fold when PEG-cRGD was present, indicating that the cRGD ligand does indeed increase cellular uptake *via* integrin-receptor mediated endocytosis. Cellular uptake was reduced by pre-incubation of the cells with free RGD, showing that binding and subsequent uptake is indeed cRGD-mediated (Figure 6a&b). In addition to improving cell uptake, the cRGD peptide may also affect the intracellular process of ligand equipped polyplexes. Several publications have shown that that RGD motif can destabilize the membrane at low pH and trigger the enhanced endosomal release of adenovirus [55,56]. To investigate the subcellular distribution of fluorescent-labelled siRNA, lysosome compartments were stained with LysoTracker Red, which is a specific marker for acidic organelles. With the co-localisation analysis of siRNA and lysosome by software ImageJ, PEG-cRGD modified polyplexes showed a significantly reduced co-localization with lysosomal compartments, compared with PEG modified polyplexes (Figure 6c). This implies that the cRGD decorated polyplexes may facilitate the siRNA transport to cytosol, as also shown in previous studies [7,57] and might explain the highly increased siRNA knock-down efficiency of RGD ligand equipped polyplexes observed (Figure 5a).

In vivo toxicity study in C57BL/6 mice

Finally, to assess the PEG-cRGD polyplexes safety profile *in vivo*, polyplexes were prepared with scrambled siRNA as described above and mice randomized into treatment groups. Mice received PEG-cRGD polyplexes (or PBS), either systemically *via* intravenous injection (IV) into the lateral tail vein or locally into the brain *via* stereotaxic intracranial injection (IC) (Figure 7). Mice were monitored for 3 weeks following final polyplex administration for signs of overt toxicity. Figure 7 demonstrates that there were no adverse effects in any treatment group when compared to PBS control cohort. Mice did not show significant changes with respect to dehydration, lethargy or ataxia. Furthermore, no weight loss was apparent between the control and treatment groups with no group demonstrating >6% fluctuation in weight (Figure 7). Moreover, no neurological, behavioral or movement issues were observed as a result of local administration (IC) or systemic administration (IV) of the polyplex at any point in the study. Following study termination, necropsy was performed and rodent tissues were excised and sent for full pathological assessment by a Board Certified Veterinary Pathologist. Cerebrum, cerebellum, skin, heart, lung, liver, spleen and kidney were collected and fixed in formalin, sectioned and hematoxylin and eosin stained for histopathology assessment. No abnormalities were detected in any tissue assessed in any group.

| Conclusions

We have described the preparation, characterization and *in vivo* toxicity assessment of a novel RGD-targeting and cholesterol stabilized polyplex system for siRNA delivery in GBM. Relative to pDHA polyplexes alone, these, stable and targeted c-pDHA polyplexes demonstrate improved cellular uptake in targeted U87R-GFP-Luc2 cells, and mediate an efficient gene silencing effect while demonstrating a low cytotoxicity profile. Our novel polyplex system shows no acute

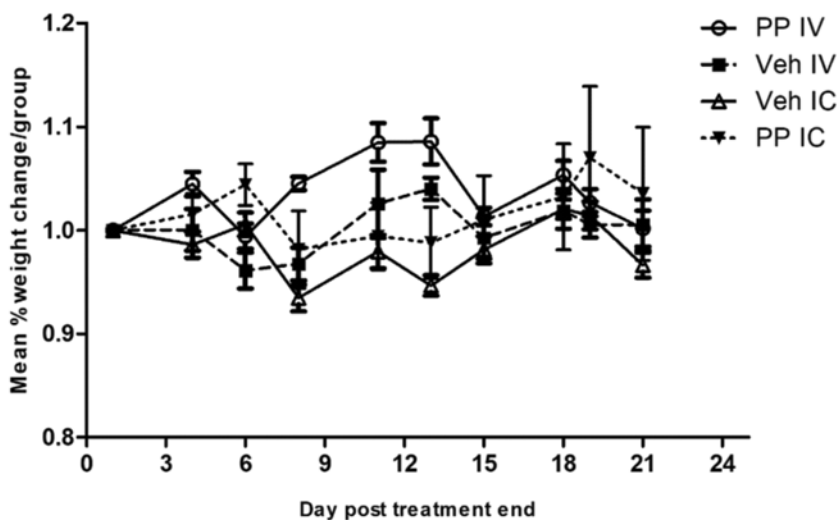
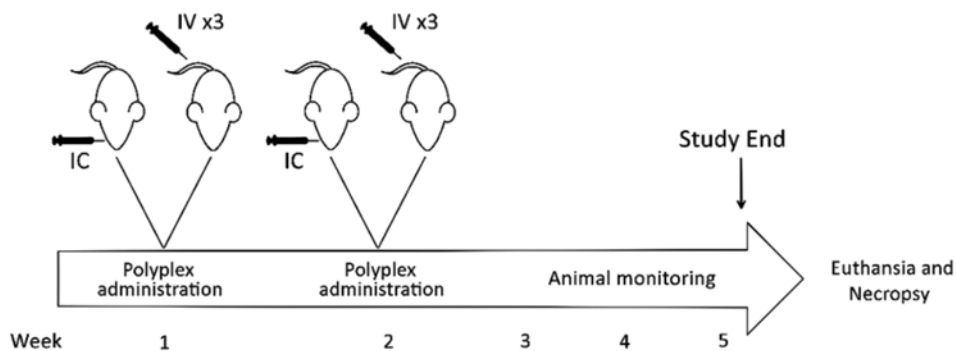


Fig. 7. *In vivo* toxicity testing of local (Intracranial: IC) or systemic (Intravenous: IV) administration of PEG-cRGD polyplexes prepared with scrambled siRNA, or PBS, in non-tumor bearing C57BL/6 mice. Mean % weight change of each non-tumor bearing C57BL/6 mice (n=6 per group) following treatment is shown. Data are represented as means \pm SEM. $p < 0.05$ is considered as statistically significant (one-way ANOVA).

toxicity *in vivo* following either parenteral or local delivery. GBM focused efficacy studies (using clinically relevant models) are now warranted; These studies should implement therapeutic siRNAs of interest in the GBM setting, packaged within newly developed polyplexes.

Acknowledgements

Bo Lou was funded by China Scholarship Council (CSC). This work was supported in part by a Science Foundation Ireland Technology Innovation Award (15/TIDA/2963). ATB is further supported by the “GLIOTRAIN” (www.gliotrain.eu) award; a Horizon 2020 Research and Innovation program funded under the Marie Skłodowska-Curie ETN initiative (Grant Agreement # 766069).

| References

1. B.A. Kohler, E. Ward, B.J. McCarthy, M.J. Schymura, L.A.G. Ries, C. Ehemann, A. Jemal, R.N. Anderson, U.A. Ajani, B.K. Edwards, Annual Report to the Nation on the Status of Cancer, 1975-2007, Featuring Tumors of the Brain and Other Nervous System, JNCI J. Natl. Cancer Inst. 103 (2011) 714–736.
2. R. Stupp, W. Mason, M.J. van den Bent, M. Weller, B.M. Fisher, M.J.B. Taphoorn, K. Belanger, A.A. Brandes, C. Marosi, U. Bogdahn, J. Curschmann, R.C. Janzer, S.K. Ludwin, T. Gorlia, A. Allgeier, D. Lacombe, G. Cairncross, E. Eisenhauer, R.O. Mirimanoff, Radiotherapy plus Concomitant and Adjuvant Temozolomide for Glioblastoma, N. Engl. J. Med. 352 (2005) 987–996.
3. P. Vader, R. Van Der Meel, M.H. Symons, M.H.A.M. Fens, E. Pieters, K.J. Wilschut, G. Storm, M. Jarzabek, W.M. Gallagher, R.M. Schiffelers, A.T. Byrne, Examining the role of Rac1 in tumor angiogenesis and growth: A clinically relevant RNAi-mediated approach, Angiogenesis. 14 (2011) 457–466.
4. E.L. Lozada-Delgado, N. Grafals-Ruiz, P.E. Vivas-Mejía, RNA interference for glioblastoma therapy: Innovation ladder from the bench to clinical trials, Life Sci. 188 (2017) 26–36.
5. J. Hou, Y. Diao, W. Li, Z. Yang, L. Zhang, Z. Chen, Y. Wu, RGD peptide conjugation results in enhanced antitumor activity of PD0325901 against glioblastoma by both tumor-targeting delivery and combination therapy, Int. J. Pharm. 505 (2016) 329–340.
6. S. Liu, W. Huang, M.J. Jin, B. Fan, G.M. Xia, Z.G. Gao, Inhibition of murine breast cancer growth and metastasis by survivin-targeted siRNA using disulfide cross-linked linear PEI, Eur. J. Pharm. Sci. 82 (2016) 171–182.
7. Y. Oe, R.J. Christie, M. Naito, S.A. Low, S. Fukushima, K. Toh, Y. Miura, Y. Matsumoto, N. Nishiyama, K. Miyata, K. Kataoka, Actively-targeted polyion complex micelles stabilized by cholesterol and disulfide cross-linking for systemic delivery of siRNA to solid tumors, Biomaterials. 35 (2014) 7887–7895.
8. C. Lin, J.F.J. Engbersen, Effect of chemical functionalities in poly(amido amine)s for non-viral gene transfection., J. Control. Release. 132 (2008) 267–272.
9. L. Novo, E.V.B. van Gaal, E. Mastrobattista, C.F. van Nostrum, W.E. Hennink, Decationized crosslinked polyplexes for redox-triggered gene delivery., J. Control. Release. 169 (2013) 246–56.
10. L. Wang, J. Kristensen, D.E. Ruffner, Delivery of antisense oligonucleotides using HPMA polymer: synthesis of A thiol polymer and its conjugation to water-soluble molecules., Bioconjug. Chem. 9 (1998) 749–57.
11. A.W. York, F. Huang, C.L. McCormick, Rational design of targeted cancer therapeutics through the multiconjugation of folate and cleavable siRNA to RAFT-synthesized (HPMA-s-APMA) copolymers, Biomacromolecules. 11 (2010) 505–514.
12. J. Kopecek, P. Kopecková, HPMA copolymers: origins, early developments, present, and future., Adv. Drug Deliv. Rev. 62 (2010) 122–49.
13. T. Lammers, K. Ulbrich, HPMA copolymers: 30 years of advances, Adv. Drug Deliv. Rev. 62 (2010) 119–121.
14. A.M. Funhoff, C.F. Van Nostrum, A.P.C.A. Janssen, M.H.A.M. Fens, D.J.A. Crommelin, W.E. Hennink, Polymer Side-Chain Degradation as a Tool to Control the Destabilization of Polyplexes, Pharm. Res. 21 (2004) 170–176.
15. H.K. De Wolf, J. Luten, C.J. Snel, G. Storm, W.E. Hennink, Biodegradable, cationic methacrylamide-based polymers for gene delivery to ovarian cancer cells in mice, Mol. Pharm. 5 (2008) 349–357.
16. S.K. Samal, M. Dash, S. Van Vlierberghe, D.L. Kaplan, E. Chiellini, C. van Blitterswijk, L. Moroni, P. Dubruel, Cationic polymers

- and their therapeutic potential, *Chem. Soc. Rev.* 41 (2012) 7147.
17. B.M. Cooper, D. Putnam, *Polymers for siRNA Delivery: A Critical Assessment of Current Technology Prospects for Clinical Application*, *ACS Biomater. Sci. Eng.* 2 (2016) 1837–1850.
 18. C. Scholz, E. Wagner, *Therapeutic plasmid DNA versus siRNA delivery: Common and different tasks for synthetic carriers*, *J. Control. Release.* 161 (2012) 554–565.
 19. J.S. Suk, Q. Xu, N. Kim, J. Hanes, L.M. Ensign, *PEGylation as a strategy for improving nanoparticle-based drug and gene delivery*, *Adv. Drug Deliv. Rev.* 99 (2016) 28–51.
 20. F.M. Mickler, Y. Vachutinsky, M. Oba, K. Miyata, N. Nishiyama, K. Kataoka, C. Bräuchle, N. Ruthardt, *Effect of integrin targeting and PEG shielding on polyplex micelle internalization studied by live-cell imaging*, *J. Control. Release.* 156 (2011) 364–373.
 21. K.M. Takeda, K. Osada, T.A. Tockary, A. Dirisala, Q. Chen, K. Kataoka, *Poly(ethylene glycol) Crowding as Critical Factor To Determine pDNA Packaging Scheme into Polyplex Micelles for Enhanced Gene Expression*, *Biomacromolecules.* 18 (2017) 36–43.
 22. J.-M. Williford, Y. Ren, K. Huang, D. Pan, H.-Q. Mao, *Shape transformation following reduction-sensitive PEG cleavage of polymer/DNA nanoparticles*, *J. Mater. Chem. B.* 2 (2014) 8106–8109.
 23. F.J. Verbaan, C. Oussoren, C.J. Snel, D.J. a Crommelin, W.E. Hennink, G. Storm, *Steric stabilization of poly(2-(dimethylamino)ethyl methacrylate)-based polyplexes mediates prolonged circulation and tumor targeting in mice.*, *J. Gene Med.* 6 (2004) 64–75.
 24. T. Blessing, M. Kurs, R. Holzhauser, R. Kircheis, E. Wagner, *Different strategies for formation of PEGylated EGF-conjugated PEI/DNA complexes for targeted gene delivery*, *Bioconjug. Chem.* 12 (2001) 529–537.
 25. U. Lachelt, E. Wagner, *Nucleic Acid Therapeutics Using Polyplexes: A Journey of 50 Years (and Beyond)*, *Chem. Rev.* 115 (2015) 11043–11078.
 26. Y. Lee, K. Kataoka, *Biosignal-sensitive polyion complex micelles for the delivery of biopharmaceuticals*, *Soft Matter.* 5 (2009) 3810.
 27. H.J. Kim, M. Oba, F. Pittella, T. Nomoto, H. Cabral, Y. Matsumoto, K. Miyata, N. Nishiyama, K. Kataoka, *PEG-detachable cationic polyaspartamide derivatives bearing stearyl moieties for systemic siRNA delivery toward subcutaneous Bxpc3 pancreatic tumor*, *J. Drug Target.* 20 (2012) 33–42.
 28. L. Novo, L.Y. Rizzo, S.K. Golombek, G.R. Dakwar, B. Lou, K. Remaut, E. Mastrobattista, C.F. Van Nostrum, W. Jahnen-Dechent, F. Kiessling, K. Braeckmans, T. Lammers, W.E. Hennink, *Decationized polyplexes as stable and safe carrier systems for improved biodistribution in systemic gene therapy*, *J. Control. Release.* 195 (2014) 162–175.
 29. B. Lou, N. Beztsinna, G. Mountrichas, J.B. van den Dikkenberg, S. Pispas, W.E. Hennink, *Small nanosized poly(vinyl benzyl trimethylammonium chloride) based polyplexes for siRNA delivery*, *Int. J. Pharm.* 525 (2017) 388–396.
 30. E. Amar-Lewis, A. Azagury, R. Chintakunta, R. Goldbart, T. Traitel, J. Prestwood, D. Landesman-Milo, D. Peer, J. Kost, *Quaternized starch-based carrier for siRNA delivery: From cellular uptake to gene silencing*, *J. Control. Release.* 185 (2014) 109–120.
 31. L. Liu, M. Zheng, D. Librizzi, T. Renette, O.M. Merkel, T. Kissel, *Efficient and Tumor Targeted siRNA Delivery by Polyethylenimine-graft-polycaprolactone-block-poly(ethylene glycol)-folate (PEI-PCL-PEG-Fol)*, *Mol. Pharm.* 13 (2016) 134–143.
 32. H.J. Kim, K. Miyata, T. Nomoto, M. Zheng, A. Kim, X. Liu, H. Cabral, R.J. Christie, N. Nishiyama, K. Kataoka, *siRNA delivery from triblock copolymer micelles with spatially-ordered compartments of PEG shell, siRNA-loaded intermediate layer, and hydrophobic core*, *Biomaterials.* 35 (2014) 4548–4556.

33. D. Oupický, Č. Koňák, K. Ulbrich, DNA complexes with block and graft copolymers of N-(2-hydroxypropyl)methacrylamide and 2-(trimethylammonio)ethyl methacrylate, *J. Biomater. Sci. Polym. Ed.* 10 (1999) 573–590.
34. E.D. Goddard-Borger, R. V. Stick, An efficient, inexpensive, and shelf-stable diazotransfer reagent: Imidazole-1-sulfonyl azide hydrochloride, *Org. Lett.* 9 (2007) 3797–3800.
35. J. Moraes, I.-M. Simionca, H. Ketari, H.-A. Klok, Avoiding compositional drift during the RAFT copolymerization of N-(2-hydroxypropyl)methacrylamide and N-acryloxysuccinimide: towards uniform platforms for post-polymerization modification, *Polym. Chem.* 6 (2015) 3245–3251.
36. K.L. Heredia, G.N. Grover, L. Tao, H.D. Maynard, Synthesis of heterotelechelic polymers for conjugation of two different proteins, *Macromolecules.* 42 (2009) 2360–2367.
37. Y. Shi, E. T. a. van den Dungen, B. Klumperman, C.F. van Nostrum, W.E. Hennink, Reversible Addition–Fragmentation Chain Transfer Synthesis of a Micelle-Forming, Structure Reversible Thermosensitive Diblock Copolymer Based on the N -(2-Hydroxypropyl) Methacrylamide Backbone, *ACS Macro Lett.* 2 (2013) 403–408.
38. X. Jiang, A. van der Horst, M.J. van Steenbergen, N. Akeroyd, C.F. van Nostrum, P.J. Schoenmakers, W.E. Hennink, Molar-mass characterization of cationic polymers for gene delivery by aqueous size-exclusion chromatography, *Pharm. Res.* 23 (2006) 595–603.
39. Lutz Nuhn, Size-Dependent Knockdown Potential of siRNA- Loaded Cationic Nanohydrogel Particles, *Biomacromolecules.* 0033 (2014) 4111–4121.
40. A.L.M. Johnston, X. Lun, J.J. Rahn, A. Liacini, L. Wang, M.G. Hamilton, I.F. Parney, B.L. Hempstead, S.M. Robbins, P.A. Forsyth, D.L. Senger, The p75 neurotrophin receptor is a central regulator of glioma invasion, *PLoS Biol.* 5 (2007) 1723–1737.
41. R. Kumar, D.S. Conklin, V. Mittal, High-throughput selection of effective RNAi probes for gene silencing, *Genome Res.* 13 (2003) 2333–2340.
42. R.J. Naik, P. Chandra, A. Mann, M. Ganguli, Exogenous and cell surface glycosaminoglycans alter DNA delivery efficiency of arginine and lysine homopeptides in distinctly different ways, *J. Biol. Chem.* 286 (2011) 18982–18993.
43. H. Willcock, R.K. O'Reilly, End group removal and modification of RAFT polymers, *Polym. Chem.* 1 (2010) 149–157.
44. S. Averick, R.A. Mehl, S.R. Das, K. Matyjaszewski, Well-defined biohybrids using reversible-deactivation radical polymerization procedures, *J. Control. Release.* 205 (2015) 45–57.
45. W. Ming, Z. Xiaofeng, R. Xiaojiao, Y. Bailiang, C. Long, L. Feizhuan, T. Jinfu, J. Feizhao, L. Shaotang, Efficacy and safety of first-line chemotherapy plus bevacizumab in patients with metastatic colorectal cancer: a met, *Chin Med J.* 127 (2014) 538–546.
46. M. Oba, K. Miyata, K. Osada, R.J. Christie, M. Sanjoh, W. Li, S. Fukushima, T. Ishii, M.R. Kano, N. Nishiyama, H. Koyama, K. Kataoka, Polyplex micelles prepared from ω -cholesteryl PEG-polycation block copolymers for systemic gene delivery, *Biomaterials.* 32 (2011) 652–663.
47. Y. Song, B. Lou, P. Zhao, C. Lin, Multifunctional Disulfide-based cationic dextran conjugates for intravenous gene delivery targeting ovarian cancer cells, *Mol. Pharm.* 11 (2014) 2250–2261.
48. J.Y. Cherng, P. vandeWetering, H. Talsma, D.J.A. Crommelin, W.E. Hennink, Effect of size and serum proteins on transfection efficiency of poly((2-dimethylamino)ethyl methacrylate)-plasmid nanoparticles, *Pharm. Res.* 13 (1996) 1038–1042.

49. J. Luten, N. Akeroyd, A. Funhoff, M.C. Lok, H. Talsma, W.E. Hennink, Methacrylamide polymers with hydrolysis-sensitive cationic side groups as degradable gene carriers, *Bioconjug. Chem.* 17 (2006) 1077–1084.
50. S. Shin, Y.S. Kim, J. Kim, H.-M. Kwon, D.-E. Kim, S.S. Hah, Sniffing for gene-silencing efficiency of siRNAs in HeLa cells in comparison with that in HEK293T cells: correlation between knockdown efficiency and sustainability of siRNAs revealed by FRET-based probing, *Nucleic Acid Ther.* 23 (2013) 152–9.
51. K. Hayashi, H. Chaya, S. Fukushima, S. Watanabe, H. Takemoto, K. Osada, N. Nishiyama, K. Miyata, K. Kataoka, Influence of RNA Strand Rigidity on Polyion Complex Formation with Block Cationomers, *Macromol. Rapid Commun.* 37 (2016) 486–493.
52. F. Danhier, A. Le Breton, V. Pr eat, RGD-based strategies to target $\alpha(v)\beta(3)$ integrin in cancer therapy and diagnosis, *Mol. Pharm.* 9 (2012) 2961–2973.
53. H. Takemoto, K. Miyata, T. Ishii, S. Hattori, S. Osawa, N. Nishiyama, K. Kataoka, Accelerated Polymer – Polymer Click Conjugation by Freeze – Thaw Treatment, *Bioconjug. Chem.* 23 (2012) 1503–1506.
54. D.W. Murray, S. Didier, A. Chan, V. Paulino, L. Van Aelst, R. Ruggieri, N.L. Tran, A.T. Byrne, M. Symons, Guanine nucleotide exchange factor Dock7 mediates HGF-induced glioblastoma cell invasion via Rac activation, *Br. J. Cancer.* 110 (2014) 1307–1315.
55. D.M. Shayakhmetov, A.M. Eberly, Z.-Y. Li, A. Lieber, Deletion of penton RGD motifs affects the efficiency of both the internalization and the endosome escape of viral particles containing adenovirus serotype 5 or 35 fiber knobs., *J. Virol.* 79 (2005) 1053–61.
56. a Ch avez, M. Pujol, I. Haro, M.A. Alsina, Y. Cajal, Membrane fusion by an RGD-containing sequence from the core protein VP3 of hepatitis A virus and the RGA-analogue: implications for viral infection., *Biopolymers.* 58 (2001) 63–77.
57. M.R. Alam, X. Ming, M. Fisher, J.G. Lackey, K.G. Rajeev, M. Manoharan, R.L. Juliano, Multivalent Cyclic RGD Conjugates for Targeted Delivery of Small Interfering RNA, *Bioconjug. Chem.* 22 (2011) 1673–1681.

| Supplementary information

3

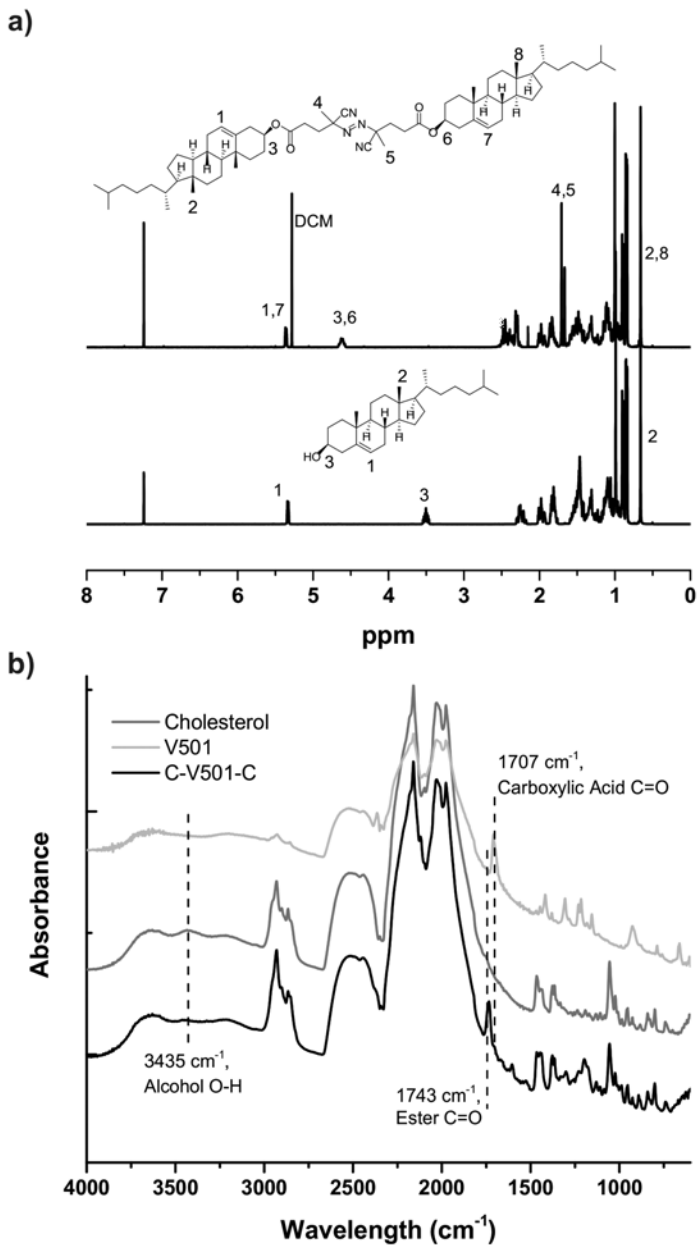


Fig. S1. ^1H NMR (CDCl_3) (a) and ATR-IR spectra (b) of C-V₅₀₁-C.

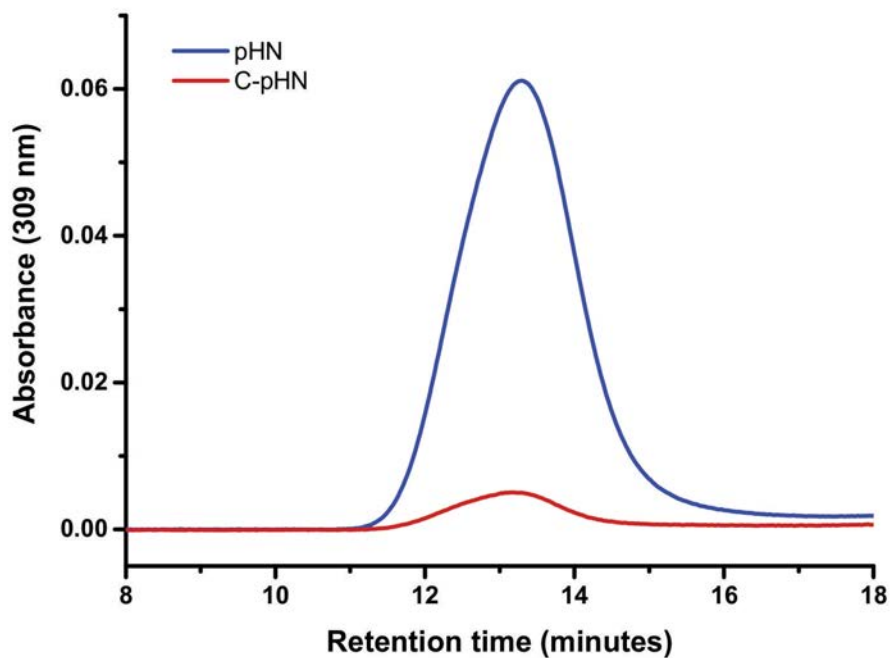


Fig. S2. GPC chromatograms using UV detection (309 nm) for pHN (blue) and C-pHN (red).



Scheme S1. Synthesis of 2-((2-azidoethyl) disulfanyl) ethan-1-amine hydrochloride (AEDA).

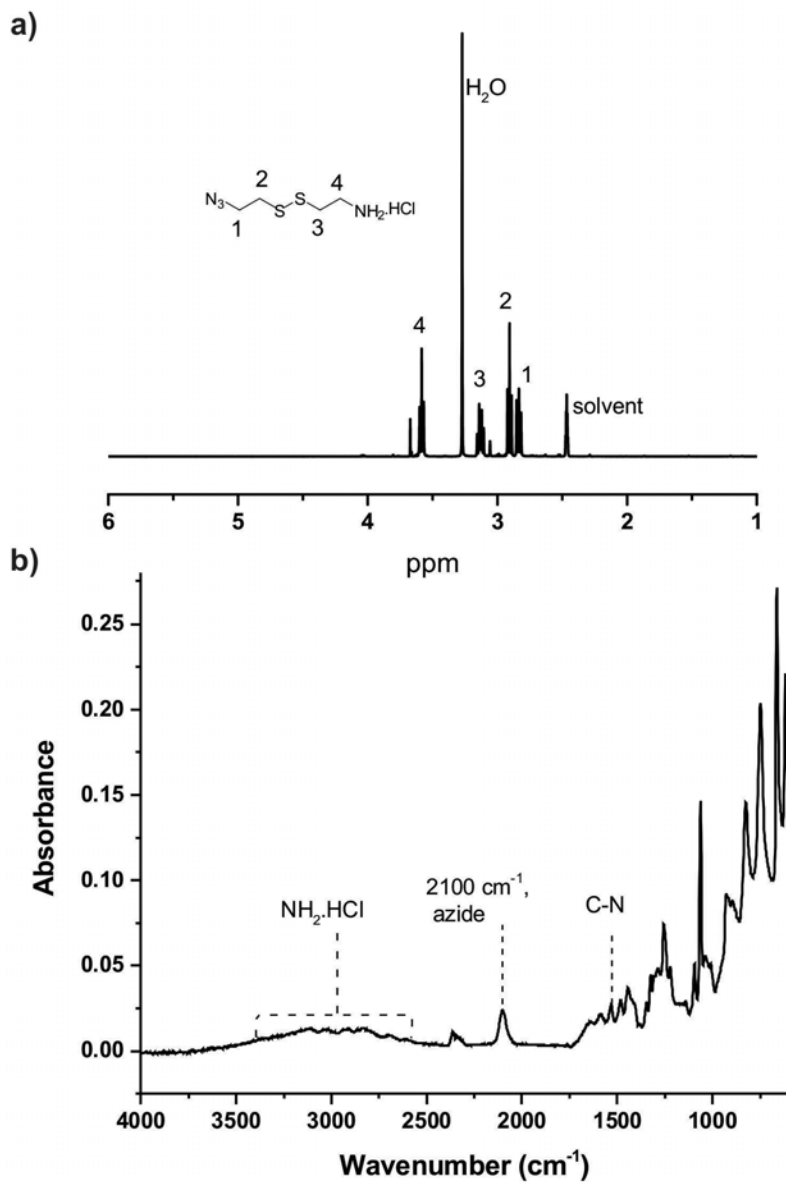


Fig. S3. ¹H NMR (DMSO-D₆) (a) and ATR-IR spectrum (b) of 2-((2-azidoethyl) disulfanyl) ethan-1-amine hydrochloride.

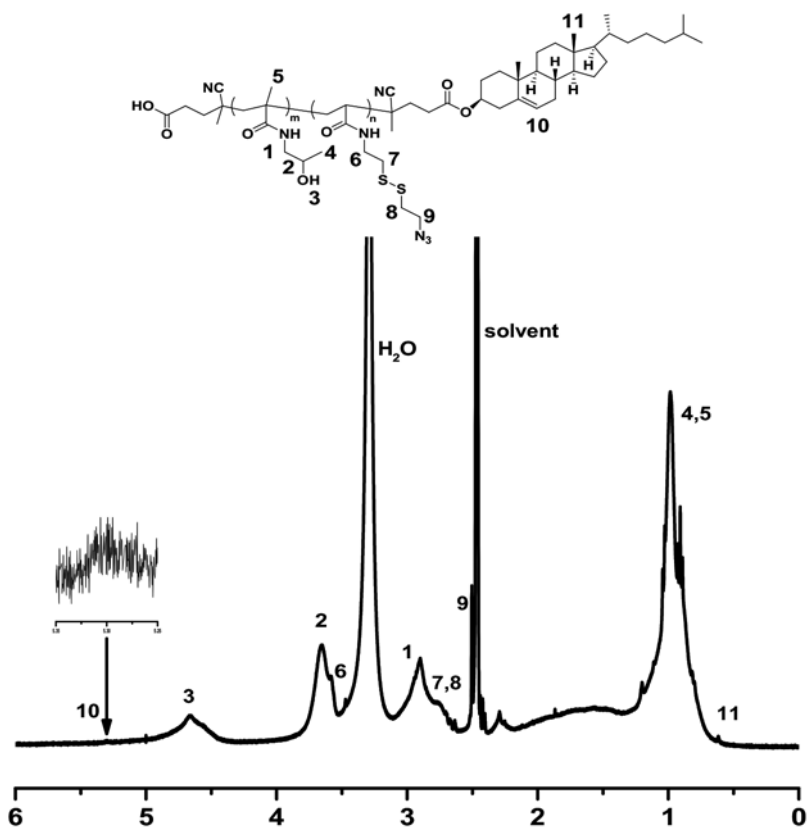


Fig. S4. ¹H NMR (DMSO-D₆) spectrum of C-pHNA.

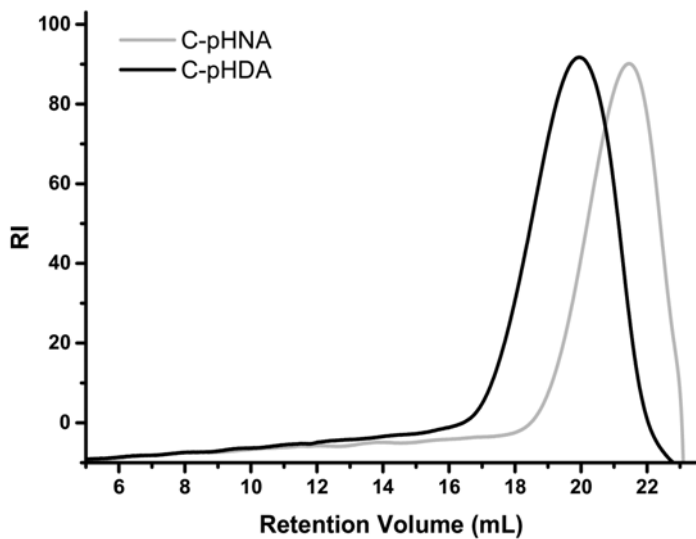


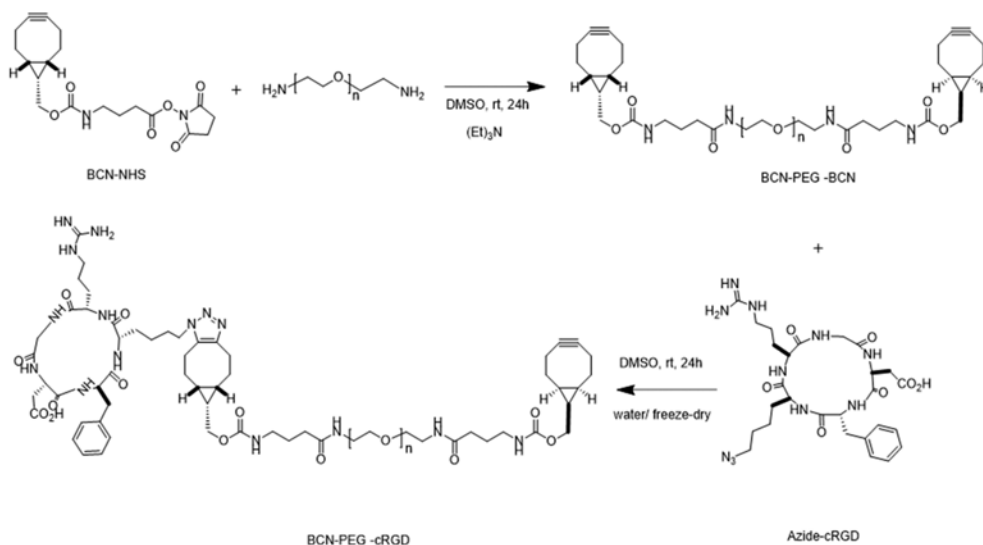
Fig. S5. SEC chromatograms of C-pHNA and C-pHDA.

Table S1. Size, zeta potential, polydispersity index (PDI) and scattering light intensity (SLI) of siRNA polyplexes prepared at varying N/P ratio

N/P ratio ^a	Size (nm) \pm S.D.	Zeta potential (mV) \pm S.D.	PDI	SLI
0.5	70 \pm 1	-27.9 \pm 1.5	0.12	173
1	130 \pm 3	-31.4 \pm 0.7	0.04	402
2	319 \pm 1	5.3 \pm 0.5	0.17	327
4	43 \pm 3	25.9 \pm 0.4	0.32	162
8	37 \pm 2	25.0 \pm 1.4	0.34	175
12	35 \pm 1	26.3 \pm 1.8	0.94	82

^a Polyplexes micells were prepared at siRNA concentration of 10 μ g/ml in pH7.4, 10mM hepes buffer.

3

**Scheme S2.** Synthesis of BCN-PEG-cRGD.

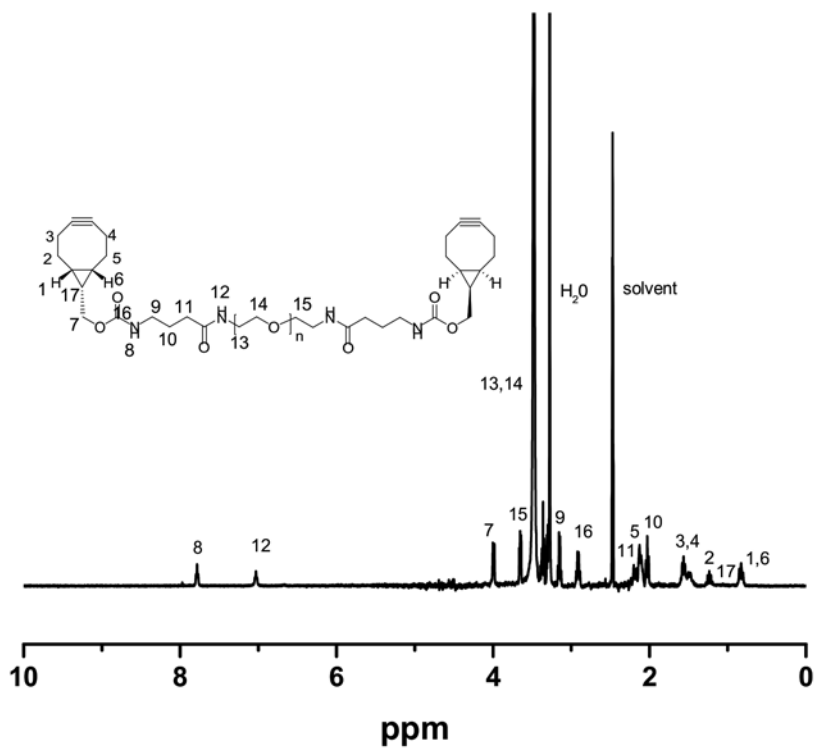


Fig. S6. ¹H NMR (DMSO-*D*₆) spectrum of BNC-PEG₆₀₀₀-BCN.

3

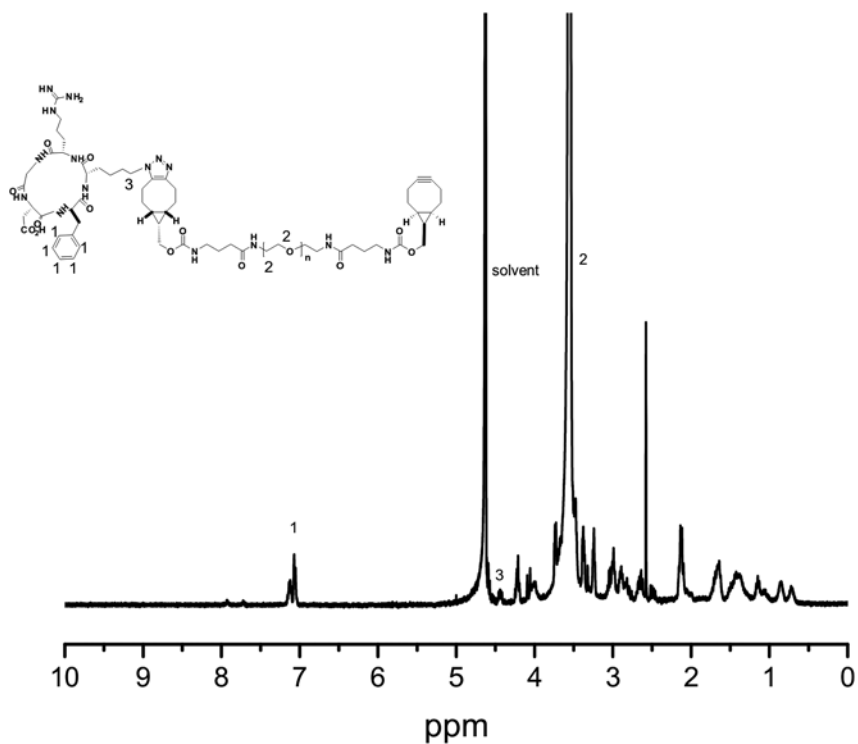


Fig. S7. ¹H NMR (D₂O) spectrum of BNC-PEG₆₀₀₀-cRGD.

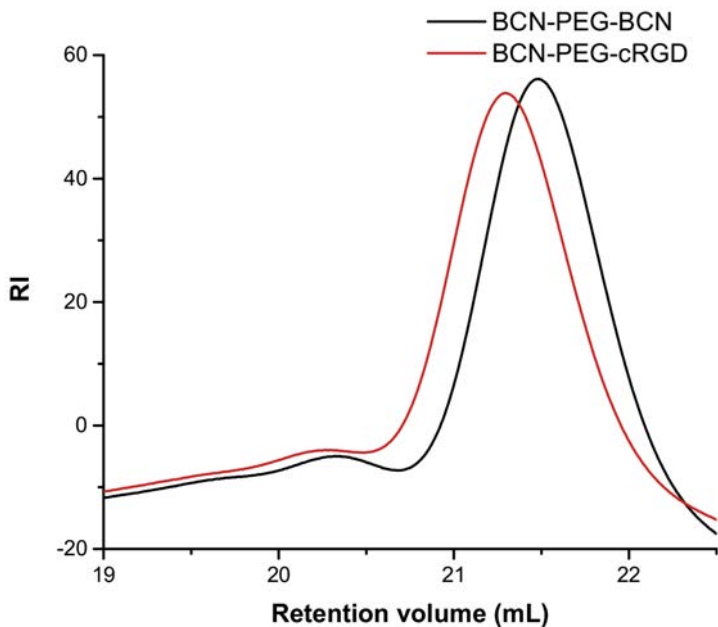
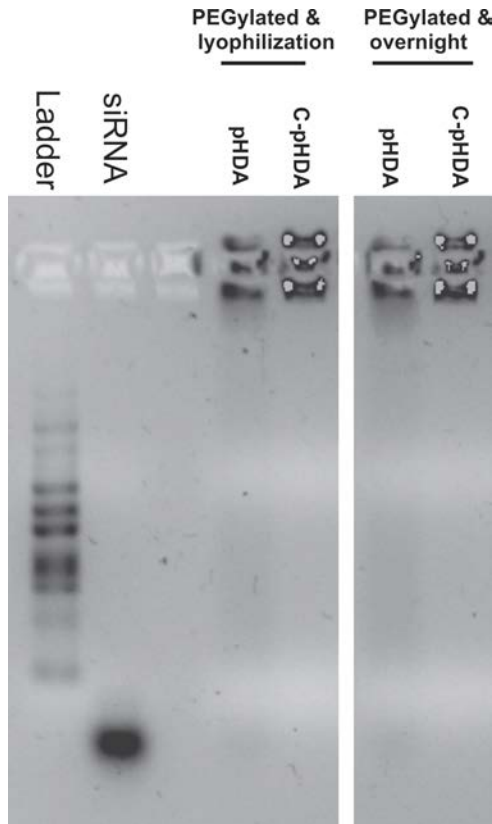


Fig. S8. SEC chromatograms (RI) of BCN-PEG-BCN and BCN-PEG-cRGD.



3

Fig. S9. Agarose gel retardation assay of the polymer/siRNA polyplexes before and after PEGylation by freeze-dry treatment.

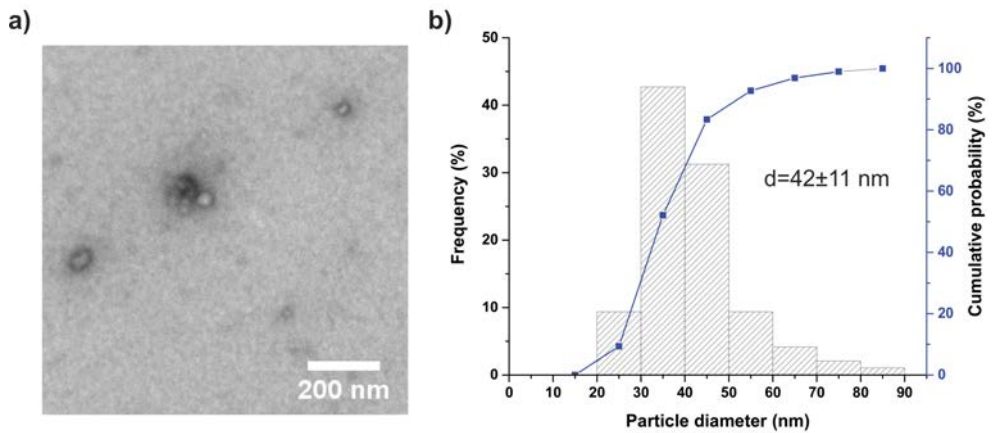


Fig. S10. Representative TEM images of PEG-cRGD post-functionalized C-pHDA siRNA polyplexes, bar indicates 200 nm.

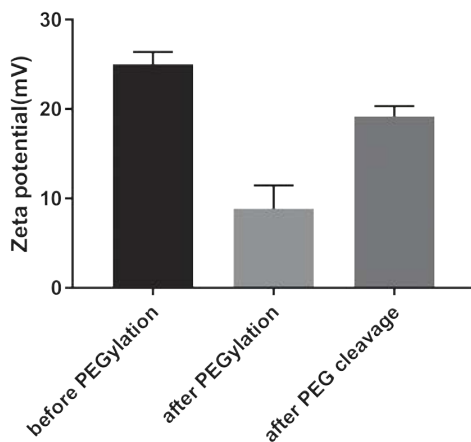


Fig. S11. Average zeta potential of C-pHDA siRNA polyplexes before PEGylation, and after PEGylation (both after being freeze-dried and resuspended in 10 mM HEPES buffer), and after PEG cleavage by incubation with 10 mM DTT for 1 h.

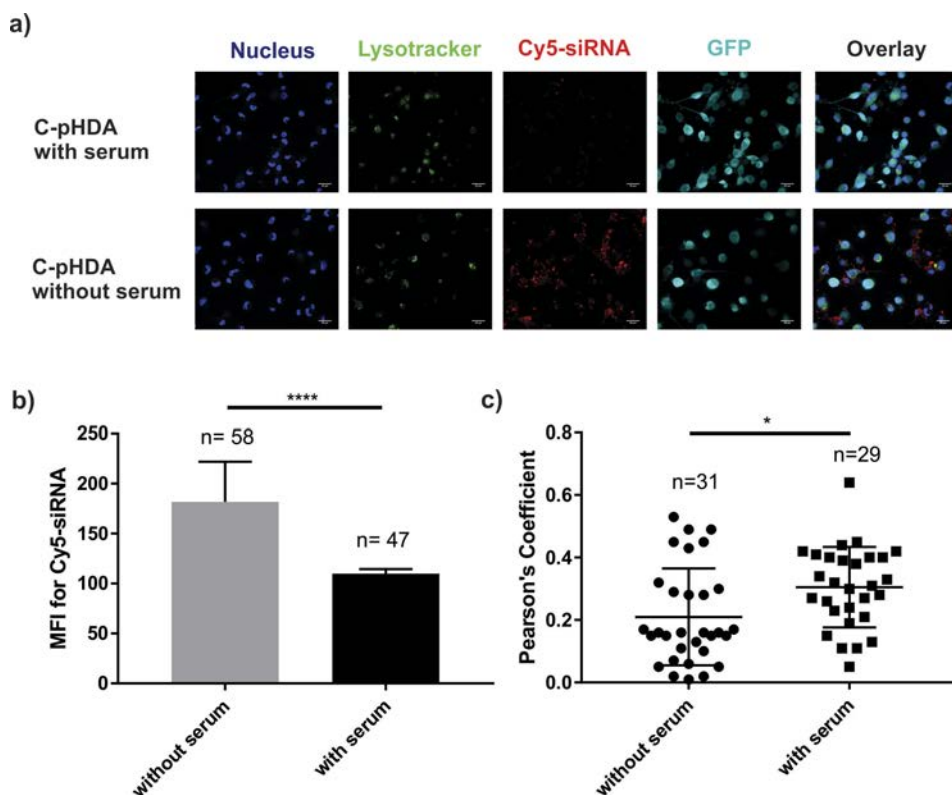


Fig. S12. Confocal microscopy images of U87R_GFP_Luc cells after 4 h incubation at 37 °C with different polyplexes in presence or absence of serum (a); (b) mean fluorescence intensity of Cy5-siRNA; (c) and co-localization analysis of siRNA and lysotracker via software ImageJ. Bar indicates 25 μ m.

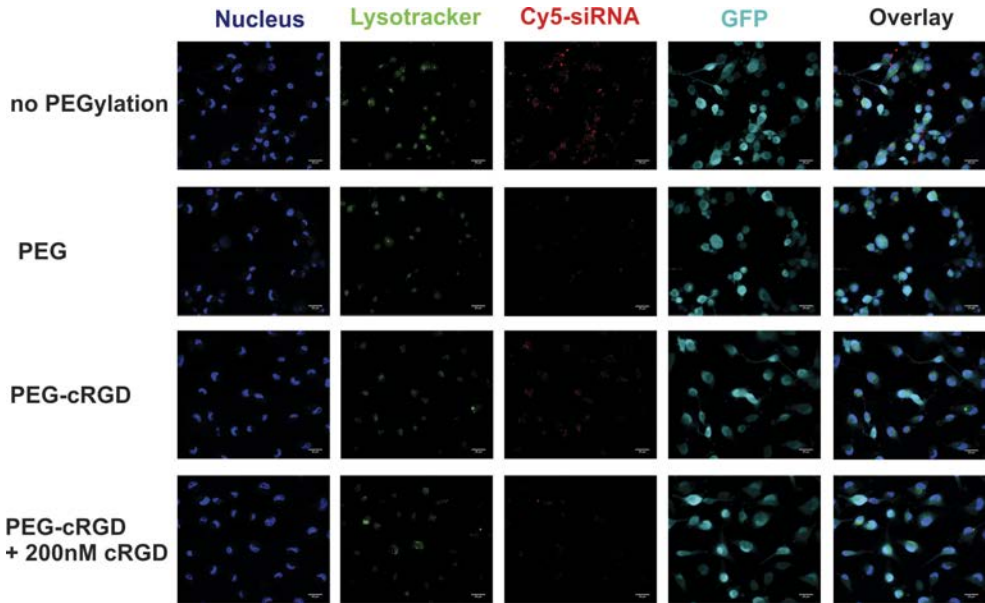


Fig. S13. Confocal microscopy images of U87R_GFP_Luc cells after 4 h incubation at 37 °C with different C-pHDA/siRNA polyplexes in the presence of serum. Bar indicates 25 μ m.

3

CHAPTER

4

Post-PEGylated and crosslinked polymeric ssRNA nanocomplexes as adjuvants targeting lymph nodes with increased cytolytic T cell inducing properties

Bo Lou^{1,§}, Ans De Beuckelaer^{2,§}, George R. Dakwar³, Katrien Remaut³, Johan Grooten², Kevin Braeckmans², Bruno G. De Geest⁴, Enrico Mastrobattista¹, Stefaan De Koker², Wim E. Hennink^{1*}

¹Department of Pharmaceutics, Utrecht Institute for Pharmaceutical Sciences, Utrecht University, 3584 CG Utrecht, The Netherlands

²Laboratory of Molecular Immunology, Department of Biomedical Molecular Biology, Ghent University, 9052 Zwijnaarde, Belgium

³Laboratory for General Biochemistry and Physical Pharmacy, Ghent University, 9000 Ghent, Belgium

⁴Department of Pharmaceutics, Ghent University, 9000 Ghent, Belgium

[§]These authors contributed equally to this work

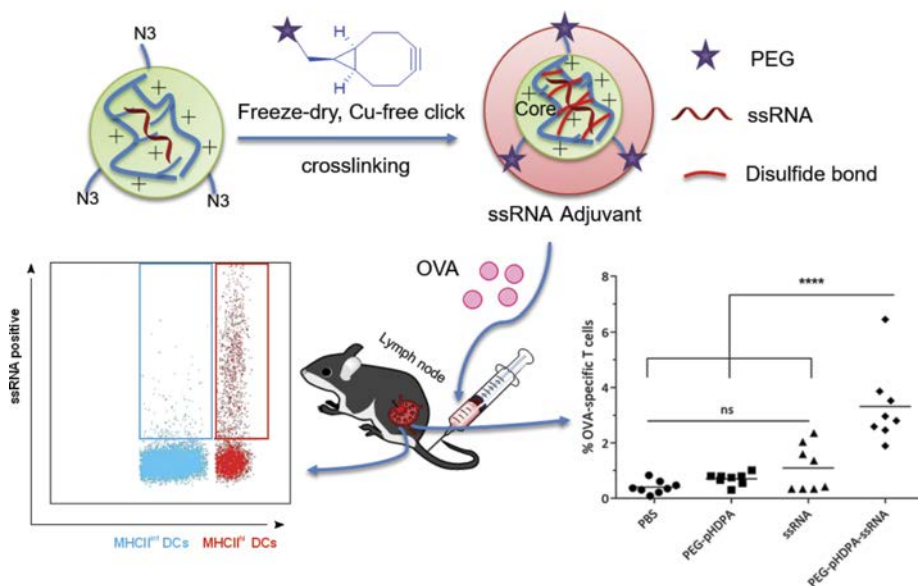
* Corresponding author

| Abstract

Potent adjuvants are highly demanded for most protein and peptides based vaccine candidates in clinical development. Recognition of viral single stranded (ss)RNA by innate toll-like receptors 7/8 in dendritic cells results in a cytokine environment supportive to the establishment of long lasting antibody responses and Th1 oriented T cell immunity. To fully exploit the immunestimulatory properties of ssRNA, it needs to be adequately formulated to ensure its optimal delivery to dendritic cells in the vaccine draining lymph nodes. In the present paper, we report on the design of ssRNA nanocomplexes formed by complexation of the cationic poly(carbonic acid 2-dimethylamino-ethyl ester 1-methyl-2-(2-methacryloylamino)-ethyl ester) (pHPMA-DMAE) based polymeric carrier and ssRNA. The resulting ssRNA nanocomplexes were subsequently PEGylated through copper-free click chemistry using PEG-bicyclo[6.1.0]nonyne (PEG-BCN) and cross-linked via disulfide bonds to increase their stability. The obtained near-neutral charged PEGylated ssRNA nanocomplexes (~150 nm) combined ssRNA protection with highly efficient delivery of ssRNA to DCs in the vaccine draining lymph nodes after subcutaneously administration. When co-administrated with a model antigen (soluble ovalbumin (OVA)), ssRNA nanocomplexes were far more efficient at inducing CD8 cytolytic T cells when compared to OVA co-administrated with naked ssRNA. Furthermore, IgG2c antibody titers, indicative of Th1 skewed T cell responses, were > 10 times increased by complexing ssRNA into the PEGylated nanocomplexes. This study highlights the potential of post-functionalizing ssRNA nanocomplexes by copper-free click chemistry and these findings indicate that this potent ssRNA adjuvant may profoundly improve the efficacy of a variety of vaccines requiring Th1-type immunity.

4

Graphical abstract



| Introduction

The design of effective immunotherapies against malignancies and insidious intracellular pathogens necessitates improved vaccine adjuvants with a strong capacity to stimulate CD8 cytolytic T cell responses in addition to humoral responses [1–3]. Activation of Toll-like receptors 7 and 8 (TLR7/8) triggers a profound secretion of interleukin 12 (IL-12) and of type I interferons (IFN), the key cytokines that guide the differentiation of CD8+ T cells into cytolytic effector T cells and of CD4+ T cells into Th1 effector cells. Hence, agonists of TLR7/8 have emerged as highly promising vaccine adjuvants to evoke cellular immune responses [4–6]. Guanidine and uridine rich single stranded RNAs (ssRNA) constitute the natural agonists of TLR7/8 present in the endosomes of dendritic cells (DCs), the most potent antigen presenting cells and initiators of T cell immunity [7,8]. Successful development of ssRNA as vaccine adjuvants, however, requires several hurdles to be taken. As natural ssRNA cannot efficiently penetrate cell membranes and are highly sensitive to ubiquitous RNases, they need to be formulated into nanosized complexes to prevent premature degradation upon injection and to reach the endosomal compartment of DCs. To this end, ssRNA have been complexed to liposomes containing cationic lipids including 1,2-dioleoyl-3-trimethylammonium-propane (DOTAP) [9,10] or to cationic polymers such as polyethyleneimine (PEI) [8] and protamine [11]. Although such approaches indeed have augmented the adjuvanticity of ssRNA, these ssRNA lipoplexes and polyplexes show limited mobility *in vivo* after local administration, resulting in limited ssRNA prevalence in DCs in the vaccine draining lymph nodes, the crucial sites of induction of adaptive immunity [7]. The limited mobility is most likely caused by the overall positive charge of these lipo/polyplexes which results in binding to extracellular matrix constituents [12–14].

Multiple studies have demonstrated that PEGylation, shields the surface charge and enhances the colloidal stability of nanoparticles and prevents their aggregation upon topical administration, which strongly aids nanoparticle trafficking to the draining lymph nodes [15–17]. Incorporation of poly(ethylene glycol) (PEG) in polyplexes is commonly achieved through the use of PEGylated block copolymers (e.g. PEG-polylysine [18,19], PEG-poly(aspartamide) [20,21], PEG-poly(amido amine)s [22,23] and PEG-PEI [24,25]) as condensing agents. A major drawback of this strategy is the crowding effect of the neutral polymer (PEG), which hinders proper nucleic acid complexation in dense particles [26–28]. Post-PEGylation – the PEGylation of preformed nucleic acid polyplexes – has emerged as an appealing alternative, with several studies indicating post-PEGylated polyplexes exhibit prolonged circulation times in mice after IV administration [29,30].

Here we aimed to design a polymeric nanocomplex system, using post-PEGylation via copper free click chemistry [31–33], to efficiently deliver ssRNA to DCs in the lymph node thus enabling effective immunomodulation. Previous studies have demonstrated that poly(carbonic acid 2-dimethylamino-ethyl ester 1-methyl-2-(2-methacryloylamino)-ethyl ester) (pHPMA-DMAE) based nucleic acid delivery systems combine excellent efficiency with a beneficial safety profile [34–37]. pHPMA-DMAE can be hydrolysed at 37 °C and at pH 7.4 (half-life, 9.6 hours) [38], enabling removal of the cationic side-chains, to yield pHPMA, a frequently studied water-

soluble polymer for drug delivery purposes [39,40]. Based on this previous work, we designed and synthesized a new series of random copolymers containing reactive azides, poly(HPMA-DMAE-co-PDTEMA-co-AzEMAm) (referred as pHDPA, Fig. 1a and Fig. S1a). ssRNA was complexed into polyplexes by electrostatic interaction with cationic pHDPA. The resulting ssRNA polyplexes were subsequently PEGylated through a copper-free chemistry using PEG-bicyclo[6.1.0]nonyne (PEG-BCN) and crosslinked via disulfide bonds to increase the stability. Upon subcutaneously injection, the generated PEG-pHDPA ssRNA nanocomplexes were expected to increase the amount of ssRNA present in lymph node DCs, which will maximize the adjuvant effect of the immune-stimulatory ssRNA when co-injected with soluble ovalbumin (OVA) protein antigen, especially at the level of the cytolytic T cell response evoked.

| Materials and methods

Materials

All chemicals were purchased in the highest purity and used without further purification. Carbonic acid 2-dimethylamino-ethyl ester 1-methyl-2-(2-methacryloylamino)-ethyl ester (HPMA-DMAE) [38] and N-[2-(2-pyridyldithio)]ethyl methacrylamide (PDTEMA) [35,41] were synthesized as previously reported. 2-Azidoethylmethacryl amide (AzEMAm) was synthesized as described previously with slightly modification [42]. Lipofectamine 2000 was obtained from Thermo Fisher Scientific (Etten-Leur, The Netherlands). Single chain RNA_{luc}-mRNA and Cy5-mRNA_{luc} were purchased from Tebu-bio (TRiLink biotechnologies); Polyuridylic acid [poly(U)] ssPolyU was purchased from InvivoGen. Agarose multi-purpose was purchased from Roche Molecular Biochemicals (Mannheim, Germany). 6 × DNA Loading Dye was purchased from Fermentas (St. Leon-Roth, Germany). SYBR Safe DNA gel stain, Opti-MEM, DMEM medium and dialyzed fetal bovine serum (FBS) were purchased from Life Technologies (Breda, The Netherlands).

Synthesis and characterization of p(HPMA-DMAE-co-PDTEMA-co-AzEMAm)

p(HPMA-DMAE-co-PDTEMA-co-AzEMAm) (pHDPA) was synthesized by radical polymerization under a nitrogen atmosphere. The polymers were synthesized using a monomer to initiator molar ratio (M/I) of 50. Different molar feed ratios of HPMA-DMAE, PDTEMA and AzEMAm were used, as shown in Table S1. In a typical experiment to synthesize p(HPMA-DMAE₇₀-co-PDTEMA₂₀-co-AzEMAm₁₀), 200 mg (0.77 mmol) HPMA-DMAE, 56.7 mg (0.22 mmol) PDTEMA, 17 mg (0.11 mmol) AzEMAm and 3.6 mg (0.022 mmol) AIBN were dissolved in dry DMSO (1 mL) in flasks sealed with rubber septa and subjected to three vacuum-N₂ cycles. The polymerization was carried at 70 °C for 48 h. Next, the polymer was precipitated in cold diethyl ether, redissolved in DMF and repeating this procedure 3 times. After extensive dialysis (8 kDa) against an NH₄OAc buffer of pH 5.0 (10 mM, last step 5 mM) at 4 °C, the polymer was collected after freeze drying. The yield of polymer is between 30-40%.

The molecular weights and polydispersity (M_w/M_n) of pHDPA were determined by size exclusion chromatography (SEC) analysis using a Viscotek-GPCmax (Viscotek, Oss,

The Netherlands) light scattering ($\lambda = 670$ nm, right (90°) and low (7°) angle)/viscosimetric detection system, using ultrahydrogel 2000 7.8×300 mm columns in series with a ultrahydrogel 6.0×40 mm guard column and 0.3 M NaAc pH 4.4, 30% acetonitrile as eluent [43]. The flow rate was 0.6 mL/min and the run time was 60 minutes. PolyCALTM PEO standards ($M_n=24$ kDa, PDI=1.01, Malvern) was used for calibration. The copolymer composition was determined by ^1H NMR analysis performed with a Gemini 400 MHz spectrometer (Varian Associates Inc., NMR Instruments, Palo Alto, CA) in D_2O . The ratio HPMA-DMAE/PDTEMA/AzEMAm was determined by comparison of the integrals at δ 4.3 ppm (bs, OCH₂CH₂, HPMA-DMAE), δ 7.69 ppm (bs, pyridyl group proton, PDTEMA) and δ 3.14-3.51 ppm (m, CH₂CH₂N₃, AzEMAm) (δ 4.3/ δ 7.69/ δ 4.08/2).

Synthesis of PEG-BCN and BCN-PEG-Cy5

NH_2 -PEG₅₀₀₀-COOH (100 mg, 0.02 mmol, 1 equiv), and cyclooctyne-NHS (BCN-NHS; 9.0 mg, 0.024 mmol, 1.2 equiv) and triethylamine (8.5 μL , 0.06 mmol, 3 equiv) were dissolved in 1.3 mL DMSO, the reaction mixture was stirred at room temperature overnight. The final product was precipitated in cold ether twice, then dissolved in milliQ water, followed by dialysis against water (MWCO: 3000) for 2 days. After filtration and freeze-drying, the polymer was obtained as a white powder. Yield 90 mg, 85.7%. ^1H NMR (400 MHz, DMSO): δ = 7.05(s, 1H; OC(=O)NH), 7.05(s, 1H; C=ONH), 4.52 (t, 2H; PEG-OH), 4.00 (d, 2H; BCN-CH₂-O(=O)), 3.66 (t, 2H; PEG-CH₂), 3.48 (bs, 440H; PEG), 3.04 (s, 2H; OCONHCH₂), 2.90 (s, 2H; C=ONHCH₂), 2.0-2.21(m, 4H; CH₂C(=O)NH₂, alkane), 1.99 (m, 2H; NHCH₂CH₂), 1.69-1.41 (m, 6H; alkane), 1.54-1.13 (m, 1H; alkane), 0.80-0.71 (m, 2H; alkane) (Figure S3).

To conjugate Cy5 to PEG-BCN, 50 mg of PEG-BCN (0.0095 mmol) was first dissolved in 1 mL DMSO, 2.34 mg of dicyclohexylcarbodiimide (DCC, 0.0114 mmol) and 1.32 mg of N-hydroxysuccinimide (NHS, 0.0114 mmol) were added and stirred for 4 h at room temperature. Then, 7.45 mg of Cy5-amine (0.0114 mmol) and 3.48 mg of triethylamine (0.0342 mmol) were added to the mixture. After overnight reaction, the mixture was diluted with water (10 mL), followed by dialysis against water (MWCO: 3000) for another 2 days. Next, the solution was filtered with 0.2 μm filter and freeze-dried. The resulting polymer was obtained as blue powder. The success of Cy5 coupling was confirmed by ^1H NMR, and no free Cy5 was present in the conjugate as confirmed by SEC analysis.

Reaction of PEG-BCN with polymer-azide (pHDPA2)

pHDPA2 and PEG-BCN were separately dissolved in 10 mM HEPES buffer (pH 7.4) at a concentration of 10.0 mg/mL (4.9 mM of azide groups) and 20 mg/mL (3.7 mM of BCN groups), respectively. Samples of the polymer solution (13.2 μL) and PEG-BCN solution (17.3 μL , azide/BCN molar ratio 1:1 or 8.7 μL , azide/BCN molar ratio 2:1) were mixed and diluted with 10 mM HEPES buffer (pH 7.3) (69.5 μL or 78.2 μL). The reaction mixtures were incubated at room temperature and collected at incubation times of 0, 1, 2, 3, 4, 8, 12 and 24 h.

The collected samples were analyzed by size exclusion chromatography (SEC) described in the previous section. The unreacted PEG-BCN concentration was calculated based on RI peak

intensity using a PEG-BCN calibration curve (Figure S3d). For the sample with freeze-dry treatment, the reaction mixture (after reacted at RT after defined time as mentioned above) were rapid frozen using liquid nitrogen. The polymer was collected after freeze drying and subsequently dissolved in water (100 μ L) and analyzed by SEC. For the sample with freeze-thaw treatment, the reaction mixture (after reacted at RT after defined time as mentioned above) were frozen at -30°C for 16 hours and thawed at 4°C for two hours.

Preparation of RNA polyplexes

For the preparation of RNA polyplexes, 3-steps can be distinguished, namely complexation, post-PEGylation, and crosslinking (Figure. 1a). In a typical example, polyplexes were prepared at N/P molar ratio of 4, with RNA concentration of 100 $\mu\text{g}/\text{mL}$. pHDDPA2 and BCN-PEG were first dissolved in 10 mM HEPES buffer, pH 7.4 with a concentration of 10 mg/mL . Next, 28.8 μL of pHDDPA2 was diluted with 100 μL HEPES buffer and the resulting solution was added to 260 μL ssRNA (60 μg , HEPES buffer) solution, vortexed for 5 s and incubated on ice for 10 minutes. Next, 76.4 μL of BCN-PEG was added to the polyplex mixture and incubated at room temperature for 2 h. Polyplexes were subsequently crosslinked by addition of 14.5 μL dithiothreitol (DTT, 5 mM dissolved in water) corresponding with a half molar equivalent to PDS groups of pHDDPA2, for 1 h at room temperature. After addition of 60 μL sucrose (50% in water) to a final concentration 5% and 15.6 μL NaCl (5 M in water) to a final salt concentration of 150 mM, the polyplexes were frozen in liquid nitrogen and freeze-dried. The obtained cake was resuspended in RNAase-free water (600 μL , final RNA concentration of 100 $\mu\text{g}/\text{mL}$) for further use.

4

Determination of the content of free pHDDPA2 in RNA polyplexes dispersion

pHDDPA2/RNA polyplexes (100 $\mu\text{g}/\text{mL}$) without PEGylation and crosslinking were formulated in 500 μL 10 mM HEPES or PBS buffer at N/P ratios from 2 to 12 as described above. After complexation and incubation at room temperature for 10 minutes, the polyplex dispersion was added to 50 μL NaCl (1.65 M) for 4 h incubation to cause polyplexes aggregation, followed by centrifugation (15,000 rpm for 60 mins) to pellet the aggregated polyplexes [44]. The supernatant was separated and the amount of free polymer was quantified by UV spectroscopy. Briefly, 90 μL of the supernatant was removed and combined with 10 μL of freshly prepared DTT solution (100 mM). After incubating these samples for 30 mins at room temperature, the UV absorbance at 343 nm was measured to determine the amount of free polymer. The concentration of free pHDDPA2 in the supernatant was quantified using a calibration curve of varying amount pHDDPA2 with the same treatment. The percentage of pHDDPA2 polymer associating with ssRNA using following formula: $100 - 100 * ((W_{\text{total}} - W_{\text{free}}) / W_{\text{total}})$, where W_{total} means total amount of pHDDPA2 used to prepare ssRNA polyplexes and W_{free} means amount of free pHDDPA2 in polyplexes dispersion.

Evaluation of post-PEGylation efficiency of PEG-BCN to the polyplexes (ultrafiltration methods)

An ultrafiltration method instead of Vivaspin was used, because it enables a higher recovery efficiency of BCN-PEG-Cy5 and PEGylated pHDPA (~95%), and polyplexes particles (>80%), by using polyethersulfone ultrafiltration membrane (MWCO, 300kDa). The RNA polyplexes were post-pegylated with BCN-PEG-Cy5 as mentioned above. The polyplexes dispersion (50 µg/mL) was then purified by ultrafiltration with an Amicon® selector valve with 10 mM HEPES buffer, pH 7.4, to remove unreacted BCN-PEG-Cy5. After the buffer was exchanged 10 times, the concentrate was analyzed by UV spectroscopy at wavelength 200 - 700 nm. The RNA and PEG-Cy5-BCN concentration were quantified by measuring the UV absorbance at 260 and 646 nm, respectively.

PEGylation conjugation efficiency determined by Fluorescence Correlation Spectroscopy (FCS)

The BCN-PEG-Cy5 coupling efficiency after incubation with RNA polyplexes in 10 mM HEPES pH 7.4 for 3 hours at room temperature was determined by FCS as previously described by Buyens et al.[23,36]. Briefly, FCS measurements were performed using free BCN-PEG-Cy5 ($\lambda_{\text{excitation}} = 646 \text{ nm}$ and $\lambda_{\text{emission}} = 662 \text{ nm}$) and RNA encapsulated in PEG-pHDPA polyplexes (0.5 µg/mL), on a C1si laser scanning confocal microscope (Nikon, Japan), equipped with a time-correlated single photon counting (TCSPC) data acquisition module (Picoquant, Berlin, Germany), and water immersion objective lens (Plan Apo 60 ×, NA 1.2, collar rim correction, Nikon, Japan). During the measurements, the glass bottom 96-well plate (Grainer Bio-one, Frickenhausen, Germany) was covered with adhesive plates seals (ThermoScientific, U.K.) to avoid evaporation of water. For each sample, fluorescence intensity fluctuations were recorded using Symphotime (Picoquant, Berlin, Germany), during 1 min in triplicate. Because the baseline fluorescence intensity of the fluorescence fluctuation profiles recorded by FCS is proportional to the concentration of BCN-PEG-Cy5, the percentage of conjugated and free form BCN-PEG-Cy5 can be calculated as described by Buyens et al. [36].

Particle size and zeta-potential measurements

The size of the polyplexes was measured with DLS using an ALV CGS-3 system (Malvern Instruments, Malvern, UK) equipped with a JDS Uniphase 22 mW He-Ne laser operating at 632.8 nm, an optical fiber-based detector, a digital LV/LSE-5003 correlator with temperature controller set at 25 °C. The zeta-potential (ζ) of the polyplexes was measured using a Malvern Zetasizer Nano-Z (Malvern, UK) with universal ZEN 1002 'dip' cells and DTS (Nano) software (version 4.20) at 25 °C. Polyplex measurements were performed in 10 mM HEPES pH 7.4 and a RNA concentration of 15 µg/mL.

The size distribution of the polyplexes was also determined by nanoparticles tracking analysis (NTA) using a NanoSight LM 10SH (NanoSight, Amesbury, United Kingdom), equipped with a sample chamber with a 532 nm Laser. Typically, RNA polyplexes were diluted with PBS to

a concentration of 0.5 µg/ml and measured for 120 s with manual shutter and gain adjustments. The captured videos were analyzed by the NTA 2.0 image analysis software.

Stability study using fluorescence single particle tracking (fSPT)

fSPT was performed to measure the stability of the PEG-pHDPA Cy5-RNA nanocomplexes in 10% serum. fSPT is a fluorescence microscopy technique that uses widefield and a fast and sensitive CCD camera to record movies of diffusion particles in fluids. These movies were analysed using in-house developed software, to obtain size distributions as previously described [45].

Gel retardation study

Polyplex (in)stability was studied by addition of dithiothreitol (DTT) (as reducing agent) and/or heparin (as counter polyanion) and /or serum. Two microliters of DTT (100 mM) and/or 1 µL heparin sodium salt (50 mg/mL) and/or 2.5 µL FBS were added to 20 µL of polyplex dispersion in HBS (40 µg/mL of RNA) yielding a final concentration of 10 mM DTT, 200 µg/mL heparin, and 10% serum. After 0.5 h incubation at 37 °C, for the sample incubated with 10% serum, 4 µL of 0.5M EDTA (pH 8.0) was added and the sample was then placed on ice for 10 min. Next, 20 µL of the sample was mixed with 3 µL 6×Loading Dye and loaded into 1% agarose gel in Tris-acetate-EDTA (TAE) buffer containing GelGreen (Biotium). Electrophoresis was done at 120 V for 30 min. RNA was detected using a Gel Doc™ XR + system (BioRad Laboratories Inc., Hercules, CA) with Image Lab software.

DC2.4 Maturation and cellular uptake

DC2.4 cells were seeded into 96-well plate (10^5 cells/ well) and incubated for 24 h. Cy5-mRNA_{luc} was loaded to the PEG-pHDPA nanocomplexes (N/P 4) as described above. The cells were treated with nanocomplexes (0.25 µg Cy5-RNA) for 24 hours with serum. Next, the cells were incubated with 0.4 % trypan blue-containing PBS buffer for 5 min and washed with PBS. Internalized RNA polyplexes were examined by flow cytometry (Canto II, BD). To measure the maturation level of D2.4 cells, after incubation cells with ssPolyU PEG-pHDPA nanocomplexes for 24 h, the cells were washed with FACS buffer and subsequently stained with anti-CD40-FITC and anti-CD86-PE antibodies (2 µg/mL, 50 µL per well, eBioscience) for 30 min on ice. These D2.4 cells were subsequently analyzed by flow cytometry after being washed with FACS buffer.

Mice

Female wild type C57BL/6 mice were purchased from Janvier (Le Genest Saint Isle, France). OT-I mice carrying a transgenic CD8⁺ T cell receptor specific for the MHC I-restricted ovalbumin (OVA) peptide SIINFEKL were donated by Dr. Bart Lambrecht from Ghent University (Ghent, Belgium). All mice were 7-12 weeks old at the start of the experiment and maintained under specific pathogen-free conditions. Animals were treated according to the European guidelines

for animal experimentation. All experiments were approved by the local ethical committee for animal experiments of Ghent University (Ghent, Belgium).

Drainage of Cy5-labeled ssRNA polyplexes to popliteal lymph nodes

C57BL/6 mice were subcutaneously injected with Cy5-mRNA_{luc} loaded PEG-pHDPA nanocomplexes and DOTAP ssRNA lipoplexes using DOTAP/DOPE at N/P ratio of 1 (Avanti Polar Lipids, Alabaster, AL, USA), referred as DOTAP ssRNA, in the footpad. The injected dose of RNA was 5 µg (20 µl in 5% glucose HBS buffer). Popliteal lymph nodes were isolated 24 hours post injection and analysed by flow cytometry. Cells were stained with α-CD16/CD32 (BD Biosciences, San Diego, CA, USA) to block non-specific FcR binding, and with Live/Dead Fixable Aqua stain (Invitrogen) to eliminate dead cells. Antibodies used were MHC-II-FITC, α-CD11c PerCP-Cy5.5, α-F4/80 PerCP (all BD Biosciences, San Diego, CA, USA). Analysis was performed on a triple-laser (B-V-R) LSR-II (Becton Dickinson, San Jose, CA, USA) followed by FlowJo (Treestar, OR) data processing.

CD8⁺ T cell dextramer staining

Subcutaneous immunizations were performed in C57BL/6 mice twice at tail base in a 3 week interval (Figure 5a). Ten µg of ssPolyU loaded PEG-pHDPA nanocomplexes or DOTAP/DOPE lipoplexes (as mentioned above), together with 10 µg soluble OVA protein (InvivoGen) in a total volume of 40 µl of 5% glucose in water (Ambion, Life technologies, USA). The formulations were injected at tail base of the mice. Five days after last boost injections, blood samples were taken and red blood cells were removed using ACK lysis buffer (BioWhittaker, Walkersville, MD, USA). Cells were stained with α-CD16/CD32 (BD Biosciences, San Diego, CA, USA), Live/Dead Fixable Aqua stain (Invitrogen), α-CD8 PerCP, α-CD3 Pacific blue, α-CD19 APC-Cy7 (all BD Biosciences, San Diego, CA, USA) and MHC dextramer H-2 K_b/SIINFEKL-PE (Immudex, Copenhagen, Denmark).

Cytotoxic T Lymphocyte activity *in vivo*

Mice immunized with different formulations were same as described above. Two weeks after last boost injection, mice were injected intravenously with 1.5×10^7 target splenocyte cells. Splenocytes were pulsed with 1 µg/ml of MHC-I OVA peptide (SIINFEKL, Invitrogen) or HIV-1 Gag peptide (AnaSpec) as a control before labelling with 5 µM (Termed CFSE^{hi}) or 0.5 µM (termed CFSE^{low}) 5-(and 6)-carboxyfluorescein diacetate succinimidyl ester (CFSE, Invitrogen), respectively. Labeled cells were mixed at a 1:1 ratio and were adoptively transferred into immunized mice. Two days later, splenocytes from host mice were analysed by flow cytometry after staining with α-F4/80 (BD Biosciences, San Diego, CA, USA) to exclude auto-fluorescent macrophages. Percentage antigen-specific killing cells was determined using the following formula: $100 - 100 * ((\% \text{ CFSE}^{\text{hi}} \text{ cells} / \% \text{ CFSE}^{\text{low}} \text{ cells})^{\text{immunized mice}} / (\% \text{ CFSE}^{\text{hi}} \text{ cells} / \% \text{ CFSE}^{\text{low}} \text{ cells})^{\text{non-immunized mice}})$.

Measurement of Ab titers

To measure the OVA specific Ab titers, 96-well plates were coated with 100 μl of a 10 $\mu\text{g}/\text{ml}$ OVA solution overnight at 4 $^{\circ}\text{C}$. The plates were washed (1×5 min) with washing buffer (PBS containing 0.05% Tween 20) and incubated for 2 h with blocking buffer (PBS containing 2% BSA and 0.05% Tween 20). After blocking, the plates were incubated with 5-fold serially diluted (blocking buffer) serum starting with a dilution of 1:50 for 2 h. To detect bound antibodies, the plates were washed (3×5 min) and incubated for 1 h with HRP-conjugated anti-mouse total IgG1 and IgG2c Ab (Southern Biotech, Birmingham, AL) with a dilution of 1:3000 in blocking buffer. After the plates were washed (3×5 min), 100 μl TMB substrate solution (Sigma-Aldrich, The Netherlands) was added to each well to initiate the color reaction at room temperature in the dark for 30 minutes. The reaction was stopped with 2 N H_2SO_4 (50 $\mu\text{L}/\text{well}$), and the OD was measured at a wavelength of 450 nm (OD_{450}).

| Results and discussion

Polymer synthesis and characterization

2-Azidoethylmethacryl amide (AzEMAm) (Scheme S1a, Fig. S2) was used to introduce azide moieties in the copolymer structure to enable post polyplex modification using click chemistry. A series of pHDPAs with different number of azide units were synthesized by free radical polymerization in dry DMSO (at a fixed monomer/initiator molar ratio of 50/1) (Fig. 1a and Fig. S1). The characteristics of the synthesized polymers (molecular weights determined by SEC and compositions determined by ^1H NMR (Fig. S1b)) are shown in Table S1. This table shows AzEMAm content of the copolymers is higher than that in the feed (feed: 5 to 20 mol%, copolymer contents: 17 to 27 mol%). The incorporation of pyridine disulfide groups (PDS) in the obtained polymers was determined by NMR analysis and was in agreement with the values obtained by UV spectroscopy, used to calculate the amount of dithiothreitol (DTT) needed to crosslink the polyplexes. Table S1 also shows that the molecular weights of the obtained polymers were around the same (~ 10 kDa). pHDPA2 has highest amount of PDS groups of the three polymers, which are favourable for high cross-link density, and enough moieties of azide (~ 10 units per polymer chain) for post-PEGylation; this polymer was therefore selected for the further studies.

The clickable PEG-BCN was synthesized by coupling (1R,8S,9s)-Bicyclo[6.1.0]non-4-yn-9-ylmethyl N-succinimidyl carbonate (BCN-NHS) to the amine group of the distal end of a PEG chain ($M_n \sim 5000$ Da) (Scheme S1b), as confirmed by ^1H NMR analysis (Fig. S3). The coupling efficiency between PEG-BCN and azide containing pHDPA (pHDPA2) was studied at room temperature in aqueous solution (10 mM HEPES, pH 7.4). The conjugation was confirmed by FTIR analysis (Fig. S4; disappearance of the N_3 vibration at 2130 cm^{-1}) and quantified by size exclusion chromatographical (SEC) analysis (Fig. S5). The conjugation efficiency of pHDPA and PEG-BCN was time (Fig. 1c) and concentration (Fig. S5b) dependent. These figures show that a higher coupling degree was reached at higher concentration and longer incubation time. At BCN/ N_3 molar ratio of 1/1, after 3 h incubation with a reactant concentration of 64.5 μM ,

the conjugation efficiency was 33%. Interestingly, it was found that freeze-drying of the reaction mixture accelerated the conjugation efficiency (Fig. 1c). After a 1 h reaction at room temperature followed by a freeze-drying treatment, the conjugation ratio was 80%, whereas it was only 17% before freeze-drying. The higher conjugation efficiency is likely caused by the increased micro-environmental reactant concentration as a consequence of the freeze-drying process, which leads to a high chance of coupling. It should be mentioned, the conjugation efficiency was also increased by only freeze-thawing (freeze at $-30\text{ }^{\circ}\text{C}$ and thaw at $4\text{ }^{\circ}\text{C}$) the reactant mixture (Fig. S5c), which is in line with previously published results of the reaction of azide modified siRNA and dibenzocyclooctyne (DBCO) modified PEG [46].

PEG-pHDPA ssRNA nanocomplexes preparation and characterization

PEG-pHDPA ssRNA nanocomplexes were formed via a three steps process as illustrated in Fig. 1a. We first evaluated the self-assembly behaviour of pHDPA and ssRNA (step a). It was shown that ssRNA was completely bound to the polymer at nitrogen/phosphate (N/P) ratios above 1 (Fig. S6a). ssRNA release upon the addition of negatively charged heparin proved that ssRNA complexation is reversible. To obtain particles with a small size, an N/P ratio of 4 instead of 2 was selected for further studies, resulting polyplexes of around 150 nm with zeta potential of 16 mV (Fig. S6b). In step b, the ssRNA polyplexes were post-modified with PEG-BCN. As shown in Fig. S7a, the zeta potential of the polyplexes decreased as a function of time upon incubation with PEG-BCN due to shielding of the surface charge of the particles by the coupled PEG chains. The zeta potential remained stable after 2 hours incubation ($\sim 10\text{ mV}$), indicating

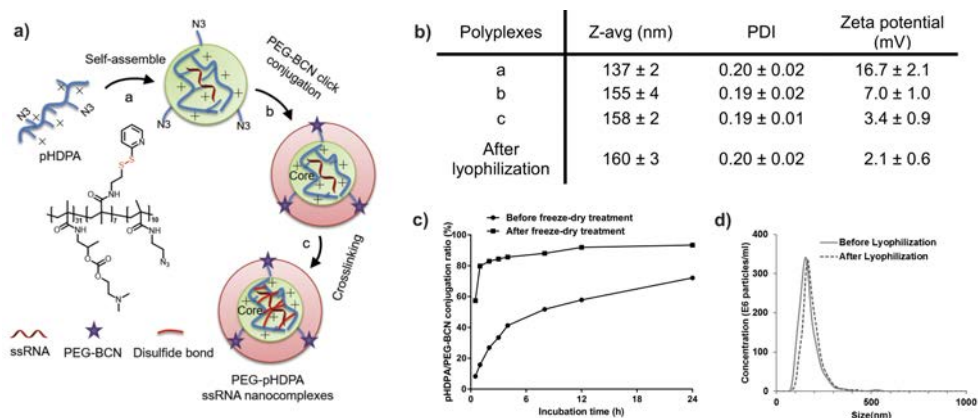


Fig. 1. Preparation and characterization of PEG-pHDPA ssRNA nanocomplexes. a) Schematic illustrations of polyplex preparation: (a) self-assembling of the cationic polymer pHDPA and ssRNA; (b) PEG-BCN was clicked on pHDPA polyplexes; (c) crosslinking the polymer chains via the addition of dithiothreitol (DTT). b) Size and zeta-potential of ssRNA polyplexes for each preparation step ($n=3$). c) pHDPA and PEG-BCN conjugate efficiency at room temperature at concentration of $64.5\text{ }\mu\text{M}$ for both reactants. d) Size distribution of PEG-pHDPA ssRNA polyplexes before and after lyophilisation/rehydration measured in PBS buffer by Nanosight. The polyplexes were prepared at N/P molar ratio of 4/1 with a final ssRNA concentration of $100\text{ }\mu\text{g/mL}$.

the post-PEGylation was completed. Conversely, incubation with non-functionalized PEG had no effect on the zeta potential, which means that the shielding was indeed due to the covalent coupling of PEG chains to the surface of the polyplexes. Different amount of PEG-BCN were added to polyplexes to establish under which conditions the surface charge of polyplexes was efficiently shielded with a minimum unreacted amount of BCN-PEG in solution. Fig. S7b shows that at PEG-BCN/ N_3 molar ratios above 0.6, no further reduction of the zeta potential (~ 10 mV) was observed (3 hours incubation). Therefore, a PEG-BCN/ N_3 ratio of 0.6 was chosen for further experiments. Previous studies demonstrated that disulfide crosslinked polyplexes have a better colloidal stability than their non-crosslinked counterparts, even in the presence of serum [47,48]. In step c, DTT was added at half molar equivalent to the pyridine disulfide groups of the polymer to induce self-crosslinking via disulfide bonds formation [49]. This final step yielded PEGylated and crosslinked polyplexes with near neutral surface charge and a diameter of 158 nm (Fig. 1b). Notably, the polyplexes' PDI (~ 0.2) and intensity of the scattered light (data not shown) remained stable during this step, proving that crosslinking of the polyplexes resulted in neither destabilization nor aggregation of the polyplexes. Importantly, the size of PEG-pHDPA ssRNA nanocomplexes was similar before and after lyophilization (Fig. 1b&d) and this dry powder form could be stored at 4 °C for at least 4 weeks without negatively affecting its size and size distribution after rehydration of the polyplexes in buffer.

To quantify the amount of PEG coupled to the ssRNA polyplexes, we first determined the amount of free cationic polymer pHDAP2 in the polyplex dispersion. It has been well documented that for most polyplex formulations, free polymer chains are present in the dispersion [44,50–52]. Here we used precipitation method (by incubating ssRNA polyplexes with 150 mM NaCl to cause polyplexes aggregation followed by centrifugation) combined with UV analysis to determine the content of uncomplexed pHDPA chains in the ssRNA polyplex dispersion. As shown in Fig. S8, around 60% of pHDPA associated with ssRNA when the polyplexes were prepared at N/P molar ratio of 4. With correction for amount of free polymer present in the polyplexes dispersion, the conjugation efficiency of the PEG-BCN and the pHDPA/ssRNA polyplexes was determined via ultrafiltration method using Cy5-labeled PEG-BCN (Scheme S1b). It is noted that after ultrafiltration, the polyplexes size and PDI were stable (data not shown). By measuring the UV absorbance of Cy5 and ssRNA in the concentrate, the amount of PEG-BCN coupled to the polyplexes surface was calculated and it turned out that around 15 mol% of the azide groups of the polyplexes was successfully modified with PEG-BCN (Fig. S9a). This means that on the average each polymer had been modified with 1.5 units of PEG. To further verify the PEG conjugation efficiency by post-PEGylation, fluorescence correlation spectroscopy (FCS) analysis was applied (Fig. S9b).[53] After incubation of the polyplexes with BCN-PEG-Cy5, the decrease of the fluorescence signal of Cy5 pointing to the coupling of BCN-PEG-Cy5 to the ssRNA polyplexes. After 3 hours incubation, the conjugation efficiency was calculated to be around 17%, which is in good agreement with the results of Fig. S9a ($\sim 15\%$).

PEG-pHDPA ssRNA nanocomplexes stability

The stability and nuclease resistance of PEG-pHDPA ssRNA nanocomplexes was investigated in the presence of serum using fluorescence single particle tracking (fSPT) analysis and a gel retardation assay (Fig. 2). fSPT is a microscopy technique that allows to visualize the movement of individual fluorescently labelled nanoparticles in a certain medium [54,55]. As shown in Fig. 2a, the size distribution of polyplexes formulated with Cy5-labeled ssRNA did not show significant changes after two hours incubation in 10% serum, which demonstrates an excellent colloidal stability of these PEGylated polyplexes. Agarose gel retardation study was conducted to test whether the loaded ssRNA in the polyplexes is protected against degradation by RNases present in serum. Fig. 2b shows that after incubation of the polyplexes with 10% serum, the ssRNA band of PEG-pHDPA nanocomplexes was detected on the top (lane 7). In contrast, naked ssRNA was fully degraded during the same conditions (lane 6). Besides, DTT (10 mM) was added to ssRNA polyplexes to break the disulfide bonds of the crosslinks. Fig. 2b (lane 3) shows that only part of the entrapped ssRNA was released in the presence of DTT. Likely, the non-crosslinked cationic polymers still complexed ssRNA. Indeed, when heparin (as counter polyanion) was added, the pHDPA/ssRNA nanocomplexes dissociated and ssRNA was fully released (lane 4).

In vitro DCs cellular uptake and maturation

To fulfil its role as an adjuvant, ssRNA needs to reach the endosomal compartment of DCs where it can trigger TLR7/8 [56]. When the crosslinked ssRNA polyplexes without PEG coating were prepared (similar procedure as Fig. 1a without step b), severe aggregation of polyplexes

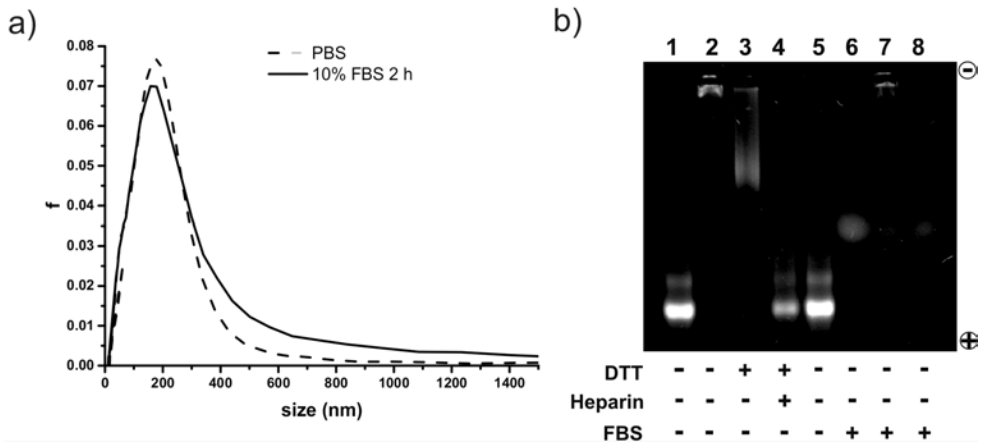


Fig. 2. Stability and nuclease resistance of PEG-pHDPA ssRNA nanocomplexes. a) Size distribution of PEG-pHDPA polyplexes of Cy5-mRNA_{luc} after incubation with 10% of serum at 37 °C for 2 hours measured via fSPT. b) Agarose gel retardation assay of PEG-pHDPA ssRNA nanocomplexes with different treatments. Polyplexes were incubated with 10 mM DTT or 10% FBS for 0.5 hour at 37 °C and subsequently incubated with heparin (final concentration of 200 µg/mL) before loading into the agarose gel. Lane 1&5-6: naked ssRNA; Lane 2-4&7: PEG-pHDPA ssRNA polyplexes; Lane 8: 10% FBS only.

4

was observed, which may be due to the inter-polyplexes crosslinking after DTT addition. Therefore, benchmark DOTAP ssRNA lipoplexes (~250 nm with zeta potential -20 mV) were used as a control. The cellular uptake of non-complexed (free) ssRNA, and PEG-pHPDA ssRNA nanocomplexes by DC2.4 cells was investigated using Cy5 labelled ssRNA. Flow cytometric analysis as well as confocal imaging revealed a strong internalization of ssRNA by DCs in the form of DOTAP and PEG-pHPDA nanocomplexes, while low uptake of ssRNA in its free form was observed (Fig. 3a&b). As shown in Fig. 3b, a higher cellular uptake of DOTAP ssRNA lipoplexes compared to PEG-pHPDA ssRNA nanocomplexes was observed, which may be due to the bigger size of the lipoplexes than the polyplexes (250 vs 150 nm; particle size plays an important role in DCs cellular uptake [57]). The confocal images were analyzed for colocalization of Cy5-labeled ssRNA and LysoTracker using ImageJ software (Fig. S10). The obtained results demonstrate that most of PEG-pHPDA nanocomplexes were trapped in organelles such as late endosome/lysosomes as evident from their colocalization with the green organelles, compared with DOTAP ssRNA lipoplexes (Pearson's colocalization coefficient: 0.70 vs 0.15 for PEG-pHPDA ssRNA nanocomplexes and DOTAP ssRNA lipoplexes, respectively). This might be ascribed to the low buffering capacity of pHPDA ($pK_a \sim 9.5$) [58] at pH values of the late endosome/lysosomes. Therefore, PEG-pHPDA ssRNA nanocomplexes will be retained in the endosome after cellular endocytosis. On the other hand, the DOTAP lipoplexes are taken up by DCs via macropinosomes and eventually merge with acidic lysosomal compartment [9,59]. The endosomal TLRs7/8 are crucial sites of interaction with ssRNA for immune stimulation, and consequently the trapped PEG-pHPDA ssRNA nanocomplexes in the endosomes enhanced the immune-stimulatory activity of ssRNA (Fig. 3c). This figure indeed shows that PEG-pHPDA ssRNA nanocomplexes evoked DCs maturation by upregulating of CD40 and CD86 expression on the surface of DC2.4 cells. Considering that both naked ssRNA and soluble PEG-pHPDA failed to significantly activate DC maturation, PEG-pHPDA ssRNA nanocomplexes caused a pronounced upregulation of CD40 and CD86, which strictly is ascribed to the ssRNA loaded in the polyplexes that is released after cellular endocytosis and subsequent disulphide bonds reduction [60–63]. Importantly, PEG-pHPDA ssRNA nanocomplexes were equally potent in activation of DCs as the benchmark DOTAP ssRNA lipoplexes (Fig. 3c).

PEG-pHPDA ssRNA nanocomplexes targeting to lymph node DCs

The induction of effector T cell responses relies on the presentation of antigens by activated DCs to T cells in the draining lymph nodes. Potency of vaccines is consequently considered to benefit from strategies that augment adjuvant uptake by DCs in the draining lymph nodes, or alternatively, DCs take up the adjuvant/vaccine at the site of injection (e.g. subcutaneous injection) and then drain to the lymph nodes [64]. To investigate whether ssRNA delivery in the form of PEG-pHPDA RNA nanocomplexes would augment ssRNA uptake by lymph node DCs, we used a fluorescently labelled (Cy5) ssRNA enabling the assessment of ssRNA uptake efficiency by lymph node DCs. Cy5-ssRNA was injected either non-complexed or loaded into both PEG-pHPDA ssRNA nanocomplexes and DOTAP ssRNA lipoplexes. One day

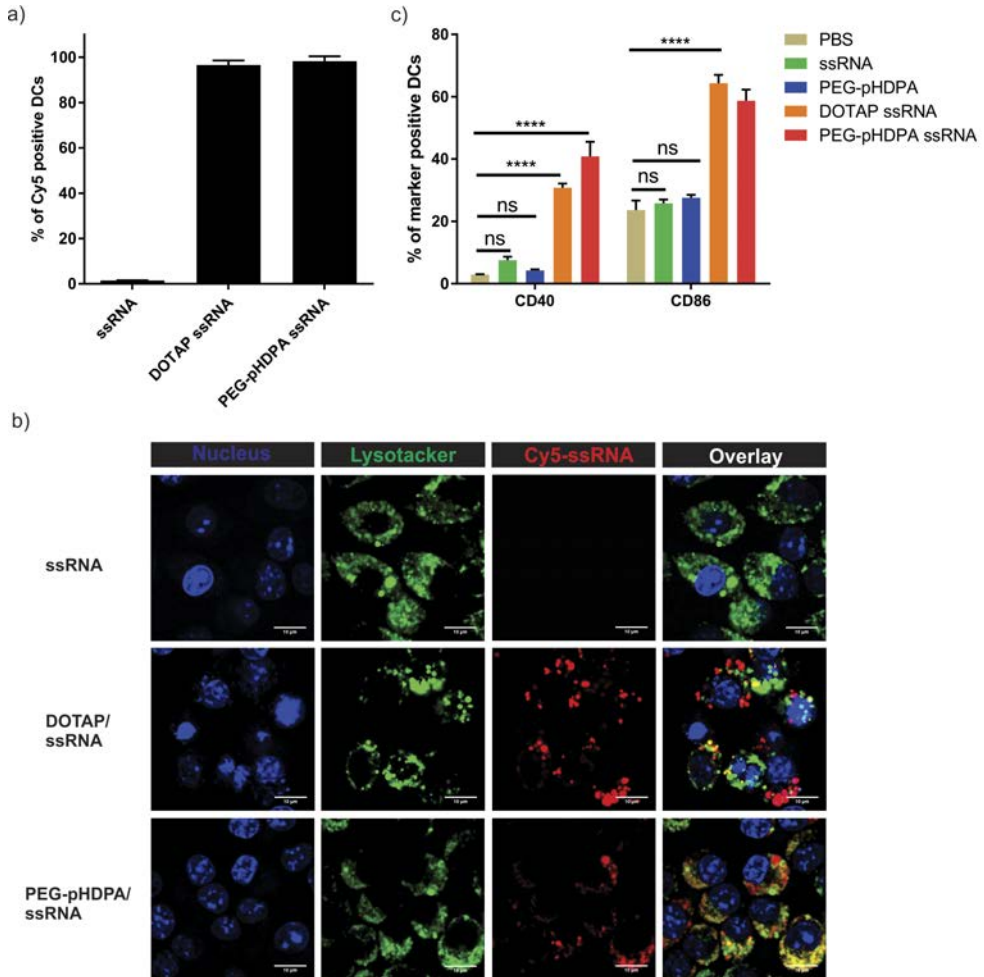


Fig. 3. Internalized ssRNA nanocomplexes promote DCs maturation *in vitro*. a) DC2.4 dendritic cells were incubated for 24 hours with 0.25 μg Cy5-ssRNA in its free form, complexed with DOTAP, and loaded in PEG-pHDPA nanocomplexes followed by flow cytometric analysis. b) Representative confocal laser scanning images of DC2.4 cultured with indicated formulation for 24 hours, bar indicated 10 μm. Yellow puncta in the overlay images indicate colocalization of ssRNA and lysotracker. c) Percentages of DC2.4 cells expressing CD40 and CD86 in response to incubation 24 h with PBS, ssRNA, PEG-pHDPA, DOTAP ssRNA and PEG-pHDPA ssRNA (herein, ssPolyU were used to form polyplexes). Two-way ANOVA analysis followed by Bonferroni multiple comparison tests (**** $p < 0.0001$).

after injection, draining popliteal lymph nodes were isolated and analysed by flow cytometry (Fig. S11). DCs were identified based on their expression of CD11c and MHCII and further subdivided into MHCII^{int} DCs (blue population) and MHCII^{hi} DCs (red population) (Fig. 4). Injection of ssRNA loaded in PEG-HDPA polyplexes resulted in a marked increase in numbers (and thus percentages) of lymph node DCs that contained ssRNA when compared to non-

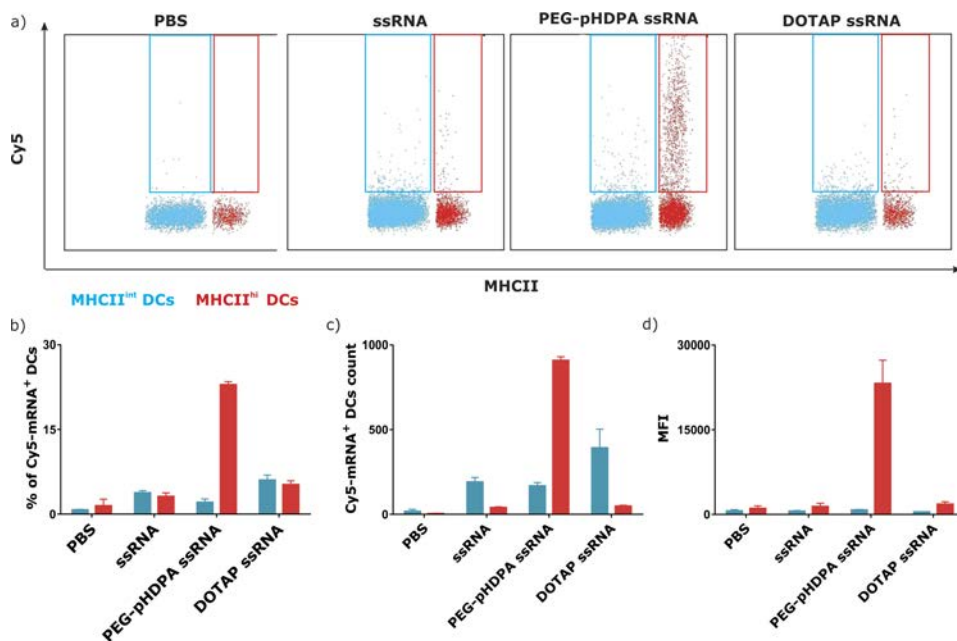


Fig. 4. ssRNA nanocomplexes efficiently target dendritic cells inside lymph nodes *in vivo*. Mice were s.c. injected in the footpad with PBS, 10 μ g of uncomplexed ssRNA or the equivalent dose of ssRNA complexed in PEG-pHDPA ssRNA nanocomplexes or DOTAP ssRNA lipoplexes. 24 Hours after injection, popliteal lymph nodes were isolated and prepared for flow cytometric analysis. DCs (CD11c+ MHCII+) were subdivided into MHCII^{hi} DCs (red population) and into MHCII^{int} DCs (blue population) and analysed for Cy5-labeled ssRNA uptake. a) Representative flow cytometry plots. b) Percentage of Cy5-positive MHCII^{hi} DCs and MHCII^{int} DCs. c) Total cell count of Cy5-positive DCs. d) Mean fluorescence intensity (MFI) of the Cy5-signal of all Cy5-positive DCs. Data are presented as means \pm SD of 5 mice/group.

formulated ssRNA or to DOTAP ssRNA lipoplexes (Fig. 4a-c). The low accumulation of DOTAP ssRNA lipoplexes in lymph nodes can likely be ascribed to their particle size (\sim 250 nm), since it has been shown that liposomes larger than 170 nm show poor lymphatic disposition [65]. Administration of PEG-pHDPA RNA nanocomplexes did not only result in higher numbers of Cy5-labeled ssRNA positive DCs in the draining lymph node, but also strongly increased the copies number of ssRNA endocytosed by DCs on a cell-per-cell basis as measured by the mean fluorescence intensity in the Cy5 channel (Fig. 4d). Most DCs that had internalized Cy5-ssRNA displayed a MHCII^{hi} phenotype corresponding to mature DCs (Fig. 4a&b). Such MHCII^{hi} DCs likely correspond to skin DCs that have migrated to the popliteal lymph nodes after ingestion of the PEG-pHDPA ssRNA nanocomplexes at the injection site. Alternatively, they also might represent lymph node resident DCs that have ingested the PEG-pHDPA ssRNA nanocomplexes (transported from the site of injection to these lymph nodes) and upregulated their MHCII expression. Taken together, the data of Fig. 4 shows that formulating the RNA into PEG-pHDPA ssRNA nanocomplexes substantially increases the amount of ssRNA in the target cell population - DCs - at the relevant site of T cell priming, the draining lymph node.

PEG-pHDPA ssRNA nanocomplexes promote adaptive immunity against co-delivery antigens

Inspired by the efficiently delivery of ssRNA to the draining lymph node (Fig. 4), the immunostimulating capacity of PEG-pHDPA ssRNA nanocomplexes *in vivo* was assessed by co-injection of these polyplexes with the soluble model antigen ovalbumin (OVA). Mice were immunized in accordance to the prime boost schedule shown in Fig. 5a. Soluble OVA was injected as saline solution or adjuvanted with respectively free ssRNA, DOTAP ssRNA lipoplexes or PEG-pHDPA ssRNA nanocomplexes. To exclude any adjuvant effects of the pHDPDA and PEG, mice were immunized with OVA admixed with PEG-pHDPA without ssRNA. Six days after the booster immunization, blood was collected and the percentages OVA-specific CD8⁺ T cells were determined via flow cytometry. As shown in Fig. 5b, solely PEG-pHDPA ssRNA nanocomplexes significantly amplified the percentages of OVA-specific CD8⁺ T cells responses in the blood. Induction of cytolytic T cells was further assessed through an *in vivo* killing assay. In brief, mice were challenged two weeks after the second boost with a 1:1 ratio of OVA peptide-pulsed CFSE^{hi} splenocytes (target cells) and non-pulsed CFSE^{low} splenocytes (non-target cells) (Fig. 5a). Two days later, spleens were isolated and the ratio of target versus non-target cells was analysed by flow cytometry. Mice that received OVA co-delivered with pHDPDA showed no significant improvement in cytolytic T cell responses compared to mice injected with soluble OVA only (Fig. 5c), arguing against intrinsic adjuvant effects of the soluble polymer itself. When compared to mice immunized with OVA in PBS only, administration of free ssRNA did not cause a statistical significance increased cytolytic T cell response in immunized mice. Fig. 5b-e shows that injection of soluble OVA in PBS resulted in a very low immune response. Therefore, the observed antigen specific killing in some mice and Ab response in all mice are very likely due to the adjuvanticity of ssRNA. Significant increases in cytolytic responses were evoked by co-administration of OVA with DOTAP ssRNA lipoplexes, but importantly, the most robust cytolytic T cell responses were clearly achieved when using PEG-pHDPA ssRNA nanocomplexes as adjuvant. The humoral immune responses using ssRNA as an adjuvant was also investigated. Mice immunized with ssRNA as adjuvant - regardless of the format the ssRNA was delivered into - showed a strong increase in IgG1 titers (Fig. 5d). Loading of ssRNA into PEG-pHDPA nanocomplexes strongly promoted antibody isotype switching to IgG2c - a feature dependent of IFN- γ and indicative for the induction of Th1 immunity [66]. As can be appreciated from Fig. 5e, PEG-pHDPA ssRNA nanocomplexes were more potent at instigating IgG2c compared to free or DOTAP complexed ssRNA.

| Conclusions

In summary, we have developed and demonstrated an alternative way to post-functionalize polyplexes via copper-free click chemistry. After post-PEGylation, the near neutral polyplexes were colloidal stable and able to protect the RNA against enzymatic degradation. PEG-pHDPA ssRNA nanocomplexes were efficiently taken up by DCs and promote DC maturation *in vitro*. More importantly, up to 25-30% of DCs in the lymph nodes had internalized the ssRNA

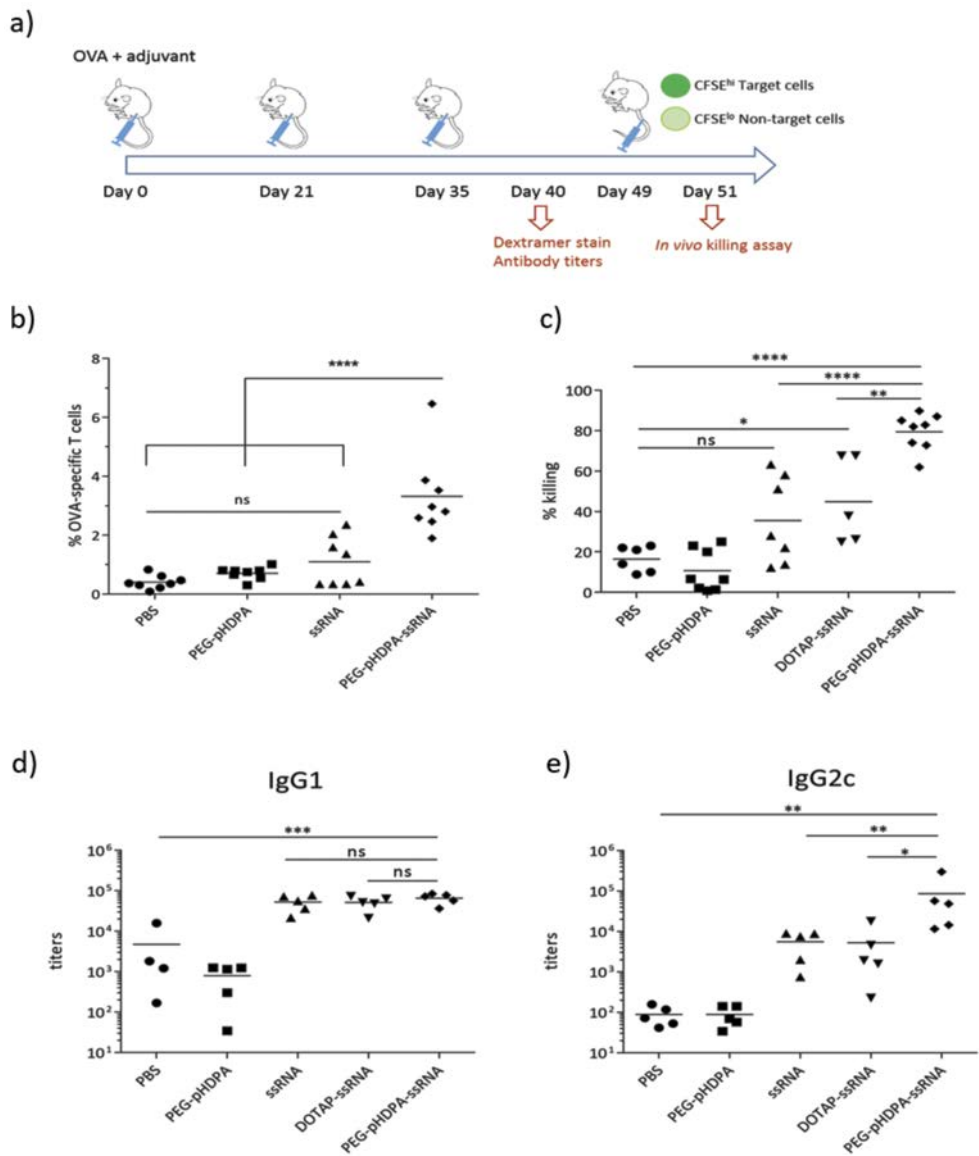


Fig. 5. Adaptive immune responses evoked by PEG-pHDPA ssRNA nanocomplexes adjuvanted protein vaccination. a) Immunization schedule and experimental set up. b) Percentages of OVA-specific CD8+ T cells induced by immunization with the indicated OVA/adjuvant formulations. Data are shown as means of 8 mice per group. c) Specific killing of target cells in response to each vaccine formulation. % killing was calculated using the formula: $100 - 100 \times ((CFSE^{high}/CFSE^{low})_{immunized\ mice} / (CFSE^{high}/CFSE^{low})_{non-immunized\ mice})$. Data are shown as means of 6-8 mice/group. Antibody titers of IgG1 (d) and IgG2c (e) as measured by ELISA in response to the indicated OVA/adjuvant formulations. Data are shown as means of 4-5 mice per group. * $p < 0.05$; ** $p < 0.01$; *** $p < 0.001$; **** $p < 0.0001$ (one-way ANOVA).

nanocomplexes, and thereafter were able to efficiently promote adaptive immunity against co-delivered antigens, which points that PEG-pHDP A ssRNA nanocomplexes are an attractive candidate as novel adjuvant.

| Conflict of interest

The authors declare no competing financial interest.

| Acknowledgments

Bo Lou was funded by China Scholarship Council. This work was supported by grants from the UGhent Concerted Research Consortium BOF12/GOA-B/12424/01, the Fund for Scientific Research Flanders project G.0226.10. De Beuckelaer A. acknowledges IWT (Agentschap voor innovatie door wetenschap en technologie, Vlaanderen) for a PhD scholarship.

| References

1. R.L. Coffman R.L. et al. Vaccine adjuvants: Putting innate immunity to work, *Immunity*. 33 (2010) 492–503.
2. W.C. Koff, D.R. Burton, P.R. Johnson, B.D. Walker, C.R. King, G.J. Nabel, R. Ahmed, M.K. Bhan, S.A. Plotkin, Accelerating next-generation vaccine development for global disease prevention, *Science*. 340 (2013) 1232910–1232910.
3. R. Arens, T. van Hall, S.H. van der Burg, F. Ossendorp, C.J.M. Melief, Prospects of combinatorial synthetic peptide vaccine-based immunotherapy against cancer, *Semin. Immunol.* 25 (2013) 182–190.
4. R.J. Mancini, L. Stutts, K.A. Ryu, J.K. Tom, A.P. Esser-Kahn, Directing the immune system with chemical compounds, *ACS Chem. Biol.* 9 (2014) 1075–1085.
5. K. Kastenmüller, U. Wille-Reece, R.W.B. Lindsay, L.R. Trager, P.A. Darrach, B.J. Flynn, M.R. Becker, M.C. Udey, B.E. Clausen, B.Z. Igyarto, D.H. Kaplan, W. Kastenmüller, R.N. Germain, R.A. Seder, Protective T cell immunity in mice following protein-TLR7/8 agonist-conjugate immunization requires aggregation, type I IFN, and multiple DC subsets, *J. Clin. Invest.* 121 (2011) 1782–1796.
6. R. Heidenreich, E. Jasny, A. Kowalczyk, J. Lutz, J. Probst, P. Baumhof, B. Scheel, S. Voss, K.J. Kallen, M. Fotin-Mleczek, A novel RNA-based adjuvant combines strong immunostimulatory capacities with a favorable safety profile, *Int. J. Cancer*. 137 (2015) 372–384.
7. A. Kowalczyk, F. Doener, K. Zanzinger, J. Noth, P. Baumhof, M. Fotin-Mleczek, R. Heidenreich, Self-adjuvanted mRNA vaccines induce local innate immune responses that lead to a potent and boostable adaptive immunity, *Vaccine*. 34 (2016) 3882–3893.
8. S.S. Diebold, T. Kaisho, H. Hemmi, S. Akira, C. Reis E Sousa, Innate Antiviral Responses by Means of TLR7-Mediated Recognition of Single-Stranded RNA, *Science*. 303 (2004) 1529–1531.
9. L.M. Kranz, M. Diken, H. Haas, S. Kreiter, C. Loquai, K.C. Reuter, M. Meng, D. Fritz, F. Vascotto, H. Hefesha, C. Grunwitz, M. Vormehr, Y. Hüsemann, A. Selmi, A.N. Kuhn, J. Buck, E. Derhovanessian, R. Rae, S. Attig, J. Diekmann, R.A. Jabulowsky, S. Heesch, J. Hassel, P. Langguth, S. Grabbe, C. Huber, Ö. Türeci, U. Sahin, Systemic RNA delivery to dendritic cells exploits antiviral defence for cancer immunotherapy, *Nature*. 534 (2016) 396–401.
10. D. Rajagopal, C. Paturel, Y. Morel, S. Uematsu, S. Akira, S.S. Diebold, Plasmacytoid dendritic cell-derived type I interferon is crucial for the adjuvant activity of Toll-like receptor 7 agonists, *Blood*. 115 (2010) 1949–1957.
11. A.E. Sköld, J.J.P. van Beek, S.P. Sittig, G. Bakdash, J. Tel, G. Schreiberl, I.J.M. de Vries, Protamine-stabilized RNA as an ex vivo stimulant of primary human dendritic cell subsets, *Cancer Immunol. Immunother.* 64 (2015) 1461–1473.
12. J.H. van den Berg, K. Oosterhuis, W.E. Hennink, G. Storm, L.J. van der Aa, J.F.J. Engbersen, J.B.A.G. Haanen, J.H. Beijnen, T.N. Schumacher, B. Nuijen, Shielding the cationic charge of nanoparticle-formulated dermal DNA vaccines is essential for antigen expression and immunogenicity, *J. Control. Release*. 141 (2010) 234–240.
13. R.N. Palumbo, X. Zhong, D. Panus, W. Han, W. Ji, C. Wang, Transgene expression and local tissue distribution of naked and polymer-condensed plasmid DNA after intradermal administration in mice, *J. Control. Release*. 159 (2012) 232–239.
14. R. Tang, R.N. Palumbo, L. Nagarajan, E. Krogstad, C. Wang, Well-defined block copolymers for gene delivery to dendritic cells: Probing the effect of polycation chain-length, *J. Control. Release*. 142 (2010) 229–237.
15. J.S. Suk, Q. Xu, N. Kim, J. Hanes, L.M. Ensign, PEGylation as a strategy for improving nanoparticle-based drug and gene delivery, *Adv. Drug Deliv. Rev.* 99 (2016) 28–51.
16. S. De Koker, J. Cui, N. Vanparijs, L. Albertazzi, J. Grooten, F. Caruso, B.G. De Geest,

- Engineering Polymer Hydrogel Nanoparticles for Lymph Node-Targeted Delivery, *Angew. Chemie - Int. Ed.* 55 (2016) 1334–1339.
17. H. Jiang, Q. Wang, L. Li, Q. Zeng, H. Li, T. Gong, Z. Zhang, X. Sun, Turning the Old Adjuvant from Gel to Nanoparticles to Amplify CD8+T Cell Responses, *Adv. Sci.* 5 (2017) 1700426.
 18. C.H. Ahn, S.Y. Chae, Y.H. Bae, S.W. Kim, Synthesis of biodegradable multi-block copolymers of poly(L-lysine) and poly(ethylene glycol) as a non-viral gene carrier, *J. Control. Release.* 97 (2004) 567–574.
 19. R.J. Christie, Y. Matsumoto, K. Miyata, T. Nomoto, S. Fukushima, K. Osada, J. Hahnaut, F. Pittella, H.J. Kim, N. Nishiyama, K. Kataoka, Targeted polymeric micelles for siRNA treatment of experimental cancer by intravenous injection, *ACS Nano.* 6 (2012) 5174–5189.
 20. S. Uchida, H. Kinoh, T. Ishii, A. Matsui, T.A. Tockary, K.M. Takeda, H. Uchida, K. Osada, K. Itaka, K. Kataoka, Systemic delivery of messenger RNA for the treatment of pancreatic cancer using polyplex nanomicelles with a cholesterol moiety, *Biomaterials.* 82 (2016) 221–228.
 21. Z. Ge, Q. Chen, K. Osada, X. Liu, T.A. Tockary, S. Uchida, A. Dirisala, T. Ishii, T. Nomoto, K. Toh, Y. Matsumoto, M. Oba, M.R. Kano, K. Itaka, K. Kataoka, Targeted gene delivery by polyplex micelles with crowded PEG palisade and cRGD moiety for systemic treatment of pancreatic tumors, *Biomaterials.* 35 (2014) 3416–3426.
 22. C. Lin, J.F.J. Engbersen, PEGylated bioreducible poly(amido amine)s for non-viral gene delivery, *Mater. Sci. Eng. C.* 31 (2011) 1330–1337.
 23. P. Vader, L.J. Van Der Aa, J.F.J. Engbersen, G. Storm, R.M. Schiffelers, Physicochemical and biological evaluation of siRNA polyplexes based on PEGylated poly(amido amine)s, *Pharm. Res.* 29 (2012) 352–361.
 24. H.-K. Nguyen, P. Lemieux, S. V Vinogradov, C.L. Gebhart, N. Guerin, G. Paradis, T.K. Bronich, V.Y. Alakhov, a V Kabanov, Evaluation of polyether-polyethylenimine graft copolymers as gene transfer agents., *Gene Ther.* 7 (2000) 126–138.
 25. C. Zhang, S. Gao, W. Jiang, S. Lin, F. Du, Z. Li, W. Huang, Targeted minicircle DNA delivery using folate-poly(ethylene glycol)-polyethylenimine as non-viral carrier, *Biomaterials.* 31 (2010) 6075–6086.
 26. P. Erbacher, T. Bettinger, P. Belguise-Valladier, S. Zou, J.L. Coll, J.P. Behr, J.S. Remy, Transfection and physical properties of various saccharide, poly(ethylene glycol), and antibody-derivatized polyethylenimines (PEI)., *J. Gene Med.* 1 (1999) 210–22.
 27. K.M. Takeda, K. Osada, T.A. Tockary, A. Dirisala, Q. Chen, K. Kataoka, Poly(ethylene glycol) Crowding as Critical Factor To Determine pDNA Packaging Scheme into Polyplex Micelles for Enhanced Gene Expression, *Biomacromolecules.* 18 (2017) 36–43.
 28. J.-M. Williford, Y. Ren, K. Huang, D. Pan, H.-Q. Mao, Shape transformation following reduction-sensitive PEG cleavage of polymer/DNA nanoparticles, *J. Mater. Chem. B.* 2 (2014) 8106–8109.
 29. T. Blessing, M. Kurs, R. Holzhauser, R. Kircheis, E. Wagner, Different strategies for formation of PEGylated EGF-conjugated PEI/DNA complexes for targeted gene delivery, *Bioconjug. Chem.* 12 (2001) 529–537.
 30. F.J. Verbaan, C. Oussoren, C.J. Snel, D.J. a Crommelin, W.E. Hennink, G. Storm, Steric stabilization of poly(2-(dimethylamino)ethyl methacrylate)-based polyplexes mediates prolonged circulation and tumor targeting in mice., *J. Gene Med.* 6 (2004) 64–75.
 31. Y. Jiang, J. Chen, C. Deng, E.J. Suuronen, Z. Zhong, Click hydrogels, microgels and nanogels: Emerging platforms for drug delivery and tissue engineering, *Biomaterials.* 35 (2014) 4969–4985.
 32. J. Dommerholt, O. Van Rooijen, A. Borrmann, C.F. Guerra, F.M. Bickelhaupt, F.L. Van Delft, Highly accelerated inverse electron-demand cycloaddition of electron-deficient azides with aliphatic cyclooctynes, *Nat. Commun.* 5 (2014) 1–7.

33. J. Dommerholt, S. Schmidt, R. Temming, L.J.A. Hendriks, F.P.J.T. Rutjes, J.C.M. Van Hest, D.J. Lefeber, P. Friedl, F.L. Van Delft, Readily accessible bicyclononynes for bioorthogonal labeling and three-dimensional imaging of living cells, *Angew. Chemie - Int. Ed.* 49 (2010) 9422–9425.
34. L. Novo, L.Y. Rizzo, S.K. Golombek, G.R. Dakwar, B. Lou, K. Remaut, E. Mastrobattista, C.F. Van Nostrum, W. Jahnen-Dechent, F. Kiessling, K. Braeckmans, T. Lammers, W.E. Hennink, Decationized polyplexes as stable and safe carrier systems for improved biodistribution in systemic gene therapy, *J. Control. Release.* 195 (2014) 162–175.
35. L. Novo, E.V.B. van Gaal, E. Mastrobattista, C.F. van Nostrum, W.E. Hennink, Decationized crosslinked polyplexes for redox-triggered gene delivery., *J. Control. Release.* 169 (2013) 246–56.
36. L. Novo, K.M. Takeda, T. Petteta, G.R. Dakwar, J.B. Van Den Dikkenberg, K. Remaut, K. Braeckmans, C.F. Van Nostrum, E. Mastrobattista, W.E. Hennink, Targeted decationized polyplexes for siRNA delivery, *Mol. Pharm.* 12 (2015) 150–161.
37. A.M. Funhoff, C.F. van Nostrum, M.C. Lok, J. a W. Kruijtzter, D.J. a Crommelin, W.E. Hennink, Cationic polymethacrylates with covalently linked membrane destabilizing peptides as gene delivery vectors., *J. Control. Release.* 101 (2005) 233–46.
38. A.M. Funhoff, C.F. Van Nostrum, A.P.C.A. Janssen, M.H.A.M. Fens, D.J.A. Crommelin, W.E. Hennink, Polymer Side-Chain Degradation as a Tool to Control the Destabilization of Polyplexes, *Pharm. Res.* 21 (2004) 170–176.
39. J. Kopecek, P. Kopecková, HPMA copolymers: origins, early developments, present, and future., *Adv. Drug Deliv. Rev.* 62 (2010) 122–49.
40. B. Říhová, M. Kovář, Immunogenicity and immunomodulatory properties of HPMA-based polymers, *Adv. Drug Deliv. Rev.* 62 (2010) 184–191.
41. G.T. Zugates, D.G. Anderson, S.R. Little, I.E.B. Lawhorn, R. Langer, Synthesis of poly(beta-amino ester)s with thiol-reactive side chains for DNA delivery., *J. Am. Chem. Soc.* 128 (2006) 12726–34.
42. M.F. Ebbesen, D.H. Schaffert, M.L. Crowley, D. Oupický, K.A. Howard, Synthesis of click-reactive HPMA copolymers using RAFT polymerization for drug delivery applications, *J. Polym. Sci. Part A Polym. Chem.* 51 (2013) 5091–5099.
43. X. Jiang, A. van der Horst, M.J. van Steenberghe, N. Akeroyd, C.F. van Nostrum, P.J. Schoenmakers, W.E. Hennink, Molar-mass characterization of cationic polymers for gene delivery by aqueous size-exclusion chromatography., *Pharm. Res.* 23 (2006) 595–603.
44. Y. Yue, F. Jin, R. Deng, J. Cai, Y. Chen, M.C.M. Lin, H.F. Kung, C. Wu, Revisit complexation between DNA and polyethylenimine - Effect of uncomplexed chains free in the solution mixture on gene transfection, *J. Control. Release.* 155 (2011) 67–76.
45. G.R. Dakwar, K. Braeckmans, J. Demeester, W. Ceelen, S.C. De Smedt, K. Remaut, Disregarded Effect of Biological Fluids in siRNA Delivery: Human Ascites Fluid Severely Restricts Cellular Uptake of Nanoparticles, *ACS Appl. Mater. Interfaces.* 7 (2015) 24322–24329.
46. H. Takemoto, K. Miyata, T. Ishii, S. Hattori, S. Osawa, N. Nishiyama, K. Kataoka, Accelerated Polymer – Polymer Click Conjugation by Freeze – Thaw Treatment, *Bioconjug. Chem.* 23 (2012) 1503–1506.
47. R.J. Christie, K. Miyata, Y. Matsumoto, T. Nomoto, D. Menasco, T.C. Lai, M. Pennisi, K. Osada, S. Fukushima, N. Nishiyama, Y. Yamasaki, K. Kataoka, Effect of polymer structure on micelles formed between siRNA and cationic block copolymer comprising thiols and amidines, *Biomacromolecules.* 12 (2011) 3174–3185.
48. M. Neu, O. Germershaus, M. Behe, T. Kissel, Bioreversibly crosslinked polyplexes of

- PEI and high molecular weight PEG show extended circulation times in vivo., *J. Control. Release.* 124 (2007) 69–80.
49. J.-H. Ryu, R.T. Chacko, S. Jiwpanich, S. Bickerton, R.P. Babu, S. Thayumanavan, Self-cross-linked polymer nanogels: a versatile nanoscopic drug delivery platform., *J. Am. Chem. Soc.* 132 (2010) 17227–35.
 50. Y. Niebel, M.D. Buschmann, M. Lavertu, G. De Crescenzo, Combined analysis of polycation/ODN polyplexes by analytical ultracentrifugation and dynamic light scattering reveals their size, refractive index increment, stoichiometry, porosity, and molecular weight, *Biomacromolecules.* 15 (2014) 940–947.
 51. S.M. Zou, P. Erbacher, J.S. Remy, J.P. Behr, Systemic linear polyethylenimine (L-PEI)-mediated gene delivery in the mouse., *J. Gene Med.* 2 (2000) 128–34.
 52. S. Boeckle, K. von Gersdorff, S. van der Piepen, C. Culmsee, E. Wagner, M. Ogris, Purification of polyethylenimine polyplexes highlights the role of free polycations in gene transfer, *J. Gene Med.* 6 (2004) 1102–1111.
 53. K. Braeckmans, K. Buyens, B. Naeye, D. Vercauteren, H. Deschout, K. Raemdonck, K. Remaut, N.N. Sanders, J. Demeester, S.C. De Smedt, Advanced fluorescence microscopy methods illuminate the transfection pathway of nucleic acid nanoparticles, *J. Control. Release.* 148 (2010) 69–74.
 54. K. Braeckmans, K. Buyens, W. Bouquet, C. Vervaet, P. Joye, F. De Vos, L. Plawinski, L. Doeuvre, E. Angles-Cano, N.N. Sanders, J. Demeester, S.C. De Smedt, Sizing nanomatter in biological fluids by fluorescence single particle tracking, *Nano Lett.* 10 (2010) 4435–4442.
 55. V. Filipe, A. Hawe, W. Jiskoot, Critical evaluation of nanoparticle tracking analysis (NTA) by NanoSight for the measurement of nanoparticles and protein aggregates, *Pharm. Res.* 27 (2010) 796–810.
 56. M. Sioud, Innate sensing of self and non-self RNAs by Toll-like receptors, *Trends Mol. Med.* 12 (2006) 167–176.
 57. M.O. Oyewumi, A. Kumar, Z. Cui, Nano-microparticles as immune adjuvants: Correlating particle sizes and the resultant immune responses, *Expert Rev. Vaccines.* 9 (2010) 1095–1107.
 58. J. Luten, N. Akeroyd, A. Funhoff, M.C. Lok, H. Talsma, W.E. Hennink, Methacrylamide polymers with hydrolysis-sensitive cationic side groups as degradable gene carriers, *Bioconjug. Chem.* 17 (2006) 1077–1084.
 59. M.C. Kerr, M.R. Lindsay, R. Luetterforst, N. Hamilton, F. Simpson, R.G. Parton, P.A. Gleeson, R.D. Teasdale, Visualisation of macropinosome maturation by the recruitment of sorting nexins., *J. Cell Sci.* 119 (2006) 3967–80.
 60. J. Yang, H. Chen, I.R. Vlahov, J.-X. Cheng, P.S. Low, Evaluation of disulfide reduction during receptor-mediated endocytosis by using FRET imaging, *Proc. Natl. Acad. Sci.* 103 (2006) 13872–13877.
 61. F. Meng, W.E. Hennink, Z. Zhong, Reduction-sensitive polymers and bioconjugates for biomedical applications, *Biomaterials.* 30 (2009) 2180–2198.
 62. L. Brülisauer, M.A. Gauthier, J.C. Leroux, Disulfide-containing parenteral delivery systems and their redox-biological fate, *J. Control. Release.* 195 (2014) 147–154.
 63. Y. Song, B. Lou, P. Zhao, C. Lin, Multifunctional Disulfide-based cationic dextran conjugates for intravenous gene delivery targeting ovarian cancer cells, *Mol. Pharm.* 11 (2014) 2250–2261.
 64. S. Rahimian, J.W. Kleinovink, M.F. Fransen, L. Mezzanotte, H. Gold, P. Wisse, H. Overkleef, M. Amidi, W. Jiskoot, C.W. Löwik, F. Ossendorp, W.E. Hennink, Near-infrared labeled, ovalbumin loaded polymeric nanoparticles based on a hydrophilic polyester as model vaccine: In vivo tracking and evaluation of antigen-specific CD8+ T cell immune response, *Biomaterials.* 37 (2015) 469–477.
 65. C. Oussoren, J. Zuidema, D.J.A. Crommelin, G. Storm, Lymphatic uptake and biodistribution of liposomes after subcutaneous injection. II. Influence of liposomal size, lipid composition

and lipid dose, *Biochim. Biophys. Acta - Biomembr.* 1328 (1997) 261–272.

66. N.P.H. Knudsen, A. Olsen, C. Buonsanti, F. Follmann, Y. Zhang, R.N. Coler, C.B. Fox, A. Meinke, U. D'Oro, D. Casini, A. Bonci, R. Billeskov, E. De Gregorio, R. Rappuoli, A.M. Harandi, P. Andersen, E.M. Agger, Different human vaccine adjuvants promote distinct antigen-independent immunological signatures tailored to different pathogens, *Sci. Rep.* 6 (2016) 19570.

| Supplementary data

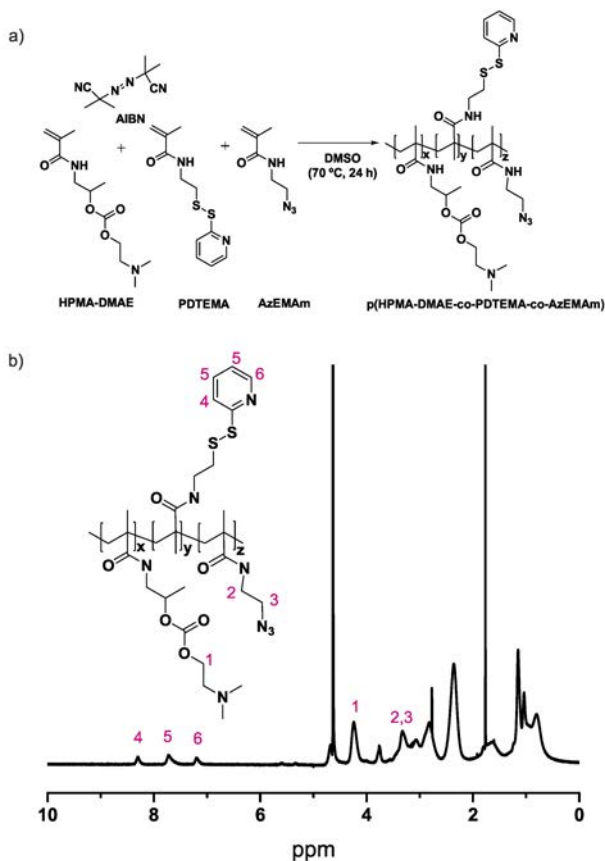
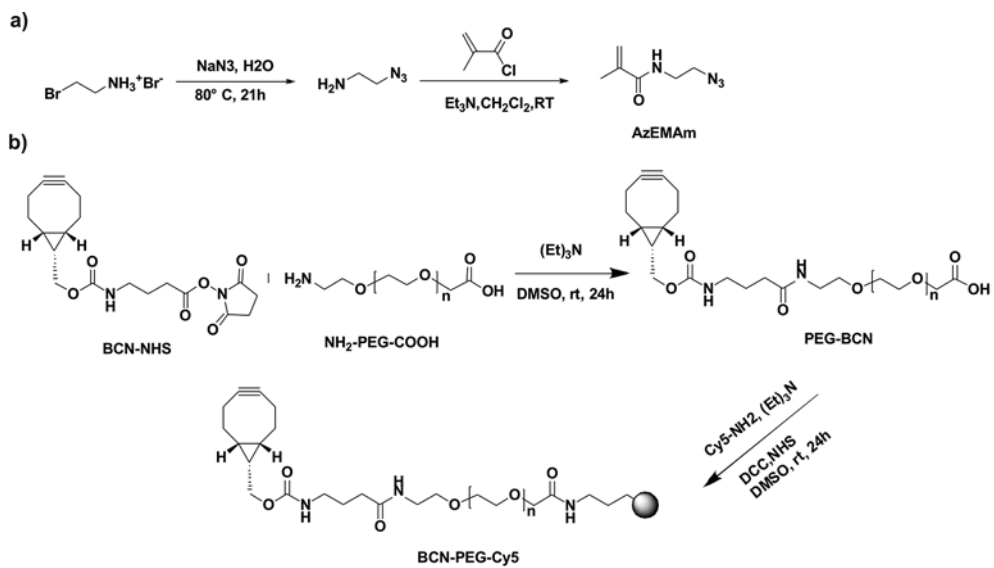


Fig. S1. a) synthesis route of random copolymers p(HPMA-DMAE-co-PDTEMA-co-AzEMAm) (abbreviated as pHDPA) of different compositions and b) a representative ^1H NMR spectrum of pHDPA in D_2O .

Table S1. Characteristics of the synthesized polymers as determined by ^1H NMR, Viscotek GPC analysis and UV spectroscopy.

Polymer	HPMA-DMAE/PDTEMA/AzEMAm			M_n^b (kDa)	M_w/M_n^b	PDS/polymer (nmol/mg) ^a	PDS/polymer (nmol/mg) ^c
	Feed (mol/mol/mol)	Copolymer (mol/mol/mol) ^a					
pHDPA1	75/20/5	68/16/17		9.6	1.7	524	484
pHDPA2	70/20/10	66/14/20		11.1	1.9	590	505
pHDPA3	60/20/20	59/14/27		9.9	2.0	521	515

^a Determined by ^1H NMR. ^b Determined by SEC. ^c Determined by UV spectroscopy.



Scheme S1. Synthesis route of a) AzEMAm, b) BCN-PEG and BCN-PEG-Cy5.

4

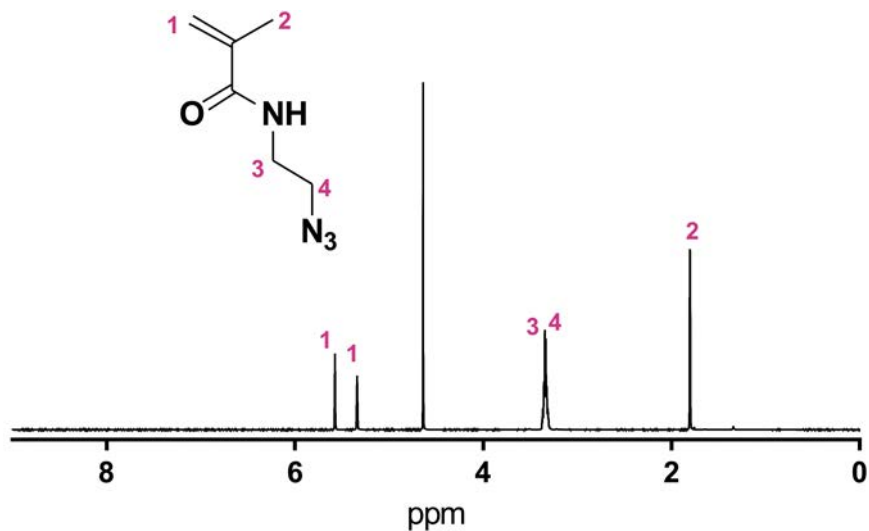


Fig. S2. ^1H NMR spectrum of AzEMAm in D_2O .

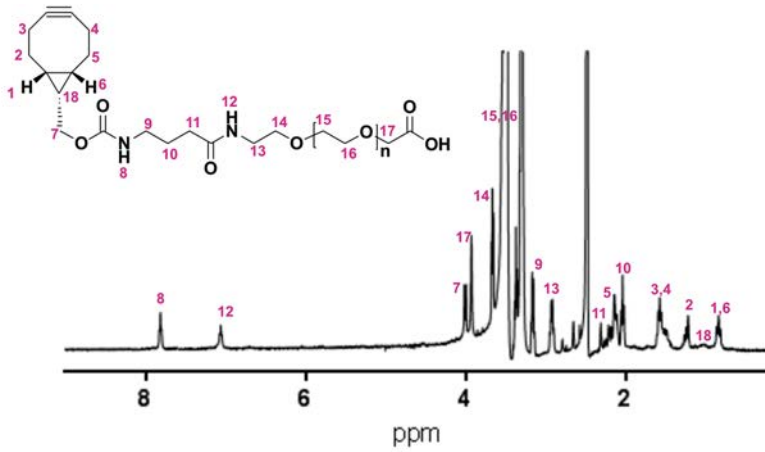


Fig. S3. ^1H NMR spectrum of PEG-BCN in DMSO-d_6 .

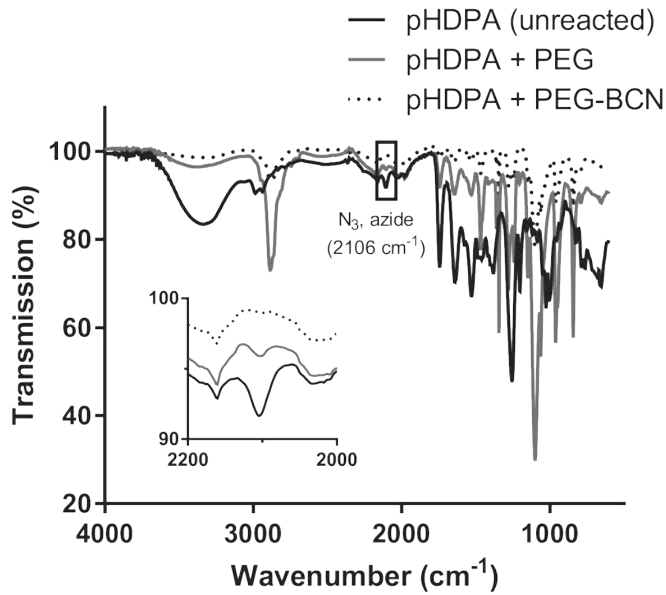


Fig. S4. FTIR spectra of the pHDP2, PEG-BCN and their reaction mixture. The mixture was reacted at room temperature for 3 h in 5 mM pH 5, NH_4OAc buffer, molar ratio 1:1.5, the spectrum was obtained after freeze drying of the mixture. The disappearance of the peak (2106 cm^{-1}) of pHDP2 after the reaction with PEG-BCN demonstrates quantitative reaction of the azide groups of pHDP2 with the cyclooctyne group of PEG-BCN.

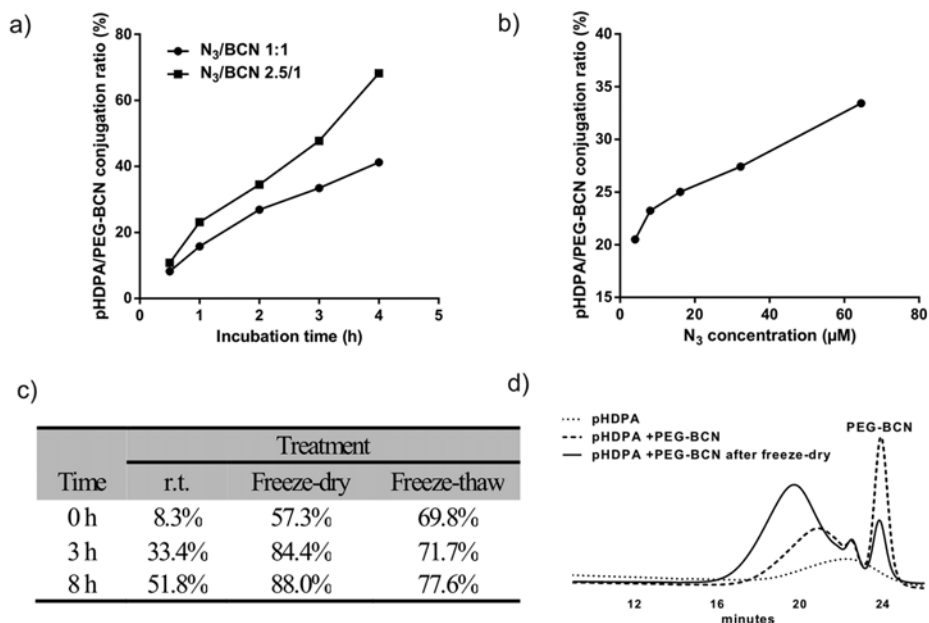


Fig. S5. a) pHDPA and PEG-BCN conjugate efficiency determined by size exclusion chromatography (SEC) at room temperature as a function of time and at different N₃/BCN ratios at a fixed azide concentration 64.5 μM in the reaction mixture, or b) as a function of azide concentration after 3 h incubation (BCN/N₃ = 1 (mol/mol)). c) pHDPA and PEG-BCN conjugation efficiency after different treatment methods; d) SEC chart (RI signal) of reaction mixture after 3 hours incubation at room temperature before and after freeze-drying (BCN/N₃ = 1 (mol/mol), 64.5 μM azide in the reaction mixture).

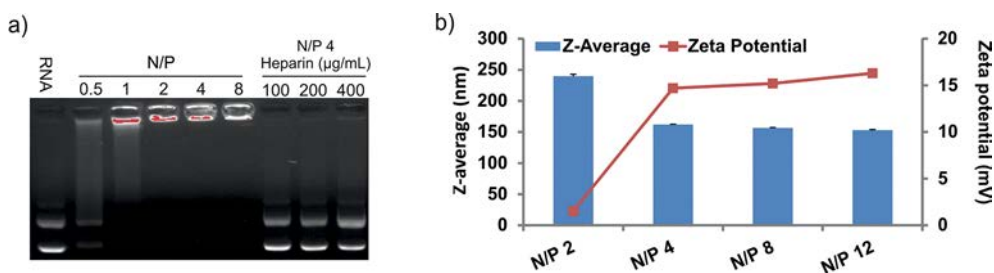


Fig. S6. a) Agarose gel retardation assay of the pHDPA ssRNA polyplexes prepared at different N/P ratios in the absence and presence of heparin; b) Average particle size and zeta potential of pHDPA ssRNA polyplexes formed at different N/P ratios from 2/1 to 12/1 (mol/mol) in HEPES buffer (20 mM, pH 7.4). Polyplexes were prepared with a ssRNA concentration of 100 μg/mL and diluted to 10 μg/mL to measure the size and zeta potential of the polyplexes.

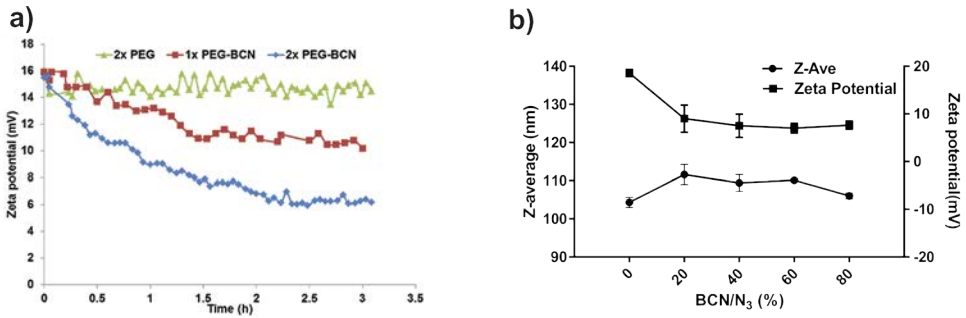


Fig. S7. a) Zeta potential of polyplexes during post-PEGylation in 10 mM pH5 NH₄OAc buffer; b) size and zeta potential of polyplexes post-modified with different amounts of PEG after 3 hour of incubation.

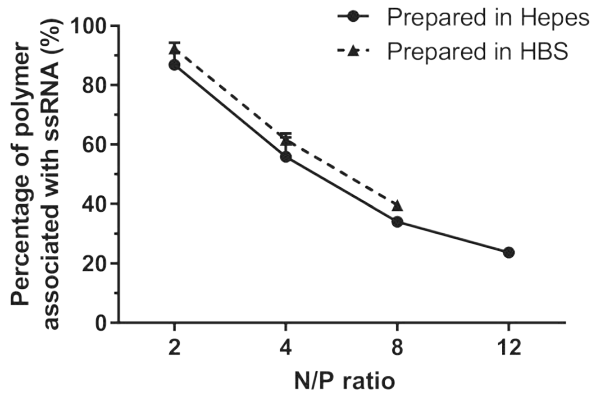


Fig. S8. Percentage of PHDA polymer associating with ssRNA in the polyplex dispersion at different N/P ratios (n=3).

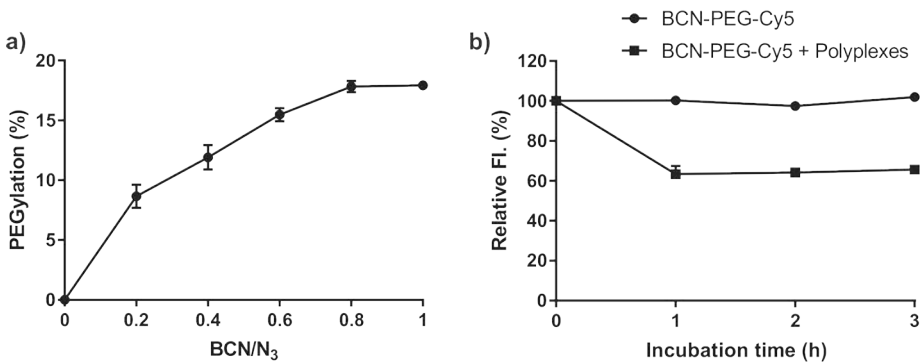


Fig. S9. Quantity of RNA polyplex post-PEGylation efficiency by BCN-PEG-Cy5 via ultrafiltration a) and fluorescence correlation spectroscopy (FCS) method (BCN/N₃ molar ratio of 0.6). The PEGylation efficiency was calculated as the moles of reacted azide compared to the initial moles of azide within the polyplexes (n=3).

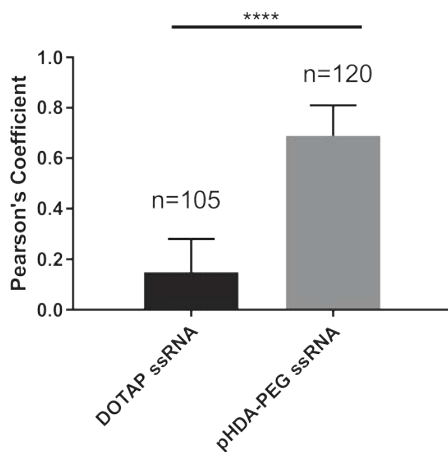


Fig. S10. Averages of the Cy5-mRNA_luc colocalization coefficients with lysotracker of Figure 2b. Images were analyzed by ImageJ with Pearson's correlation coefficient. **** p < 0.0001.

4

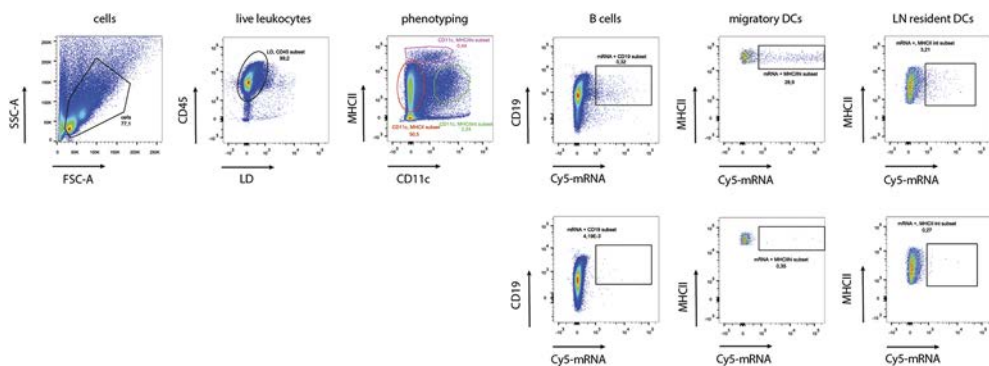


Fig. S11. Gating strategy that was applied to identify B cells, and MHCII^{hi} and MHCII^{low} DCs in the popliteal lymph nodes.

CHAPTER

5

Modular core-shell polymeric nanoparticles mimicking viral structures for vaccination

Bo Lou¹, Ans De Beucklaer², Eger Boonstra¹,
Dandan Li¹, Bruno G. De Geest³, Stefaan De Koker²,
Enrico Mastrobattista¹, Wim E. Hennink^{1,*}

¹Department of Pharmaceutics, Utrecht Institute for Pharmaceutical science,
Utrecht University, 3584CG Utrecht, the Netherlands

²Laboratory of Molecular Immunology, Department of Biomedical Molecular
Biology, Ghent University, 9052 Zwijnaarde, Belgium

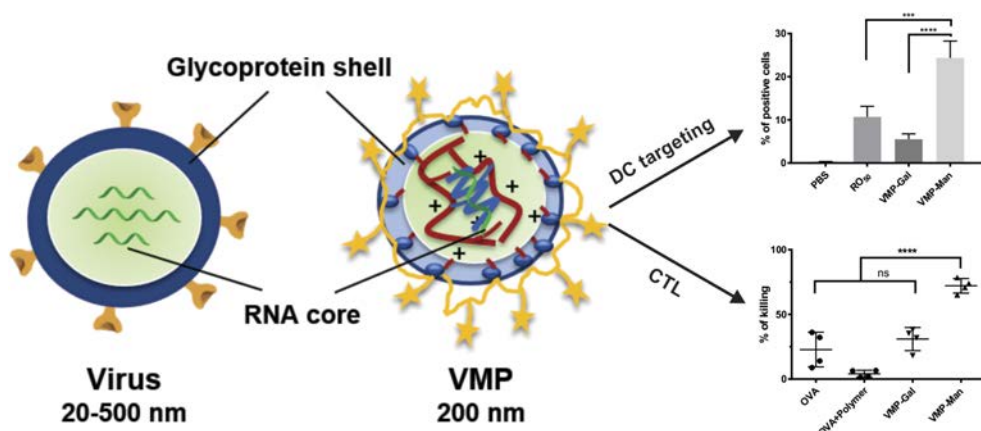
³Department of pharmaceutics, Ghent University, 9000 Ghent, Belgium

| Abstract

Recent advances in the development of protein-based vaccines have expanded the opportunities for preventing and treating both infectious diseases as well as cancer. However, readily and efficient antigen delivery systems capable of stimulating strong cytotoxic T-lymphocyte (CTL) responses remain a challenge. With the attempt to closely mimic the properties of viruses in terms of their size and molecular organization, we constructed RNA (which is a ligand for Toll-like receptor 7 (TLR7) and TLR8) and antigen-loaded nanoparticles resembling the structural organization of viruses. Cationic polymers containing either azide or bicyclo[6.1.0]nonyne (BCN) groups were synthesized as electrostatic glue that binds negatively charged single stranded RNA (PolyU) to form self-crosslinked polyplex core. BCN-modified antigen protein (ovalbumin, OVA) shell and glycosylated polymer were sequentially conjugated to the RNA core via disulfide bonds using copper free click chemistry. The generated reducible virus mimicking particles (VMP) with a diameter of 200 nm and negatively surface charge (-14 mV) were colloidal stable in physiological environment. The immunogenicity of these VMP vaccines was evaluated both *in vitro* and *in vivo*. The surface mannosylated VMP (VMP-Man) showed 5 times higher cellular uptake by Bone marrow derived DCs (BMDCs) compared to galactosylated VMP (VMP-Gal) counterpart. Moreover, VMP-Man efficiently activated DCs and greatly facilitated MHC I Ag presentation *in vitro*. Vaccination of mice with VMP-Man elicited strong OVA-specific CTL responses as well as humoral immune responses. These results demonstrate that the modular core-shell polymeric nanoparticles described in this paper are superior in inducing strong and durable immune responses compared to adjuvanted protein subunit vaccines and offer therefore a flexible platform for personalized vaccines

5

Graphical abstract



| Introduction

Protein subunit vaccines have been extensively investigated as a safe alternative to classical vaccines consisting of whole, attenuated or inactivated pathogens [1]. Also for cancer immunotherapy, vaccines based on tumor-associated antigens or tumor neoantigens are being explored [2–4]. Recombinant or purified protein antigens for vaccination have a good safety profile and have been extensively tested in clinical studies [5,6]. However, protein subunit vaccines are poorly immunogenic by themselves [7]. Thus, the inclusion of an adjuvant in the vaccine formulation is necessary to induce a more potent immune response. The mostly used adjuvants in the clinical trials are emulsions (e.g. AS03 and MF59[®]), which can enhance the antigen persistence at the injection site and increase recruitment and activation of antigen presenting cells (APCs). Nonetheless, repeated immunization can cause antigen-specific T cell sequestration, dysfunction and deletion [8], and is also associated with the risk to induce autoimmunity [9].

Alternatively, nanoparticles have been used to adjuvant protein vaccine formulations [10,11]. The use of nanoparticles in vaccinology is inspired by the fact that most pathogens have a dimension within the sub-micron size range, and therefore can be processed efficiently by the immune system, leading to a potent immune response. One of the most intensively studied polymer-based protein delivery systems are biodegradable poly(lactic-co-glycolic acid) (PLGA) nanoparticles [12–14]. The co-delivery of Toll-like receptor ligands (TLRs) and protein antigens in PLGA particles can efficiently induce strong CD8⁺ T cell responses with the capacity to inhibit the growth of tumors or protect against a viral challenge [15,16]. Besides PLGA, a whole spectrum of different nanocarriers systems, both polymeric as well as lipidic, has been developed for vaccination purposes, with most of these systems relying on the entrapment of antigens in the core of the nanoparticles to efficiently deliver their loading to antigen presenting cells [17–20]. The pharmaceutical limitation of this approach is that one needs to empirically optimize the vaccine formulation in terms of encapsulation efficiency and antigen release, which is often time consuming with different requirements for different antigens. For this reason, the encapsulation approach is not recommended for manufacturing of personalized vaccines.

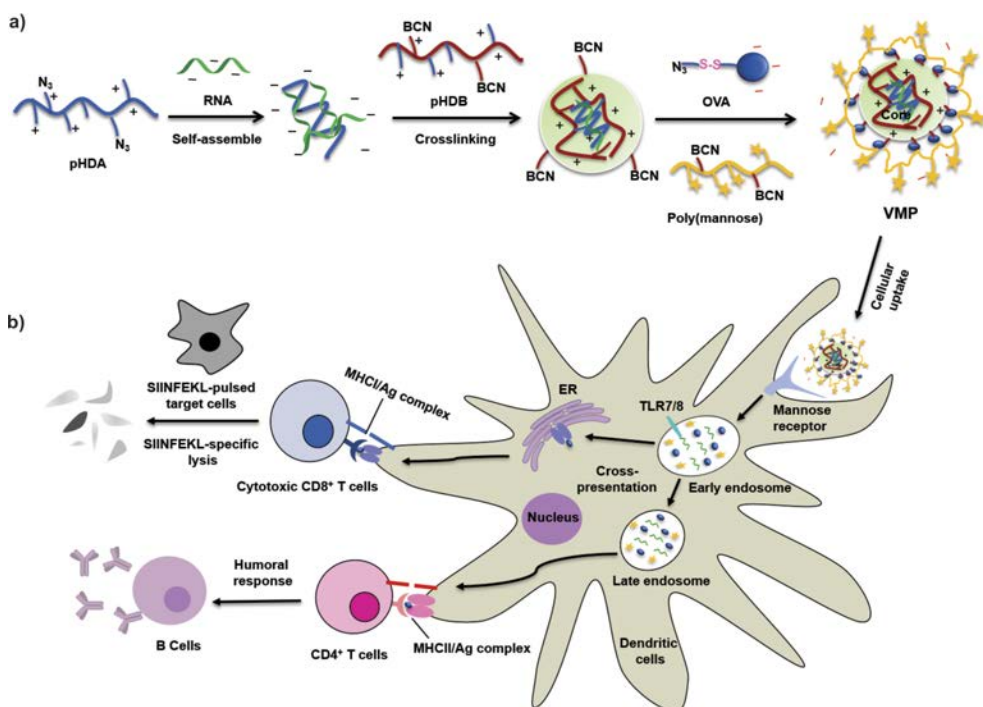
Here, we propose an alternative and simple strategy to produce antigen and adjuvant loaded nanoparticles by using synthetic biodegradable polymers (Scheme 1). Our strategy is based on the formation of a universal crosslinked core nanoparticle containing virus-mimicking single chain RNA (PolyU) as TLR-adjuvant to which different layers of functional shells (e.g. antigen and stabilizer poly(mannose)) can be coupled using copper-free click chemistry (Scheme 1a). Such a modular core-shell polymeric nanoparticle resembles viruses in terms of size and supramolecular organization and as such is expected to efficiently boost the immune system. Virus-mimicking nanoparticles (VMPs) were constructed by sequential self-assembly of single stranded RNA (adjuvant), ovalbumin (as model antigen) with cationic polymers and stabilized with poly(mannose) for targeting the mannose-receptors on the surface of DCs [21]. VMP particles surface modified with poly (galactose) were prepared as a negative control, as galactose has extremely low binding affinities to mannose receptors. The strength of this vaccine delivery

system lies in the flexibility at which different antigen shell layers can be “clicked” onto the VMP core, enabling versatile adaptation for different vaccine application. As the antigen is covalently linked to the RNA core, antigen loading becomes independent on the properties of antigen used. To ensure antigen release once delivered into the antigen presenting cells, reducible disulfide bonds were introduced between the polymeric shell and the antigen, enabling intracellular antigen release [22–24]. These VMP were tested for antigen-specific immune activation both *in vitro* and *in vivo* and showed robust antigen-specific immune activation that warrants its further investigation as a modular vaccine platform.

Materials and methods

Materials

Imidazole-1-sulfonyl azide hydrochloride [25], N-(2-hydroxyl propyl)-methacrylamid (HPMA) and DMAE-CI [26] were synthesized as previously described. Azobis(isobutyronitrile) (AIBN), 4-cyano-4-[(dodecylsulfanylthiocarbonyl)sulfanyl]pentanoic acid (CDTPA), azidoacetic acid N-hydroxysuccinimide ester, acrylic acid N-hydroxysuccinimide ester (NAS) and all other



Scheme 1. Design of synthetic virus mimicking particles (VMP) vaccines. (a) Schematic illustration of sequential assembly of VMP particles. pHDA: cationic polymer containing azide groups; pHDB: cationic polymer containing cyclooctyne groups (bicyclo[6.1.0]nonyne (BCN)). (b) The VMP particles specifically target to dendritic cells, promote antigen cross-presentation, and induce DC maturation, resulting in elicitation of robust antigen-specific cytotoxic T lymphocytes responses and superior antibody production.

reagents and solvents used were obtained from Sigma (Zwijndrecht, The Netherlands) and were used without further purification. 2,5-Dioxopyrrolidin-1-yl 4-((((1R,8S,9s)-bicyclo [6.1.0] non-4-yn-9-ylmethoxy)carbonyl)amino)butanoate (BCN, SX-A1036) was purchased from Synaffix BV (Oss, The Netherlands). Ovalbumin (OVA) and PolyU were purchased from InvivoGen (Toulouse, France). Cy5-mRNA_luc was from Teu-bio (TRiLink biotechnologies, San Diego, USA). Agarose multi-purpose was purchased from Roche Molecular Biochemicals (Mannheim, Germany). 6× DNA Loading Dye was purchased from Fermentas (St. Leon-Roth, Germany). SYBR Safe DNA gel stain, Dulbecco's phosphate buffered saline (DPBS), RPMI-1640/IMDM medium, Opti-MEM, and heat inactivated fetal bovine serum (HI-FBS) were purchased from Life Technologies (Breda, the Netherlands).

Monomer synthesis

Synthesis of 1,2-bis(2-azidoethyl) disulfane

The synthesis procedures were similar as the methods described above (Scheme S1). Typically, imidazole-1-sulfonyl azide hydrochloride chloride salt (5.0 g, 23.9 mmol) was added to cystamine dihydrochloride salt (2.2, 9.9 mmol), K_2CO_3 (6.1g, 44.2 mmol) and $CuSO_4 \cdot 5H_2O$ (59.6 mg, 238.5 μ mol) in MeOH (100 mL) and the mixture was stirred at room temperature for 12 h. Next, the mixture was concentrated, diluted with H_2O (200 mL), and extracted with DCM (3×100 mL). The combined organic layers were dried ($MgSO_4$), filtered and concentrated. Flash chromatography gave the aimed product as a yellow oil (DCM/MeOH/ NH_4OH , 3/1/0.1). The yield was 1.9 g (94%, $R_f = 0.5$). The monomer was characterized by 1H NMR spectroscopy (Fig. S4).

Synthesis of 3-((2-azidoethyl) disulfanyl) propanoic acid NHS ester (ADDP)

The synthesis procedure of 3-((2-azidoethyl)disulfanyl)propanoic acid was based on a previous study (Scheme S2) [27]. In detail, 1,2-bis(2-azidoethyl) disulfane (1.9 g, 9.3 mmol) was dissolved in MeOH (100 mL) and cooled in an ice bath. A solution of 3-chloroperbenzoic acid (mCPBA, Sigma-Aldrich, the Netherlands) (75%, 2.6 g, 11.2 mmol) in DCM (20 mL) was added dropwise. The reaction mixture was stirred overnight at room temperature and the solvent was subsequently evaporated in vacuo to give a white residue. The obtained solid was suspended in MeOH (50 mL), to which dropwise 3-mercaptopropionic acid (0.81 mL, 9.3 mmol) was added. The resulting solution was stirred overnight at room temperature. The solvent was removed in vacuo and the resulting oil was purified by basic Al_2O_3 gel, eluted with MeOH/ $CHCl_3$ /AcOH= 10/100/1. The aimed compound was obtained as a pale yellow oil. The yield was 1.4g (75%, $R_f = 0.4$) and characterized by 1H NMR spectroscopy (400 MHz, DMSO-d6) (Fig. S5).

Next, 3-((2-azidoethyl) disulfanyl) propanoic acid was activated with NHS. Briefly, 1.0 g of 3-((2-azidoethyl) disulfanyl) propanoic acid (4.8 mmol) and 0.9 mg of N-hydroxysuccinimide (NHS, 7.2 mmol) were dissolved in 15 mL dichloromethane. Then, 1.5 g of dicyclohexylcarbodiimide (DCC, 7.2 mmol) was added and the mixture was stirred overnight at room temperature. After filtration of insoluble dicyclohexylurea (DCU) and evaporation of

DCM, the mixture was purified using a silica gel column (DCM/MeOH=50/2). The yield was 0.9 g (59%, $R_f = 0.8$) and the product was characterized by ^1H NMR spectroscopy (400 MHz, DMSO- d_6) (Fig. S6).

Synthesis of 3-(2-aminoethylthio) propyl α -D-mannopyranoside/galactopyranoside (Man-NH₂/Gal-NH₂)

The reaction consists of elongation of the alkyne group of allyl α -D-mannopyranoside/galactopyranoside (Sigma-Aldrich, the Netherlands) by adding 2-aminoethanethiol according to reaction Scheme S3 [28]. Typically, 1.2 g of allyl α -D-mannopyranoside (5.5 mmol) was dissolved in 2 mL deoxygenated water in which 570 mg of cysteamine hydrochloride (5.0 mmol) was also dissolved. The solution was then irradiated with UV light of 254 nm for 17 h. Next, the solution was diluted with 100 mL methanol and dried (MgSO_4), filtered and concentrated. The resulting oil residue was purified by silica gel chromatography (methanol/ NH_4OH , 100:1), to give final product Man-NH₂ as a colorless oil (1.2 g, 73%, $R_f = 0.25$). The products were characterized by the ^1H NMR spectroscopy (Fig. S11).

Synthesis of the polymers

*Synthesis of p(HPMA-*r*-NAS) (pHN) by RAFT*

p(HPMA-*r*-NAS) was synthesized by reversible addition fragmentation chain transfer (RAFT) copolymerization as previously published [29]. Briefly, 4-cyano-4-[(dodecylsulfanylthiocarbonyl)sulfanyl] pentanoic acid (CDTPA) was used as chain transfer agent (CTA), and AIBN as initiator (I). The polymer was synthesized using monomers (HPMA and NAS) to chain transfer agent and initiator ratio (M/CTA/I) of 100/1/0.1 (mol/mol/mol) and a feed ratio HPMA/NAS of 70/30 (mol/mol). 1,3,5-Trioxane (Sigma-Aldrich, the Netherlands) was added as internal NMR standard with a final concentration of 0.1 M. The polymerization was carried at 70 °C for 9 h in dry DMF under argon after purging for half an hour, using a final total monomer concentration of 1.0 M. After polymerization, the conversion of the monomers was analyzed by ^1H NMR analysis by dilution (10x) a sample of the reaction mixture with DMSO- d_6 . The product was precipitated into a mixture of anhydrous acetone and diethyl ether (50/50 v/v). To remove the trithiocarbonate end group [30], the polymer and AIBN (50 times excess, mol/mol) were dissolved in anhydrous DMF and purged with argon. The solution was heated at 80 °C for 90 min, and the polymer was subsequently precipitated in 100 mL of anhydrous acetone, collected by centrifugation, and dried under vacuum for 24 h. The procedure was repeated for three times and the polymer was dried in vacuo prior to ^1H NMR and GPC analysis (yield: 55%, $M_n = 15$ kDa, $M_w/M_n = 1.43$). ^1H NMR (400 MHz, DMSO- d_6); δ ppm; 0.95–1.52 (backbone- CH_3 , $\text{CH}_3\text{CH}(\text{OH})$), 1.55–2.41 (backbone CH_2 , backbone- CH), 3.00–3.33 (CH_2NH), 3.5 (NHS- CH_2), 3.90 (CHOH).

Synthesis of p(HPMA-DMAE-r-AEDA) (pHDA) and p(HPMA-DMAE-r-BCN) (pHDB)

Hundred mg of the copolymer p(HPMA-r-NAS) (pHN) (0.19 mmol of NAS, 0.48 mmol of HPMA) was dissolved in 1 mL dry DMSO and purged with argon for 30 min. After that, 40 mg of 2-((2-azidoethyl) disulfanyl) ethan-1-amine hydrochloride (AEDA) or 73 mg (0.22 mmol) of BCN-amine (A-10004, Synaffix BV) was added to this solution under argon purge. Subsequently 113 mg (1.12 mmol) of triethylamine was injected into the reaction vessel and the solution was stirred at 40 °C. After 48 h, 28 mg (0.37 mmol) of d,l-amino-2-propanol was introduced into the reaction mixture which was subsequently stirred overnight at room temperature. The modified polymers were precipitated twice into a mixture of anhydrous acetone and diethyl ether (50/50 v/v) and dried under vacuum to get the white colored products (pHNA and pHNB; yields: 63% and 56% for pHNA and pHNB respectively). Next, the obtained polymers were dissolved in 2 mL dry DMSO, DMAE-Cl (3.4 g, 14.4 mmol) was loaded under argon purging. After 72 h reaction at room temperature, the resulting mixture was diluted with 20 mL 2.5 mM ammonium acetate buffer (pH 5) were ultra-filtrated for 24 h with a membrane MWCO of 3000 Da. The resulting polymer solutions were filtered with 0.2 µm sterile filter before freeze-drying. Yield 57% for pHDA and 71% for pHDB.

RAFT Synthesis of the homopolymer of NAS (pNAS)

A typical polymerization procedure for pNAS with a degree of polymerization (DP) of 120 is described in a previously published paper [31]. A reaction vial (8 mL) was charged with NAS (0.5 g, 2.95 mmol) in anhydrous DMF (1.4 mL, 2 M solution) and 4-cyano-4-[(dodecylsulfanylthiocarbonyl)sulfanyl]pentanoic acid (5.96 mg, 0.014 mmol) (CTA, CDTA). A solution of AIBN (24 µL, 0.24 mg, 1.4 µmol) in anhydrous DMF was transferred into the vial. The [M]/[CTA] ratio was 200/1 (mol/mol), whereas the [CTA]/[Initiator] ratio was kept at 10/1 (mol/mol). The mixture was degassed by three freeze–evacuate–thaw cycles and then heated under argon in an oil bath at 70 °C for a period of 7 h. The vial was removed from the oil bath, cooled with ice-water and exposed to air to terminate the polymerization. Finally, a small fraction of the sample (30 µL) was withdrawn and characterized by ¹H NMR spectroscopy (in DMSO-d₆) to determine the monomer conversion. The polymer was precipitated in anhydrous acetone (50 mL) and recovered by centrifugation. The procedure was repeated three times and the obtained pellet was subsequently dried under vacuum for 24 h (yield: 0.31 g, 58%). The absence of residual monomers in the obtained polymer was confirmed by ¹H NMR spectroscopy (in DMSO-d₆). The trithiocarbonate end group of the polymer was removed according to a procedure similar as described in section 2.3.1 [30]. Typically, pNAS (0.25 g, degree of polymerization 116 calculated from conversion 63%, thus 11.5 µmol of end-groups) and AIBN (94.5 mg, 57.5 µmol, 50 times molar excess over pNAS) were dissolved in anhydrous DMF (2 mL). The solution was heated for 90 min at 80 °C. Subsequently, the homopolymer was precipitated in 100 mL of anhydrous acetone, collected by centrifugation, and dried under vacuum for a period of 24 h (yield: 0.21 g, 83%). The absence of the trithiocarbonate end group was confirmed by GPC analysis (disappearance of the UV absorbance at 309 nm).

Synthesis of *p*(Man-*r*-BCN)/*p*(Gal-*r*-BCN)

Functionalization of pNAS with mannose and BCN groups was carried out shown in scheme 3. In detail, 60 mg of pNAS (0.33 mmol of NAS) was dissolved in anhydrous dimethyl sulfoxide (DMSO, 1.2 mL), followed by addition 9 mg of BCN-amine (0.03 mmol, A-10004, Synaffix BV, the Netherlands) and 28 mg of triethylamine (0.27 mmol), the mixture was stirred at room temperature for one hour. Then, 118 mg of 3-(2-aminoethylthio) propyl α -D-mannopyranoside (0.39 mmol) and 402 mg of triethylamine (3.97 mmol) were added. The reaction was carried out at 40 °C for 36 h followed by quenching of the unreacted active ester groups with NH_4OH (1 mL) for half an hour and the polymer was subsequently precipitated in 100 ml methanol. The polymer was re-dissolved in water and ultrafiltrated against MilliQ water for 5 h to remove unreacted mannose and BCN-amine. The resulting polymer solution was filtered with 0.2 μm sterile filter and subsequently freeze-dried. The conjugation efficiency was calculated from ^1H NMR spectroscopy (91% for the mannose polymer). The same procedure was performed to synthesize of *p*(Gal-*r*-BCN) with a 97% galactose conjugation efficiency. The polymer yield was around 85%. The molar ratio of mannose/ galactose and BCN into the polymer chain was determined by ^1H NMR spectroscopy (Fig. S12) and it was shown that the molar ratio of BCN in the polymers was 8-9% for both polymers, as calculated from the peak intensity ratio of the hydroxyl group protons of sugar (4.97-5.11 ppm, 4H) and methylene protons of BCN (OCOCH_2 , 4.02 ppm, 2H).

Characterization of the polymers

The copolymer composition of the different polymers was determined by ^1H NMR analysis performed with a Gemini 400 MHz spectrometer (Varian Associates Inc., NMR Instruments, Palo Alto, CA). The polymers were dissolved in D_2O or DMSO-d_6 . The molecular weights and molecular weight distributions of the synthesized copolymers pHN and pNAS were determined by gel permeation chromatography (GPC), using two serial PLgel 5 μm MIXED-D columns (Polymer Laboratories, UK) and PEGs of narrow molecular weight distribution as calibration standards. The eluent was DMF containing 10 mM LiCl, the flow rate was 1 mL/min and the temperature was 60 °C. For pHDA and pHDB, the molecular weights and molecular weight distributions were determined by GPC using a Viscotek-GPC max (Viscotek, Oss, The Netherlands) light scattering ($\lambda = 670$ nm, right (90°) and low (7°) angle)/viscosimetric detection system, using an ultrahydrogel 2000, 7.8 \times 300 mm column in series with an ultrahydrogel 6.0 \times 40 mm guard column (Waters) and 0.3 M NaAc, pH 4.4, 30% acetonitrile as eluent [32]. The flow rate was 0.6 mL/min and the run time was 50 min. PolyCALTM PEO standard ($M_n = 24$ kDa, PDI=1.01, Malvern) was used for calibration.

Modification of ovalbumin (OVA) with azide groups

ADDP (7 or 14 μL , 30 mg/mL in dry DMSO) was added to 2.5 mL of OVA (2.5 mg/mL in DPBS, Serva Electrophoresis GmbH) resulting in molar ratios of azide and OVA of 5:1 and 10:1, respectively. The mixtures were incubated for 1 h at room temperature. The modified OVA

was subsequently purified with PD 10 column chromatography using nuclease-free water as eluent and subsequently freeze-dried. The number of modified lysine residues was determined by using the TNBS assay (Thermo Fisher Scientific) according to the protocol of the supplier. Sulfo-Cy3 modified OVA was synthesized using the same procedure as for the azide modified OVA with a molar ratio sulfo-cy3/OVA of 2/1.

Spectral analysis of azide modified OVA

UV absorption spectra of 0.5 mg/mL native and modified OVA in DPBS buffer were measured in the range of 250–350 nm using a Shimadzu UV-2450 UV-vis spectrophotometer (Shimadzu Corporation, Kyoto, Japan). UV-CD spectra of 0.5 mg/mL native and modified OVA in DPBS buffer were recorded from 250 to 195 nm using a dual-beam DSM 1000 CD spectropolarimeter (On-Line Instruments Systems, Bogart, GA) using cuvettes with a path length of 0.5 mm. Fluorescence measurements were carried out with Jasco FP8300 Spectrofluorometer (JASCO, Easton, USA). The excitation wavelength was set at 280 nm and the emission spectra were recorded in the range of 300–350 nm. Native and modified OVA were measured at a concentration of 0.1 mg/mL in DPBS at pH 7.4.

Particle preparation and characterization

Preparation of self-crosslinked RNA polyplexes

pHDA and pHDB were dissolved in 10 mM NaAc buffer (pH 5) at 10 mg/mL. As shown in Fig. 2a, RNA polyplexes were prepared by mixing 100 μ L of pHDA dissolved in 5 mM NaAc buffer (pH 5) with 100 μ L of RNA solution (PolyU or Cy5-mRNA_{luc}) solution in the same buffer at different N/P molar ratios from 0.2 to 2 and a final fixed RNA concentration of 50 μ g/ml. The mixture was vortexed for 5 s and incubated at room temperature for 10 min. To prepare the self-crosslinked (pHDA+pHDB) polyplexes, typically, 100 μ L of pHDA dissolved in 5 mM NaAc buffer (N/P ratio of 0.5 mol/mol) was mixed with 100 μ L of RNA solution (50 μ g/ml). After vortexing for 5 s and equilibration for 10 min, 100 μ L of pHDB solution in 5 mM NaAc buffer (N/P ratio of 1.2) was added to the RNA/pHDA polyplex dispersion, followed by vortexing and incubating for 10 min at RT. To accelerate the crosslink process, sucrose (final concentration 5%) was added to the resulting (pHDA+pHDB)/RNA polyplexes which were subsequently frozen for one hour at - 20 °C and thawed at 4 °C (~ 1 h) [33].

Preparation of RNA (core)-OVA(shell) polyplexes (RO)

The remaining BCN groups of the RNA polyplexes were subjected to further copper-free click conjugation with azide modified OVA to immobilize this antigen onto the surface of the RNA polyplexes. To this end, azide modified OVA (OVA SS 10) was dissolved in 5 mM NaAc buffer (pH 5, 2.5 mg/mL) and added to the RNA polyplex dispersion (prepared as described in section 2.6.1 at OVA/(OVA+polymer) of 33, 50, 66, 75 and 80%, resulting in (N_3 in OVA) / (remaining BCN groups of the polyplexes) ratios of 0.35, 0.7, 1.4, 2.1 and 2.8 mol/mol, followed by vortexing and incubating at 4 °C for 5 min. The modified polyplexes were frozen in liquid nitrogen and

freeze-dried. The resulting RNA-OVA polyplexes are further termed RO_x, with x corresponding with the percentage of OVA added to the formulation. To evaluate the conjugation efficiency of OVA to the RNA polyplexes, azide modified OVA and labeled with Sulfo-Cy3 were used to prepare the formulations. The resulting RNA-OVA polyplexes dispersion was freeze-dried and re-dissolved in DPBS. Next, after 1 hour, the unconjugated OVA was removed by Vivaspin® 500 centrifugal filter with a molecular cut-off 300 kDa. The concentration of OVA in the filtrate was measured with UV spectroscopy (548 nm). The conjugation efficiency (CE) was calculated as follows: CE= (total OVA-OVA in filtrate)/total OVA ×100%. The conjugation efficiency of azide functionalized OVA with RNA polyplexes (50% OVA added) was 87%.

Preparation of virus mimicking particles (VMP)

The RNA-OVA (RO₅₀) polyplexes prepared as described in section 2.6.2 containing 60 µg RNA were dispersed in 600 µL 5 mM NaAc buffer. Next, 20.2 µL p(Man-r-BCN) or p(Gal-r-BCN) (10 mg/ml in water) was added to OVA/RNA polyplexes at (BCN in sugar polymer)/(azide in OVA) molar ratio of 1.2 and followed by freeze-drying. The resulting virus mimicking particles (VMP-Man/VMP-Gal) were stored at 4 °C and resuspended in DPBS for further experiments.

Lectin binding assay and stability assay

The ability of the VMP-Man to bind to a mannose-specific lectin was investigated using a Concanavalin A (ConA, 104 kDa, Sigma-Aldrich, the Netherlands) agglutination assay [34]. Sixty µL of VMP-Man dispersion (RNA concentration was 100 µg/mL in DPBS) was pipetted into a DLS microcuvet and subsequently diluted with 240 µL phosphate buffering solution (DPBS, pH 7.4) containing CaCl₂ and MgCl₂ (0.901 mM and 0.493 mM, respectively). DLS measurements were recorded every 60 s at room temperature. After 5 min, 300 µL of a 0.5 mg/mL ConA in DPBS was pipetted into the microcuvette under continuous recording of the DLS data. The size was measured for another 10 mins. Analogous to the above-described assay, the interaction of VMP-Gal with Con A was investigated under identical conditions. For stability assay, 1 mL of VMP-Man dispersion (RNA concentration 10 µg/mL in DPBS) was pipetted into a microcuvette under continuous recording of the DLS data for 6 h at 37 °C. The stability of the VMP-Man particles was also studied under reducing conditions. Therefore, DTT was added to VMP-Man dispersion in DPBS to a final concentration of 10 mM and the size of the particles was recorded by DLS for 6 h at 37 °C.

Particle size and zeta-potential measurements

The size and size distribution of the polyplexes were measured with DLS using an ALV CGS-3 system (Malvern Instruments, Malvern, UK) equipped with a JDS Uniphase 22 mW He-Ne laser operating at 632.8 nm, an optical fiber-based detector, a digital LV/LSE-5003 correlator with temperature controller set at 25 or 37 °C. The zeta-potential (ζ) of the polyplexes was measured using a Malvern Zetasizer Nano-Z (Malvern, UK) with universal ZEN 1002 'dip' cells and DTS (Nano) software (version 4.20) at 25 or 37 °C. Polyplex measurements were performed

in 5 mM HEPES pH 7.4 and at an RNA concentration of 10 µg/mL. For the stability study, polyplexes were resuspended or diluted in DPBS with a final RNA concentration of 10 µg/mL.

Uptake of RO by DC2.4 cells

DC2.4 cells were seeded into a 48-well plate (70,000 cells/well) and incubated in RPMI-1640 medium (10% HI-FBS, 50 µM 2-mercaptoethanol and 2 mM l-glutamine) for 24 h at 37 °C. RO polyplexes (OVA with Cy3 labeled and RNA (luc_mRNA) with Cy5 labeled) were diluted with cell culture medium to a final OVA concentration of 7.5 µg/mL. Next, the cell medium was changed with 200 µL medium containing the different formulations and incubated for 4 h at 37 °C. The cells were washed with DPBS and 50 µL EDTA (2 mM) was added to detach the cells from the plates. The presence of internalized RO polyplexes was examined by flow cytometry (Canto II, BD). For confocal microscopy, DC 2.4 cells were seeded into 96-well µClear® black plates (10,000 cells/well) and incubated for 24 h at 37 °C. Then, the medium was replaced with fresh medium containing different RO formulations (OVA labeled with Cy3 and RNA labeled with Cy5) at a final OVA concentration of 7.5 µg/mL and the cells were subsequently incubated for another 4 h at 37 °C. Next, the medium was replaced with fresh medium containing Hoechst33342 for staining the nuclei (incubation at 37 °C for 10 min). After washing with DPBS, CLSM images were recorded using Yokogawa CV7000S imager (Yokogawa group, Tokyo, Japan) equipped with a 60x water immersion objective at excitation wavelength of 405, 561 and 646 nm for Hoechst33342, Cy3-OVA and Cy5-RNA, respectively.

In vitro antigen presentation and cytotoxicity study

MHC class I antigen presentation assay

D2.4 cells (50,000 cells/well) were seeded in a 96-well plate and cultured for 24 h at 37 °C and subsequently incubated with soluble OVA, soluble OVA + polymer (same concentrations of pHDA and pHDB as used to prepare VMP formulations) and VMP at titrated amounts of OVA (12.5-75 µg/mL) for 18 h at 37 °C. Subsequently, B3Z cells (CD8+ T cell hybridoma cells, 50,000 cells/well), in 100 µL IMDM medium (10% HI-FBS, 25 µM 2-mercaptoethanol and 2 mM Glutamax) were added to the D2.4 cells and co-incubated for 24 h at 37 °C. The hybridoma B3Z cells produce β-galactosidase after being activated by DCs that present SIINFEKL in MHC molecules, thus allowing measurement of antigen presentation by a colorimetric assay using β-galactosidase assay (CPRG) [35]. β-Galactosidase activity of B3Z cells was measured by incubating the cells with 100 µL of CPRG buffer [35] for 1 h at 37 °C. β-Galactosidase converts the yellow–orange substrate CPRG into the chromophore chlorophenol red that absorbs at 590 nm, and the absorbance was read by SPECTROstar (BMG Labtech, Germany). To determine the relative maximum B3Z T cell activation, DCs were loaded with 1 µg/mL of the H-2K^b-restricted OVA class I epitope SIINFEKL (Invitrogen) as positive control and the extinction value was set as 100% [13].

Cytotoxicity of VMP formulations

To determine cytotoxicity of VMP formulations, the Alamar Blue cell viability assay (Invitrogen, Karlsruhe, Germany) was performed. In short, 24 h after incubation with the indicated formulations as described above, the cell medium was replaced with culture medium containing Alamar Blue (50 nM) and cultured for another 4 h at 37 °C. Next, 80 µL of medium was transferred into a flat-bottom 96-well plate to measure the light absorbance. The relative cell metabolic activity was calculated by normalizing the absorbance at 570 nm (reference wavelength of 630 nm) with the absorbance of DPBS-treated cells.

Murine Bone Marrow Derived DCs cellular uptake and maturation

Bone marrow derived DCs (BMDCs) were generated using a protocol as described by Coen et al [34]. After harvesting BMDC from C57BL/6 mice with 6 days culturing, the cells were pulsed with different VMP formulations (Cy5-luc_mRNA) at an OVA concentration of 7.5 µg/mL. After 1 h of incubation at 37 °C, the cells were detached and transferred into Eppendorf tubes and centrifuged (10 min, 250 x g, 4 °C). The supernatant was aspirated, discarded, and the cell pellets were stained with 50 µL L/D -Amcyan / CD11c-PE-Texa-red (BD Biosciences) for 30 mins on ice. Next, 200 µL of FACS buffer (1% BSA in DPBS) was added to the samples prior to centrifugation (10 min, 250xg, 4 °C). The supernatant was aspirated, and the cell pellets were suspended in 200 µL of FACS buffer and kept on ice to prevent cell lysis. The cells were then subjected to flow cytometry analysis. To measure the maturation level of the BMDCs, after their incubation with the VMP particles for 24 h, the cells were washed with FACS buffer and subsequently stained with an antibody cocktail solution containing L/D-Amcyan, CD11c-PE-Texa-red, CD40-APC and MHCII-FITC antibodies (2 µg/mL, 50 µL per well, eBioscience) for 30 min on ice. The BMDCs were subsequently analyzed by flow cytometry after being washed with FACS buffer. FACS analysis was performed using a BD Accuri C6 (BD Biosciences) and data were processed by FlowJo software.

5

Cytotoxic T Lymphocyte activity *in vivo*

Female wild type C57BL/6 mice were purchased from Janvier (Le Genest Saint Isle, France). All mice were 7-12 weeks old at the start of the experiment and maintained under pathogen-free conditions. Subcutaneous immunizations were performed in C57BL/6 mice twice at tail base in a 3 week interval (Fig. 8a). Mice were injected with OVA (InvivoGen), OVA+polymer (same amount of pHDA and pHDB used for the preparation of the VMP formulations), OVA+PolyU polyplexes (chapter 4 in this thesis), VMP-Gal and VMP-Man with an OVA dose of 25 µg (plus 5 µg PolyU) in a total volume of 40 µl of 5% glucose in saline RNase-free water (Ambion, Life technologies, USA). Two weeks after boost injection, mice were injected intravenously with 1.5×10^7 target splenocyte cells. Splenocytes were pulsed with 1 µg/ml of MHC-I OVA peptide (SIINFEKL, Invitrogen) or HIV-1 Gag peptide (AnaSpec) as a control before labelling with 5 µM (Termed CFSE^{hi}) or 0.5 µM (termed CFSE^{low}) 5-(and 6)-carboxyfluorescein diacetate succinimidyl ester (CFSE, Invitrogen), respectively. Labeled cells were mixed at a 1:1 ratio

and were adoptively transferred into immunized mice. Two days later, splenocytes from host mice were analyzed by flow cytometry after staining with α -F4/80 (BD Biosciences, San Diego, CA, USA) to exclude auto-fluorescent macrophages. Percentage antigen-specific killing cells was determined using the following formula: $100 - 100 * ((\% \text{ CFSE}^{\text{hi}} \text{ cells} / \% \text{ CFSE}^{\text{low}} \text{ cells})_{\text{immunized mice}} / (\% \text{ CFSE}^{\text{hi}} \text{ cells} / \% \text{ CFSE}^{\text{low}} \text{ cells})_{\text{non-immunized mice}})$.

Measurement of Ab titers

The mice were immunized as described in section 2.11 and 7 days after the boost administration, serum was collected from the mice for antibody titer analyses. To measure the OVA specific Ab titers, 96-well plates were coated with 100 μ l OVA (10 μ g/mL in DPBS) solution overnight at 4 $^{\circ}$ C. The plates were washed (1 \times 5 min) with buffer (DPBS containing 0.05% Tween 20) and incubated for 2 h with blocking buffer (DPBS containing 2% BSA and 0.05% Tween 20). Next, the plates were incubated with 5-fold serially diluted serum in blocking buffer starting with a dilution of 1:50 for 2 h. To detect bound Ab, the plates were washed (3 \times 5 min) and incubated for 1 h with HRP-conjugated anti-mouse total IgG1 and IgG2c Ab (Southern Biotech, Birmingham, USA) with a dilution of 1: 3,000 in blocking buffer. After the plates were washed (3 \times 5 min), 100 μ l TMB substrate solution (Sigma-Aldrich, the Netherlands) was added to the wells to initiate the color reaction at room temperature in the dark for 30 min. The reaction was stopped with 2 N H_2SO_4 (50 μ L/well), and the OD was measured at a wavelength of 450 nm (OD_{450}).

Statistical analysis

Unless otherwise mentioned, triplicate data were obtained and presented as mean \pm standard deviation. Statistical analysis for comparison between means was performed with software Graphpad Prism 7 and a value of $p < 0.05$ was considered significant.

| Results and discussion

Synthesis and characterization of polymers

The building block polymers with azide and BCN functional groups were synthesized as shown in Scheme 2. Firstly, p(HPMA-r-NAS) was synthesized via RAFT polymerization using a similar procedure as previously published [29] with 27 mol% of NAS in the copolymer ($M_n = 14$ kDa, PDI = 1.31) (Fig. S1a). No significant peak shift in the RI chromatogram and decrease of UV absorbance at 309 nm (the absorbance maximum of the trithiocarbonate group [36]) of the polymer before and after incubation with AIBN confirmed the successful end removal of the RAFT trithiocarbonate end group (>92%) (Fig. S1 b&c). Next, the copolymer was reacted either with 2-((2-azidoethyl) disulfanyl) ethan-1-amine hydrochloride (AEDA) or BCN-amine in a 1.2:1 molar ratio relative to the number of NAS units in the copolymer, followed the addition of an excess of 1-amino-propam-2-ol to fully convert remaining unreacted NAS groups (Scheme 2). ^1H NMR analysis of the modified polymers after purification showed that the azide

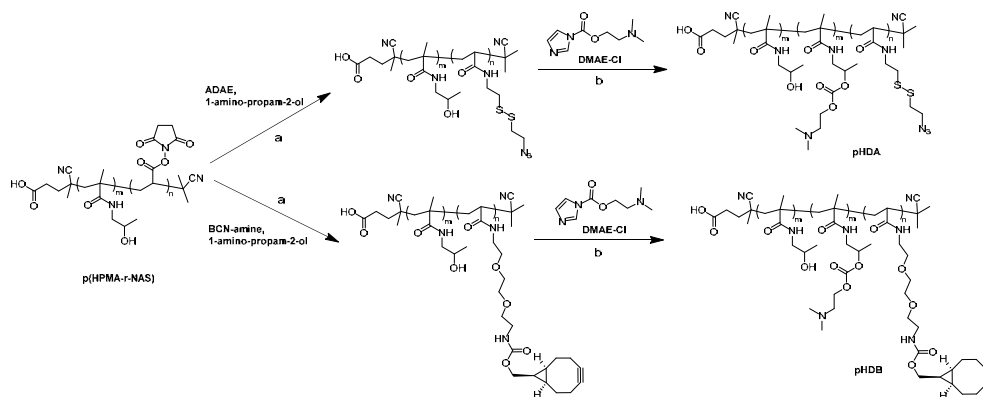
and BCN groups were indeed incorporated into the polymers with a conjugation efficiency of 77 and 75%, relative to NAS group (Table 1).

In the last step (scheme 2), the azide and BCN functionalized polymers were reacted with DMAE-Cl to yield the cationic polymers p(HPMA-DMAE-r-AEDA) (pHDA) and p(HPMA-DMAE-r-BCN) (pHDB). After purification of the polymers by ultrafiltration, ^1H NMR (Fig. S3 for pHDA and Fig. S4 for pHDB) showed the appearance of a new peak at δ 4.75 ppm (2H, OCH_2CH_2 , HPMA-DMAE), confirming the successful reaction of the OH group of HPMA with DMAE-Cl. By comparing the integral ratio of the peak at δ 4.75 ppm and the remaining peak at δ 3.74 ppm (1H, $\text{CH}_2\text{CHCH}_3\text{O}$, HPMA), it is calculated that the conjugation efficiencies with DMAE-Cl are 63 and 68% for pHDA and pHDB, respectively (Table 1). GPC analysis of the final polymers showed that pHDA had a relatively low PDI (1.40) after post-polymerization, while pHDB had a broader molecular weight distribution (PDI of 2.01). This broader molecular weight distribution can likely be ascribed to a side reaction of BCN with the thiol at the ω -end of

Table1. Characteristics of the synthesized copolymers used in the present study.

Polymers	Abbreviation	HPMA (% mol) ^a	NAS (% mol)	HPMA-DMAE (% mol)	ADA/E/BCN (% mol)	M_n^c (g/mol)	M_w/M_n
P(HPMA-r-NAS)	pHN	72 (62%) ^b	28 (58%) ^b	0	0	14,400	1.31
P(HPMA-DMAE-r-ADA/E)	pHDA	26	0	49 (63%) ^b	25 (87%) ^b	21,600	1.40
P(HPMA-DMAE-r-BCN)	pHDB	29	0	53 (68%) ^b	18 (61%) ^b	28,100	2.01

a Copolymer composition as determined by ^1H NMR; b Conversion (percentage) calculated from ^1H NMR; c Determined by GPC viscotek analysis (0.3 M NaAc, pH 4.4, with 30% acetonitrile as eluent).



Scheme 2. Post-polymerization modification of p(HPMA-r-NAS) copolymer to yield azide-containing polymer pHDA and BCN-containing polymer pHDB: (a) TEA, dry DMSO, 35 °C, 50 h; (b) TEA, DMSO, RT, 72 h.

the polymer by thiol-yne reaction [37,38], because around 10% of the polymer chains still carry a trithiocarbonate group after end group removal, which can be subsequently be converted into a free thiol group by aminolysis during post-polymerization modification [36,39].

Modification of OVA with azide groups

To covalently conjugate OVA to the RNA polyplexes (Scheme 1), the OVA antigen was modified with azide groups using 3-((2-azidoethyl) disulfanyl) propanoic acid NHS ester (ADDP, Scheme S3) for subsequent coupling with BCN groups present on the particles. The disulfide bond between OVA and particles enables the intracellular release of OVA due to the presence of glutathione (2–10 mM) [40,41]. Varying amounts of azide groups were introduced by reaction of OVA with ADDP at different molar ratio (Fig. 1a). The number of azide groups introduced to OVA was determined by a TNBS assay. This assay determines the number of free lysine residues in proteins and thus the number of lysine per protein reacted with ADDP can be calculated. The results of the TNBS assay show that 1.5 and 3.6 of azide groups per OVA molecule were introduced when ADDP was added at a 5 and 10 molar excess, respectively (Fig. 1a). The maximum modification of 3-4 azide groups is in line with the observation that three of lysine groups are easily accessible in native OVA [42]. The modified OVA was further characterized

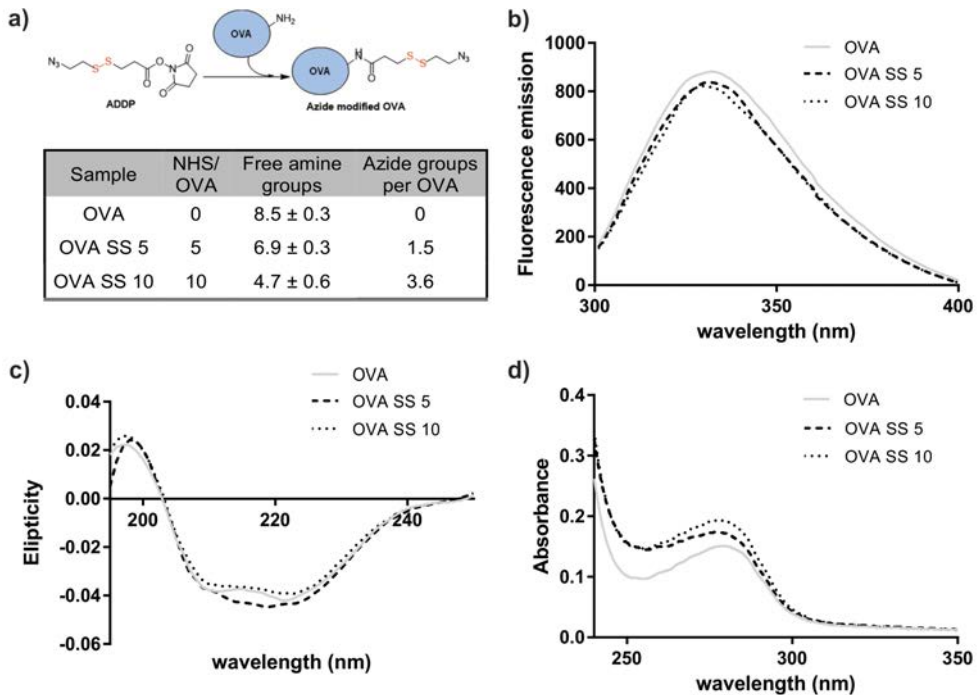


Fig.1. Characteristics of azide-modified OVA. (a) Table summarizing the number of free amines of OVA as determined by the TNBS assay (n=3). Fluorescence emission spectra (b), far-UV CD (circular dichroism) spectra (c) and UV-vis spectra of azide-modified OVA samples.

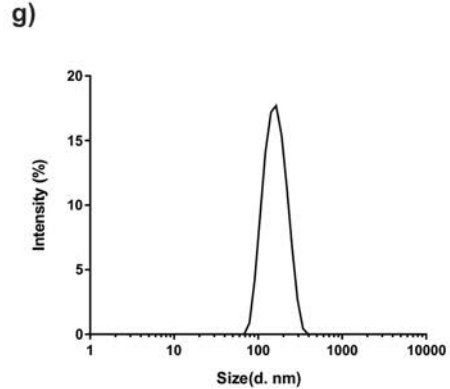
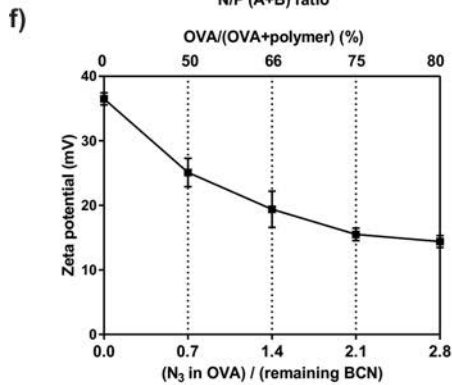
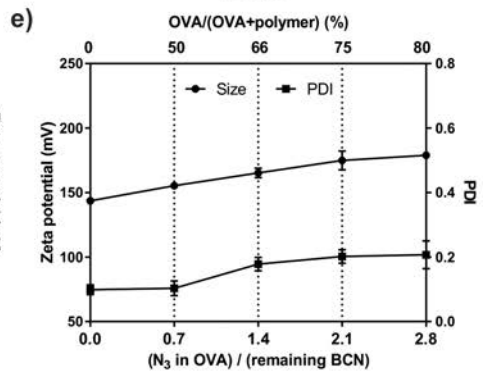
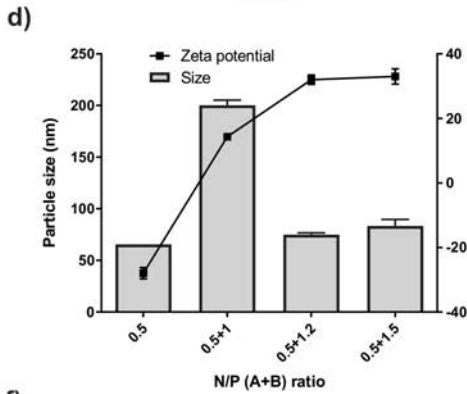
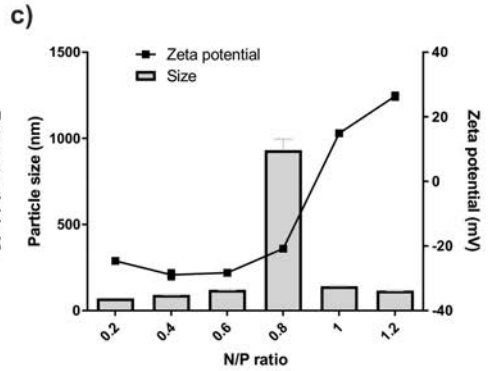
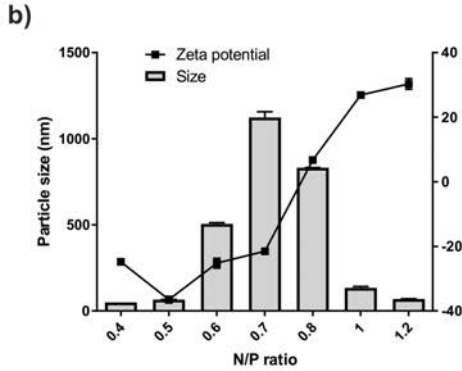
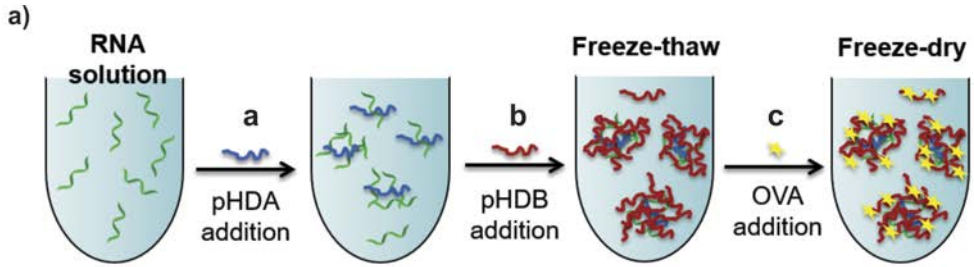
with spectral analysis (Fig. 1b-d). The fluorescence and circular dichroism (CD) spectra showed no significant differences between native and modified protein, which demonstrates that neither aggregation nor significant changes in secondary or tertiary structures occurred after OVA modification. As shown in Fig. 1d, the increase of UV absorbance at 280 nm for the modified OVA might be attributed to the contribution to the absorption of the introduced disulfide bonds [42]. OVA modified with an average of 3.6 azide groups (OVA SS 10, Fig. 1a) was used for the experiments discussed in the following sections.

Preparation and characterization of RNA-OVA polyplexes

It has been shown in previous studies that the physicochemical properties of polyelectrolyte complexes are dependent on the mixing sequence of the negatively charged polyanion (e.g. a nucleic acid) and the cationic polymer [43,44]. As illustrated in Fig. 2a, three steps can be distinguished in the preparation of the RNA (core)-OVA (shell) polyplexes. pHDA was first mixed with RNA (PolyU) to form negatively charged particles (at N/P ratio <1), followed by coating of the formed polyplexes with a slight excess of pHDB to yield positively charged particles. The freeze-thaw treatment likely accelerates the click reaction [45] between azide (from pHDA) and BCN (from pHDB) groups to form the crosslinked RNA core, and the excess amount of BCN groups relative to azide groups was subsequently used for conjugation of azide modified OVA to the particles as shell. It should be noted that the addition of azide modified OVA to these cationic polyplexes (zeta potential was 18 mV) at pH 7.4 (5 mM HEPES buffer) resulted in the formation of aggregates (> 1 μ m; Fig. S7) likely because of the highly negative charge (-25 mV) of OVA (pI = 4.9 [46]). The net surface charge of OVA is dependent on the pH of the buffer in which the protein is dissolved, and therefore to decrease the surface charge of OVA, the formulations were prepared in pH 5 ammonium acetate (NH₄OAc, 5 mM) buffer, in which OVA has a slightly positive charge (9 mV). Another advantage of the NH₄OAc buffer is that this ammonium salt can be evaporated during freeze-drying [47].

To obtain insight into the self-assembling properties (electrostatic interactions) of pHDA/pHDB and RNA, RNA (PolyU) was mixed with pHDA or pHDB at varying N/P ratios from 0.2 to 1.2, where the N/P ratio refers to the molar ratio of amines (N, cationic groups, pK_a=9.5) in the polymers to phosphates (P, anionic groups, pK_a<1) in the nucleic acid. As shown in Fig. 2b, pHDA formed small negatively charged RNA polyplexes at an N/P ratio of 0.5 (around 60 nm in diameter; zeta potential -32 mV). At this stage, pHDA plays a role as an electrostatic

Fig. 2. a) Schematic representation of the preparation of RNA-OVA (RO) polyplexes. Particle size and zeta potential of pHDA/RNA polyplexes (b), pHDB/RNA polyplexes (c) and (pHDA+pHDB)/RNA polyplexes (d) as a function of N/P ratio. Surface modification of RNA core ((pHDA(0.5)+pHDB(1.2))/RNA polyplexes) with azide modified OVA (OVA SS10) at various mixing (N₃ in OVA) / (remaining BCN groups of the polyplexes) ratios to yield RNA-OVA polyplexes, termed as RO. (e) Size and PDI and (f) zeta potential of RO polyplexes. (g) DLS histogram of RO₇₅ prepared at (N₃ in OVA) / (remaining BCN groups of the polyplexes) = 2.1, which means 75% weight ratio of OVA added. The polyplexes were prepared in 5 mM NH₄Ac buffer, with a final RNA concentration of 50 μ g/mL. Data are presented as mean \pm SD. ▶



glue and binds the negatively charged RNA, as depicted in step a of Fig. 2a. At an N/P ratio of 0.8, pHDA/RNA aggregates (830 nm, 6 mV) were formed. Positively charged polyplexes with size of < 150 nm were formed at an N/P ratio of 1 and higher. A similar trend was observed for the pHDB/RNA polyplexes (Fig. 2c), in line with the other studies of PEI/DNA polyplexes [44] and pDMEAEM/DNA complexes [48].

To prepare small RNA polyplexes, RNA was first complexed with the azide containing polymer pHDA at an N/P ratio of 0.5 (Fig. 2b). Next, pHDB at different N/P ratios was added to these preformed polyplexes dispersion to find the optimal N/P ratio, at which positively charged polyplexes were formed with low amounts of free pHDB in the polyplex dispersion. As shown in Fig. 2d, after addition of pHDB at an N/P ratio of 1.2 and higher, polyplexes with a size of around 75 nm and positive zeta potential (33 mV) were formed. Agarose gel electrophoresis (Fig. S8) showed that no free RNA was present in the dispersion. The resulting pHDA(0.5)+pHDB(1.2)/RNA polyplexes were subsequently frozen (-20 °C for 1 h) and thawed (4 °C for 1 h) to accelerate the copper-free click reaction between the azide and BCN groups [33], to yield the self-crosslinked RNA core. This freeze/thawing procedure resulted in an increase of size (from 75 to 150 nm), while the zeta potential only showed a slight decrease (from 33 to 30 mV) (Fig. S9a). After incubation with 150 mM NaCl (pH 5, 5 mM NH₄Ac buffer) for 5 h at room temperature, the size of the non-crosslinked pHDB/RNA (N/P = 1.7) polyplexes increased from 180 to 1500 nm, which is normal for cationic charged polyplexes like PEI/RNA [49]. In contrast, the RNA core showed a limited increase in size from 150 to 450 nm after 5 h incubation (Fig. S9b). This increase can be ascribed to swelling of the RNA polyplexes and demonstrates that indeed crosslinked polyplexes were formed. It should be noted that the overall BCN (from pHDB) to azide (from pHDA) molar ratio in the RNA polyplexes dispersion was 1.5, and therefore, the resulting crosslinked RNA core still has an excess of BCN groups which are available for further modification.

The prepared RNA/pHDB core was subjected to surface grafting with azide modified OVA (OVA SS 10, Fig. 1a) through copper-free click conjugation between the azide groups of OVA and remaining BCN moieties of the core, generating a reducible disulfide bonds between the RNA core and the OVA shell (Fig. 2a, step c). Different ratios of OVA SS10 were mixed with the RNA core dispersions. With an increasing of OVA, the size of the RNA-OVA (RO) polyplexes slightly increased from 145 to 178 nm (Fig. 2e). Regardless of the amount of OVA added, the PDI of particles remained low (< 0.2), indicating that the original structure of RNA polyplexes was maintained after OVA coupling. Fig. 2f shows that a gradual decrease in zeta potential from 36 to 14 mV was observed with an increasing amount of OVA added. As shown in Fig. 2g, the narrow distribution of the RO polyplexes was preserved when 75% weight ratio of OVA was added. To accelerate the conjugation reaction between the azide groups of OVA and the BCN groups, the RO polyplexes were freeze-dried (chapter 4 in this thesis). As shown in Table 2, after freeze-drying and redispersion in 5 mM HEPES buffer, pH 7.4, the RO polyplexes size slightly increased; for example, the size of RO₅₀ (refers to 50% OVA loaded particles) increased from 155 to 177 nm. The RO₇₅ particles had a slightly bigger size (195 vs 177 nm) and a lower zeta potential (-13.3 vs -3.2 mV) as compared to the RO₅₀ particles. These negative zeta

Table 2. Particle size and zeta potential of polyplexes.

Sample	Before freeze-drying (pH 5)		After freeze-drying (pH 7.4) ^b	
	Z _{ave} (nm)	Zeta potential (mV)	Z _{ave} (nm)	Zeta potential (mV)
RNA core	141 ± 2	33.2 ± 1.5	156 ± 1	16.4 ± 2.2
RO ₅₀	155 ± 3	25.2 ± 2.2	177 ± 3	-3.2 ± 0.3
RO ₇₅	169 ± 7	15.5 ± 1.4	195 ± 5	-13.3 ± 0.8
OVA + polymer ^a	244 ± 1	20.2 ± 0.8	1263 ± 17	-5.2 ± 0.2

^a Same amount of OVA SS 10 and (pHDA+pHDB) used to prepare RO₅₀. ^b Polyplexes were prepared at 5 mM NH₄OAc buffer (pH 5), after freeze-drying, the particles were resuspended in 5 mM HEPES buffer (pH 7.4). mean ± SD are shown.

potential values can be explained by the negative charge of OVA at pH 7.4. It is important to note that OVA conjugation and the freeze-dry treatment did not lead to detectable RNA release, as demonstrated by agarose gel electrophoresis (Fig. S8).

The uptake of RO polyplexes by DC 2.4 cells was investigated. The RO polyplexes were prepared by using Cy5-labeled mRNA_{luc} and sulfo-Cy3 conjugated OVA (sulfo-Cy3-OVA SS 10, Table S1). As shown in Fig. 3a, DC cells took up RO₅₀ efficiently and the fluorescence signals from RNA and endocytosed OVA confirmed the colocalization, which indicates that RNA (adjuvant) and OVA (antigen) were present the same subcellular compartment. The uptake efficacy of RO polyplexes, soluble OVA and OVA+polymer (OVA was mixed with same amount of polymer used for the preparation of polyplexes) was also studied by confocal microscopy as well as flow cytometry. Strong green fluorescence signals were observed in the DCs incubated with RO polyplexes (both RO₅₀ and RO₇₅) compared to the those incubated with soluble OVA and OVA+polymer (Fig. 3b). The percentage of DCs that internalized OVA when cells incubated with RO₅₀ was about two-fold higher as compared to soluble OVA, whereas a similar uptake percentage was observed for OVA+polymer (Fig. 3c). However, the amount of OVA internalized by DCs measured via mean fluorescence intensity (MFI) in the Cy5 channel of the RO₅₀ formulation was about two times higher than for OVA+polymer (Fig.S10a). The higher cellular uptake of OVA+polymer formulation compared to soluble OVA can probably be ascribed to the formation of micrometer sized particles (Table 2). Likely, the azide modified OVA is conjugated to the BCN moieties of pHDB during the freeze-dry treatment, as studies have shown that the coupling of OVA to a cationic polymer enhances the OVA cellular uptake [50,51]. It should be noticed that although the RO₅₀ and RO₇₅ particles have around the same particle size (177 and 195 nm, respectively), the cellular uptake of RO₇₅ was significantly lower than that of the RO₅₀ particles (Fig. 3c), which may be ascribed to the lower zeta potential of the RO₇₅ polyplexes (-13 and -3 mV, respectively, Table 2). Apart from that, the RNA cellular uptake percentage of RO₅₀ was around 100%, which was two times higher (MFI, five times higher) than observed for the uptake of RO₇₅ (Fig. S10b). Importantly, the RO₅₀ instead of RO₇₅ polyplexes showed that all DCs that have endocytosed OVA also internalized RNA (Fig. 3c),

which is ideal and critical for immune activation and antigen presentation [52,53]. On the basis of these results, the RO₅₀ formulation was selected for further investigations described later.

Preparation and characterization of virus mimicking particles (VMP)

To mimic glycans of glycoproteins present on the envelope of viruses (e.g. HIV and influenza), a polyvalent copolymer with mannose repeating units and BCN groups in the side chain was synthesized (Scheme 3) and coated on the surface of RO polyplexes to yield virus mimicking particles (VMP) which potentially can target DCs. Similarly, a polymer modified with galactose and BCN units that likely does not target DCs was also synthesized and used as a non-functionalized control.

Firstly, poly(N-acryloyloxysuccinimide) (pNAS) with a degree of polymerization of 120 was synthesized by RAFT polymerization (PDI = 1.4, Table S2). After removal of the end trithiocarbonate group, pNAS was reacted with either mannose-amine or galactose-amine (Fig. S12) together with BCN-amine (Scheme 3) followed by hydrolysis of the unreacted NAS

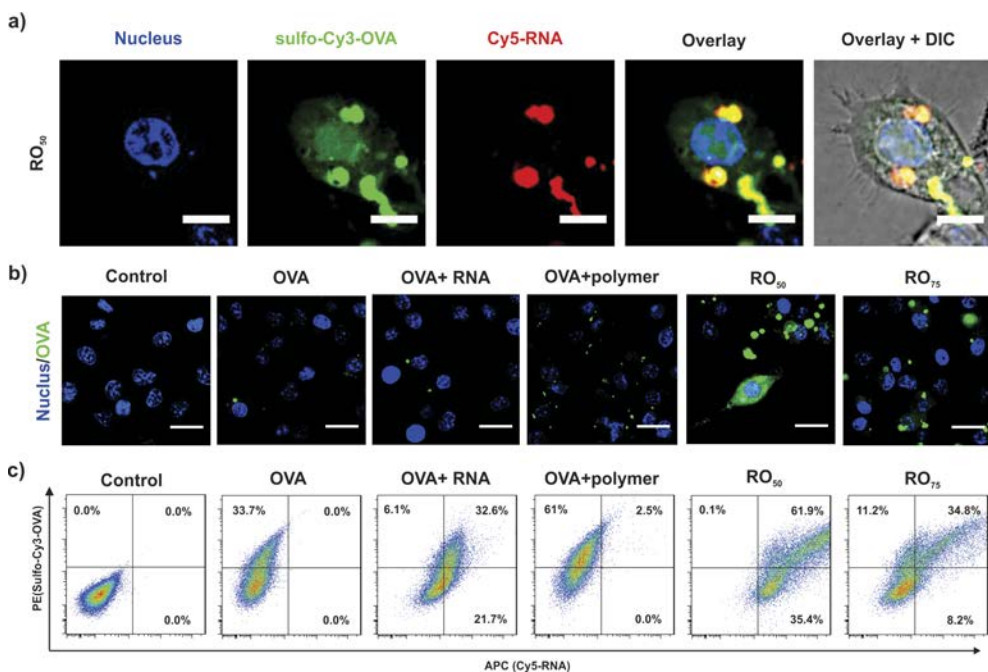
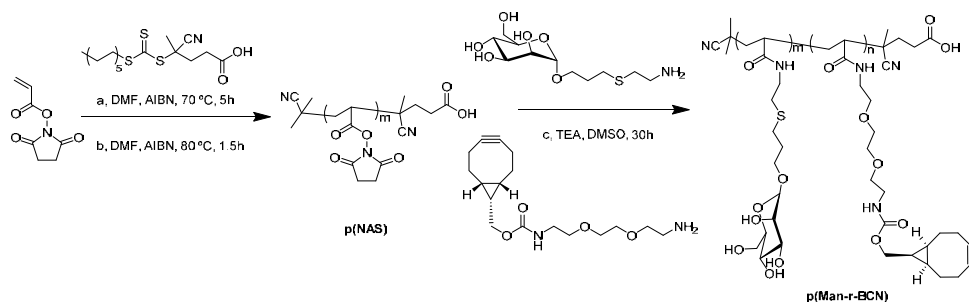


Fig. 3. Co-localization and cellular uptake of RNA-OVA (RO) particles. DC 2.4 cells were incubated with the indicated formulations for 4 h at 37 °C, with a final sulfo-Cy3-OVA (sulfo-Cy3-OVA SS 10, Table S1) concentration of 7.5 μg/mL. (a) representative confocal fluorescence microscopy images of DCs incubated with RO₅₀ polyplexes demonstrate the co-localization of the RNA core (Cy5-labeled luc_mRNA) and the OVA shell (labeled with sulfo-Cy3); bar indicates 10 μm. (b) Representative fluorescence microscopy images of indicated formulations (sulfo-Cy3 labeled OVA) after cellular uptake; bar indicates 20 μm. (c) DC 2.4 cells cellular uptake efficiencies of indicated formulations (Cy5-labeled luc_mRNA and sulfo-Cy3 labeled OVA) was analyzed by flow cytometry.

groups with ammonium hydroxide. The resulting polymers p(Man-r-BCN)/p(Gal-r-BCN) were characterized by ^1H NMR (Fig. S12) and GPC analysis (Fig. S13). The results are summarized in Table S2. The resulting p(Man-r-BCN) and p(Gal-r-BCN) showed narrow and unimodal molecular weight distribution ($M_n \sim 30$ kDa).

The p(Man-r-BCN) or p(Gal-r-BCN) was next added to the RO₅₀ dispersion at a BCN groups in p(Man-r-BCN)/p(Gal-r-BCN) to azide in OVA molar ratio of 1.2, the resulting mannoseylated or galactosylated RO₅₀ polyplexes are termed as VMP-Man and VMP-Gal, respectively. We assume that the unreacted azide groups of OVA during preparation of RO polyplexes are available for reaction with BCN moieties of the p(Man-r-BCN)/p(Gal-r-BCN). As shown in Table 3, the generated VMP particles after freeze-drying and rehydrated in DPBS had a size around 200 nm and a negative zeta potential (-14.3 mV). The smaller particle size and lower surface charge of VMP compared to RO₅₀ can be ascribed to surface shielding by p(Man-r-BCN)/p(Gal-r-BCN), confirming that indeed surface glycans coating occurred. Dynamic light scattering (DLS) measurements of VMP-Man (Fig. 4a) particles in DPBS at room temperature showed that the particles had an excellent colloidal stability (no significant changes in size and scattering intensity for 6 h). Interestingly, these results show that the surface coating of RO₅₀ with poly(mannose) not only provides targeting ability to RO₅₀, but also stabilizes the RO₅₀



Scheme 3. Synthesis routine of the multivalent polymer p(Man-r-BCN). (a) A homopolymer p(NAS) was first synthesized by RAFT polymerization in dry DMF with CPADB as chain transfer agent and AIBN as initiator; (b) The trithiocarbonate group at ω -end of the polymer was removed using AIBN as the initiating species [54]; (c) p(NAS) was further modified with mannose-NH₂ or galactose-NH₂ and BCN-NH₂ in DMSO to yield the final polymers p(Man-r-BCN) or p(Gal-r-BCN).

Table 3. Particle size and zeta potential of different formulations.

Sample	After freeze-drying and redispersion		
	Z_{ave} (nm) ^a	Zeta potential (mV) ^b	PDI ^a
RO ₅₀	504 ± 4	-4.3 ± 1.6	0.097
VMP-Man	198 ± 5	-14.3 ± 1.1	0.196
VMP-Gal	186 ± 4	-15.2 ± 0.5	0.170

^a Particle size and PDI were measured in DPBS. ^b Zeta potential was measured in 5 mM HEPES buffer, pH 7.4.

particles in DPBS. The reduction sensitive property of VMP-Man was studied by exposing these particles to DTT (mimicking the intracellular reductive environment) and continuously monitoring their size by DLS. Fig. 4b shows that the light scattering intensity (SLI) gradually decreased during 160 min of incubation while the particle size remained stable (~250 nm). Upon ~150 min of incubation, a rapid decrease in scattering intensity was observed which was associated with a substantial increase in size of the particles. This points to swelling and dissociation of the VMP-Man particles due to reduction of the disulfide bonds that crosslinks the particles. After 300 min incubation, the scattering intensity was low, which implies that most of particles have been dissociated.

The possible exposure of mannose on the surface of the VMP-Man particles was investigated by testing whether these particles showed affinity for concanavalin A (ConA), a lectin that has four binding sites for α -D-mannosyl and α -D-glucosyl residues, but not for α -D-galactosyl residues [55]. As shown in Fig. 4c, after addition of ConA to VMP-Man particles, the size and SLI increased, while no changes were observed for VMP-Gal particles (Fig. 4d). The results convincingly demonstrate that the mannose units were indeed exposed on the surface of VMP-Man particles.

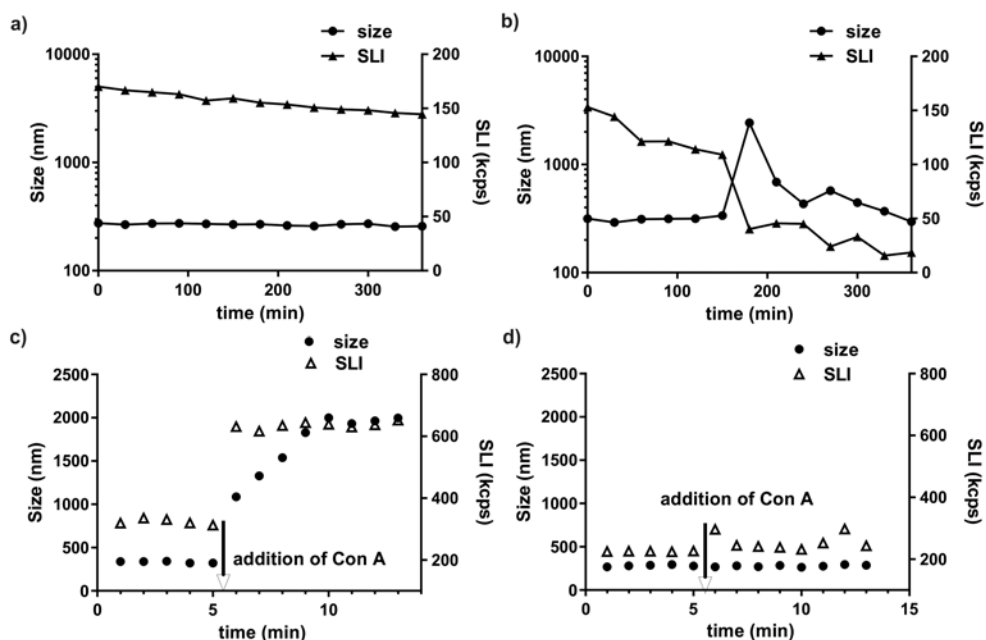


Fig. 4. Particle size and scattered light intensity (SLI) measured by DLS of VMP-Man upon incubation in DPBS in the absence (a) and presence (b) 10 mM DTT at 37 °C. Evolution of size and SLI upon addition of concanavalin A (ConA) to (c) VMP-Man and (d) VMP-Gal particles measured by DLS.

In vitro BMDC cellular uptake and maturation

The potential of VMP-Man particles to specifically target and activate bone marrow derived DCs (BMDCs) was investigated. BMDCs are known to express higher levels of mannose receptor compared to the immortalized cell line DC 2.4 [34]. After 1 h incubation of BMDCs with the different formulations at 37 °C, around 10 and 25% of the cells had taken up the RO₅₀ and VMP-Man particles, respectively (Fig.5a). Importantly, despite having similar particle size (~ 200 nm) and zeta-potential (-15 mV) as the VMP-Man nanoparticles, the latter polyplexes exhibited a very low cellular association with BMDCs cells (5-folds less), which demonstrates that the uptake of VMP-Man particles indeed mainly occurred via mannose-receptor mediated endocytosis.

The capability of VMP-Man/ VMP-Gal particles to induce BMDCs maturation was evaluated with flow cytometry by measuring the upregulation of the co-stimulatory makers CD40 and of MHCII on the surface of DCs. As shown in Fig. 5b, soluble OVA with and without soluble PolyU did not exhibit activation of BMDCs. In contrast, the expression of maturation maker MHCII and CD40 was highly increased when BMDCs were incubated with either VMP-Man or VMP-Gal. It has been shown that the synthetic RNA (PolyU) which is loaded in the core the formulation of VMP-man polyplexes, mimics a single chain RNA of viruses, and therefore activates the endosomal toll like receptor TLR7/8 leading to the maturation of DCs [56]. The results proved that the VMP particles protect RNA against degradation by RNase in the medium and have the capacity to deliver RNA to the endosome of DC to activate TLR 7/8 after being released from the particles.

In vitro antigen presentation and cytotoxicity

The potential of the VMP particles to enhance MHC class I antigen cross-presentation was investigated *in vitro* using DC 2.4 cells exploiting the B3Z cell assay [53]. As shown in

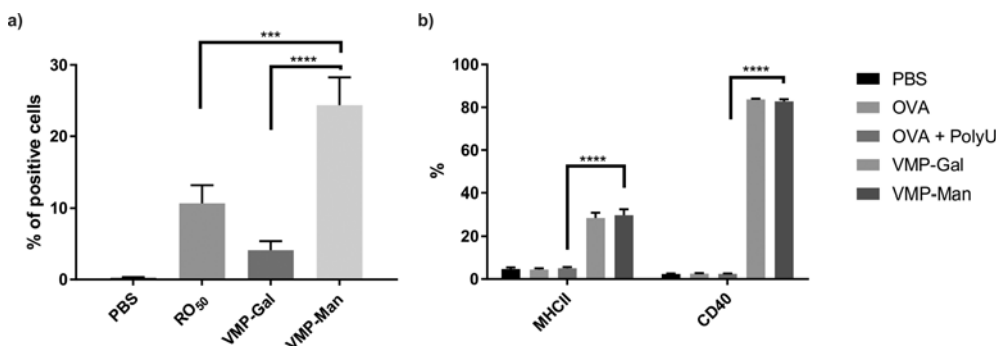


Fig. 5. Flow cytometry analysis of bone-marrow derived DCs (BMDC) cellular uptake efficiency (a) of RO₅₀, VMP-Gal and VMP-Man. The particles formulated with Cy5-mRNA_{luc} were incubated with BMDC at 37 °C for 1h. (n=3; **p<0.01; ****p<0.0001). (b) Percentage of BMDCs that expressed the maturation makers MHCII and CD40 studied by flow cytometry analysis after incubation of BMDCs with the indicated formulations for 24 h (n=4, ****p<0.0001).

Fig. 6a, the three different OVA particulate formulations were more efficient in stimulating B3Z T cells than soluble OVA as also observed for other particulate OVA delivery systems due to the enhanced uptake and cross-presentation [57,58]. All three formulations showed similar T cell activation at high OVA concentration (25 $\mu\text{g}/\text{mL}$). However, at low OVA concentration (12.5 $\mu\text{g}/\text{mL}$), the VMP-Man particles showed the highest T cell activation, with a factor of 2~3 higher activation of T cells activation compared with the VMP-Gal formulation and 1.5 times higher than RO₅₀. The higher cellular uptake (Fig. 5a) likely contributes to this difference in T cell activation. Importantly, all the formulations did not show any toxicity even at the high concentration tested (75 $\mu\text{g}/\text{mL}$, Fig. S14).

In vivo immunogenicity

To investigate to which extent the targeting ability and the enhanced MHC class I presentation of the VMP-Man observed *in vitro* would confer improved antigen specific cellular immune response *in vivo*. Mice were immunized with soluble OVA, VMP-Gal and VMP-Man, following a prime-boost scheme as shown in Fig. 7a. To exclude any intrinsic adjuvant effects of the polymer used to prepare the nanoparticles, mice were immunized with a mixture of soluble OVA and polymer (pHDA+pHDB). For the adjuvant positive control, PEGylated polyplexes loaded with PolyU, which showed strong adjuvant effect in our previous study (chapter 4 in this thesis), was used. Cytotoxic T cell responses were assessed using a standard *in vivo* killing assay. Three weeks after the boost immunization, mice were challenged with a 1:1 ratio of OVA peptide-pulsed CFSE^{hi} splenocytes (target cells) and non-pulsed CFSE^{low} splenocytes (non-target cells) (Fig. 7a). Two days after this adoptive transfer, the spleens were isolated and the ratio of target cells versus non-target cells was analysed by flow cytometry. The stronger the evoked

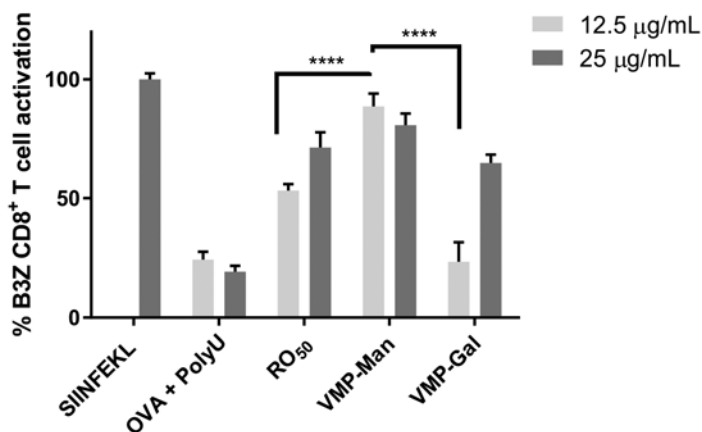


Fig. 6. Efficient MHC class I cross-presentation of VMP particles *in vitro*. D2.4 cells were incubated for 24 h with different OVA formulations. MHC class I presentation of processed OVA was detected by co-culture with H-2Kb/SIINFEKL-specific B3Z cells. Normalized values were calculated based on the OD₅₉₀ nm values obtained by using DC pulsed with SIINFEKL (1 $\mu\text{g}/\text{mL}$) cultured together with B3Z T cells (OD_{590nm} = 0.84 = 100% CD8+ T cell activation). **** p < 0.0001 (two-way ANOVA).

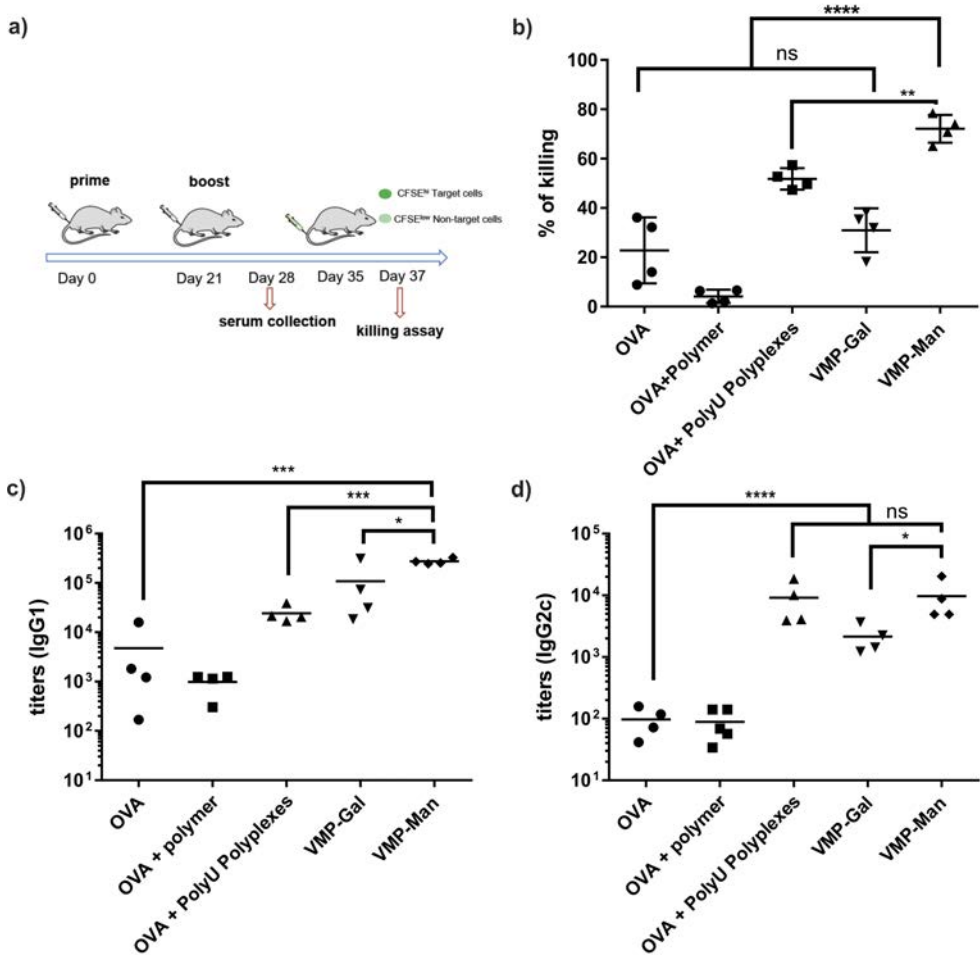


Fig. 7. Adaptive immune responses evoked by VMP particles. (a) Schematic representation of the experimental set-up of the immunization protocol. (b) Specific killing of target cells in response to each vaccine formulation. Antibody titers of IgG1 (c) and IgG2c (d) in serum. Data are shown as means of 4 mice /group. * $p < 0.05$; ** $p < 0.01$; *** $p < 0.001$; **** $p < 0.0001$ (one-way ANOVA).

cytotoxic T cell response, the more targeted cells are killed, leading to a higher killing percentage. Fig. 7b shows that the mice immunized with the mixture of soluble OVA and polymer exhibited even lower level of antigen specific cell lysis as compared to soluble OVA, indicating the poor adjuvant effects of the soluble polymer used in this study. Immunization with VMP-Gal antigen particles did not result in antigen specific cell lysis levels above those induced by immunization with antigen in saline. Importantly, The VMP-Man formulation induced the most strongest cytolytic T cell responses. The observed differences in the killing assay between VMP-Man and VMP-Gal can likely be ascribed to the enhanced DC cellular uptake of VMP-Man by binding to the mannose receptors followed by endocytosis and MHC I antigen presentation [59]. On

the level of the humoral immune response, VMP-Man strongly promoted IgG1 responses (Fig. 7c), as well as IgG2c (Fig. 7d), which are indicative for the strength of Th1 immunity induction [60]. All formulations with PolyU were potent in eliciting the IgG2c response as compared to soluble OVA (Fig. 7d). A similar phenomenon was observed in previous studies when mice were immunized OVA together with TLR ligands like polyU and resiquimod [13,60–62]. Taken together, VMP-Man particles achieved synergistic effects in terms of effector T cell and humoral responses.

| Conclusions

In summary, we have developed a virus mimicking synthetic vaccine with mannose ligands on the surface, for the effective and simultaneous delivery of an antigen (OVA) and adjuvant (PolyU) to DCs. This reduction-sensitive vaccine can be readily formulated by sequential self-assembly of RNA and OVA with polymers, and followed by surface modification with mannose ligands by employing copper-free click chemistry. The mannosylated VMP-Man particles with a size around 200 nm exhibited enhanced cellular uptake by BMDCs as compared to VMP-Gal and induced DC maturation. These VMP-Man particles had a good cytocompatibility and enabled enhanced MHC I antigen presentation by DCs *in vitro*. Immunization with VMP-Man showed superior antibody and cytolytic T cell responses. In summary, the synthetic polymer-based vaccine that mimicks the structure and function of viruses, is a promising modality to develop vaccines against diseases such as HIV and cancer that require Th1/cytotoxic T cell responses in addition to antibodies for protection.

5

| Acknowledgements

Bo Lou is financially supported by China Scholarship Council (CSC).

References

1. T.J. Moyer, A.C. Zmolek, D.J. Irvine, Beyond antigens and adjuvants: formulating future vaccines, *J. Clin. Invest.* 126 (2016) 799–808.
2. C. Giefing, A.L. Meinke, M. Hanner, T. Henics, M.D. Bui, D. Gelbmann, U. Lundberg, B.M. Senn, M. Schunn, A. Habel, B. Henriques-Normark, A. Ortqvist, M. Kalin, A. von Gabain, E. Nagy, Discovery of a novel class of highly conserved vaccine antigens using genomic scale antigenic fingerprinting of pneumococcus with human antibodies., *J. Exp. Med.* 205 (2008) 117–131.
3. T.N. Schumacher, R.D. Schreiber, Neoantigens in cancer immunotherapy, *Science.* 348 (2015) 69–74.
4. T.C. Wirth, F. Kühnel, Neoantigen Targeting—Dawn of a New Era in Cancer Immunotherapy?, *Front. Immunol.* 8 (2017) 1848.
5. R. Arens, T. van Hall, S.H. van der Burg, F. Ossendorp, C.J.M. Melief, Prospects of combinatorial synthetic peptide vaccine-based immunotherapy against cancer, *Semin. Immunol.* 25 (2013) 182–190.
6. L. Li, S.P. Goedegebuure, W.E. Gillanders, Preclinical and clinical development of neoantigen vaccines, *Ann. Oncol.* 28 (2017) xiii11–xiii17.
7. A. Pasquale, S. Preiss, F. Silva, N. Garçon, Vaccine Adjuvants: from 1920 to 2015 and Beyond, *Vaccines.* 3 (2015) 320–343.
8. Y. Hailemichael, Z. Dai, N. Jaffarzar, Y. Ye, M.A. Medina, X.-F. Huang, S.M. Dorta-Estremera, N.R. Greeley, G. Nitti, W. Peng, C. Liu, Y. Lou, Z. Wang, W. Ma, B. Rabinovich, R.T. Sowell, K.S. Schluns, R.E. Davis, P. Hwu, W.W. Overwijk, Persistent antigen at vaccination sites induces tumor-specific CD8+ T cell sequestration, dysfunction and deletion, *Nat. Med.* 19 (2013) 465–472.
9. J.W. van der Laan, S. Gould, J.Y. Tanir, Safety of vaccine adjuvants: Focus on autoimmunity, *Vaccine.* 33 (2015) 1507–1514.
10. M.D. Joshi, W.J. Unger, G. Storm, Y. van Kooyk, E. Mastrobattista, Targeting tumor antigens to dendritic cells using particulate carriers, *J. Control. Release.* 161 (2012) 25–37.
11. L.A. Brito, D.T. O'Hagan, Designing and building the next generation of improved vaccine adjuvants, *J. Control. Release.* 190 (2014) 563–579.
12. L.J. Cruz, P.J. Tacken, R. Fokkink, B. Joosten, M.C. Stuart, F. Albericio, R. Torensma, C.G. Figdor, Targeted PLGA nano- but not microparticles specifically deliver antigen to human dendritic cells via DC-SIGN *in vitro.*, *J. Control. Release.* 144 (2010) 118–126.
13. A.L. Silva, R.A. Rosalia, E. Varypataki, S. Sibuea, F. Ossendorp, W. Jiskoot, Poly-(lactic-co-glycolic-acid)-based particulate vaccines: Particle uptake by dendritic cells is a key parameter for immune activation, *Vaccine.* 33 (2015) 847–854.
14. S. Rahimian, M.F. Fransen, J.W. Kleinovink, M. Amidi, F. Ossendorp, W.E. Hennink, Particulate Systems Based on Poly(Lactic-co-Glycolic)Acid (pLGA) for Immunotherapy of Cancer., *Curr. Pharm. Des.* 21 (2015) 4201–4216.
15. S.L. Demento, N. Bonafé, W. Cui, S.M. Kaech, M.J. Caplan, E. Fikrig, M. Ledizet, T.M. Fahmy, TLR9-targeted biodegradable nanoparticles as immunization vectors protect against West Nile encephalitis., *J. Immunol.* 185 (2010) 2989–2997.
16. A. Gutjahr, C. Phelip, A.-L. Coolen, C. Monge, A.-S. Boisgard, S. Paul, B. Verrier, Biodegradable Polymeric Nanoparticles-Based Vaccine Adjuvants for Lymph Nodes Targeting, *Vaccines.* 4 (2016) 34.
17. D. Li, N. Kordalivand, M.F. Fransen, F. Ossendorp, K. Raemdonck, T. Vermonden, W.E. Hennink, C.F. Van Nostrum, Reduction-sensitive dextran nanogels aimed for intracellular delivery of antigens, *Adv. Funct. Mater.* 25 (2015) 2993–3003.
18. Y. Fan, J. Moon, Nanoparticle Drug Delivery Systems Designed to Improve

- Cancer Vaccines and Immunotherapy, *Vaccines*. 3 (2015) 662–685.
19. M. Dierendonck, K. Fierens, R. De Rycke, L. Lybaert, S. Maji, Z. Zhang, Q. Zhang, R. Hoogenboom, B.N. Lambrecht, J. Grooten, J.P. Remon, S. De Koker, B.G. De Geest, Nanoporous hydrogen bonded polymeric microparticles: Facile and economic production of cross presentation promoting vaccine carriers, *Adv. Funct. Mater.* 24 (2014) 4634–4644.
 20. S. Tandrup Schmidt, C. Foged, K. Smith Korsholm, T. Rades, D. Christensen, Liposome-Based Adjuvants for Subunit Vaccines: Formulation Strategies for Subunit Antigens and Immunostimulators, *Pharmaceutics*. 8 (2016) 7.
 21. A. Bandyopadhyay, R.L. Fine, S. Demento, L.K. Bockenstedt, T.M. Fahmy, The impact of nanoparticle ligand density on dendritic-cell targeted vaccines., *Biomaterials*. 32 (2011) 3094–3105.
 22. Y.S. Lee, S.W. Kim, Bioreducible polymers for therapeutic gene delivery, *J. Control. Release*. 190 (2014) 424–439.
 23. L. Brülisauer, M.A. Gauthier, J.C. Leroux, Disulfide-containing parenteral delivery systems and their redox-biological fate, *J. Control. Release*. 195 (2014) 147–154.
 24. F. Meng, W.E. Hennink, Z. Zhong, Reduction-sensitive polymers and bioconjugates for biomedical applications, *Biomaterials*. 30 (2009) 2180–2198.
 25. E.D. Goddard-Borger, R. V. Stick, An efficient, inexpensive, and shelf-stable diazotransfer reagent: Imidazole-1-sulfonyl azide hydrochloride, *Org. Lett.* 9 (2007) 3797–3800.
 26. A.M. Funhoff, C.F. Van Nostrum, A.P.C.A. Janssen, M.H.A.M. Fens, D.J.A. Crommelin, W.E. Hennink, Polymer Side-Chain Degradation as a Tool to Control the Destabilization of Polyplexes, *Pharm. Res.* 21 (2004) 170–176.
 27. N. Vurgun, R.F. Gómez-Biagi, M. Nitz, Access to Versatile β -Cyclodextrin Scaffolds through Guest-Mediated Monoacylation, *Chem. - A Eur. J.* 22 (2016) 1062–1069.
 28. F.L. Dufour Menno, Cellulose support containing d-mannose derivatives, 2010.
 29. J. Moraes, I.-M. Simionca, H. Ketari, H.-A. Klok, Avoiding compositional drift during the RAFT copolymerization of N-(2-hydroxypropyl) methacrylamide and N-acryloxysuccinimide: towards uniform platforms for post-polymerization modification, *Polym. Chem.* 6 (2015) 3245–3251.
 30. M. Chen, G. Moad, E. Rizzardo, Thiocarbonylthio end group removal from RAFT-synthesized polymers by a radical-induced process, *J. Polym. Sci. Part A Polym. Chem.* 47 (2009) 6704–6714.
 31. Y. Li, J. Yang, B.C. Benicewicz, Well-controlled polymerization of 2-azidoethyl methacrylate at near room temperature and click functionalization, *J. Polym. Sci. Part A Polym. Chem.* 45 (2007) 4300–4308.
 32. X. Jiang, A. van der Horst, M.J. van Steenberg, N. Akeroyd, C.F. van Nostrum, P.J. Schoenmakers, W.E. Hennink, Molar-mass characterization of cationic polymers for gene delivery by aqueous size-exclusion chromatography., *Pharm. Res.* 23 (2006) 595–603.
 33. H. Takemoto, K. Miyata, T. Ishii, S. Hattori, S. Osawa, N. Nishiyama, K. Kataoka, Accelerated Polymer – Polymer Click Conjugation by Freeze – Thaw Treatment, *Bioconjug. Chem.* 23 (2012) 1503–1506.
 34. R. De Coen, N. Vanparijs, M.D.P. Risseeuw, L. Lybaert, B. Louage, S. De Koker, V. Kumar, J. Grooten, L. Taylor, N. Ayres, S. Van Calenbergh, L. Nuhn, B.G. De Geest, PH-Degradable Mannosylated Nanogels for Dendritic Cell Targeting, *Biomacromolecules*. 17 (2016) 2479–2488.
 35. J. Karttunen, S. Sanderson, N. Shastri, Detection of rare antigen-presenting cells by the lacZ T-cell activation assay suggests an expression cloning strategy

- for T-cell antigens., *Proc. Natl. Acad. Sci. U. S. A.* 89 (1992) 6020–6024.
36. H. Willcock, R.K. O'Reilly, End group removal and modification of RAFT polymers, *Polym. Chem.* 1 (2010) 149–157.
 37. R. van Geel, G.J.M. Pruijn, F.L. van Delft, W.C. Boelens, Preventing Thiol-Yne Addition Improves the Specificity of Strain-Promoted Azide-Alkyne Cycloaddition, *Bioconjug. Chem.* 23 (2012) 392–398.
 38. H. Tian, T.P. Sakmar, T. Huber, A simple method for enhancing the bioorthogonality of cyclooctyne reagent, *Chem. Commun.* 52 (2016) 5451–5454.
 39. S. Averick, R.A. Mehl, S.R. Das, K. Matyjaszewski, Well-defined biohybrids using reversible-deactivation radical polymerization procedures, *J. Control. Release.* 205 (2015) 45–57.
 40. F.Q. Schafer, G.R. Buettner, Redox environment of the cell as viewed through the redox state of the glutathione disulfide/glutathione couple, *Free Radic. Biol. Med.* 30 (2001) 1191–1212.
 41. M.J. Heffernan, N. Murthy, Disulfide-crosslinked polyion micelles for delivery of protein therapeutics, *Ann. Biomed. Eng.* 37 (2009) 1993–2002.
 42. F.S. Steven, G.R. Tristram, The reactivity of free amino groups in native and denatured ovalbumin towards fluorodinitrobenzene., *Biochem. J.* 70 (1958) 179–182.
 43. C. Schatz, J.M. Lucas, C. Viton, A. Domard, C. Pichot, T. Delair, Formation and properties of positively charged colloids based on polyelectrolyte complexes of biopolymers, *Langmuir.* 20 (2004) 7766–7778.
 44. S.K. Cho, C. Dang, X. Wang, R. Ragan, Y.J. Kwon, Mixing-sequence-dependent nucleic acid complexation and gene transfer efficiency by polyethylenimine, *Biomater. Sci.* 3 (2015) 1124–1133.
 45. H. Takemoto, K. Miyata, T. Ishii, S. Hattori, S. Osawa, N. Nishiyama, K. Kataoka, Accelerated polymer-polymer click conjugation by freeze-thaw treatment, *Bioconjug. Chem.* 23 (2012) 1503–1506.
 46. S.A. Kidwai, A.A. Ansari, A. Salahuddin, Effect of Succinylation (3-Carboxypropionylation) on the Conformation and Immunological Activity of Ovalbumin, *Biochem. J.* 155 (1976) 171–180.
 47. F. Franks, Freeze-drying of bioproducts: putting principles into practice, *Eur. J. Pharm. Biopharm.* 45 (1998) 221–229.
 48. J.Y. Cherng, P. Van De Wetering, H. Talsma, D.J.A. Crommelin, W.E. Hennink, Effect of size and serum proteins on transfection efficiency of poly ((2-dimethylamino)ethyl methacrylate)-plasmid nanoparticles, *Pharm. Res.* 13 (1996) 1038–1042.
 49. Z. Wang, H. Zou, Z. Wang, J. Wu, Z. Xia, M. Feng, Highly stable polyglutamate derivatives/siRNA polyplex efficiently down-relegate survivin expression and augment the efficacy of cisplatin., *Int. J. Pharm.* 505 (2016) 24–34.
 50. L. Lybaert, N. Vanparijs, K. Fierens, M. Schuijs, L. Nuhn, B.N. Lambrecht, B.G. De Geest, A Generic Polymer-Protein Ligation Strategy for Vaccine Delivery, *Biomacromolecules.* 17 (2016) 874–881.
 51. B. Slütter, P.C. Soema, Z. Ding, R. Verheul, W.E. Hennink, W. Jiskoot, Conjugation of ovalbumin to trimethyl chitosan improves immunogenicity of the antigen, *J. Control. Release.* 143 (2010) 207–214.
 52. G. Zhu, F. Zhang, Q. Ni, G. Niu, X. Chen, Efficient Nanovaccine Delivery in Cancer Immunotherapy, *ACS Nano.* 11 (2017) 2387–2392.
 53. R. Kuai, L.J. Ochyl, K.S. Bahjat, A. Schwendeman, J.J. Moon, Designer vaccine nanodiscs for personalized cancer immunotherapy, *Nat. Mater.* 16 (2016) 489–496.
 54. K. V. Gujrati, M.J. Yanjarappa, A. Saraph, A. Joshi, J. Mogridge, R.S. Kane, Synthesis of homopolymers and copolymers containing an active ester of acrylic acid by RAFT: Scaffolds for controlling polyvalent ligand

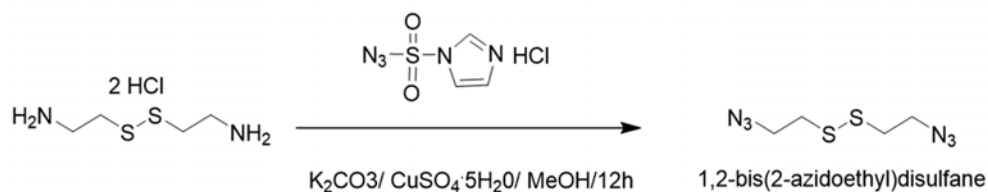
- display, *J. Polym. Sci. Part A Polym. Chem.* 46 (2008) 7249–7257.
55. D.A. Mann, M. Kanai, D.J. Maly, L.L. Kiessling, Probing low affinity and multivalent interactions with surface plasmon resonance: Ligands for concanavalin A, *J. Am. Chem. Soc.* 120 (1998) 10575–10582.
 56. S.S. Diebold, T. Kaisho, H. Hemmi, S. Akira, C. Reis E Sousa, Innate Antiviral Responses by Means of TLR7-Mediated Recognition of Single-Stranded RNA, *Science* (80-.). 303 (2004) 1529–1531.
 57. N. Benne, J. van Duijn, J. Kuiper, W. Jiskoot, B. Slütter, Orchestrating immune responses: How size, shape and rigidity affect the immunogenicity of particulate vaccines, *J. Control. Release.* 234 (2016) 124–134.
 58. A. Gomes, M. Mohsen, M. Bachmann, Harnessing Nanoparticles for Immunomodulation and Vaccines, *Vaccines.* 5 (2017) 6.
 59. S. Burgdorf, A. Kautz, V. Böhnert, P. a Knolle, C. Kurts, Distinct Pathways of Antigen Uptake, *Science.* 612 (2007) 612–616.
 60. G.M. Lynn, R. Laga, P.A. Darrah, A.S. Ishizuka, A.J. Balaci, A.E. Dulcey, M. Pechar, R. Pola, M.Y. Gerner, A. Yamamoto, C.R. Buechler, K.M. Quinn, M.G. Smelkinson, O. Vanek, R. Cawood, T. Hills, O. Vasalatiy, K. Kastenmüller, J.R. Francica, L. Stutts, J.K. Tom, K.A. Ryu, A.P. Esser-Kahn, T. Etrych, K.D. Fisher, L.W. Seymour, R.A. Seder, In vivo characterization of the physicochemical properties of polymer-linked TLR agonists that enhance vaccine immunogenicity., *Nat. Biotechnol.* 33 (2015) 1201–1210.
 61. L. Nuhn, N. Vanparijs, A. De Beuckelaer, L. Lybaert, G. Verstraete, K. Deswarte, S. Lienenklaus, N.M. Shukla, A.C.D. Salyer, B.N. Lambrecht, J. Grooten, S.A. David, S. De Koker, B.G. De Geest, pH-degradable imidazoquinoline-ligated nanogels for lymph node-focused immune activation, *Proc. Natl. Acad. Sci.* 113 (2016) 8098–8103.
 62. R. Heidenreich, E. Jasny, A. Kowalczyk, J. Lutz, J. Probst, P. Baumhof, B. Scheel, S. Voss, K.J. Kallen, M. Fotin-Mleczek, A novel RNA-based adjuvant combines strong immunostimulatory capacities with a favorable safety profile, *Int. J. Cancer.* 137 (2015) 372–384.

| Supplementary data

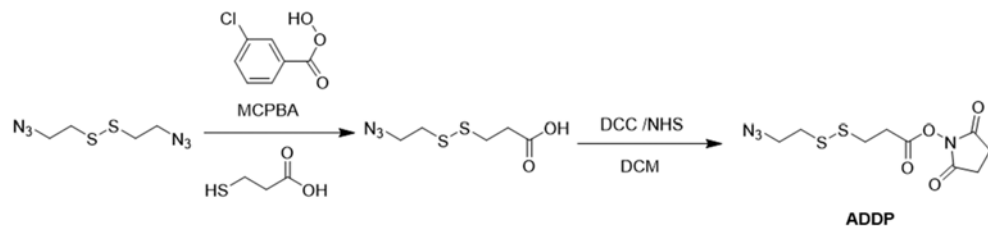
Methods

Gel retardation assay

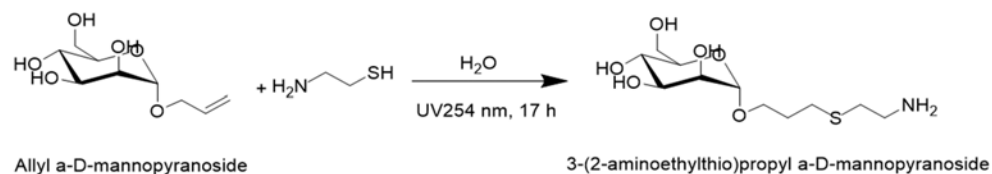
RNA-OVA polyplexes (mRNA_{luc}) after freeze-drying were resuspended in 10 mM HEPES buffer, pH 7.4, 150 mM NaCl, at a final RNA concentration of 40 µg/mL. Next, 20 µL of the sample was mixed with 3 µL 6×Loading Dye and loaded into 1% agarose gel in Tris–acetate–EDTA (TAE) buffer containing GelGreen (Biotium). Electrophoresis was done at 120 V for 30 min. RNA was detected using a Gel Doc™ XR + system (BioRad Laboratories Inc., Hercules, CA) with Image Lab software.



Scheme S1. Synthesis of 1,2-bis(2-azidoethyl) disulfane.



Scheme S2. Synthesis of 3-((2-azidoethyl) disulfanyl) propanoic acid NHS ester (ADDP).



Scheme S3. Synthesis of 3-(2-aminoethylthio) propyl α -D-mannopyranoside (Man-NH₂).

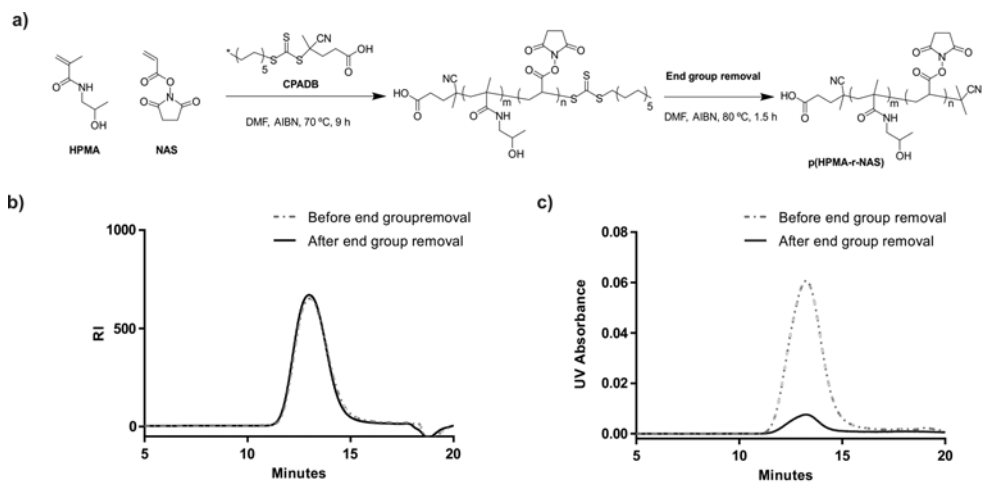


Fig. S1. (a) Polymerization of HPMA and NAS by RAFT. RI (b) and UV absorbance (309 nm) (c) of pHN before and after RAFT end group removal measured by GPC.

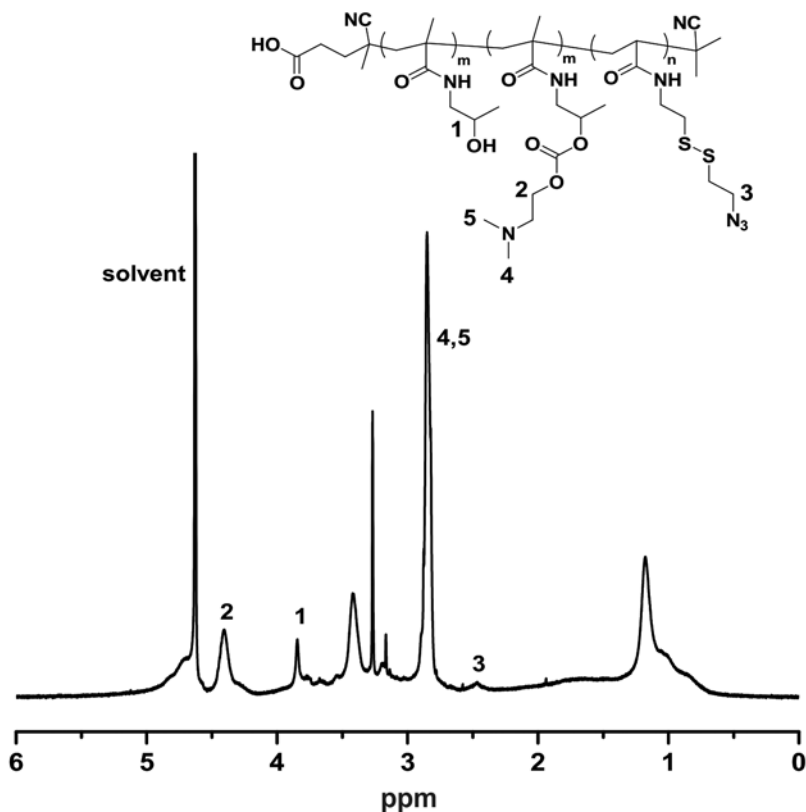


Fig. S2. ^1H NMR (D_2O) spectrum of pHDA.

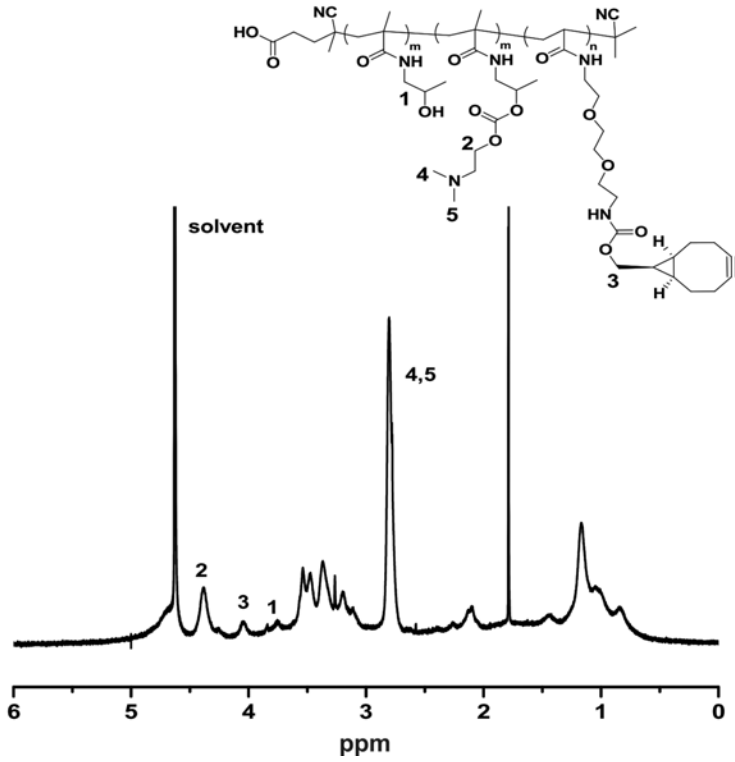


Fig. S3. ^1H NMR (D_2O) spectrum of pHDB.

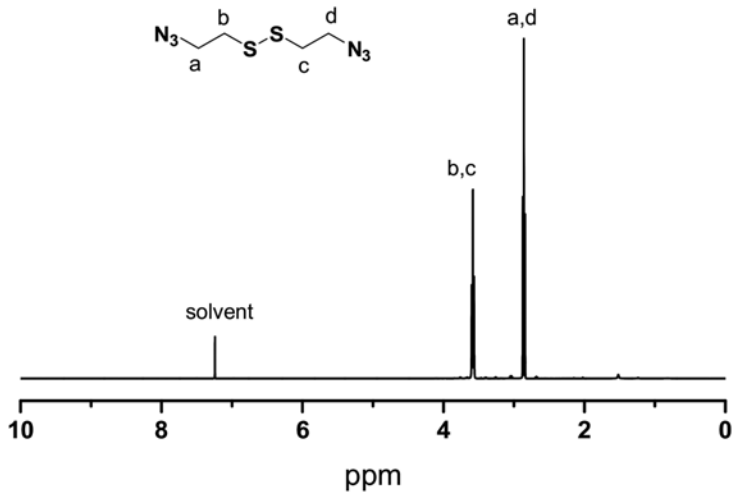


Fig. S4. ^1H NMR (CDCl_3) spectrum of 1,2-bis(2-azidoethyl) disulfane.

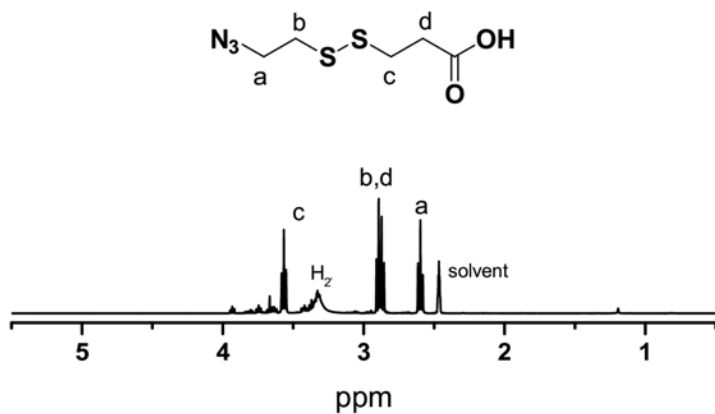


Fig. S5. ^1H NMR (DMSO-d_6) spectrum of 3-((2-azidoethyl) disulfanyl) propanoic acid.

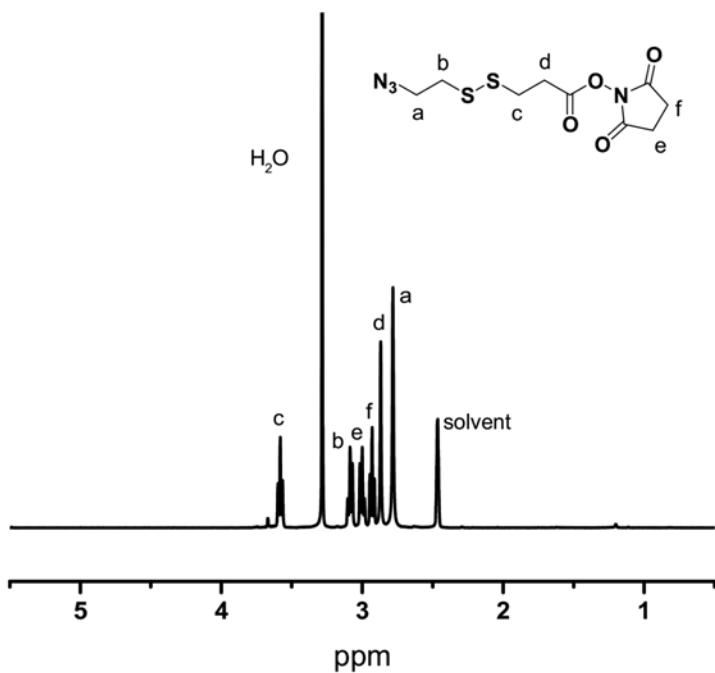


Fig. S6. ^1H NMR (DMSO-d_6) spectrum of 3-((2-azidoethyl) disulfanyl) propanoic acid NHS ester.

5

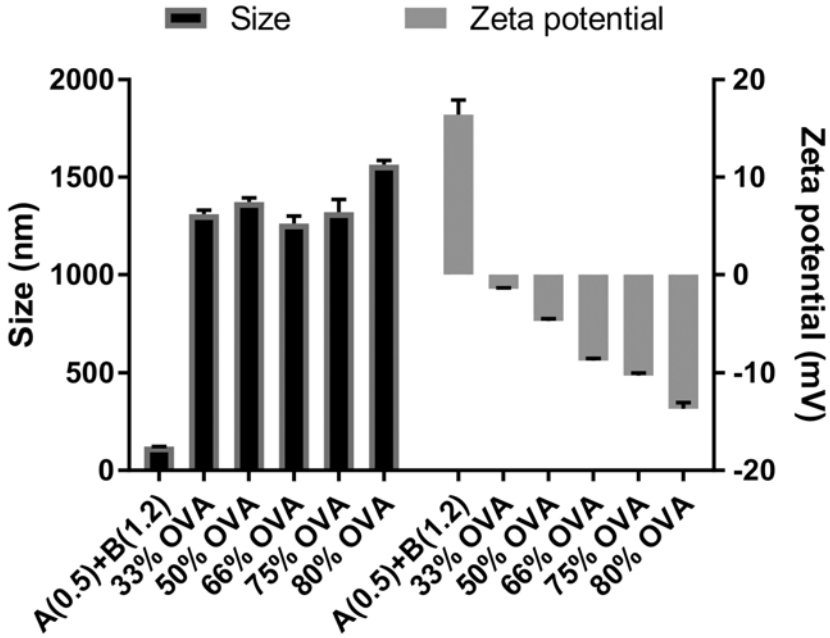


Fig. S7. Addition of OVA to preformed RNA polyplexes in pH 7.4, 5 mM HEPES buffer caused large aggregates. Size and zeta potential after addition different amount of OVA to A(0.5)+B(1.2) polyplexes.

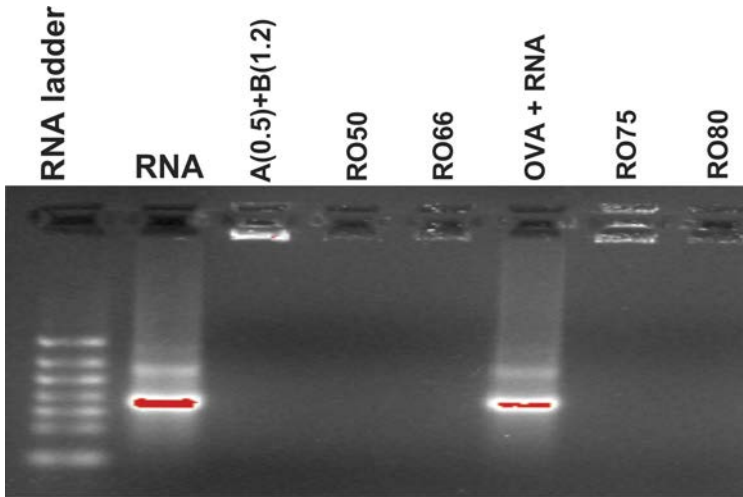


Fig. S8. Agarose gel retardation assay of the RNA polyplexes (pHDA (0.5)+pHDB (1.2)) and RNA-OVA particles after freeze-drying and rehydration in 5 mM HEPES buffer with 150 mM NaCl.

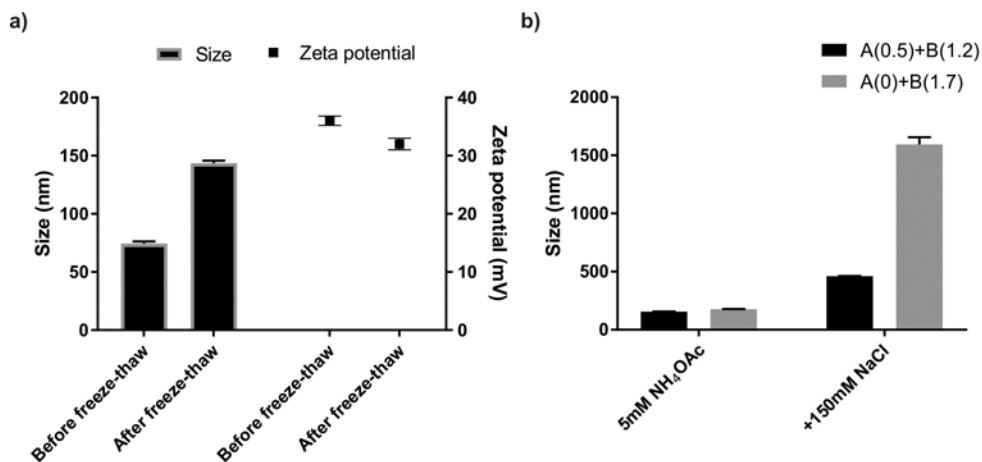


Fig. S9. (a) The A(0.5)+B(1.2)/ RNA polyplexes sizes and zeta potentials before and after freeze-thawing in 5 mM NH₄OAc buffer. (b) Particle size of crosslinked A(0.5)+B(1.2)/ RNA and non-crosslinked pHDB(1.7)/RNA polyplexes after incubation in 5 mM NH₄OAc buffer or 5 mM NH₄OAc buffer with 150 mM NaCl.

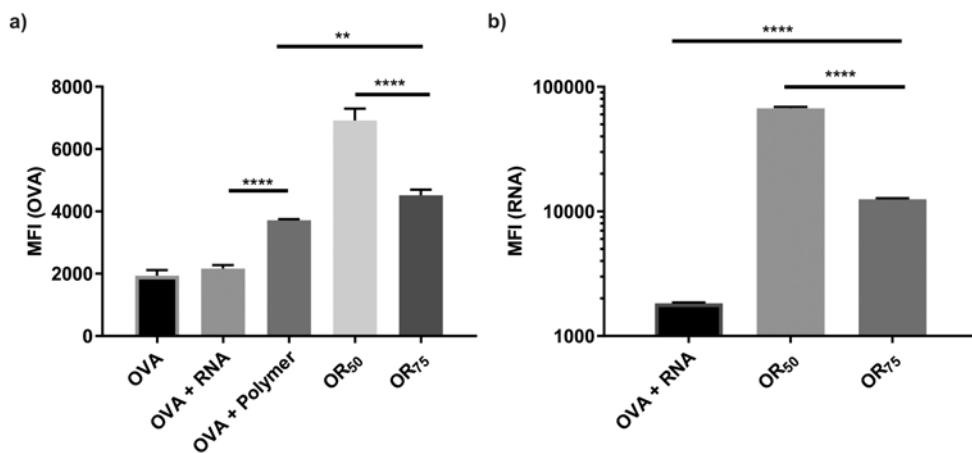


Fig. S10. Mean fluorescence intensity (MFI) of sulfo-Cy3-OVA (a) and Cy5-RNA (b) of indicated formulations incubated with DC 2.4 cells was analyzed by flow cytometry. The OVA concentration was 15 µg/mL. Data are presented as mean±SD (**p< 0.01, ****p<0.0001).

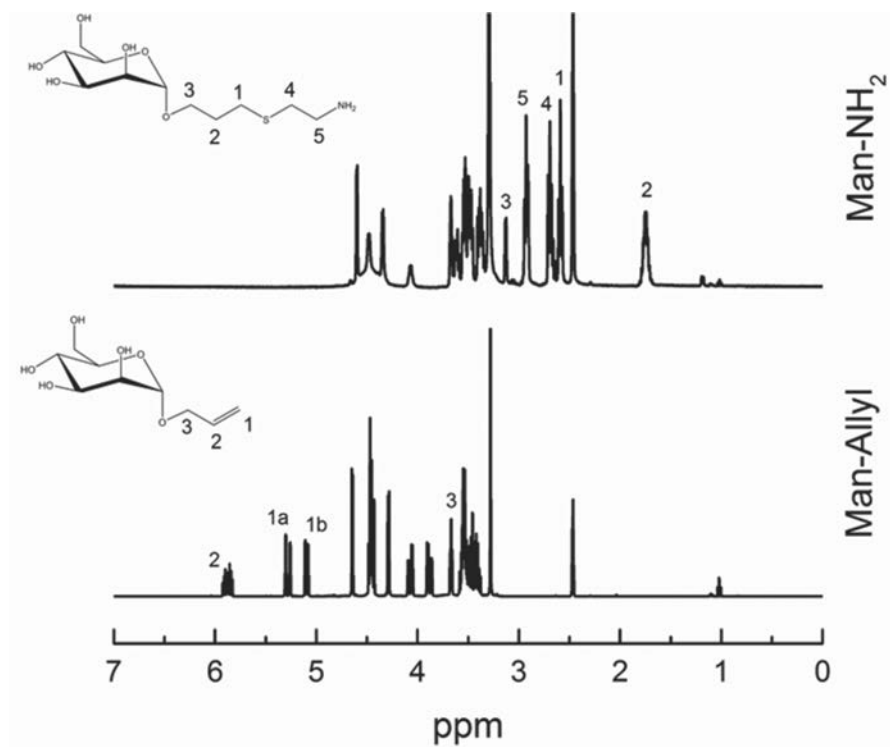


Fig. S11. ¹H NMR (DMSO-d₆) spectra of 3-(2-aminoethylthio) propyl α-D-mannopyranoside.

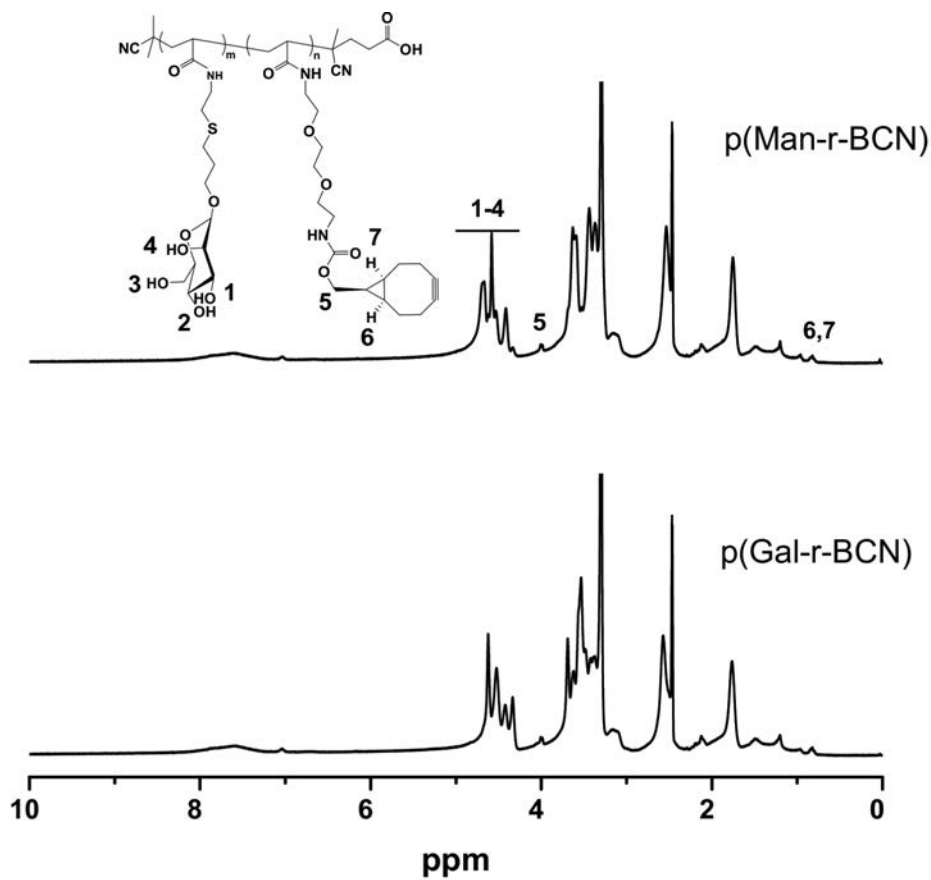


Fig. S12. ¹H NMR (DMSO-*d*₆) spectra of polymer p(Man-r-BCN) and p(Gal-r-BCN).

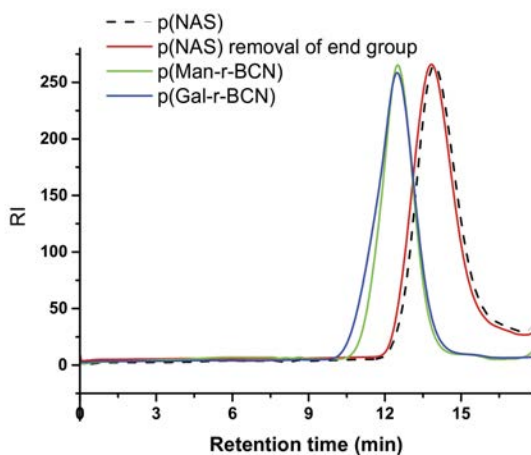


Fig. S13. GPC chromatograms of the pNAS and after chain transfer agent end group removal, p(Man-r-BCN) and p(Gal-r-BCN) in DMF.

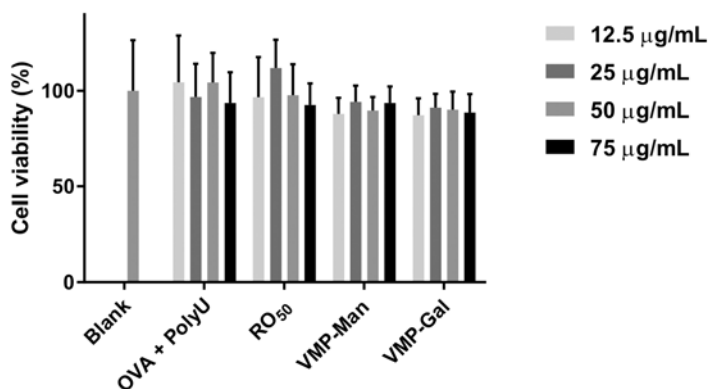


Fig. S14. Cell viability of DC2.4 cells after incubation with indicated formulation for 24 h.

Table S1. Number of free NH_2 groups and azide/Cy3 groups after modification of OVA with 2 or 10 equivalents of NHS as determined by the TNBS assay ($n = 3$).

Sample	NHS/OVA (mol/mol)	Free amine groups	Azide/Sulfo-Cy3 groups per OVA
OVA	0	8.5 ± 0.3	0
Sulfo-Cy3-OVA	2	7.6 ± 0.1	0.9
Sulfo-Cy3-OVA SS 10	10	5.3 ± 0.2	3.2

Table S2. Characteristics of the synthesized polymer as determined by ^1H NMR and GPC.

Polymer	Saccharide unit/BCN		M_n^a (kDa)	M_n^b (kDa)	M_w/M_n^b
	Feed (mol/mol)	Copolymer (mol/mol) ^a			
pNAS	0	0	21.7	8.3	1.4
p(Man-r-BCN)	90/10	92/8	39.4	31.6	1.4
p(Gal-r-BCN)	90/10	91/9	41.4	33.3	1.6

^aTheoretical M_n determined by ^1H NMR. ^b Determined by GPC.

CHAPTER

6

mRNA polyplexes with post-conjugated GALA peptides efficiently target, transfect and activate antigen presenting cells

Bo Lou [†], Stefaan De Koker[§], Chun Yin Jerry Lau[†],
Wim E. Hennink[†], Enrico Mastrobattista^{†*}

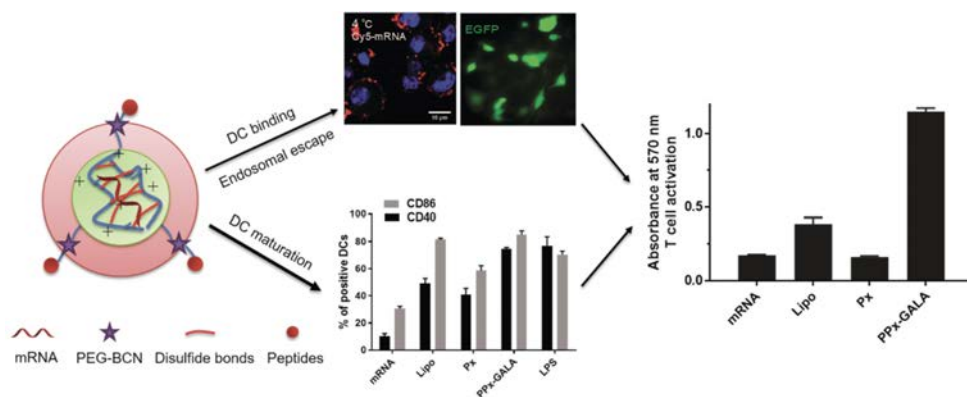
[†]Department of Pharmaceutics, Utrecht Institute for Pharmaceutical Science (UIPS), Utrecht University, 3584CG Utrecht, the Netherlands

²Laboratory of Molecular Immunology, Department of Biomedical Molecular Biology, Ghent University, 9052 Zwijnaarde, Belgium

| Abstract

Vaccines based on messenger RNA (mRNA) have emerged as potent systems to elicit CD8⁺ T cell responses against various cancers and viral infectious diseases. The efficient intracellular delivery of mRNA molecules encoding antigens into the cytosol of antigen-presenting cells (APCs) is still challenging, requiring cell attachment, active uptake and subsequent endosomal escape. Here, we report a facile approach for the formulation of peptide-functionalized mRNA polyplexes using copper-free click chemistry to promote presentation of mRNA antigen by dendritic cells (DCs). After screening different membrane active peptides, GALA modified mRNA polyplexes (PPx-GALA) with a size around 350 nm and with a slightly negative surface charge (-7 mV), exhibited the highest EGFP-mRNA transfection in RAW 246.7 macrophages (~ 36%) and D1 dendritic cells (~ 50%) as compared to polyplexes decorated with melittin or LEDE peptides. Interestingly, we found that PPx-GALA enters DCs through sialic acid mediated endo/phagocytosis, which was not influenced by DC maturation. The PPx-GALA formulation exhibited 18-fold higher cellular uptake compared to a lipofectamine mRNA formulation without inducing cytotoxicity. Live cell imaging showed that PPx-GALA that were taken up by endocytosis induced calcein release from endosomes into the cytosol. DCs treated with PPx-GALA containing mRNA encoding for OVA displayed enhanced T cell responses and DC maturation. Collectively, these data provide a strong rationale for further study of this PPx-GALA formulation *in vivo* as a promising mRNA vaccine platform.

Graphical abstract



| Introduction

The induction of robust antigen-specific T cell responses is a necessity for effective immunotherapy of cancer and for the treatment of persistent viral infections [1,2]. Recent clinical successes on chimeric antigen receptor T cell (CAR T cell) therapies in blood cancers have led to the approval of two CAR-T cell therapies by the Food and Drug Administration (FDA) in 2017 [3]. While exciting, these engineered CAR T cell therapies so far have limited efficacy for solid tumors and are costly for widespread application and are thus less suitable to be used for treating infectious diseases [4]. An alternative and traditional way to activate antigen-specific T cell responses is to use dendritic cells (DCs)-based vaccines [5]. DCs, as potent antigen presenting cells (APCs), play a crucial role in the initiation and regulation of adaptive immune responses and are the key orchestrators of T cell responses. For efficient induction of cytolytic T cell responses, the antigen needs to be delivered into the cytosol of DCs and, after processing, incorporated into the major histocompatibility complex (MHC) class I molecules for presentation on the cell surface and potential recognition by CD8⁺ T lymphocytes. Nucleotide vaccines, especially mRNA vaccines, are very attractive, since they exhibit the ability to induce a strong CD8⁺ T cell response without the potential danger of genome integration from DNA vaccines or the limitation of antigen selection from peptide vaccines [6,7]. However, the lack of efficient delivery systems for transfection of APCs remains a major hurdle in the development of mRNA-based vaccines. The main challenges for non-viral mRNA vaccine delivery include therefore: (1) selectively delivering mRNA to antigen presenting cells, most preferentially DCs inside the lymph nodes, (2) triggering efficient cellular uptake and endosomal escape to release mRNA into the cytosol, (3) circumventing the detrimental impact of type I interferon (IFN) secretion triggered by exogenous mRNA uptake [8,9].

Various delivery systems originally developed for cellular transfection with DNA and small interfering RNAs (siRNA) have been employed as mRNA delivery agents [10]. Among them, the most studied and promising are lipoplexes (i.e. mRNA complexed with cationic lipids) or lipid nanoparticles (i.e. solid or vesicular nanoparticles with an outer lipid bilayer structure) based on synthetic/natural lipids [11–13]. Lipid-based delivery systems have shown good transfection levels with APCs both *in vitro* and *in vivo*, however, the maturation of DCs induced by the self-adjuncting effect of mRNA via Toll like receptor (TLR7/8) activation hampers further RNA internalization due to abrogated micropinocytosis, which is the predominant DC cellular uptake pathway of lipid-based mRNA particles [14,15]. This drawback can be overcome by using mRNA containing modified nucleosides to diminish the DC maturation. However, additional TLR agonists were then required to exploit the full potential of the mRNA vaccine [16]. Cationic polymers as an alternative, such as polyethyleneimine (PEI), poly(L-lysine) (PLL), poly(dimethylaminoethyl methacrylate) (pDMAEMA) and polyaspartamides (PAsp(DET)) have been studied over the past decades to deliver pDNA and siRNA [9,17]. Despite the fact that these polymers have shown successful delivery of mRNA into tumor cells with acceptable levels of protein expression, only a few studies have been reported to effectively transfect APCs [18–20]. Several novel cationic polymers and peptides have shown to deliver mRNA into

APCs *in vitro* with efficiencies of 20-80% of transfected cells [21–24]. Although promising for *in vitro* applications, due to their highly positive surface charge they are less suitable for direct *in vivo* application.

Previously, we developed single-stranded poly-uridine (PolyU) polyplexes that were post-modified with PEG as a novel particulate RNA adjuvant. These PEGylated RNA polyplexes (Px) exhibited superior targeting ability to DCs in the lymph nodes, and successfully elicited strong CD8⁺ cytolytic T cell responses when co-administered with OVA via the subcutaneous route [25].

In present study, the aim was to further employ this delivery system as mRNA vaccine platform and to obtain efficient endosomal escape of antigen-encoding mRNA by post-functionalizing the RNA polyplexes with different membrane-active peptides at the distal end of the surface-exposed PEG chains. These peptides included the cationic and hemolytic peptide melittin [26,27], a pH-sensitive fusogenic peptide GALA [28,29] and an anti-microbial peptide LEDE [30–32] (sequence see Fig.1, gift from Leiden University). Preliminary experiments showed that the LEDE peptide has mild membrane leakage properties and that LEDE-functionalized Luc-mRNA polyplexes (PPx-LEDE) showed 100 times increase in luciferase expression in mouse fibroblast NIH3T3 cells compared to PEGylated mRNA polyplexes without the peptide (Px) (Fig. S2). All three peptides were post-conjugated to the mRNA polyplexes and screened for mRNA transfection in different antigen presenting cells. Our data revealed that GALA-modified mRNA polyplexes (PPx-GALA) efficiently transfected macrophages and DCs with EGFP mRNA to a comparable or higher transfection level as compared to formulation of mRNA with the commercial lipofectamine and without any noticeable cytotoxicity. We further investigated the cellular uptake mechanism and intracellular trafficking process of PPx-GALA in DCs and found that the GALA peptides serve a dual function: they selectively bind to sialic acid terminated glycans on DCs leading to internalization and subsequent cytosolic release, presumably by facilitating endo/phagosome membrane disruption. Moreover, delivery of OVA mRNA with these GALA-functionalized polyplexes resulted in efficient transfection and activation of DCs, thereby promoted strong OVA-specific T cell activation *in vitro*.

6

| Experimental Procedures

Materials

All chemicals were purchased in the highest purity and used without further purification. Carbonic acid 2-dimethylamino-ethyl ester 1-methyl-2-(2-methacryloylamino)-ethyl ester (HPMA-DMAE) [33], N-[2-(2-pyridyldithio)]ethyl methacrylamide(PDTEMA) [34,35] and 2-azidoethylmethacryl amide (AzEMAm) (Chapter 4) were synthesized as previously reported. Lipofectamine 2000 was obtained from Thermo Fisher Scientific (Etten-Leur, the Netherlands). The EGFP-mRNA Cy5-EGFP-mRNA and Cy5-luc_mRNA (5-methoxyuridine) were purchased from Tebu-bio (TRiLink biotechnologies, San Diego, CA). LEDE-azide [30–32] was a gift from Dr. Jan Wouter Drijfhout, Faculty of Medicine, Leiden University). GALA-azide and Melittin-azide was provided by ChinaPeptides Co.,Ltd. (Shanghai, China). Maackia amurensis agglutinin,

Opti-MEM, DMEM medium and heat inactivated fetal bovine serum (HI-FBS) were purchased from Sigma-Aldrich (Darmstadt, Germany).

Polymer synthesis and characterization

p(HPMA-DMAE-co-PDTEMA-co-AzEMAm) (pHDPA) was synthesized as reported [25]. The polymer was synthesized by radical polymerization using a monomer to initiator molar ratio (M/I) of 50 under a nitrogen atmosphere. The feed molar ratio of HPMA-DMAE, PDTEMA and AzEMAm was 70/20/10. In brief, 200 mg (0.77 mmol) HPMA-DMAE, 56.7 mg (0.22 mmol) PDTEMA, 17 mg (0.11 mmol) AzEMAm and 3.6 mg (0.022 mmol) AIBN were dissolved in dry DMSO (1 mL) in flasks sealed with rubber septa and subjected to three vacuum- N_2 cycles. The polymerization was carried at 70 °C for 48 h. Next, the polymer was precipitated in cold diethyl ether, redissolved in DMF and precipitated in cold diethyl ether. This procedure was repeated 3 times. After extensive dialysis (5 kDa) against an ammonium acetate (NH_4OAc) buffer of pH 5.0 (10 mM, last step 2.5 mM) at 4 °C, the polymer was collected after freeze drying. The yield of the polymer was 40%.

The molecular weights and polydispersity (M_w/M_n) of pHDPA were determined by size exclusion chromatography (SEC) analysis using a Viscotek-GPCmax (Viscotek, Oss, The Netherlands) light scattering ($\lambda = 670$ nm, right (90°) and low (7°) angle)/viscosimetric detection system, using ultrahydrogel 2000 7.8×300 mm columns in series with a ultrahydrogel 6.0×40 mm guard column and 0.3 M NaAc pH 4.4, 30% acetonitrile as eluent [36]. The flow rate was 0.6 mL/min and the run time was 60 minutes. A PolyCALTM PEO standard ($M_n = 24$ kDa, PDI=1.01, Malvern) was used for calibration. The copolymer composition was determined by 1H NMR analysis (polymer dissolved in D_2O) and performed with a Gemini 400 MHz spectrometer (Varian Associates Inc., NMR Instruments, Palo Alto, CA). The ratio HPMA-DMAE/PDTEMA/AzEMAm was determined by comparison of the integrals at δ 4.3 ppm (bs, OCH_2CH_2 , HPMA-DMAE), δ 7.69 ppm (bs, pyridyl group proton, PDTEMA) and δ 3.14-3.51 ppm (m, $CH_2CH_2N_3$, AzEMAm).

Peptide conjugate synthesis

The BCN-PEG₆₀₀₀-peptides were synthesized as previously described (Chapter 3 of this thesis, Fig. S1B). Briefly, for the synthesis of BCN-PEG₆₀₀₀-GALA, 20.9 mg of BCN-PEG₆₀₀₀-BCN (6510 g/mol, 3.2 μ mol) was dissolved in 1 mL dry DMSO, followed by the addition 10.0 mg of GALA-azide (3115 g/mol, 3.2 μ mol) and the obtained solution was subsequently stirred for 16 h at room temperature. Next, 10 mL water was added, followed by freeze-drying. Subsequently, the product was re-dissolved in 2.5 mL nuclease-free water and purified with PD 10 column chromatography to remove unreacted peptide using nuclease-free water as eluent and freeze-dried. The product was obtained at a yield of 80%. It should be noted that the applied procedure resulted in the formation of a statistical mixture of BCN-PEG-GALA, GALA-PEG-GALA and unreacted BCN-PEG-BCN. The BCN-PEG₆₀₀₀-Melittin and BCN-PEG₆₀₀₀-LEDE was synthesized in a similar way.

Preparation and characterization of peptide functionalized mRNA polyplexes

The preparation of RNA polyplexes consisted of 3 consecutive steps: complexation, post-PEG-peptide modification, and crosslinking (Fig. 1A). Briefly, complexation was achieved by mixing four volumes of polymer and one volume of nucleic acid in 10 mM HEPES buffer, pH 7.4, at an N/P ratio of 4. For control polyplexes modified with PEG, BCN-PEG₅₀₀₀-COOH [25] was added to preformed mRNA polyplexes a BCN/N₃ mole of 0.6. The peptide modification process was performed by mixing BCN-PEG₆₀₀₀-peptide (synthesis described in section 2.3) at either a low (30%) or high (60%) molar ratio to BNC/N₃ in HEPES buffer pH 7.4 to react for 2 h at room temperature. For the low amount of peptide modification, another 30% equivalent of BCN-PEG₅₀₀₀-COOH was first mixed together BCN-PEG₆₀₀₀-peptide before addition to the mRNA polyplex dispersion. Next, surface modified mRNA polyplexes were crosslinked by addition of dithiothreitol (DTT) corresponding with a half molar equivalent to PDS groups of the polymer used in particle formation and subsequent incubation for 1 h at room temperature. After adding 5% sucrose as cryoprotectant, the polyplexes were freeze-dried and stored at 4 °C. Unless indicated otherwise, the polyplexes were prepared with a final RNA concentration of 100 µg/mL. The mRNA polyplex dry powder was re-suspended in RNAase-free water 30 mins before addition to the cells.

The size of the polyplexes was measured with DLS using an ALV CGS-3 system (Malvern Instruments, Malvern, UK) equipped with a JDS Uniphase 22 mW He-Ne laser operating at 632.8 nm, an optical fiber-based detector, a digital LV/LSE-5003 correlator with temperature controller set at 25 °C. The zeta-potential (ζ) of the polyplexes was measured using a Malvern Zetasizer Nano-Z (Malvern, UK) with universal ZEN 1002 'dip' cells and DTS (Nano) software (version 4.20) at 25 °C. Polyplex measurements were performed in 10 mM HEPES pH 7.4 and with an RNA concentration of 15 µg/mL.

The size distribution of the polyplexes was also determined by nanoparticle tracking analysis (NTA) using a NanoSight LM 10SH (NanoSight, Amesbury, United Kingdom), equipped with a sample chamber with a 532 nm Laser. Typically, RNA polyplexes were diluted with PBS to a concentration of 0.5 µg/ml and measured for 120 s with manual shutter and gain adjustments. The captured videos were analyzed by the NTA 2.0 image analysis software.

Transfection of DCs

Immortalized DC2.4 cells were used to test protein expression activity of the peptide modified mRNA polyplexes. Briefly, DC2.4 cells were seeded into a 96-well plate at a seeding density of 3.0×10^4 cells/well, and cell culture was done in 100 µL complete culture medium for 24 h at 37 °C. Prior to transfections, the medium on the cells was refreshed with either 100 µL OPTI-MEM or full medium and incubated with EGFP mRNA polyplexes prepared as described in section 2.4 for 4 h at 37°C, and then another 100 µL full medium was added without removing polyplexes. After incubation for 20 h at 37°C in a CO₂ incubator, EGFP expression was visualized using Keyence BZ-9000 Microscope (Keyence, Osaka, Japan). Flow cytometry was performed to measure the percentage of GFP-positive cells compared to non-transfected cells as control

using a BD FACS Canto II flow cytometer (Becton Dickinson, BD, Franklin Lakes, NJ, USA). The same procedure was also applied to determine EGFP expression in D1 dendritic cells, RAW 246.7 macrophages, and HEK293T human embryonic kidney cells. Lipofectamine 2000 (Lipo) was used as positive control (Lipo/mRNA were prepared at volume/weight ratio of 1.5/1). Unless specified cells were incubated with mRNA at dose of 250 ng per well.

In vitro cytotoxicity

To determine possible cytotoxic effects of the polyplexes, the Alamar Blue cell viability assay (Invitrogen, Karlsruhe, Germany) was performed essentially as described by the manufacturer. In short, 20 h after transfection, the cell medium was replaced with culture medium containing Alamar Blue (50 nM) and the cells were cultured for another 4 h. Next, 80 μ L of medium from each well was transferred into a flat-bottom 96-well plate to measure the light absorbance. The relative cell metabolic activity was calculated by normalizing the absorbance at 570 nm (reference wavelength of 630 nm) with the absorbance of PBS-treated cells.

The capability of PPx-GALA to interfere with cell membrane integrity was analyzed with the CytoTox-ONE kit, which determines the lactate dehydrogenase (LDH) release from cells after exposure to the different polyplex formulations. The assay was performed using a 96-well plate, in which 10,000 D1 cells were plated 24 h before the treatment. Before sample addition, the culture medium was replaced with OPTI-MEM. Next, polyplex dispersions containing 62.5, 125, 250 and 500 ng of mRNA/well were added. After 4 h incubation at 37 °C, the supernatant was collected, LDH activity was determined according to the manufacturer's protocol. For the positive control, cells were 100% lysed with 1% triton X-100.

In vitro DCs cellular uptake studies of GALA-modified polyplexes (PPx-GALA)

To determine the route of cellular internalization of the PPx-GALA, D1 cells were seeded at a density of 3.0×10^4 cells/well in a 96-well plate or in 96-well μ Clear® black plates and incubated for 24 h at 37 °C. The cells were then incubated with Cy5-labeled luc_mRNA loaded in PPx-GALA as described in section 2.4 at dose of 250 ng of mRNA/well for 1, 6, 12 and 24 h. For inhibition studies, cells were pre-treated with 1 μ g/mL lipopolysaccharide (LPS, Invitrogen) for 15 h, 10 μ M Maackia amurensis agglutinin for 30 min (MAM, sialic acid binding lectin, Sigma), 10 μ M cytochalasin D (Cyto-D, phagocytosis inhibitor, Sigma) for 3 h, 15 μ M chlorpromazine (CPZ, clathrin-mediated endocytosis inhibitor, Sigma) for 1 h or different concentrations of free GALA peptide (1-150 μ M) for 15 minutes in full medium prior to addition of PPx-GALA to the cells. The cells were then incubated for 1 h (inhibitor present during transfection) at 37 °C before they were washed with ice-cold FACS buffer (1% BSA in PBS) and applied to determine particle uptake using a BD FACSCanto II flow cytometer and high content confocal fluorescent microscope Yokogawa Cell Voyager CV7000s (Yokogawa Electric Corporation, Tokyo, Japan). For binding assay of PPx-GALA, cells were first incubated on ice for 1 h and then incubated together with PPx-GALA for another 1 h on ice before taking confocal images. For colocalization studies, cells were co-transfected with PPx-GALA and 200

$\mu\text{g/mL}$ rhodamine-labeled dextran (70,000 Da, ThermoFisher) or 150 $\mu\text{g/mL}$ cell impermeable dye Calcein (Sigma, the Netherlands) for 3 h at 37 °C. To study the sub-cellular distribution, after 3 h co-incubation with PPx-GALA, the cells were incubated with 100 nM lysotracker green (Invitrogen, the Netherlands) for 30 min before confocal imaging.

In vitro DCs maturation and antigen presentation

D1 cells were seeded in 96-well plates at a density of 25,000 cells/well in 100 μL complete medium and allowed to adhere overnight. Polyplexes or lipoplexes were added at 0.25 μg mRNA/well in 100 μL serum-free media. Control cells were treated with 0.1 mM SIINFEKL peptide (in vitrogen, the Netherlands). After incubation for 6, 12 and 24 h at 37 °C, the cells were washed with medium, new fresh complete medium was added and incubated for overnight at 37 °C. Next, 100,000 B3Z cells/well in 100 μL complete medium were added and incubated for 24 h at 37 °C. The medium was then replaced with 100 μL /well lysis buffer containing 0.1 mM 2-mercaptoethanol, 9 mM MgCl_2 , 0.1% Triton X-100, and 0.15 mM chlorophenol red b-D-galactopyranoside (CPRG) in DPBS. After 2 h incubation at 37 °C, absorbance measurements were recorded at 570 nm. To measure the maturation level of the D1 cells, after incubation of the cells with the different formulations for 24 h at 37 °C, the cells were washed with FACS buffer and subsequently stained with anti-CD40-FITC and anti-CD86-PE antibodies (2 $\mu\text{g/mL}$, 50 μL /well, eBioscience, U.S.) for 30 min on ice. The D1 cells were subsequently analyzed by flow cytometry after 2 washing steps with FACS buffer.

Statistical analysis

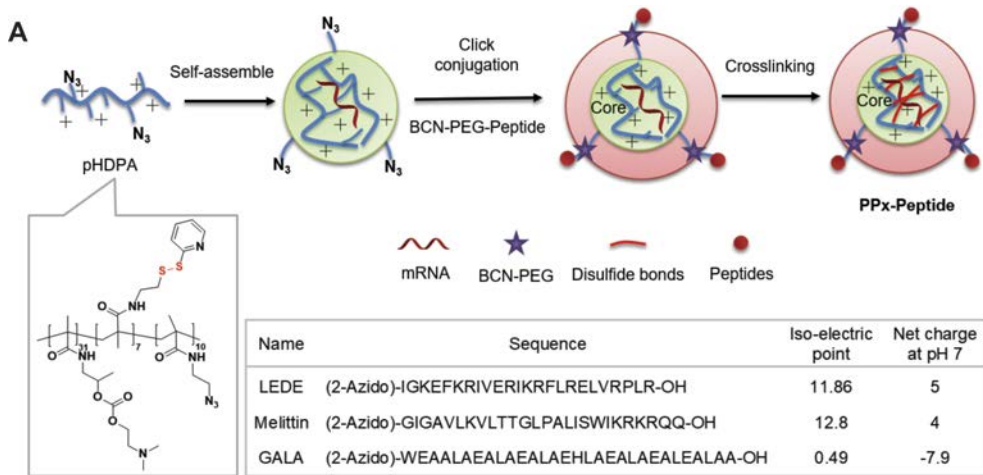
Two-tailed Student t-test was applied for comparison between experimental groups. $P < 0.05$ was considered statistically significant.

| Results and Discussion

Preparation and characterization of peptide modified mRNA polyplexes

In this study, a random copolymer p(HPMA-DMAE-co-PDTEMA-co-AzEMAm) (pHDPA) containing azide functional groups was synthesized (Fig. 1A and S1, $M_n = 11.2$ kDa (PEG calibration), $M_w/M_n = 1.9$).

Peptide modified mRNA polyplexes (PPx) were prepared in three steps as illustrated in Fig. 1A. mRNA was first complexed with pHDPA via electrostatic interactions with an amine to phosphate (N/P) molar ratio of 4:1, according to a previous publication [25]. DLS analysis showed the formation of mRNA polyplexes with a diameter of ~ 150 nm with a narrow distribution (polydispersity index (PDI) < 0.15), and with a positive zeta potential of 16 mV. Next, the prepared mRNA polyplexes were post-modified with BCN-PEG₆₀₀₀-peptide through copper-free click conjugation between the BCN and N₃ moieties, generating stable covalent bonds between the PEG-peptides (forming the polyplex shell) and the polyplex core. To optimize the surface peptide density, two different amounts of BCN-PEG₆₀₀₀-peptide conjugates were added to the mRNA polyplexes: 30 or 60% BCN/N₃ molar ratio, respectively. In the last step,



Nomenclature:

BCN-PEG modified mRNA polyplexes = Px

BCN-PEG-peptide modified mRNA polyplexes = PPx, e.g. PPx-LEDE, PPx-Melittin and PPx-GALA

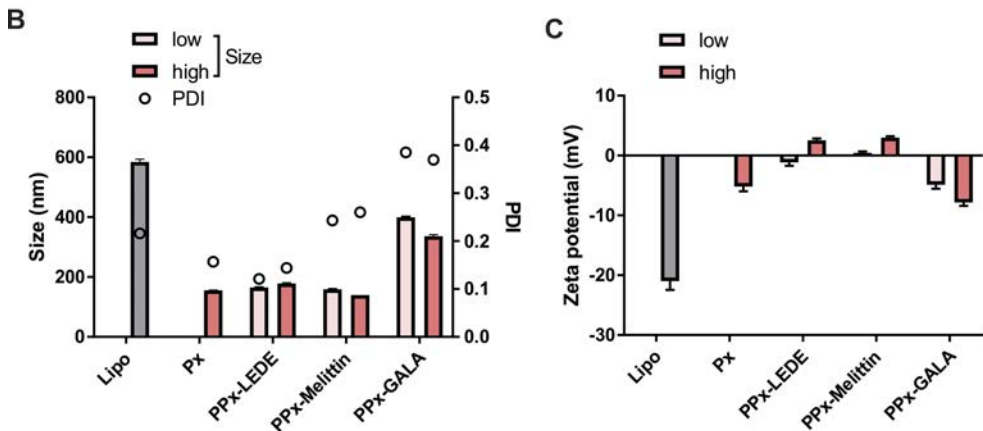


Fig. 1. Preparation and characterization of peptide-modified mRNA polyplexes (PPx). (A) Schematic illustration of the 3-step preparation method of PPx: (a) core self-assembly by mixing the cationic polymer and mRNA; (b) low or high degree of BCN-PEG-peptide is conjugated to the pHDPA/mRNA polyplexes by click chemistry, and (c) particle stabilization by crosslinking the polymer chains of the core with DTT. (B) Particle size, polydispersity index (PDI) and zeta potential (C) of peptide modified EGFP mRNA PPx at low or high amount of peptide surface modification. mRNA polyplexes were diluted to 10 $\mu\text{g}/\text{mL}$ in 10 mM Hepes buffer pH 7.4. Lipo represents mRNA formulated with Lipofectamine 2000 into lipoplexes. Data are the mean \pm SD, n=3.

interchain disulfide crosslinking of the polyplexes was induced by the addition of DTT at a 50% molar equivalent of the PDS groups of the polymer, yielding final peptide-modified mRNA polyplexes (named as PPx-Peptide). Finally, PPx formulations were freeze-dried in the presence of 5% sucrose and stored at 4 $^{\circ}\text{C}$ no longer than two weeks before use. Freeze-drying and cold storage did not result in a change in the particle size distribution of PPx after their redispersion

in buffer. Similarly, the mRNA polyplexes post-modified with BCN-PEG₅₀₀₀-COOH at a 60% BCN/N₃ molar ratio were prepared using the same steps, yielding PEGylated mRNA polyplexes (named as Px) as a control.

The size and zeta potential of the control Px and various PPx formulations were determined. As shown in Fig. 1B, after post-PEGylation, the size of Px was around 155 nm, which is slightly higher than the size of mRNA polyplexes before PEGylation (140 nm). The decrease of zeta potential after PEGylation (from 16 to -5 mV) confirmed the success of conjugation of PEG to the preformed mRNA polyplexes (Fig. 1C). After modification with either the LEDE or melittin peptide, independent of the added amount (low or high) of peptides, the size of PPx was around 150-200 nm, with a relatively low polydispersity (PDI, 0.15-0.3), which is similar as the size of Px that has no peptide attached. In contrast, the size of GALA modified PPx significantly increased from 140 to 350-400 nm together with an increased PDI of around 0.4. This increase in size and PDI is presumably due to the negative charge of GALA (Fig. 1A), which might be caused by inter-polyplex crosslinking due to the presence of BCN-PEG₆₀₀₀-BCN and the low repulsive forces between the polyplexes because of their low zeta-potential. This assumption was confirmed by nanoparticle tracking analysis (NTA), a technique that allows the simultaneous analysis of individual particles in suspension and gives information of the true size distribution (Fig. S3). Px showed a similar particle size as found with DLS analysis (~150 nm), whereas PPx-GALA clearly showed two populations with average sizes around 200 and 300 nm and the peak around 300 nm can be ascribed to inter-crosslinking of two polyplex nanoparticles of ~150 nm. Compared to Px that had a negative zeta potential, the zeta potential of PPx-LEDE and PPx-Melittin polyplexes was near-neutral with a slight increase in zeta potential when the highest amount of peptide was coupled. This is because of these peptides have a net positive charge at neutral pH (Fig. 1A). In contrast, PPx-GALA polyplexes have a negative zeta potential due to the net charge of -7.9 of this peptide at neutral pH (Fig. 1C). The zeta potential of PPx-GALA decreases when the highest amount of GALA peptide was added during formulation (low vs high: -5 vs -8 mV), which implied that indeed more GALA peptides were conjugated to the surface of mRNA polyplexes at the higher peptide feed.

6

Peptide-mediated mRNA delivery to antigen presentation cells

To be able to quantify the transfection activity of the different PPx formulations, mRNA encoding for EGFP was used. Flow cytometry analysis of EGFP fluorescence following mRNA delivery allows for simultaneous quantification of the fraction of cells exhibiting above-baseline levels of fluorescence (percent transfection) as well as shifts in the mean fluorescence intensity of the entire cell population. mRNA expression after incubation of the cells with PPx in the absence of serum was compared with expression obtained with EGFP mRNA Lipoplexes based on the commercial agent Lipofectamine 2000 (Lipo, positive control) as well as Px. The cells were transfected with PPx modified with low or high amounts of peptides. Bone marrow derived dendritic cell line DC 2.4, macrophage cell lines RAW246.7 and normal cell line HEK 293T were used to evaluate the transfection activities of the different PPx formulations (Fig. 2 and S4). As shown in Fig. 2A, modest levels of EGFP expression (~ 20%) were observed in DC

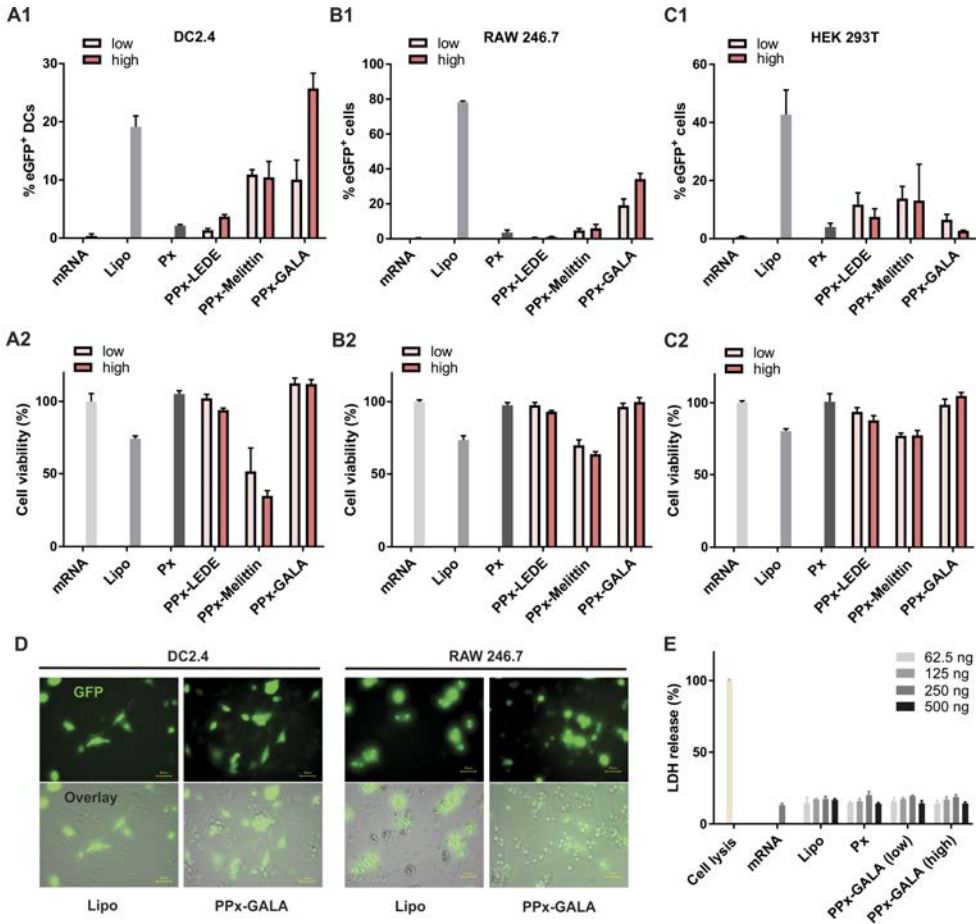


Fig. 2. Evaluation of PPx formulations for EGFP mRNA delivery. EGFP expression (upper panels) detected by flow cytometry and normalized cell viability (lower panels) in comparison to untreated cells (100% cell viability) determined with the AlamarBlue assay using DC2.4 (A), RAW246.7 (B) and HEK 293T(C) cells 24 h after incubation with free mRNA or PPx. (D) Epifluorescence microscopy images showing EGFP fluorescence alone and a bright-field overlay of DC2.4 (left panel) and RAW 246.7 cells (right panel) treated with mRNA complexed with Lipofectamine 2000 (Lipo), Gala modified mRNA polyplexes (PPx-GALA, high). (E) Lactate dehydrogenase (LDH) assay of DC 2.4 cells after incubation for 4 h in the absence of serum with the indicated formulations and with various amounts of mRNA added per well. For Fig. 2A-D. the cells were transfected with 250 ng mRNA/well in 96-well plates. Data are the mean \pm SD, n=3. Size bar corresponds to 40 μ m.

2.4 cells when transfected with Lipo, which is in line with previously reported work (~25%) [24]. Naked mRNA and the Px formulation showed no transfection at all. The PPx-LEDE or PPx-Melittin formulations both exhibited a weak EGFP expression (<12%), irrespective of the amount of peptide grafted on the surface. Interestingly, PPx-GALA formulations with a high peptide density showed the highest EGFP expression with 28% transfection efficiency, and which is more than 2 times higher than the PPx-GALA formulations with a low peptide

density. A similar trend was also observed in RAW246.7 cells (Fig. 2B), with lipofectamine and PPx-GALA being the only formulations that showed transfection but with higher levels of transfection as compared to DC 2.4 cells. By increasing the GALA density on the surface of PPx, the transfection efficiency increased from 23 to 36%. In contrast, HEK293T cells incubated with PPx-LEDE and PPx-melittin induced moderate levels of EGFP expression (10-25%), whereas incubation with PPx-GALA showed expression in less than 5% of cells (Fig. 2C). The EGFP expression was also confirmed by epifluorescence microscopic analysis (Fig. 2D).

The possible cytotoxicity of the different PPx formulations was evaluated by an AlamarBlue assay using DC2.4, RAW 264.7 macrophages and HEK 293T cells (Fig. 2). Cells were incubated with the PPx formulations for 24 h, after which cell viability was quantified based on their total metabolic activity resulting in reduction of the AlamarBlue reagent. In all these three cell lines, incubation with the lipofectamine formulation showed acceptable levels of cytotoxicity with >75% cell viability. Compared with RAW 246.7 and HEK 293T cell lines, PPx-Melittin showed higher toxicity towards DC2.4 (40% viability). Importantly, the PPx-GALA and PPx-LEDE formulations exhibited high cytocompatibility (>95% viability) in all three cell lines. We further evaluated in DC2.4 cells the cell membrane-destabilizing capability of PPx-GALA at different concentrations using a lactate dehydrogenase (LDH) release assay. As shown in Fig. 2E, released LDH from cells incubated with the indicated formulations was comparable to naked mRNA, again pointing to an excellent cytocompatibility of PPx-GALA. Overall, PPx-GALA with high GALA density was identified as best formulation as it was able to specifically transfect antigen presentation cells like macrophages and dendritic cells with a superior cytocompatibility. This formulation was therefore selected for further testing.

mRNA expression kinetics in dendritic cells

We further examined the capacity of PPx-GALA to transfect the spleen-derived D1 cell line, a growth factor-dependent cell line derived from splenic C57BL/6 mouse DCs that behaves like freshly isolated bone marrow DCs [37,38]. D1 cells were transfected with PPx-GALA, loaded with Cy5-EGFP mRNA both in the presence and absence of serum. When the D1 cells were incubated with PPx-GALA in the absence of serum, ~ 50% of cells expressed EGFP, which is significantly higher than that of Lipo (~28%) (Fig. S5A). In contrast, P_x with the same amount of unconjugated GALA showed no transfection at all, which indicates that immobilized GALA peptides contributed to the enhanced transfection. In the presence of serum, the relative transfection efficiency significantly decreased, from 50% to 15% for PPx-GALA and from 30% to 20% for the Lipo formulation. The same trends were also observed by fluorescence microscopy (Fig. S5B). This decrease in transfection efficiency in the presence of serum is partly due to the reduced cellular uptake, with a 23% and 46% decrease in mRNA uptake for Lipo and PPx-GALA, respectively (Fig. S5C).

Next, kinetics of cellular uptake of PPx-GALA by D1 cells and subsequent mRNA expression was investigated (Fig. 3). Upon incubation of D1 cells with PPx-GALA in the absence of serum, transfection reached ~20% EGFP-positive cells at 6 h, and, reached 45% of transfection at 12 h, which sustained for 24 h (Fig. 3A). In strong contrast, the D1 cells already showed maximum

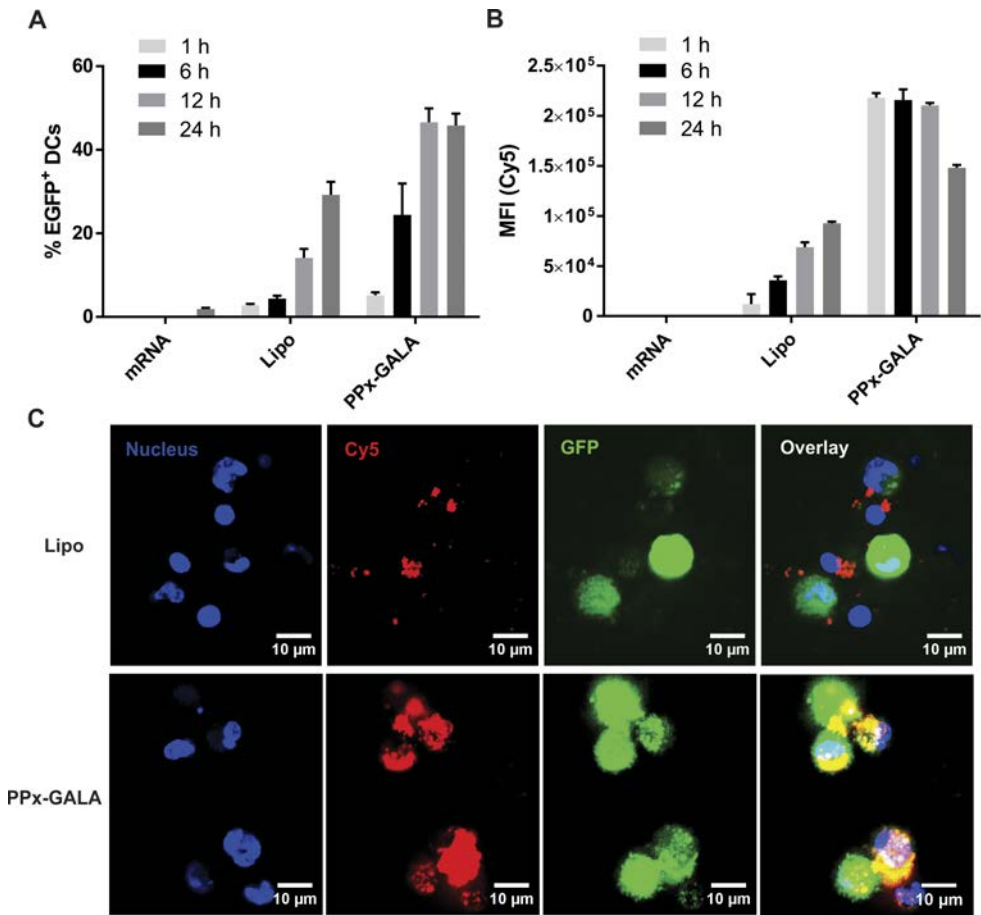


Fig. 3. Transfection (A) and cellular uptake (B) kinetics of Cy5-EGFP mRNA on D1 cells following incubation with the indicated formulations by flow cytometry. (C) Confocal microscopy of D1 cells incubated with Cy5-EGFP-mRNA complexes after 12 h. The cells were transfected in the absence of serum and were incubated with 250 ng mRNA/well in 96-well plates. Data are the mean \pm SD, $n=3$. Bar indicates 10 μ m.

cellular uptake of PPx-GALA after 1 h incubation and lasted to 12 h, the Cy5-EGFP mRNA intensity inside the cells then decreased after 24 h incubation (Fig. 3B). On the other hand, the percentage of cells expressing EGFP and cellular uptake after Lipo transfection was still increasing at 24 h of incubation. As shown in Fig. 3B, the cellular uptake level of PPx-GALA was 18 and 3-fold higher than Lipo at 1 and 12 h of incubation, respectively. The same results were observed by confocal microscope images (Fig. 3C). D1 cells incubated with PPx-GALA showed much higher Cy5-EGFP uptake than cells incubated with the Lipo formulation. Despite the rapid delivery of high amounts of mRNA into D1 cells upon incubation with PPx-GALA, the mRNA expression peak was observed at only 12 h, which is later than the typical mRNA expression peak at 6-7 h post-transfection in DCs or other cell types [39,40]. The rapid and

sustained uptake of PPx-GALA compared to Lipo points towards a different uptake mechanism for PPx-GALA by dendritic cells that leads to functional delivery of mRNA at later time points.

DC cellular uptake mechanisms of PPx-GALA

To elucidate potential mechanisms that underlie efficient DC uptake by PPx-GALA, the uptake level of PPx-GALA was compared to Px in D1 and HEK 293T cells. After 1 h incubation, HEK 293T cells internalized higher amounts (~1.7 fold) of Px compared to PPx-GALA (Fig. 4A). Conversely, D1 showed higher uptake of PPx-GALA compared to Px. It has been reported that particles with a size range from 200-500 nm are more favorable for uptake by dendritic cells [41–43], thus higher cellular uptake of PPx-GALA compared to Px in D1 cells might be ascribed to the size difference (350 nm for PPx-GALA versus 150 nm for Px). However, another possibility is that the PPx-GALA entered DCs via receptor-mediated endocytosis, which is often much faster compared to adsorption-mediated endocytosis or micropinocytosis [44]. GALA is a 30 amino acid synthetic peptide with a glutamic acid-alanine-leucine-alanine (EALA) repeat, that resembles the putative fusion peptide domain of Influenza virus hemagglutinin 2 (HA2) with pH-dependent membrane fusion ability [29,45]. Recent studies have shown that GALA-modified lipid nanoparticles could actively target sialic acid-terminated sugar chains on lung endothelial cells [46,47]. Dendritic cells also present a very high amount of sialic acid-containing glycans on the cell surface [48,49]. Therefore, in the light of above findings, we hypothesize that PPx-GALA polyplexes are able to actively target the DCs via sialic acid-terminated glycans mediated endocytosis.

To test this hypothesis, a competition assay was conducted to determine whether free GALA in the cell culture medium inhibits cellular uptake of PPx-GALA. As shown in Fig. 4B, preincubation of dendritic cells with free GALA has negligible effect on the cellular uptake of Px. In contrast, free GALA significantly lowered the uptake of PPx-GALA mRNA polyplexes. The competition was dose-dependent and with an IC_{50} of around 50 μ M, which suggested that GALA peptides on the surface of mRNA polyplexes do indeed play a role in cellular uptake. To test whether the sialic acid-terminated sugar chains on the dendritic cells are involved in PPx-GALA uptake, a plant lectin *Maackia amurensis* agglutinin (MAM) [50], which specifically binds to sialic acid, was incubated with the cells before adding PPx-GALA. It is important to note that blocking sialic acid residues with MAM lectin is to be preferred above sialidase treatment, as the removal of sialic acid residues on the DC surface can stimulate the phagocytic ability of these cells as was previously reported [51,52]. As shown in Fig. 4C, the incubation of cells with MAM reduced the cellular uptake level of PPx-GALA by 50%. On the other hand, pre-incubation of MAM did not significantly influence the cellular uptake levels of Lipo and Px (Fig. S6), indicating that the inhibition of the uptake of PPx-GALA by MAM does not appear to be due to a non-specific perturbation of cellular function. Similar trends were also observed in confocal microscopy images (Fig. 4D). Importantly, when the DCs were incubated with PPx-GALA at 4 °C for 1 h, a clear signal of red fluorescence was observed at the cell membrane because of PPx-GALA binding. Considering the negative surface charge of

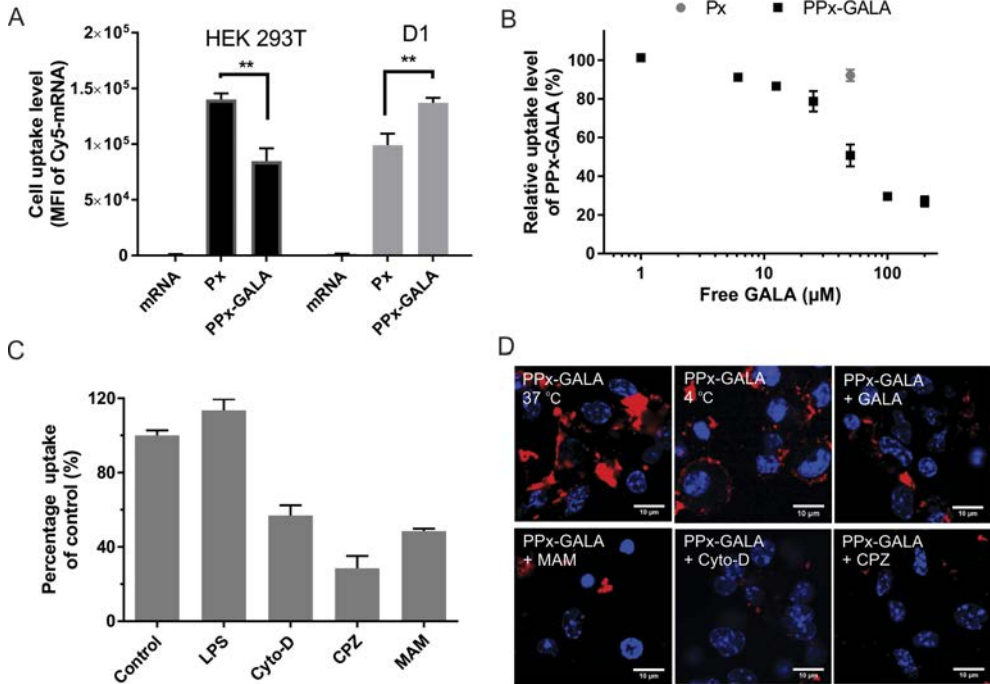


Fig. 4. Cellular uptake mechanisms of PPx-GALA. (A) Cellular uptake of naked Cy5-luc_mRNA, Lipo, Px and PPx-GALA by HEK293T (left) and D1 (right) cells after 2 h incubation in the presence of serum. (B) Inhibition of the intracellular uptake of Px and PPx-GALA by free GALA. The cellular uptake of Px or PPx-GALA by D1 was determined by FACS after incubation 1 h at 37 °C in the presence of GALA (1-120 μM). (C) Inhibition of D1 cellular uptake of PPx-GALA. D1 cells were incubated with PPx-GALA Cy5-luc_mRNA polyplexes for 2 h in the presence of LPS, Cytochalsin D (Cyto-D), Chlorpromazine (CPZ) and Maackia amurensis agglutinin (MAM). (D) Confocal microscopy of D1 cells 2 h after incubation with PPx-GALA in presence of indicated molecules at 37 or at 4 °C. Cell nuclei were stained with Hoechst (blue), Cy5-luc_mRNA is shown in red. In all the studies, 250 ng mRNA/well was added in 96-well plate. Data are the mean ± SD, n=3-5. Bar indicates 10 μm.

PPx-GALA formulation (-7 mV) and that active endocytosis is abolished at 4 °C, nonspecific binding by electrostatic interaction or nonspecific uptake mechanisms such as micropinocytosis can be excluded. Instead, the association of PPx-GALA to the DCs is most likely caused by cell surface receptor-specific binding. These results collectively suggest uptake of the PPx-GALA through sialic acid-terminated glycan-mediated endocytosis.

Furthermore, the mechanism of cellular uptake was also examined by treating D1 cells with inhibitors of endocytosis, macropinocytosis and phagocytosis. It is well documented that mature DCs show low levels of micropinocytosis [53], whereas receptor-mediated endocytosis and phagocytosis still remain highly active [54]. Maturation of D1 cells with lipopolysaccharide (LPS) had no effect on the level of internalization of PPx-GALA as compared to control (Fig. 4C). Also, PPx-GALA taken up by D1 cells showed no colocalization with

the micropinocytosis marker dextran (Fig. S7). In comparison, cytochalasin D (CytoD), an inhibitor of phagocytosis and chlorpromazine (CPZ), a clathrin-mediated endocytosis inhibitor, significantly inhibited cellular uptake of DCs by 40 and 70%, respectively (Fig. 4C&D). Altogether, these findings demonstrate that receptor-mediated endocytosis triggered by sialic acid binding as well as phagocytosis are the major uptake pathways of PPx-GALA in D1 cells.

Intracellular trafficking process of PPx-GALA

At neutral pH, GALA is water soluble and converts from a random coil to an amphipathic α -helix when the pH is lowered to 5.0. This conformational change enables binding and insertion of the GALA peptide into the lipid membrane compartment causing membrane leakage [29]. To test the endosome-disruptive capacity of PPx-GALA, D1 cells were incubated with PPx-GALA in the presence of calcein (150 $\mu\text{g}/\text{mL}$) for 1 h at 37 $^{\circ}\text{C}$. Calcein is a membrane-impermeant fluorescent small molecule that can be taken up into endocytic vesicles to make them fluorescent [55,56]. Cells treated with calcein alone or Px showed a punctuate distribution of fluorescence indicative of endo-lysosomal compartmentalization of the dye (Fig. 5A, i). In contrast, when cells were incubated with PPx-GALA in the presence of calcein, a diffused calcein fluorescence throughout the cytosol and nucleus was observed (Fig. 5A, ii). Only part of Cy5-mRNA showed a weak diffused pattern remine very closely to the site of leaking endosome (Fig. 5A, iii). To exclude the possibility that PPx-GALA might have destabilized the cell membrane allowing calcein to diffuse directly into the cytosol, total cell-associated calcein fluorescence

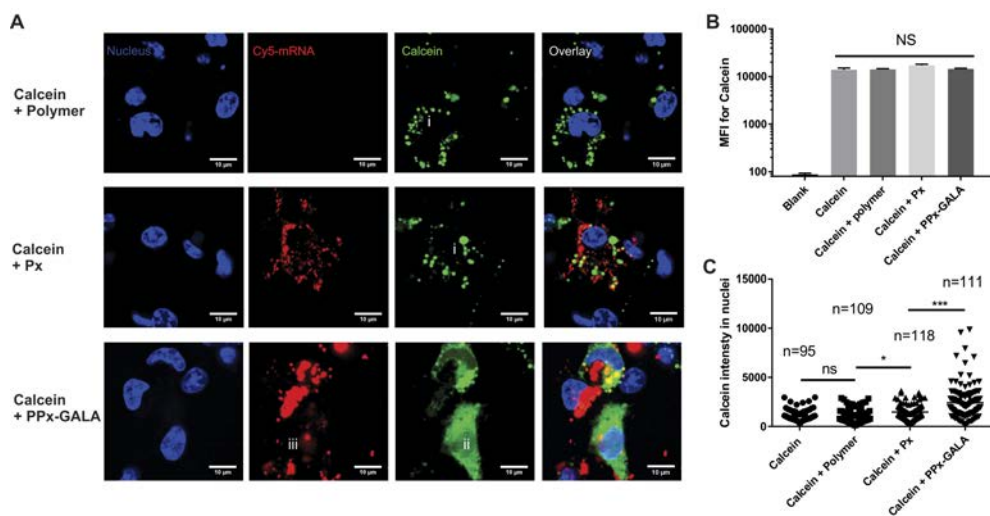


Fig. 5. PPx-GALA polyplexes facilitate the delivery of the membrane-impermeable fluorescent molecule calcein into the cytosol of dendritic cells. Confocal microscopy (A) and flow cytometry analysis (B) of the cellular uptake of calcein in D1 cells after 3 h in the presence of serum at 37 $^{\circ}\text{C}$ after incubation of polymer, Px and PPx-GALA in the presence of 150 $\mu\text{g}/\text{mL}$ calcein (blue, nuclei; red, Cy5-luc mRNA; green, calcein). Scale bar: 10 μm . (C) The mean fluorescence intensity of calcein in D1 cell nuclei measured by ImageJ from confocal microscopy pictures. Data are the mean \pm SD.

was determined by flow cytometry (Fig. 5B). The coinubation of calcein with PPx-GALA did not increase the mean fluorescence intensity (MFI) of the cells compared to control groups, excluding the option of direct influx of calcein over the cell membrane. Since calcein can freely diffuse from the cytosol into the nucleus, this organelle can be taken as a clean region of interest (ROI) to quantify cytosolic calcein release with ImageJ. Figure 5C shows the fluorescence intensity of calcein inside the nucleus of cells as measured by confocal microscopy. The average calcein fluorescence of nuclei from cells incubated with PPx-GALA was significantly higher than that of cells incubated with Px or with the soluble polymer used to prepare PPx-GALA. Based on these data, it is safe to conclude that the observed diffuse calcein fluorescence in the DCs is due the leakage of calcein from endo-lysosomes caused by the immobilized GALA peptides on internalized PPx-GALA.

The final fate of mRNA polyplexes was also evaluated by staining late-endosome/lysosome with lysotracker (green), and Px polyplexes without endosomal escape ability were used as control (Fig. 6A). As expected, the confocal images of cells transfected with PPx-GALA displayed spreading red regions into the cytoplasm and showed lower colocalization with lysotracker compared with Px (Fig. 6B). Lysotracker as a weakly basic amine can selectively accumulate into acidic compartments such as lysosomes. The lower colocalization with mRNA is most likely due to the GALA-disrupted acidic compartments resulting in an increase in pH of the endosomal lumens, which may lead to quenching and/or redistribution of the fluorescence of lysotracker [58]. These results strongly suggest that the presence of GALA on the surface of mRNA polyplexes facilitate endosomal escape.

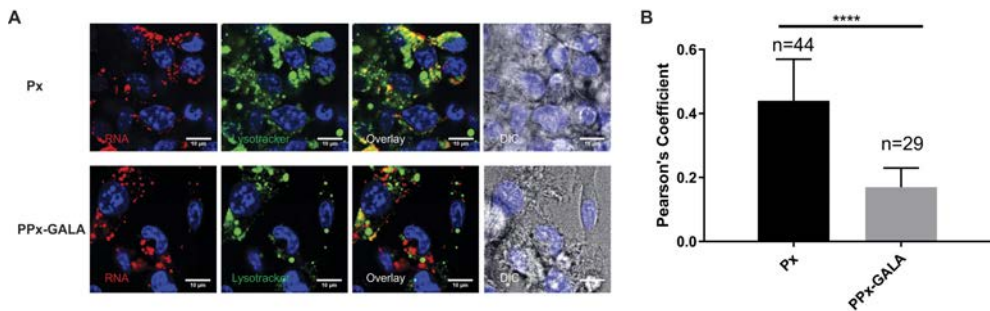


Fig. 6. Endosomal escape of PPx-GALA mRNA formulations from D1 cells. (A) Confocal microscopy of D1 cells 3 h after incubation with Px or PPx-GALA containing Cy5-luc_mRNA in the presence of serum at 37 °C. The endo-lysosomes were labeled with lysotracker green, yellow puncta in the overlay images indicate colocalization of mRNA (red) and lysotracker (green). Bar indicates 10 μ m. (B) Averages of Cy5-luc mRNA colocalization coefficients with lysotracker of images from A. Images were analyzed by ImageJ with the Pearson correlation coefficient [57].

PPx-GALA OVA-mRNA polyplexes stimulate DC antigen presentation and promote DC maturation

Antigen processing and presentation were analyzed using D1 cells incubated with PPx-GALA loaded with mRNA encoding ovalbumin. An *in vitro* MHC I antigen presentation assay was performed using the B3Z CD8⁺ T cell hybridoma, which produces β -galactosidase upon recognition of the ovalbumin CD8 epitope (SIINFEKL) presented in the context of MHC I H-2K^b on the surface of D1 cells [59]. Time course and dose response studies were performed to establish the kinetics of OVA mRNA translation, processing and presentation of the SIINFEKL peptide (Fig.7). As shown in Fig. 7A, a 6 h incubation time of D1 cells with PPx-GALA is enough to detect T cell activation. At 24 h, the PPx-GALA generated the highest T cell responses. This was further confirmed by flow cytometry, which was used to detect the amount of MHCI-OVA epitope on the cell surface by staining DCs with the 25-D1.16 monoclonal antibody directed

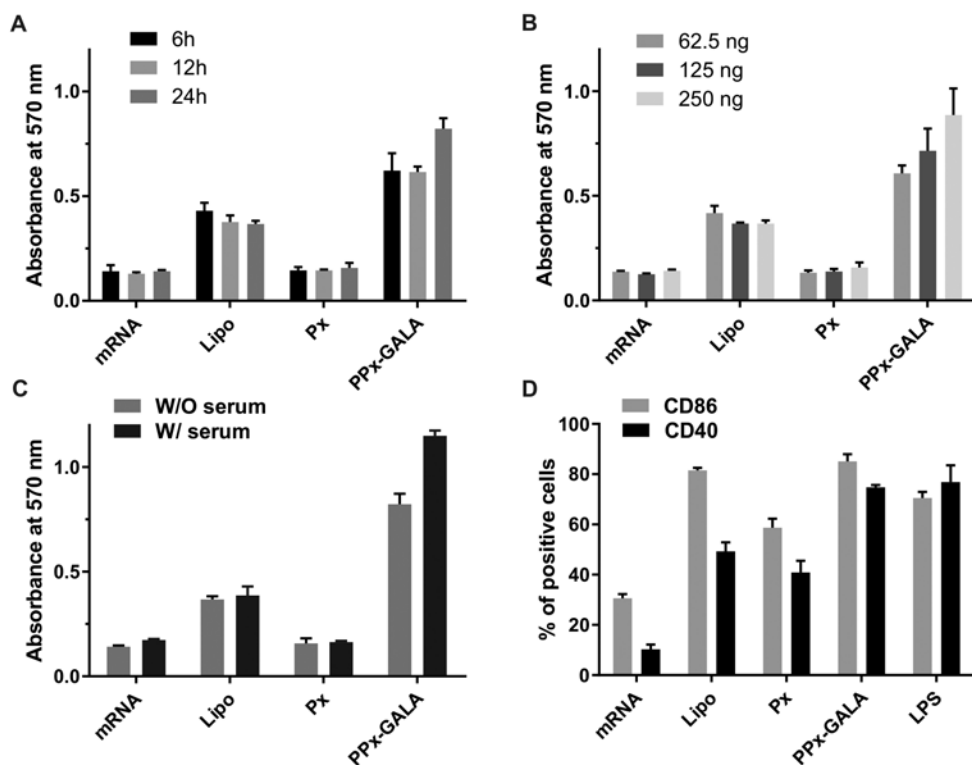


Fig. 7. B3Z T cell activation by transfected D1 dendritic cells. D1 cells were incubated with free mRNA and the indicated mRNA polyplexes encoding ovalbumin (OVA) for indicated lengths of time (A), or different mRNA dosages at a fixed incubation time (24h) (B) and different transfection conditions (C), then cocultured with B3Z T cells for 24 h. T cell activation was then quantified based on β -galactosidase activity. (D) Percentage of D1 cells expressing CD40 and CD86 in response to incubation 24h with the indicated formulations, LPS (1 μ g/mL) was used as positive control. Unless specified, all experiments were conducted with mRNA dose of 250 ng/well.

against MHC I H-2K^b complexes (Fig. S8). The kinetics of OVA antigen presentation were similar as for EGFP mRNA expression, which implies that the cytoplasmic protein production and proteasome processing were conducted at the same time. Since a 4 fold decrease in mRNA dose only lead to a minor decrease in T cell responses (Fig. 7B), it can be concluded that the proteasome degradation process is the rate limiting step for antigen presentation. A similar phenomenon was also observed in a previous study, where a mRNA core-lipid shell structured LPP/mRNA (encoding for OVA) vaccine was used to transfect DC2.4 with almost 100% efficiency with EGFP mRNA, but only have around 10% of DCs displayed MHC I H-2K^b complexes when transfected [14]. Surprisingly, when D1 cells were transfected in the presence of serum, PPx-GALA produced a higher T cell response than when serum was omitted (Fig. 7C), despite having a slightly lower EGFP mRNA transfection efficiency (Fig. S5). These results suggest that the high mRNA translation efficiency does not necessarily correlate with high T cell responses.

Subsequently, we evaluated to what extent the OVA mRNA polyplexes PPx-GALA were able to activate DCs. After D1 cells were incubated for 24 h with PPx-GALA, strong upregulation of the co-stimulatory markers CD40 and CD86 was observed (Fig.7D). PPx-GALA polyplexes were able to promote DC maturation to the same extent as D1 treated with LPS. The higher DC maturation level of PPx-GALA compared to Px may be due to the higher cellular uptake level because of the GALA targeting ability (Fig. 4A). These results indicate that DC maturation is mediated by the self-adjuvant effect of mRNA, and not so much by mRNA expression. In summary, PPx-GALA polyplexes are able to efficiently promote DC antigen presentation as well as DC maturation.

| Summarizing discussion

This study aimed to identify a peptide candidate to facilitate mRNA endosomal escape from APCs using a novel polymer-based mRNA vaccine platform. APCs are known for being notoriously difficult to transfect with non-viral transfection methods [60]. Here, three different peptides (LEDE, Melittin and GALA) were examined to promote endosomal escape of mRNA polyplexes. We found that GALA-modified mRNA polyplexes were the only formulation that successfully transfected both macrophages and DCs. Optimal exposure of GALA peptides from the surface of polyplexes was achieved by using a post-modification method in which first the mRNA polyplex core was formed, after which a functional shell was introduced using click chemistry. This method prevents shielding of immobilized GALA peptides (Fig. 1A) since previous studies have shown that GALA must be present on the surface of particles to exert its function [61]. Strikingly, the negatively charged PPx-GALA polyplexes were able to transfect both the DC 2.4 murine bone marrow derived dendritic cell line (28%) and the D1 spleen-derived cell line (50%) with a transfection efficiency comparable to that of cationic polyplexes [24,62,63] and lipoplexes [14,16,23]. The use of GALA peptides has resulted in enhanced pDNA and siRNA transfection in different tumors [28,29,64–67] and dendritic cells [68]. However, to best of our knowledge, this is the first time that GALA modified polyplexes promote mRNA delivery in APCs.

Cellular uptake studies revealed that PPx-GALA efficiently bound to the surface of DCs. Sialic acid residues on membrane proteins [46] and lipids and GALA peptides on the polyplex seemed to play a role in this binding as pre-incubation with MAM lectin blocked binding to DCs, whereas polyplexes without GALA did not show any inhibited cellular uptake (Fig.4C,D). Cell membrane binding of PPx-GALA did lead to rapid internalization (Fig. 3B). It was unexpected to see that a peptide that was initially selected for its fusogenic properties, also showed selective binding to cell surface proteoglycans on dendritic cells and thus acts as targeting ligand. As depicted in Fig. 8, the PPx-GALA mimics the cell entry mechanism of influenza viruses as both bind to sialic acid residues [69], are taken up by endocytosis/phagocytosis and trigger endosomal escape of their RNA content. Further proof for a specific interaction between GALA and sialic acid residues was given by dose-dependent binding of PPx-GALA to a variety of tumor cell lines (murine melanoma B16F10, mouse colorectal cancer CT26 and human lung carcinoma H358) that are known to over-express sialic acid residues to protect them against

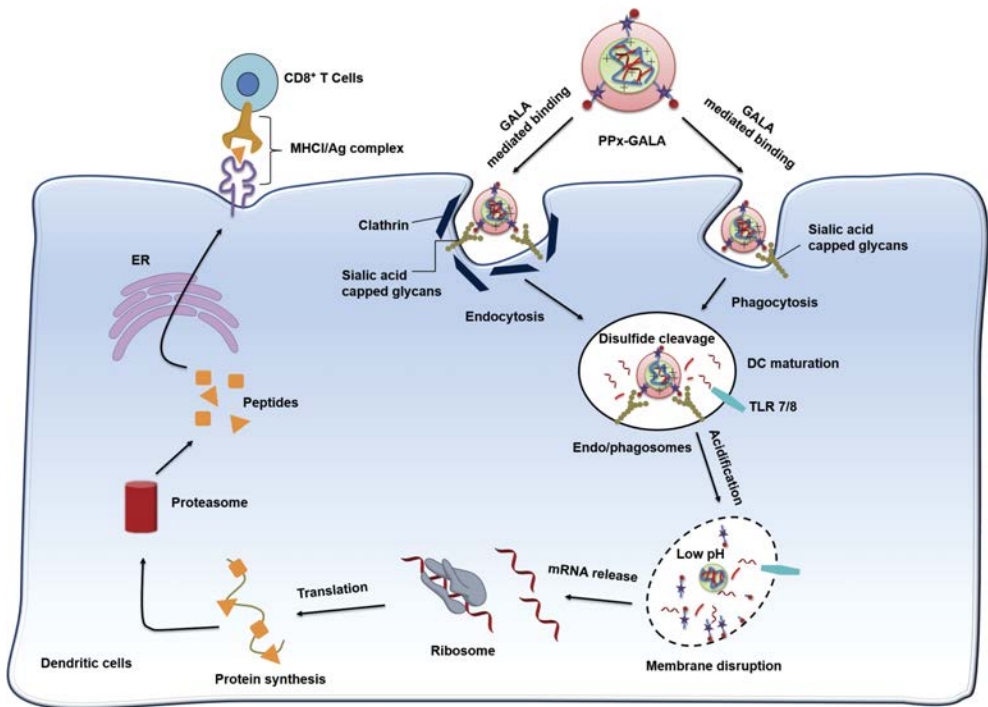


Fig.8. Proposed intracellular trafficking pathway of PPx-GALA mRNA polyplexes. The GALA peptide on the out-layer of polyplexes binds to the sialic acid capped glycans on the surface of DCs, followed by internalization by endo/phagocytosis. The disulfide bonds crosslinker inside polyplexes start to break down due to the presence of different thiols and reductive enzymes [77], and mRNA is gradually released from polyplexes and activated TLR7/8 receptor. The decreasing pH in endo/phagosomes also increases the helical content of GALA, leading to membrane disruption and to subsequent cytosolic release of mRNA, resulting in the induction of protein expression. The expressed endogenous antigen protein is processed by proteasome and presented to MHC I on the cell surface.

the immune defense system [70–73]. As shown in Fig.S9, after 24 h incubation with different tumor cells, PPx-GALA exhibited a much higher cellular uptake compared to Px. However, similar as observed for HEK 293T cells, there was no EGFP expression in these tumor cells. The specific ability to transfect APCs other than the tumor cells and normal cell lines may be due to differences in intracellular routing of internalized PPx-GALA in DCs compared to tumor cells. It is known that DCs have a longer acidification process [74–76], which could favor thiol-disulfide exchange [77] and survival of mRNA in the endosomal compartments. The cleavage of the disulfide bonds accelerated the release of mRNA which will activate the TLR7/8 before being released into the cytosol.

For most lipid-based mRNA vaccines that are predominantly internalized by micropinocytosis, internalization is abrogated upon DC maturation, resulting in a loss of transfection efficiency [1,78,79]. In contrast, the cellular uptake of PPx-GALA increased around 20% when DCs were matured with LPS (Fig. 4C). Interestingly, it has been described that LPS-induced DC maturation leads to upregulation of sialic acid residues on the cell surface [48,51]. Therefore, PPx-GALA polyplexes have a great advantage over lipid-based delivery systems if it comes to transfecting DCs.

Since the mRNA used in this study has a length more than 1000 nucleotides (nt), a much bigger molecular than siRNA (~ 20 nt), it is difficult to directly observe their endosomal escape as mRNA exhibited poor mobility in cytoplasm because of molecular crowding [80]. To have a better understanding of PPx-GALA intracellular trafficking process, we first examined the leakage properties of endo/phagosome caused by GALA using calcein as indicator molecule (Fig. 5). After 3 h co-incubation of PPx-GALA with calcein indeed a significant calcein leakage from endo/phagosomes to the cell nucleus was observed (Fig. 5). However, only 23% of total D1 cells showed calcein fluorescence signal inside nuclei even though all the cells have internalized PPx-GALA (Fig. 5C). These results imply that only a small portion of internalized PPx-GALA is able to cause endo/lysosome disruption; similar phenomena were found for PEI/pDNA polyplexes [81] and lipid siRNA formulations [82].

The ultimate goal was to make a polyplex vaccine that would induce strong CD8⁺ T cell responses. After investigating the antigen presentation kinetics *in vitro* with OVA mRNA as model antigen, we found that the mRNA protein translation and proteasome degradation is fast and occurred 6 h after transfection (Fig.7A and Fig. S8). The PPx-GALA formulations were able to induce a much stronger T cell response than the Lipo formulation and was less toxic to the cells (Fig. 2). The mRNA used in this study was chemically modified (nucleotides-modified), which have shown to produce high levels of protein, reduce the recognition by TLR7/8 and avoid the release of type I IFNs [8,16,83]. Interestingly, PPx-GALA still efficiently activated DCs to the same level as LPS, which may be related to the very high cellular uptake levels of mRNA that continued even after maturation of the DCs. In conclusion, GALA appears to fulfill a dual task: it binds to sialic acid residues on DCs and after internalization subsequently triggers endosome disruption, thereby helping the mRNA being released into the cytosol to be translated as into an endogenous antigen, which is subsequently processed and presented to the MHC class I molecules to activate T cells.

| Conclusions

We have successfully transfected antigen presenting cells via screening of different endosomal escape peptides. The mRNA polyplexes post-modified with GALA, PPx-GALA, showed high mRNA translation in dendritic cells and macrophages. PPx-GALA exhibit sialic acid ended glycan cellular uptake and are capable to help mRNA endosomal escape. This delivery system achieved superior OVA mRNA antigen transfection efficiencies and high levels of antigen specific T cell responses, along with the strong immune-stimulatory properties. These results warrant further exploration of PPx-GALA as vaccine platform for the development of personalized vaccines for cancer immunotherapy.

| Acknowledgments

Bo Lou was supported by a PhD scholarship from China scholarship Council (CSC). We thank Dr. Jan Wouter Drijfhout from Leiden University for providing the LEDE peptide.

| References

1. C. Pollard, S. De Koker, X. Saelens, G. Vanham, J. Grooten, Challenges and advances towards the rational design of mRNA vaccines., *Trends Mol. Med.* 19 (2013) 705–13.
2. M. Barry, R.C. Bleackley, Cytotoxic T lymphocytes: all roads lead to death, *Nat. Rev. Immunol.* 2 (2002) 401–409.
3. S.S. Neelapu, S. Tummala, P. Kebriaei, W. Wierda, C. Gutierrez, F.L. Locke, K. V. Komanduri, Y. Lin, N. Jain, N. Daver, J. Westin, A.M. Gulbis, M.E. Loghin, J.F. de Groot, S. Adkins, S.E. Davis, K. Rezvani, P. Hwu, E.J. Shpall, Chimeric antigen receptor T-cell therapy — assessment and management of toxicities, *Nat. Rev. Clin. Oncol.* 15 (2017) 47–62.
4. K.T. Roybal, Refining cell therapy, *Science.* 359 (2018) 1112–1113.
5. A.K. Palucka, L.M. Coussens, The Basis of Oncoimmunology, *Cell.* 164 (2016) 1233–1247.
6. C.J.M. Melief, T. van Hall, R. Arens, F. Ossendorp, S.H. van der Burg, Therapeutic cancer vaccines, *J. Clin. Invest.* 125 (2015) 3401–3412.
7. S. Pascolo, Vaccination with Messenger RNA (mRNA), in: Springer, Berlin, Heidelberg, 2008: pp. 221–235.
8. A. De Beuckelaer, J. Grooten, S. De Koker, Type I Interferons Modulate CD8+ T Cell Immunity to mRNA Vaccines, *Trends Mol. Med.* 23 (2017) 216–226.
9. H. Yin, R.L. Kanasty, A.A. Eltoukhy, A.J. Vegas, J.R. Dorkin, D.G. Anderson, Non-viral vectors for gene-based therapy, *Nat. Rev. Genet.* 15 (2014) 541–555.
10. K.J. Kauffman, M.J. Webber, D.G. Anderson, Materials for non-viral intracellular delivery of messenger RNA therapeutics, *J. Control. Release.* 240 (2016) 227–234.
11. O.S. Fenton, K.J. Kauffman, R.L. McClellan, E.A. Appel, J.R. Dorkin, M.W. Tibbitt, M.W. Heartlein, F. DeRosa, R. Langer, D.G. Anderson, Bioinspired Alkenyl Amino Alcohol Ionizable Lipid Materials for Highly Potent In Vivo mRNA Delivery, *Adv. Mater.* 28 (2016) 2939–2943.
12. M.A. Oberli, A.M. Reichmuth, J.R. Dorkin, M.J. Mitchell, O.S. Fenton, A. Jaklenec, D.G. Anderson, R. Langer, D. Blankschtein, Lipid Nanoparticle Assisted mRNA Delivery for Potent Cancer Immunotherapy, *Nano Lett.* 17 (2017) 1326–1335.
13. K. Hirschberger, A. Jarzebinska, E. Kessel, V. Kretzschmann, M.K. Aneja, C. Dohmen, A. Herrmann-Janson, E. Wagner, C. Plank, C. Rudolph, Exploring Cytotoxic mRNAs as a Novel Class of Anti-cancer Biotherapeutics, *Mol. Ther. - Methods Clin. Dev.* 8 (2018) 141–151.
14. S. Persano, M.L. Guevara, Z. Li, J. Mai, M. Ferrari, P.P. Pompa, H. Shen, Lipopolyplex potentiates anti-tumor immunity of mRNA-based vaccination, *Biomaterials.* 125 (2017) 81–89.
15. L.M. Kranz, M. Diken, H. Haas, S. Kreiter, C. Loquai, K.C. Reuter, M. Meng, D. Fritz, F. Vascotto, H. Hefesha, C. Grunwitz, M. Vormehr, Y. Hüsemann, A. Selmi, A.N. Kuhn, J. Buck, E. Derhovanessian, R. Rae, S. Attig, J. Diekmann, R.A. Jabulowsky, S. Heesch, J. Hassel, P. Langguth, S. Grabbe, C. Huber, Ö. Türeci, U. Sahin, Systemic RNA delivery to dendritic cells exploits antiviral defence for cancer immunotherapy, *Nature.* 534 (2016) 396–401.
16. R. Verbeke, I. Lentacker, L. Wayteck, K. Breckpot, M. Van Bockstal, B. Descamps, C. Vanhove, S.C. De Smedt, H. Dewitte, Co-delivery of nucleoside-modified mRNA and TLR agonists for cancer immunotherapy: Restoring the immunogenicity of immunosilent mRNA, *J. Control. Release.* 266 (2017) 287–300.
17. U. Lachelt, E. Wagner, Nucleic Acid Therapeutics Using Polyplexes: A Journey of 50 Years (and Beyond), *Chem. Rev.* 115 (2015) 11043–11078.
18. S. Uchida, H. Kinoh, T. Ishii, A. Matsui, T.A. Tockary, K.M. Takeda, H. Uchida,

- K. Osada, K. Itaka, K. Kataoka, Systemic delivery of messenger RNA for the treatment of pancreatic cancer using polyplex nanomicelles with a cholesterol moiety, *Biomaterials*. 82 (2016) 221–228.
19. S. Uchida, K. Itaka, H. Uchida, K. Hayakawa, T. Ogata, T. Ishii, S. Fukushima, K. Osada, K. Kataoka, In vivo messenger RNA introduction into the central nervous system using polyplex nanomicelle., *PLoS One*. 8 (2013) e56220.
 20. T. Bettinger, R.C. Carlisle, M.L. Read, M. Ogris, L.W. Seymour, Peptide-mediated RNA delivery: a novel approach for enhanced transfection of primary and post-mitotic cells., *Nucleic Acids Res.* 29 (2001) 3882–91.
 21. C.J. McKinlay, J.R. Vargas, T.R. Blake, J.W. Hardy, M. Kanada, C.H. Contag, P.A. Wender, R.M. Waymouth, Charge-altering releasable transporters (CARTs) for the delivery and release of mRNA in living animals, *Proc. Natl. Acad. Sci.* 114 (2017) E448–E456.
 22. N. Zheng, L. Yin, Z. Song, L. Ma, H. Tang, N.P. Gabrielson, H. Lu, J. Cheng, Maximizing gene delivery efficiencies of cationic helical polypeptides via balanced membrane penetration and cellular targeting., *Biomaterials*. 35 (2014) 1302–14.
 23. X. Su, J. Fricke, D.G. Kavanagh, D.J. Irvine, In vitro and in vivo mRNA delivery using lipid-enveloped pH-responsive polymer nanoparticles, *Mol. Pharm.* 8 (2011) 774–787.
 24. C. Cheng, A.J. Convertine, P.S. Stayton, J.D. Bryers, Multifunctional triblock copolymers for intracellular messenger RNA delivery., *Biomaterials*. 33 (2012) 6868–76.
 25. B. Lou, A. De Beuckelaer, G.R. Dakwar, K. Remaut, J. Grooten, K. Braeckmans, B.G. De Geest, E. Mastrobattista, S. De Koker, W.E. Hennink, Post-PEGylated and crosslinked polymeric ssRNA nanocomplexes as adjuvants targeting lymph nodes with increased cytolytic T cell inducing properties, *J. Control. Release*. 284 (2018) 73–83.
 26. M. Meyer, A. Philipp, R. Oskuee, C. Schmidt, E. Wagner, Breathing life into polycations: Functionalization with pH-responsive endosomolytic peptides and polyethylene glycol enables siRNA delivery, *J. Am. Chem. Soc.* 130 (2008) 3272–3273.
 27. C. Huang, H. Jin, Y. Qian, S. Qi, H. Luo, Q. Luo, Z. Zhang, Hybrid melittin cytolytic peptide-driven ultrasmall lipid nanoparticles block melanoma growth in vivo, *ACS Nano*. 7 (2013) 5791–5800.
 28. H. Hatakeyama, E. Ito, H. Akita, M. Oishi, Y. Nagasaki, S. Futaki, H. Harashima, A pH-sensitive fusogenic peptide facilitates endosomal escape and greatly enhances the gene silencing of siRNA-containing nanoparticles in vitro and in vivo, *J. Control. Release*. 139 (2009) 127–132.
 29. W. Li, F. Nicol, F.C. Szoka, GALA: a designed synthetic pH-responsive amphipathic peptide with applications in drug and gene delivery, *Adv. Drug Deliv. Rev.* 56 (2004) 967–985.
 30. M.J. Nell, G.S. Tjabringa, A.R. Wafelman, R. Verrijck, P.S. Hiemstra, J.W. Drijfhout, J.J. Grote, Development of novel LL-37 derived antimicrobial peptides with LPS and LTA neutralizing and antimicrobial activities for therapeutic application, *Peptides*. 27 (2006) 649–660.
 31. A. de Breij, M. Riool, P.H.S. Kwakman, L. de Boer, R.A. Cordfunke, J.W. Drijfhout, O. Cohen, N. Emanuel, S.A.J. Zaat, P.H. Nibbering, T.F. Moriarty, Prevention of *Staphylococcus aureus* biomaterial-associated infections using a polymer-lipid coating containing the antimicrobial peptide OP-145, *J. Control. Release*. 222 (2016) 1–8.
 32. A. Göblyös, K.J.M. Schimmel, A.R.P.M. Valentijn, L.M. Fathers, R.A. Cordfunke, H.L. Chan, J. Oostendorp, P.H. Nibbering, J.W. Drijfhout, P.S. Hiemstra, J. Den Hartigh, Development of a Nose Cream Containing the Synthetic Antimicrobial Peptide P60.4Ac for Eradication of Methicillin-Resistant *Staphylococcus aureus* Carriage, *J. Pharm. Sci.* 102 (2013) 3539–3544.
 33. A.M. Funhoff, C.F. Van Nostrum, A.P.C.A. Janssen, M.H.A.M. Fens, D.J.A. Crommelin, W.E. Hennink, Polymer Side-

- Chain Degradation as a Tool to Control the Destabilization of Polyplexes, *Pharm. Res.* 21 (2004) 170–176.
34. G.T. Zugates, D.G. Anderson, S.R. Little, I.E.B. Lawhorn, R. Langer, Synthesis of poly(beta-amino ester)s with thiol-reactive side chains for DNA delivery., *J. Am. Chem. Soc.* 128 (2006) 12726–34.
 35. L. Novo, E.V.B. Van Gaal, E. Mastrobattista, C.F. Van Nostrum, W.E. Hennink, Decationized crosslinked polyplexes for redox-triggered gene delivery, *J. Control. Release.* 169 (2013) 246–256.
 36. X. Jiang, A. van der Horst, M.J. van Steenberg, N. Akeroyd, C.F. van Nostrum, P.J. Schoenmakers, W.E. Hennink, Molar-mass characterization of cationic polymers for gene delivery by aqueous size-exclusion chromatography., *Pharm. Res.* 23 (2006) 595–603.
 37. H. Dumortier, G.J.D. van Mierlo, D. Egan, W. van Ewijk, R.E.M. Toes, R. Offringa, C.J.M. Melief, Antigen presentation by an immature myeloid dendritic cell line does not cause CTL deletion in vivo, but generates CD8+ central memory-like T cells that can be rescued for full effector function., *J. Immunol.* 175 (2005) 855–863.
 38. C. Winzler, P. Rovere, M. Rescigno, F. Granucci, G. Penna, L. Adorini, V.S. Zimmermann, J. Davoust, P. Ricciardi-Castagnoli, Maturation stages of mouse dendritic cells in growth factor-dependent long-term cultures., *J. Exp. Med.* 185 (1997) 317–28.
 39. S. Zou, K. Scarfo, M.H. Nantz, J.G. Hecker, Lipid-mediated delivery of RNA is more efficient than delivery of DNA in non-dividing cells, *Int. J. Pharm.* 389 (2010) 232–243.
 40. K.K.L. Phua, K.W. Leong, S.K. Nair, Transfection efficiency and transgene expression kinetics of mRNA delivered in naked and nanoparticle format, *J. Control. Release.* 166 (2013) 227–233.
 41. T.Z. Chang, S.S. Stadtmiller, E. Staskevicius, J.A. Champion, Effects of ovalbumin protein nanoparticle vaccine size and coating on dendritic cell processing, *Biomater. Sci.* (2016).
 42. F. Lebre, C.H. Hearnden, E.C. Lavelle, Modulation of Immune Responses by Particulate Materials, *Adv. Mater.* (2016) 5525–5541.
 43. S. Kumar, A.C. Anselmo, A. Banerjee, M. Zakrewsky, S. Mitragotri, Shape and size-dependent immune response to antigen-carrying nanoparticles, *J. Control. Release.* 220 (2015) 141–148.
 44. N.M. Zaki, N. Tirelli, Gateways for the intracellular access of nanocarriers: a review of receptor-mediated endocytosis mechanisms and of strategies in receptor targeting, *Expert Opin. Drug Deliv.* 7 (2010) 895–913.
 45. D.K. Schach, W. Rock, J. Franz, M. Bonn, S.H. Parekh, T. Weidner, Reversible Activation of a Cell-Penetrating Peptide in a Membrane Environment, *J. Am. Chem. Soc.* 137 (2015) 12199–12202.
 46. K. Kusumoto, H. Akita, T. Ishitsuka, Y. Matsumoto, T. Nomoto, R. Furukawa, A. El-Sayed, H. Hatakeyama, K. Kajimoto, Y. Yamada, K. Kataoka, H. Harashima, Lipid envelope-type nanoparticle incorporating a multifunctional peptide for systemic siRNA delivery to the pulmonary endothelium, *ACS Nano.* 7 (2013) 7534–7541.
 47. S. Santiwarangkool, H. Akita, T. Nakatani, K. Kusumoto, H. Kimura, M. Suzuki, M. Nishimura, Y. Sato, H. Harashima, PEGylation of the GALA Peptide Enhances the Lung-Targeting Activity of Nanocarriers That Contain Encapsulated siRNA, *J. Pharm. Sci.* 106 (2017) 2420–2427.
 48. H.J. Crespo, J.T.Y. Lau, P.A. Videira, Dendritic cells: A spot on sialic acid, *Front. Immunol.* 4 (2013) 1–15.
 49. N.M. Stamos, I. Carubelli, D. van de Vlekkert, E.J. Bonten, N. Papini, C. Feng, B. Venerando, A. D'Azzo, A.S. Cross, L.-X. Wang, P.J. Gomas, LPS-induced cytokine production in human dendritic cells is regulated by sialidase activity, *J. Leukoc. Biol.* 88 (2010) 1227–1239.

50. R.N. Knibbs, I.J. Goldstein, R.M. Ratcliffe, N. Shibuya, Characterization of the carbohydrate binding specificity of the leukoagglutinating lectin from *Maackia amurensis*: Comparison with other sialic acid-specific lectins, *J. Biol. Chem.* 266 (1991) 83–88.
51. P.A. Videira, I.F. Amado, H.J. Crespo, M.C. Algueró, F. Dall’Olio, M.G. Cabral, H. Trindade, Surface α 2-3- and α 2-6-sialylation of human monocytes and derived dendritic cells and its influence on endocytosis, *Glycoconj. J.* 25 (2008) 259–268.
52. M.G. Cabral, Z. Silva, D. Ligeiro, E. Seixas, H. Crespo, M.A. Carrascal, M. Silva, A.R. Piteira, P. Paixão, J.T. Lau, P.A. Videira, The phagocytic capacity and immunological potency of human dendritic cells is improved by α 2,6-sialic acid deficiency, *Immunology.* 138 (2013) 235–245.
53. F. Sallusto, M. Cella, C. Danieli, A. Lanzavecchia, Dendritic cells use macropinocytosis and the mannose receptor to concentrate macromolecules in the major histocompatibility complex class II compartment: downregulation by cytokines and bacterial products., *J. Exp. Med.* 182 (1995) 389–400.
54. C.D. Platt, J.K. Ma, C. Chalouni, M. Ebersold, H. Bou-Reslan, R.A.D. Carano, I. Mellman, L. Delamarre, Mature dendritic cells use endocytic receptors to capture and present antigens, *Proc. Natl. Acad. Sci.* 107 (2010) 4287–4292.
55. G.L. Lukacs, P. Haggie, O. Seksek, D. Lechardeur, N. Freedman, A.S. Verkman, Size-dependent DNA mobility in cytoplasm and nucleus, *J. Biol. Chem.* 275 (2000) 1625–1629.
56. R.A. Jones, C.Y. Cheung, F.E. Black, J.K. Zia, P.S. Stayton, A.S. Hoffman, M.R. Wilson, Poly(2-alkylacrylic acid) polymers deliver molecules to the cytosol by pH-sensitive disruption of endosomal vesicles., *Biochem. J.* 372 (2003) 65–75.
57. J. Adler, I. Parmryd, Quantifying colocalization by correlation: The Pearson correlation coefficient is superior to the Mander’s overlap coefficient, *Cytom. Part A.* 77 (2010) 733–742.
58. N.B. Yapici, Y. Bi, P. Li, X. Chen, X. Yan, S.R. Mandalapu, M. Faucett, S. Jockusch, J. Ju, K.M. Gibson, W.J. Pavan, L. Bi, Highly stable and sensitive fluorescent probes (LysoProbes) for lysosomal labeling and tracking, *Sci. Rep.* 5 (2015) 8576.
59. J. Karttunen, S. Sanderson, N. Shastri, Detection of rare antigen-presenting cells by the lacZ T-cell activation assay suggests an expression cloning strategy for T-cell antigens., *Proc. Natl. Acad. Sci. U. S. A.* 89 (1992) 6020–6024.
60. G. Xue, Y. Cheng, F. Ran, X. Li, T. Huang, Y. Yang, Y. Zhang, SLC gene-modified dendritic cells mediate T cell-dependent anti-gastric cancer immune responses in vitro, *Oncol. Rep.* 29 (2013) 595–604.
61. T. Kakudo, S. Chaki, S. Futaki, I. Nakase, K. Akaji, T. Kawakami, K. Maruyama, H. Kamiya, H. Harashima, Transferrin-Modified Liposomes Equipped with a pH-Sensitive Fusogenic Peptide: An Artificial Viral-like Delivery System, *Biochemistry.* 43 (2004) 5618–5628.
62. N. Zheng, L. Yin, Z. Song, L. Ma, H. Tang, N.P. Gabrielson, H. Lu, J. Cheng, Maximizing gene delivery efficiencies of cationic helical polypeptides via balanced membrane penetration and cellular targeting, *Biomaterials.* 35 (2014) 1302–1314.
63. A.S. Irvine, P.K.E. Trinder, D.L. Laughton, H. Ketteringham, R.H. McDermott, S.C.H. Reid, A.M.R. Haines, A. Amir, R. Husain, R. Doshi, L.S. Young, A. Mountain, Efficient nonviral transfection of dendritic cells and their use for in vivo immunization, *Nat. Biotechnol.* 18 (2000) 1273–1278.
64. I. Nakase, S. Futaki, Combined treatment with a pH-sensitive fusogenic peptide and cationic lipids achieves enhanced cytosolic delivery of exosomes, *Sci. Rep.* 5 (2015) 10112.
65. F.S. Nouri, X. Wang, M. Dorrani, Z. Karjoo, A. Hatefi, A recombinant biopolymeric platform for reliable evaluation of the activity of pH-responsive amphiphile fusogenic peptides, *Biomacromolecules.* 14 (2013) 2033–2040.

66. H. Youn, J.-K. Chung, . Introduction 2. Modified mRNA 3. Delivery systems for modified mRNA 4. Systemic delivery of modified mRNA for gene therapy Modified mRNA as an alternative to plasmid DNA (pDNA) for transcript replacement and vaccination therapy, *Expert Opin. Biol. Ther.* 15 (2015) 1337–1348.
67. J. Haensler, F.C. Szoka, Polyamidoamine cascade polymers mediate efficient transfection of cells in culture, *Bioconjug. Chem.* 4 (1993) 372–379.
68. H. Akita, K. Kogure, R. Moriguchi, Y. Nakamura, T. Higashi, T. Nakamura, S. Serada, M. Fujimoto, T. Naka, S. Futaki, H. Harashima, Nanoparticles for ex vivo siRNA delivery to dendritic cells for cancer vaccines: Programmed endosomal escape and dissociation, *J. Control. Release.* 149 (2011) 58–64.
69. I. Ramos, A. Fernandez-Sesma, Cell receptors for influenza A viruses and the innate immune response, *Front. Microbiol.* 3 (2012) 117.
70. A. Passaniti, W. Hart, Cell Surface Sialylation and Tumor Metastasis, *J. Biochem.* 263 (1988) 725–729.
71. J.-J. Park, M. Lee, Increasing the α 2, 6 sialylation of glycoproteins may contribute to metastatic spread and therapeutic resistance in colorectal cancer., *Gut Liver.* 7 (2013) 629–41.
72. R. Schauer, Sialic acids: fascinating sugars in higher animals and man, *Zoology.* 107 (2004) 49–64.
73. M. Kubota, K. Takeuchi, S. Watanabe, S. Ohno, R. Matsuoka, D. Kohda, S.-I. Nakakita, H. Hiramatsu, Y. Suzuki, T. Nakayama, T. Terada, K. Shimizu, N. Shimizu, M. Shiroishi, Y. Yanagi, T. Hashiguchi, Trisaccharide containing α 2,3-linked sialic acid is a receptor for mumps virus., *Proc. Natl. Acad. Sci. U. S. A.* 113 (2016) 11579–11584.
74. A. Savina, C. Jancic, S. Hugues, P. Guermonprez, P. Vargas, I.C. Moura, A.M. Lennon-Duménil, M.C. Seabra, G. Raposo, S. Amigorena, NOX2 Controls Phagosomal pH to Regulate Antigen Processing during Crosspresentation by Dendritic Cells, *Cell.* 126 (2006) 205–218.
75. K.K. Peachman, M. Rao, C.R. Alving, D.R. Palmer, W. Sun, S.W. Rothwell, Human dendritic cells and macrophages exhibit different intracellular processing pathways for soluble and liposome-encapsulated antigens, *Immunobiology.* 210 (2005) 321–333.
76. K.K. Tran, H. Shen, The role of phagosomal pH on the size-dependent efficiency of cross-presentation by dendritic cells, *Biomaterials.* 30 (2009) 1356–1362.
77. L. Brülisauer, M.A. Gauthier, J.C. Leroux, Disulfide-containing parenteral delivery systems and their redox-biological fate, *J. Control. Release.* 195 (2014) 147–154.
78. L.M. Kranz, M. Diken, H. Haas, S. Kreiter, C. Loquai, K.C. Reuter, M. Meng, D. Fritz, F. Vascotto, H. Hefesha, C. Grunwitz, M. Vormehr, Y. Hüseman, A. Selmi, A.N. Kuhn, J. Buck, E. Derhovanessian, R. Rae, S. Attig, J. Diekmann, R.A. Jabulowsky, S. Heesch, J. Hassel, P. Langguth, S. Grabbe, C. Huber, Ö. Türeci, U. Sahin, Systemic RNA delivery to dendritic cells exploits antiviral defence for cancer immunotherapy, *Nature.* 534 (2016) 396–401.
79. S. Persano, M.L. Guevara, Z. Li, J. Mai, M. Ferrari, P.P. Pompa, H. Shen, Lipopolyplex potentiates anti-tumor immunity of mRNA-based vaccination, *Biomaterials.* 125 (2017) 81–89.
80. G.L. Lukacs, P. Haggie, O. Seksek, D. Lechardeur, N. Freedman, A.S. Verkman, Size-dependent DNA mobility in cytoplasm and nucleus, *J. Biol. Chem.* 275 (2000) 1625–1629.
81. Z.U. Rehman, D. Hoekstra, I.S. Zuhorn, Mechanism of polyplex- and lipoplex-mediated delivery of nucleic acids: Real-time visualization of transient membrane destabilization without endosomal lysis, *ACS Nano.* 7 (2013) 3767–3777.
82. A. Wittrup, A. Ai, X. Liu, P. Hamar, R. Trifonova, K. Charisse, M. Manoharan,

- T. Kirchhausen, J. Lieberman, Visualizing lipid-formulated siRNA release from endosomes and target gene knockdown, *Nat. Biotechnol.* 33 (2015) 870–876.
83. M.S.D. Kormann, G. Hasenpusch, M.K. Aneja, G. Nica, A.W. Flemmer, S. Herber-Jonat, M. Huppmann, L.E. Mays, M. Ilenyi, A. Schams, M. Griese, I. Bittmann, R. Handgretinger, D. Hartl, J. Rosenecker, C. Rudolph, Expression of therapeutic proteins after delivery of chemically modified mRNA in mice, *Nat. Biotechnol.* 29 (2011) 154–159.

| Supporting information

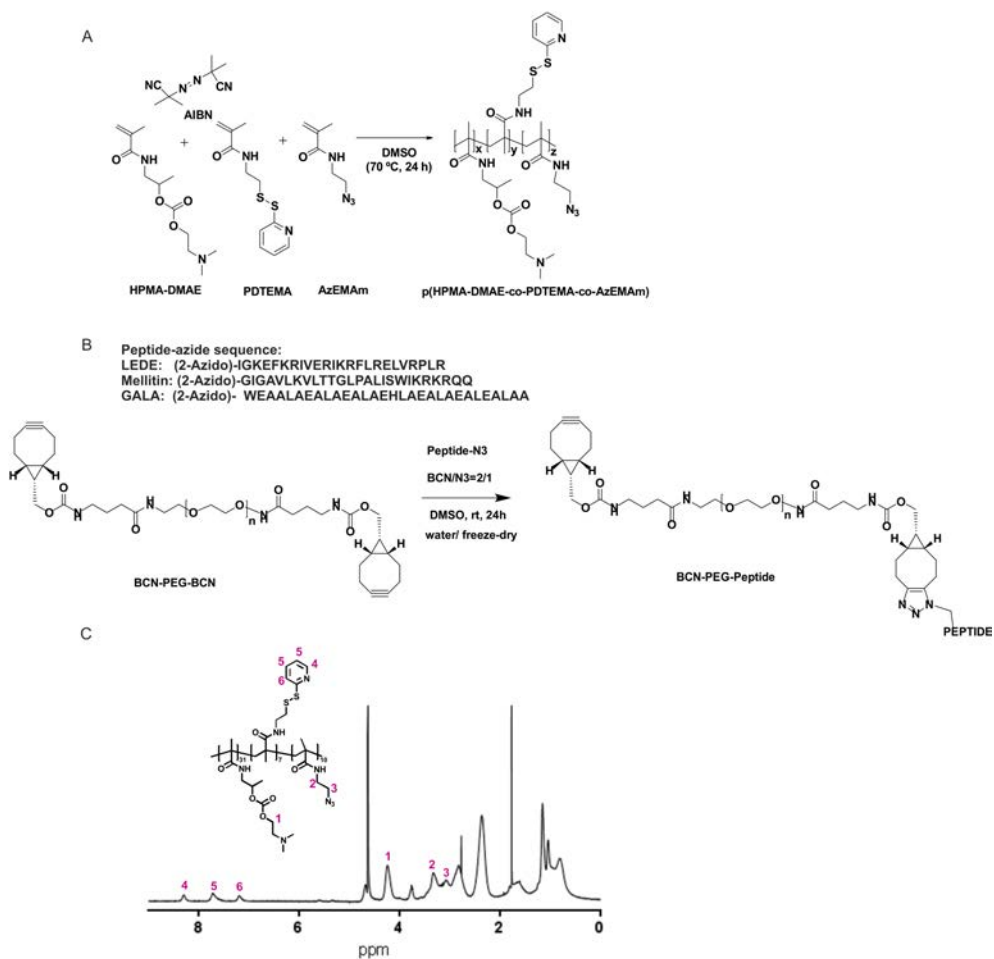


Fig. S1. Synthesis of random copolymers (A) p(HPMA-DMAE-co-PDTEMA-co-AzEMAm) (abbreviated as pHDPA), (B) BCN-PEG-peptide and (C) ^1H NMR spectrum of pHDPA in D_2O .

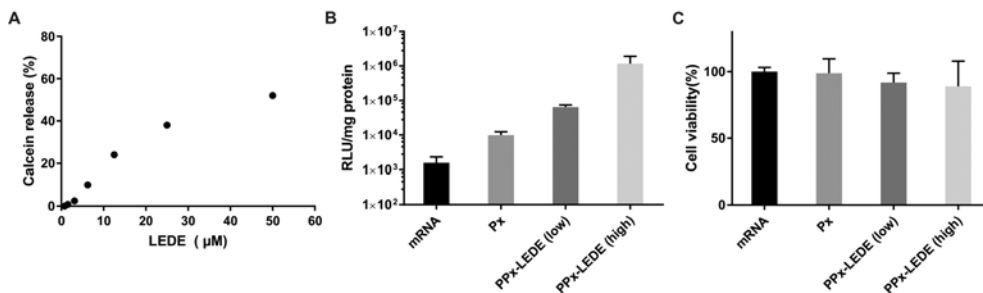


Fig. S2. (A) Membrane activity of LEDE peptide in the calcein leakage assay. Calcein release from target liposomes with self-quenched concentrations of entrapped calcein, was measured after 1 h incubation at pH 7.4. Results are plotted relative to 100% leakage, induced by addition of 0.5% Triton X-100 to the calcein liposomes (EPC:Chol in 2:1 ratio) [81]. Transfection efficiency (B) and cytotoxicity of LEDE modified luc_mRNA polyplexes on NIH3T3 cells in the absence of serum after 24 h with mRNA dose of 250 ng / well in a 96 well plate.

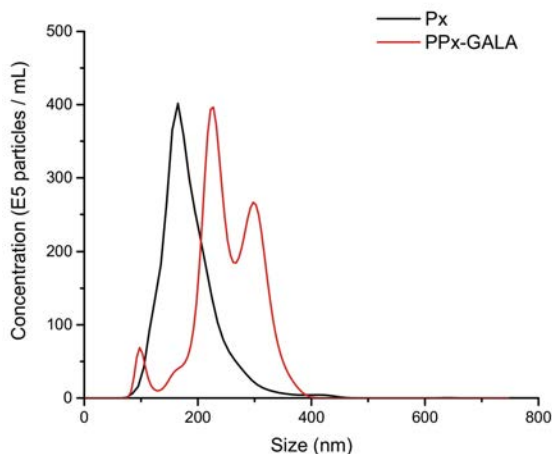


Fig. S3. Size distribution of Px (black) and PPx-GALA (red) mRNA polyplexes after lyophilization and rehydration measured in PBS buffer by Nanosight with a final mRNA concentration of 0.5 $\mu\text{g}/\text{mL}$.

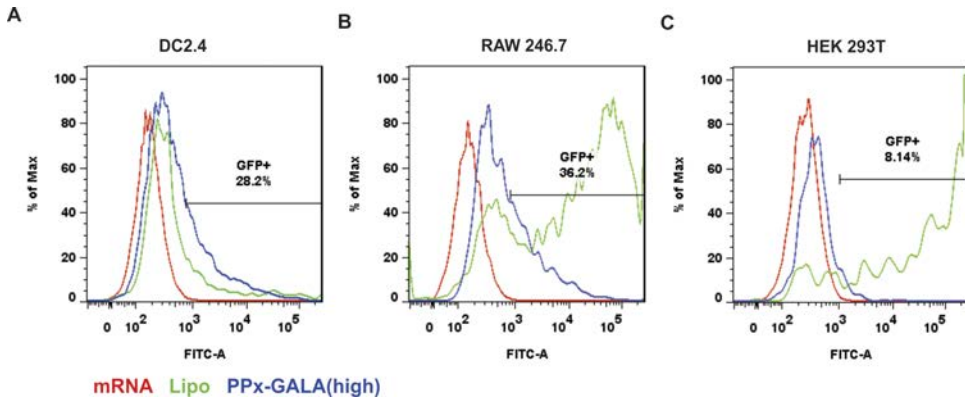


Fig. S4. Representative flow cytometry histograms of EGFP expression in DC2.4 (A), RAW246.7 (B) and HEK 293T(C) cells 24 h after incubation with free EGFP mRNA (red), Lipoplexes (Lipo, green) and PPx-GALA (blue), with a dose of 250 ng/well.

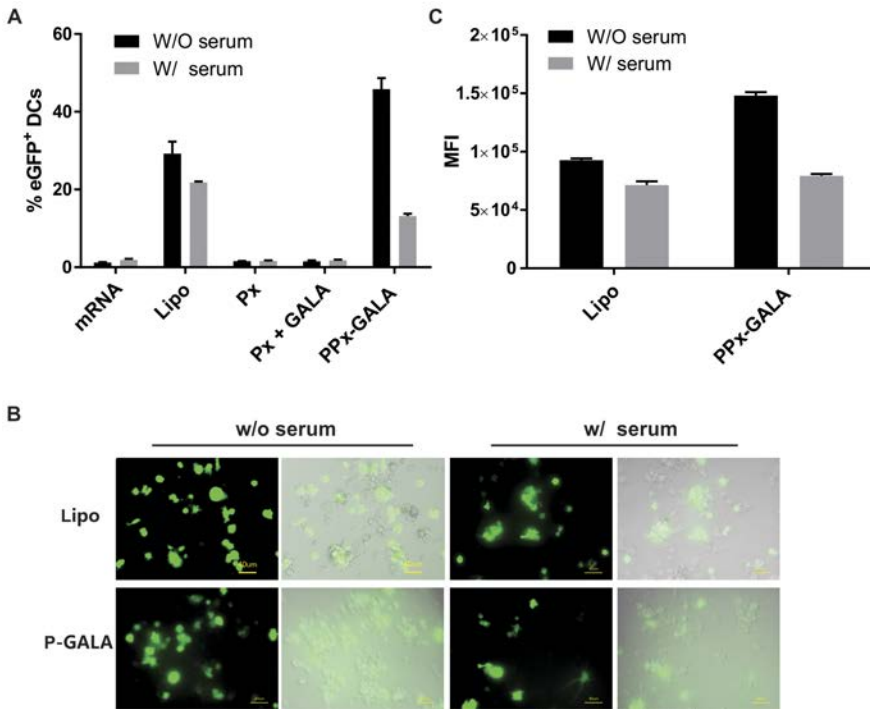


Fig. S5. The influence of serum on the transfection of D1 cells. (A) EGFP expression in D1 cells 24 h after addition of naked mRNA, lipofectamine-complexed mRNA or indicated Px and PPx formulations in the absence (W/O) or presence (W/) of serum as measured by flow cytometry. (B) Epifluorescence microscopy images showing EGFP fluorescence alone and a bright-field overlay of D1 cells. (C) D1 cellular uptake of Cy5-mRNA after 24 h when cells were transfected with (W/) or without (W/O) serum during the first 4 h of incubation. mRNA was added with a dose of 250 ng/well. Data are the mean \pm SD, n=3. Size bar represents 40 μ m.

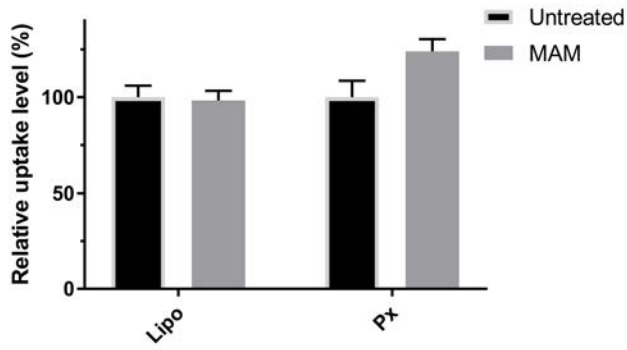


Fig. S6. D1 cellular uptake of Lipoplexes or Px (Cy5-luc_mRNA) after 1 h when cells were preincubated with Maackia amurensis agglutinin (MAM).

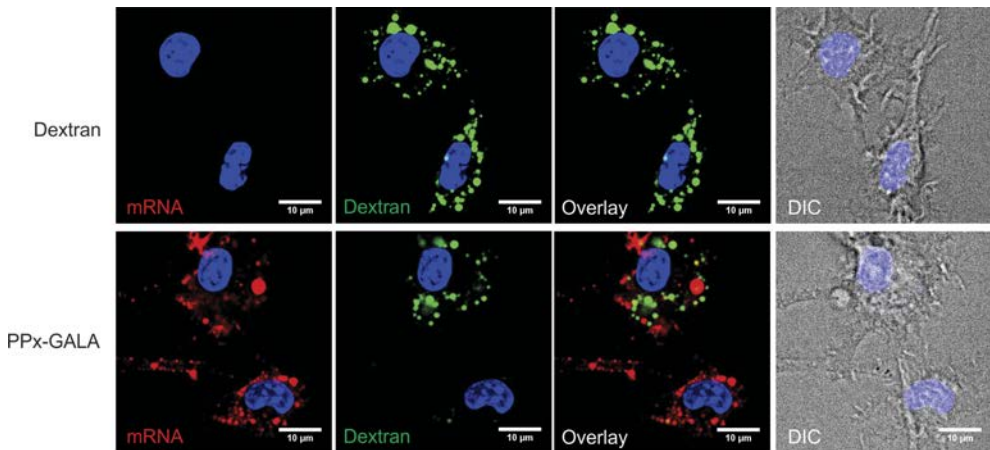


Fig. S7. Localization of Cy5-luc mRNA in D1 cells after co-transfection of PPx-GALA with dextran-FITC (70 kDa, 150 µg/mL) for 3 h.

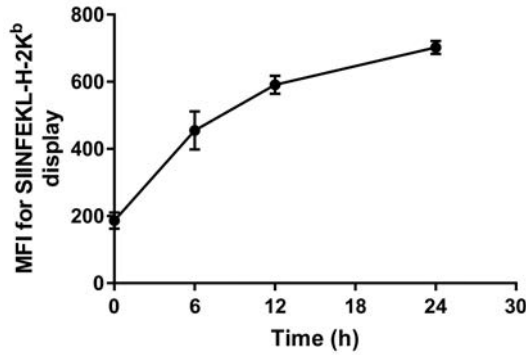


Fig. S8. D1 cells were incubated with PPx-GALA mRNA polyplexes encoding ovalbumin for the indicated times and antigen presentation was quantified by flow cytometry analysis of DCs stained with 25-D1.16 mAb that recognizes SIINFEKL-H-2K^b complexes.

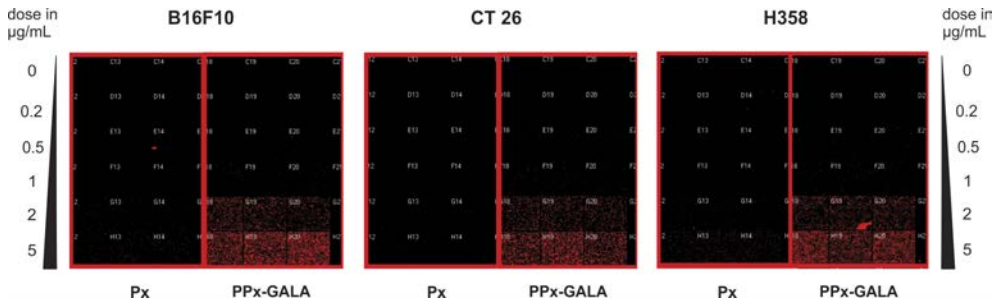


Fig. S9. Cellular uptake image of Px and PPx-GALA (high) formulation in the presence of serum. Tumor cells were plated in 384 well plates and cultured in an incubator. Cells were seeded to result in confluency at the end of the experiment (cell types tested = B16F10 – 4,000/well, CT26 4,000/well, H358 15,000/well. 50 µ media per well). The formulations were added directly to the cells (no media change) in triplicate at indicated concentration at the following day. After 24 h, the cells were fixed (4% PFA) and imaged on the ImageXpress.

CHAPTER

Summary and Perspectives

7

| Summary

Over the past decade, major advances in basic RNA biology, chemistry and gene sequencing technology have enabled RNA-based drugs to become a promising therapeutic tool to treat a wide variety of medical applications. RNA-based drugs greatly extend the domain of druggable targets beyond what can be achieved with small molecules and proteins. RNA therapeutics are in various clinical trials, for example, testing interfering RNAs (siRNA) to treat renal and hepatic disorders, messenger RNA (mRNA) to combat cancer, and, recently, CRISPR guide RNAs (gRNAs) to reprogram genetic information [1]. However, limited success has been achieved with RNA-based drugs largely due to the RNA molecule itself, because it is prone to nuclease degradation, can activate the immune system, and is too large or negatively charged to passively cross cell membranes. Therefore, functional systems that can deliver RNA therapeutics to the disease site, assist in RNA cellular entry and facilitate RNA endosomal escape into the cytoplasm are necessary and highly desired. Within the RNA delivery field, synthetic polymeric delivery systems are of particular interest by virtue of their high degree of chemical flexibility and the possibility to be tuned to integrate the various functionalities to overcome specific biological barriers as mentioned above. In this thesis, we focused on developing novel and multifunctional polymeric vectors for different RNA therapeutics, including delivery of siRNA to target tumor cells, delivery of single chain RNA (ssRNA) as adjuvant together with a protein antigen for vaccines and finally delivery of mRNA antigen to dendritic cells for cancer immunotherapy.

In **Chapter 1** a general introduction about RNA therapeutics and RNA delivery systems is given. This chapter firstly describes the categories of RNA therapeutics and briefly summarizes the current clinical achievements of RNA-based drugs. In addition, the biological barriers that need to be overcome and versatile delivery systems especially polymers-based vectors for RNA therapeutics are discussed. Furthermore, the cancer immunotherapy and advantages of mRNA cancer vaccines as well as their major challenges for clinical transformation are introduced to highlight the importance of devising multifunctional vectors for mRNA delivery.

In **Chapter 2** we tested a series of novel RAFT synthesized homopolymer poly(vinyl benzyl trimethylammonium chloride) (PVTC) and its block copolymer with poly(oligo(ethylene glycol) methacrylate) (POEGMA), which containing quaternized amines and hydrophobic benzyl groups as backbone, for siRNA delivery. The polymers formed colloiddally stable and small nanosized polyplexes (from 8 to 25 nm) with siRNA. Luciferase gene knock assay, confocal microscopy and flow cytometry showed that these polymers can efficiently delivery siRNA to human ovarian adenocarcinoma cells intracellularly, resulting in gene silencing to a level comparable to standard transfectant Lipofectamine 2000. The small and stable size combined with its high gene silencing properties, suggests that this system is suitable for treatment of solid tumors. This because of the better tumor penetration properties of small particles.

To target delivery of siRNA to glioblastoma (GBM) for down-regulation of key mediators for tumor cells invading and proliferation, **Chapter 3** describes a cholesterol stabilized polymeric siRNA delivery system that is functionalized with cRGD peptides as targeting ligands. We first

synthesized a random copolymer containing N-(2-hydroxypropyl)-methacrylamide (HPMA) and N-acryloxysuccinimide (NAS) via RAFT polymerization, followed by radical cross-coupling with cholesterol for stabilization. Next, cationic amines and azides were introduced for siRNA complexation and for post-polyplex modification. Incorporation of hydrophobic cholesterol groups resulted in the formation of stable nanosized siRNA polyplexes (~ 40 nm). Post-modification of the preformed polyplexes with PEG-cRGD for targeting via copper-free click chemistry gave rise to enhanced cellular uptake and increased luciferase gene silencing in U87R cells. In addition, a pilot *in vivo* study in healthy, non-tumor bearing C57BL/6 mice demonstrated that this PEG-cRGD polyplex system is well-tolerated and non-toxic, encouraging future evaluation of this targeted formulation for efficacy in tumor-bearing animals.

Chapter 4 reports on the design of a polymeric nanocomplex system for efficient delivery of ssRNA (PolyU, which is a ligand for Toll-like receptor 7 and 8 to DCs in the lymph nodes). It is aimed that this system is a potent adjuvant to enable effective immunomodulation for proteins or peptide-based subunit vaccines. We designed and synthesized a new series of random copolymers containing reactive azides and amines coupled to the polymer backbone via degradable carbonate bonds. The nanocomplexes were formed through a stepwise procedure, starting with the complexation of ssRNA and the cationic polymer, followed by post-PEGylation of the polyplexes through copper-free chemistry using PEG-bicyclononyne (BCN). Finally, the polyplexes were crosslinked via disulfide bonds to increase their stability. The post-PEGylation kinetics was studied by zeta-potential measurements and fluorescence correlation analysis. The generated near neutral ssRNA nanocomplexes with a size of ~150 nm were colloidally stable and able to protect RNA against enzymatic degradation. It was further shown that these particles were efficiently taken up by DCs and promote DC maturation *in vitro*. More importantly, up to 25-30% of DCs in the lymph nodes had internalized the ssRNA nanocomplexes after subcutaneous administration. When co-administered with a model antigen (soluble ovalbumin (OVA)), ssRNA nanocomplexes were far more efficient at inducing CD8 cytolytic T cells when compared to OVA co-administered with naked ssRNA. Furthermore, in contrast with naked ssRNA, IgG2c antibody titers, indicative of Th1 skewed T cell responses, were > 10 times higher when the ssRNA was complexed into the PEGylated nanocomplexes. Taken together, this chapter highlights the potential of post-functionalizing ssRNA nanocomplexes by copper-free click chemistry and these findings indicate that this potent ssRNA adjuvant formulation may profoundly improve the efficacy of a variety of vaccines requiring Th1-type immunity.

Because of the promising results regarding the adjuvant properties of ssRNA nanocomplexes in chapter 4, we are seeking a way to co-deliver ssRNA (PolyU) and antigen (OVA) in the same polymeric nanoparticle. Unlike traditional delivery systems such as PLGA and nanogel particles in which the antigen OVA and TLR agonist are both encapsulated into the core of nanoparticle, in **Chapter 5** we propose an alternative strategy to prepare nanoparticles loaded with OVA and an adjuvant by a modular core-shell assemble method. ssRNA was first self-assembled to nanocomplexes with two clickable cationic polymers which contain BCN or azide groups, that will self-crosslink via copper-free click chemistry. BCN-modified OVA and a glycosylated

polymer (containing mannose or galactose units) were sequentially clicked to the RNA core. Further, disulphide groups are present inside the crosslinked RNA core and between OVA to RNA core to allow reductive release of cargo once the particles being taken up by the cells. The strength of this vaccine delivery system lies in the flexibility at which the shell layers can be “clicked” onto the RNA core particle, enabling versatile adaptation of the vaccine. The generated particles resemble the structural organization of viruses in terms of size and supramolecular organization, and are thus named virus mimicking particles (VMP). These reduction-sensitive VMP with a size of 200 nm and negatively surface charge (-14 mV) were colloiddally stable in physiological environment. The immunogenicity of these VMP vaccines was evaluated *in vitro* and *in vivo*. The surface mannosylated VMP (VMP-Man) showed 5 times higher cellular uptake by BMDCs compared to the galactosylated VMP (VMP-Gal) counterpart. Moreover, VMP-Man efficiently activated DCs and greatly facilitated MHC I antigen presentation *in vitro*. Vaccination of mice with VMP-Man elicited strong OVA-specific cytotoxic T lymphocyte (CTL) responses as well as humoral immune responses. In summary, this modular core-shell polymeric delivery system described in this chapter is a promising modality to develop vaccines against diseases such as HIV and cancer that require Th1/cytotoxic T cell responses in addition to antibodies for protection.

Recently, mRNA have emerged as potent alternative to subunit protein and peptide-based vaccines to elicit CD8⁺ T cell immunity against various types of cancer and viral infections. Exogenous mRNA serves as ligand for specific TLR receptors both at the cell membrane as well as inside endocytic vesicles. This, combined with the fact that exogenous mRNA when delivered into the cytosol will be translated into protein and thus can provide a source of intracellular antigen for MHC I antigen presentation, makes mRNA a suitable candidate for use in cancer vaccination. *In vivo* studies (Chapter 4) have shown that PEGylated RNA polyplexes are stable and capable of targeting and activating DCs in the lymph nodes, however, most of the polyplexes likely remained entrapped inside the endo/lysosome compartments due to lack of endosomal escaping properties. To further employ this delivery system as mRNA vaccine platform, in Chapter 6 we post-functionalized the RNA polyplexes with different membrane-active peptides at the distal ends of the PEG chains to facilitate endosomal escape. Our data revealed that mRNA (encoding for EGFP) polyplexes surface decorated only with the GALA peptide (PPx-GALA), but not with other peptides such as melittin, lead to efficient transfection of macrophages and DCs (25-50% of the cells expressed EGFP). The mRNA transfection level is comparable or higher than the commercial lipofectamine formulation, without any observed cytotoxicity. To the best of our knowledge, this is the highest DCs transfection level achieved so far for a negatively charged PEGylated polymeric delivery systems. We further investigated the cellular uptake mechanism and intracellular trafficking process of PPx-GALA in DCs and found that the GALA peptide has a dual function: it actively targets sialic acid terminated glycans on DCs and subsequently mediates endosomal escape of mRNA leading to release into the cytosol. Moreover, PPx-GALA complexed with mRNA encoding OVA antigen efficiently transfected and activated DCs, resulting in strong OVA-specific T activation *in vitro*. These

results warrant further exploration of PPx-GALA as vaccine platform for the development of personalized vaccines for cancer immunotherapy.

| Future perspectives

Towards simple, smart and modular delivery system

Currently, with major breakthroughs in oncology and other life threatening diseases and extensive research of RNA biology and lipid and polymer chemistry, RNA-based therapeutics have made a fast pace of progress [2]. Even so, the lack of ‘ideal’ delivery systems has largely restricted the clinical translation of RNA-based drugs and is considered a serious bottleneck in the biopharmaceutical industry [3]. In the academic field, “smart delivery systems” employing different stimuli-responsive properties nanomaterials and nanotechnologies have been extensively developed, however, only some of them have been translated into the clinic [4]. Those delicate smart delivery systems enable the release of the RNA payload at specific target sites by responding to the spatial triggers. The triggers comprise endogenous stimuli, such as pH variations, redox gradients and enzyme concentrations, which are related to the pathological characteristics of the disease, or exogenous stimuli, including temperature, magnetic field, ultrasound and so on [5–7].

To obtain smart properties, most developed delivery systems in the past were designed with complexity to obtain sophisticated structures and formulations, which are difficult to scale up to allow industrial production. Therefore, for successful clinical translation, it is essential to reduce complexity and design facile and simple delivery platforms while maintaining the smart properties in favor of good manufacturing practice production. In addition, with the coming era of personalized medicines [8], for example, personalized cancer vaccines [9] which is a customized vaccine based on patient’s individual specific tumor-antigen, a modular delivery system which can rapidly adapted to different payloads without the need for time-consuming empirically optimization is the basis for fulfilling this purpose.

In this thesis, RNA delivery systems were designed based on this “modular” philosophy. We have utilized copper-free click chemistry for post-PEGylation (Chapter 3, 4 and 6) or antigen conjugation (Chapter 5) of preformed RNA polyplexes. As such, the formulations can be easily modified with different functionalities, e.g. targeting ligands and endosomal escape peptides. Important from a pharmaceutical perspective is that all the formulations used in this thesis can be stored in dry-powder form after freeze-drying without affecting particle size and RNA activity. Nevertheless, there is still room to further optimize these delivery systems. For instance, the mRNA delivery platform described in **Chapter 4** requires three steps for formulation, i.e. complexation, post-PEGylation and crosslinking, and the last step requires the addition of DTT to the polyplexes to activate pyridine disulfide groups (PDS). During this step, the amount of DTT added need to be precise (50 mol% of DTT against total PDS groups), because a deficient amount will result in unstable polyplexes and an excess amount will tend to cause inter-polyplexes aggregation. In addition, the by-product compounds such as pyridothione and oxidized DTT (a stable six-membered ring) will be produced during the crosslinking process. Although

those compounds have shown no toxicity in low concentrations both *in vitro* and *in vivo* [10], it would be better if we could avoid the use of such kind of crosslinking strategy for future clinical translation. One possible solution is to employ the method as presented in Chapter 5, in which the crosslinked RNA polyplexes were formed with two clickable cationic polymers which contain either BCN or azide groups. These will self-crosslink via strain promoted cycloaddition during a simple freeze-thaw treatment [11]. After that, extra BCN groups on the surface of RNA polyplexes can be further modified with various functionalities. In this way, it is much easier to control the crosslinking reaction and also more suitable for upscaling production and importantly, no by-products will be generated.

Beyond the traditional systemic administration route

Thirty years ago, Maeda and co-workers discovered the enhanced permeability and retention (EPR) effect [12] and demonstrated the potential for heightened accumulation of long-circulating macromolecules and nanoparticles by extravasation through fenestrated blood vessels in tumors compared to normal tissues [13]. Later, this EPR phenomenon has been expanded to other pathologies such as infection [14] and heart failure [15]. Ever since, extensive research efforts were applied using systemic delivery of nanoparticles to treat cancer, infection and inflammation [16]. As the nanoparticles can increase the circulation time of drug cargos (e.g. hydrophobic molecules and proteins), which leads to accumulation of drug at site of interest by passive targeting exploiting the EPR effect. The systemic administration of long circulation nanoparticle-formulated drugs indeed improved the safety and pharmacokinetics of encapsulated drugs. The most well-known examples are the FDA approved liposomal doxorubicin (Doxil) [17] and albumin-bound paclitaxel (Abraxane) [18] for treatment of cancer.

However, although similar nanoparticulate strategies have been explored for RNA therapeutics and massive efforts were examined to improve the RNA nanoparticle stability, RNA-based nanomedicines show a short circulation time after systemic delivery, mostly with a half-time of less than one hour [19]. Cationic polymer-based RNA delivery systems, for example, JetPEI/siRNA [20] and poly(ethylene glycol)-polyaspartamide (PEG- PAsp)/mRNA [21] have a circulation half-time of less than 10 mins. This is likely due to the insufficient stability of inter-polyelectrolyte complexes between RNA and cationic carriers, and the premature released RNA is subsequently rapidly degraded in the circulation by RNases. Some success has been reported to extend the circulation half-time of more than 8 hours by using lipid nanoparticles (LNP) for systemic delivery of siRNA or mRNA, but these systems show liver-only expression [22].

Alternatively, local administration of RNA therapeutics has become an attractive and effective route, allowing the use of lower doses and reducing side effects [23]. The mostly applied administration sites are the skin, the eye, the lung and nervous system. For example, subcutaneous injection of triantennary N-acetylgalactosamine (GalNAc), a high-affinity ligand for the hepatocyte-specific asialoglycoprotein receptor (ASGPR), modified siRNA [24] or antisense oligonucleotides (ASOs) [25] resulted in robust RNA-mediated gene silencing in the liver and has shown impressive benefit in clinical trials. It is likely that GalNAc-RNA

conjugates will eventually replace most therapeutic LNP efforts for liver treatments due to the safety and easy formulation. Similarly, mRNA-based drugs, especially mRNA vaccines are primarily topically applied [26]. Intramuscular injection of formulated mRNA with polymeric systems or LNP have shown extended mRNA expression and duration [26,27].

In the cancer immunotherapy field, due to the immune suppressive microenvironment inside the tumor [28], intratumoral administration has gained rising interest [29]. The direct administration of immunomodulatory agents such as mRNA encoding for immunotoxins [30], a fusion protein [31] or costimulatory factors [32] resulted in a significant reduction in tumor growth. More interestingly, recent studies have shown that local injection of TLR agonists (CpG - unmethylated CG enriched oligodeoxynucleotide - a TLR9 ligand) with co-stimulatory signals (anti-OX40 antibody, that can potentiate the action of conventional T cells) in tumors can lead to shrinkage of the injected tumors as well as distant untreated tumors resulting in long-term survival of the animals, even in a stringent spontaneous tumor model [33–35]. Another fascinating study showed that locally applied hydrogel scaffolds that gradually release agonists (for activating TLR7/8 (e.g. resiquimod) or stimulator of interferon genes (STING)) of innate immunity at the sites of tumor resection, effectively activated a systemic immune response that prevented tumor relapse and eliminated metastases [36]. The studies mentioned above show advantages of the “deliver locally, act globally” of local immunotherapy. Moreover, no toxicity that is often associated with systemic treatments is observed, thus providing a strong rationale for intratumoral therapy.

In light of the findings described above, it will be interesting to test the mRNA delivery system developed in **Chapter 6** after intratumoral administration in an appropriate syngeneic mouse tumor model. As we have found that PPx-GALA mRNA particles can selectively activate and transfect DCs and macrophages, but to a lesser extent tumor cells such as melanoma B16F10 and lung carcinoma H358, it will be interesting to locally inject this vaccine complexed with mRNA encoding tumor associated neoantigens into solid syngeneic and preferably orthotopic tumors to awake and initiate the immunosuppressive antigen presentation cells (APCs) inside tumor. Recent studies have identified that CD103⁺ DCs in the tumor microenvironment can process antigens and are crucial to the induction of an anti-tumoral T-cell response [37,38]. Therefore, we expect that PPx-GALA vaccines will play two roles. Firstly, PPx-GALA can act as an adjuvant which can actively bind to intratumoral APCs leading to internalization and activation of TLR7/8 due to the intrinsic immunogenicity of mRNA, and the production of inflammatory cytokines will further recruit more immune cells inside the tumor [39,40]. Secondly, after endosomal escape of PPx-GALA, the intratumoral DCs will express the tumor associated antigen and present it to infiltrated T cells to evoke antigen-specific anti-tumor responses. With such a dual effect, we believe that PPx-GALA will exhibit significant anti-tumor activity.

Combinational cancer vaccine treatment

Cancer immunotherapy has taken center stage as a novel and powerful approach to treat tumors [41]. A wide variety of promising immunotherapeutic strategies that aim to generate robust and

durable tumor-directed immune responses are available. These strategies include but are not limited to adoptive T cell therapy [42], immune checkpoint blockade [43], and more tolerable strategies like *ex-vivo* dendritic cell (DC)-based cancer vaccines [44] or synthetic therapeutic cancer vaccines [45]. Among them, synthetic cancer vaccines (e.g. protein/peptide vaccine or nucleic acid vaccine) which can preferentially stimulate and broaden the repertoire of T cells against tumor-specific epitopes have been extensively tested in patients with advanced cancer [46].

However, they have had little clinical success, which has largely been attributed to the immunosuppressive tumor microenvironment [47,48]. Thus, in established cancers, therapeutic cancer vaccines need the combination of immunomodulatory treatments to overcome immune evasion to become fully effective [45]. One advanced clinical example is the combination of cancer vaccines together with immune checkpoint blockades, such as the co-inhibitory receptors cytotoxic T lymphocyte antigen 4 (CTLA4) or programmed cell death protein 1 (PD1). These are antibodies which can release the brake of T cells to kill tumor cells. The best studied is PD1/PDL1, which have shown to induce remarkable long-lasting survival benefit in patients within more than thirty different kinds of tumors [49]. Recent results obtained from clinical trials have suggested that this combination immunotherapy increases the efficacy of checkpoint inhibitors as well as overall therapeutic efficacy [50–52]. In addition to immune checkpoints, a recent clinical study using a combination of DC vaccines and the vascular endothelial growth factor A (VEGF-A) blocking antibody bevacizumab and cyclophosphamide for treating ovarian cancer also shed some light onto different combination strategies for cancer vaccines. The clinical outcome showed significantly prolonged survival and demonstrated that this combination is feasible, safe and well tolerated, and importantly it elicited antitumor immunity with improved survival [53]. The rationale behind this study is that bevacizumab can induce *de novo* T cell infiltration in human tumors [54,55] and low-dose cyclophosphamide is able to attenuate systemic and tumor-infiltrating T regulatory cells [56].

Conclusion and future directions

With the continuous clinical progress and success, RNA-based therapeutics will become an increasing component of the pharmacopeia in the future. In this thesis we described different new RNA polymeric delivery systems starting from delivery siRNA to cancer cells for targeted gene therapies, followed by the delivery of protein and mRNA antigen to antigen presentation cells. We addressed stability issues that are generally related to polymeric RNA delivery systems by applying different stabilization strategies, among which the introduction of hydrophobic groups, crosslinks and surface PEGylation. To solve the targeting and endosomal escape problems, we have examined different targeting ligands (e.g. RGD and mannose) and endosomal membrane disruptive peptides. By combining different functionalities, we have obtained interesting and appealing results.

Further work on optimizing polymeric RNA delivery system is still needed to address the following two aspects: (1) increase the targeting ability to specific cell types and tissues and most importantly (2) boost endosomal escape ability of RNA-based nanomedicines. This

requires a better understanding of the fundamental pathological characteristics of tumors together with application-orientated design of delivery systems by integrating advanced technologies. For example, studies have shown that gene silencing of suppressor of cytokine signaling 1 (SOCS1) in dendritic cells leads to augmented DCs immunostimulatory capacity and results in an enhanced antitumor response [57,58]. Therefore, engineering an innovative delivery system that can transport RNA cocktails containing siRNA that target SOCS1 together with multiple tumor-associated mRNA neoantigens into DCs will be a promising approach to generate a strong immune response to combat cancer. Hopefully, with the accumulation of encouraging clinical data and basic investigations on smart polymeric delivery systems, RNA therapeutics will be translated to real-world products in a faster pace.

| References

1. A. Mullard, First in vivo gene-editing drugs enter the clinic, *Nat. Rev. Drug Discov.* 17 (2017) 7.
2. J. Lieberman, Tapping the RNA world for therapeutics, *Nat. Struct. Mol. Biol.* 25 (2018) 357–364.
3. Editorial - The commercial tipping point, *Nat. Biotechnol.* 35 (2017) 181–181.
4. C. Alvarez-Lorenzo, A. Concheiro, Smart drug delivery systems: from fundamentals to the clinic, *Chem. Commun.* 50 (2014) 7743–7765.
5. M. Uz, S. Alsoy Altinkaya, S.K. Mallapragada, Stimuli responsive polymer-based strategies for polynucleotide delivery, *J. Mater. Res.* 32 (2017) 2930–2953.
6. D. Liu, F. Yang, F. Xiong, N. Gu, The Smart Drug Delivery System and Its Clinical Potential, *Theranostics.* 6 (2016) 1306–1323.
7. J.O. Eloy, R. Petrilli, R.F. V Lopez, R.J. Lee, Stimuli-Responsive Nanoparticles for siRNA Delivery, *Curr. Pharm. Des.* 21 (2015) 4131–4144.
8. E.A. Ashley, Towards precision medicine, *Nat. Rev. Genet.* 17 (2016) 507–522.
9. U. Sahin, Ö. Türeci, Personalized vaccines for cancer immunotherapy, *Science.* 359 (2018) 1355–1360.
10. L. Novo, L.Y. Rizzo, S.K. Golombek, G.R. Dakwar, B. Lou, K. Remaut, E. Mastrobattista, C.F. Van Nostrum, W. Jahnen-Dechent, F. Kiessling, K. Braeckmans, T. Lammers, W.E. Hennink, Decationized polyplexes as stable and safe carrier systems for improved biodistribution in systemic gene therapy, *J. Control. Release.* 195 (2014) 162–175.
11. H. Takemoto, K. Miyata, T. Ishii, S. Hattori, S. Osawa, N. Nishiyama, K. Kataoka, Accelerated polymer-polymer click conjugation by freeze-thaw treatment, *Bioconjug. Chem.* 23 (2012) 1503–1506.
12. Y. Matsumura, H. Maeda, A New Concept for Macromolecular Therapeutics in Cancer Chemotherapy: Mechanism of Tumorotropic Accumulation of Proteins and the Antitumor Agent Smancs, *Cancer Res.* 46 (1986) 6387–6392.
13. H. Maeda, H. Nakamura, J. Fang, The EPR effect for macromolecular drug delivery to solid tumors: Improvement of tumor uptake, lowering of systemic toxicity, and distinct tumor imaging in vivo, *Adv. Drug Deliv. Rev.* 65 (2013) 71–79.
14. E.A. Azzopardi, E.L. Ferguson, D.W. Thomas, The enhanced permeability retention effect: a new paradigm for drug targeting in infection, *J. Antimicrob. Chemother.* 68 (2013) 257–274.
15. C.N. Marti, M. Gheorghiad, A.P. Kalogeropoulos, V. V. Georgiopoulou, A.A. Quyyumi, J. Butler, Endothelial dysfunction, arterial stiffness, and heart failure, *J. Am. Coll. Cardiol.* 60 (2012) 1455–1469.
16. E. Blanco, H. Shen, M. Ferrari, Principles of nanoparticles design for overcoming biological barriers for drug delivery, *Nat Biotechnol.* 33 (2015) 941–951.
17. Y. (Chezy) Barenholz, Doxil® — The first FDA-approved nano-drug: Lessons learned, *J. Control. Release.* 160 (2012) 117–134.
18. M.J. Hawkins, P. Soon-Shiong, N. Desai, Protein nanoparticles as drug carriers in clinical medicine, *Adv. Drug Deliv. Rev.* 60 (2008) 876–885.
19. R.L. Juliano, The delivery of therapeutic oligonucleotides, *Nucleic Acids Res.* 44 (2016) 6518–6548.
20. S. Gao, F. Dagnaes-Hansen, E.J.B. Nielsen, J. Wengel, F. Besenbacher, K.A. Howard, J. Kjems, The effect of chemical modification and nanoparticle formulation on stability and biodistribution of siRNA in mice, *Mol. Ther.* 17 (2009) 1225–1233.
21. S. Uchida, H. Kinoh, T. Ishii, A. Matsui, T.A. Tockary, K.M. Takeda, H. Uchida, K. Osada, K. Itaka, K. Kataoka, Systemic delivery of messenger RNA for the treatment of pancreatic cancer using polyplex nanomicelles with a cholesterol moiety, *Biomaterials.* 82 (2016) 221–228.

22. S.F. Dowdy, Overcoming cellular barriers for RNA therapeutics, *Nat. Biotechnol.* 35 (2017) 222–229.
23. F.T.M. de C. Vicentini, L.N. Borgheti-Cardoso, L.V. Depieri, D. De MacEdo Mano, T.F. Abelha, R. Petrilli, M.V.L.B. Bentley, Delivery systems and local administration routes for therapeutic siRNA, *Pharm. Res.* 30 (2013) 915–931.
24. J.K. Nair, J.L.S. Willoughby, A. Chan, K. Charisse, M.R. Alam, Q. Wang, M. Hoekstra, P. Kandasamy, A. V. Kelin, S. Milstein, N. Taneja, J. Oshea, S. Shaikh, L. Zhang, R.J. Van Der Sluis, M.E. Jung, A. Akinc, R. Hutabarat, S. Kuchimanchi, K. Fitzgerald, T. Zimmermann, T.J.C. Van Berkel, M.A. Maier, K.G. Rajeev, M. Manoharan, Multivalent N -acetylgalactosamine-conjugated siRNA localizes in hepatocytes and elicits robust RNAi-mediated gene silencing, *J. Am. Chem. Soc.* 136 (2014) 16958–16961.
25. T.P. Prakash, M.J. Graham, J. Yu, R. Carty, A. Low, A. Chappell, K. Schmidt, C. Zhao, M. Aghajani, H.F. Murray, S. Riney, S.L. Booten, S.F. Murray, H. Gaus, J. Crosby, W.F. Lima, S. Guo, B.P. Monia, E.E. Swayze, P.P. Seth, Targeted delivery of antisense oligonucleotides to hepatocytes using triantennary N-acetyl galactosamine improves potency 10-fold in mice, *Nucleic Acids Res.* 42 (2014) 8796–8807.
26. H. Youn, J.-K. Chung, Modified mRNA as an alternative to plasmid DNA (pDNA) for transcript replacement and vaccination therapy, *Expert Opin. Biol. Ther.* 15 (2015) 1337–48.
27. C.J. McKinlay, J.R. Vargas, T.R. Blake, J.W. Hardy, M. Kanada, C.H. Contag, P.A. Wender, R.M. Waymouth, Charge-altering releasable transporters (CARTs) for the delivery and release of mRNA in living animals, *Proc. Natl. Acad. Sci.* 114 (2017) E448–E456.
28. D.H. Munn, V. Bronte, Immune suppressive mechanisms in the tumor microenvironment, *Curr. Opin. Immunol.* 39 (2016) 1–6.
29. A. Marabelle, H. Kohrt, C. Caux, R. Levy, Intratumoral immunization: A new paradigm for cancer therapy, *Clin. Cancer Res.* 20 (2014) 1747–1756.
30. K. Hirschberger, A. Jarzebinska, E. Kessel, V. Kretzschmann, M.K. Aneja, C. Dohmen, A. Herrmann-Janson, E. Wagner, C. Plank, C. Rudolph, Exploring Cytotoxic mRNAs as a Novel Class of Anti-cancer Biotherapeutics, *Mol. Ther. - Methods Clin. Dev.* 8 (2018) 141–151.
31. K. Van der Jeught, P.T. Joe, L. Bialkowski, C. Heirman, L. Daszkiewicz, T. Liechtenstein, D. Escors, K. Thielemans, K. Breckpot, Intratumoral administration of mRNA encoding a fusokine consisting of IFN- β and the ectodomain of the TGF- β receptor II potentiates antitumor immunity, *Oncotarget.* 5 (2014) 10100–10113.
32. K. Van der Jeught, L. Bialkowski, L. Daszkiewicz, K. Broos, C. Goyvaerts, D. Renmans, S. Van Lint, C. Heirman, K. Thielemans, K. Breckpot, Targeting the tumor microenvironment to enhance antitumor immune responses, *Oncotarget.* 6 (2015) 1359–1381.
33. I. sagiv-Barfi, D.K. Czerwinski, R. Levy, In Situ Vaccination with a TLR9 Agonist and Anti-OX40 Antibody Leads to Tumor Regression and Induces Abscopal Responses in Murine Lymphoma, *Blood.* 128 (2016) 1847.
34. I. Sagiv-Barfi, D.K. Czerwinski, S. Levy, I.S. Alam, A.T. Mayer, S.S. Gambhir, R. Levy, Eradication of spontaneous malignancy by local immunotherapy, *Sci. Transl. Med.* 10 (2018) eaan4488.
35. A. Marabelle, H. Kohrt, I. Sagiv-Barfi, B. Ajami, R.C. Axtell, G. Zhou, R. Rajapaksa, M.R. Green, J. Torchia, J. Brody, R. Luong, M.D. Rosenblum, L. Steinman, H.I. Levitsky, V. Tse, R. Levy, Depleting tumor-specific Tregs at a single site eradicates disseminated tumors, *J. Clin. Invest.* 123 (2013) 2447–2463.
36. C.G. Park, C.A. Hartl, D. Schmid, E.M. Carmona, H.J. Kim, M.S. Goldberg, Extended release of perioperative immunotherapy prevents tumor recurrence and eliminates metastases, *Sci. Transl. Med.* 10 (2018) eaar1916.

37. B. Ruffell, D. Chang-Strachan, V. Chan, A. Rosenbusch, C.M.T. Ho, N. Pryer, D. Daniel, E.S. Hwang, H.S. Rugo, L.M. Coussens, Macrophage IL-10 Blocks CD8+ T Cell-Dependent Responses to Chemotherapy by Suppressing IL-12 Expression in Intratumoral Dendritic Cells, *Cancer Cell*. 26 (2014) 623–637.
38. M.L. Broz, M. Binnewies, B. Boldajipour, A.E. Nelson, J.L. Pollack, D.J. Erle, A. Barczak, M.D. Rosenblum, A. Daud, D.L. Barber, S. Amigorena, L.J. van't Veer, A.I. Sperling, D.M. Wolf, M.F. Krummel, Dissecting the Tumor Myeloid Compartment Reveals Rare Activating Antigen-Presenting Cells Critical for T Cell Immunity, *Cancer Cell*. 26 (2014) 638–652.
39. K. Li, S. Qu, X. Chen, Q. Wu, M. Shi, Promising Targets for Cancer Immunotherapy: TLRs, RLRs, and STING-Mediated Innate Immune Pathways., *Int. J. Mol. Sci.* 18 (2017).
40. K.D. Moynihan, C.F. Opel, G.L. Szeto, A. Tzeng, E.F. Zhu, J.M. Engreitz, R.T. Williams, K. Rakhra, M.H. Zhang, A.M. Rothschilds, S. Kumari, R.L. Kelly, B.H. Kwan, W. Abraham, K. Hu, N.K. Mehta, M.J. Kauke, H. Suh, J.R. Cochran, D.A. Lauffenburger, K.D. Wittrup, D.J. Irvine, Eradication of large established tumors in mice by combination immunotherapy that engages innate and adaptive immune responses, *Nat. Med.* 22 (2016) 1402–1410.
41. J. Weiden, J. Tel, C.G. Figdor, Synthetic immune niches for cancer immunotherapy, *Nat. Rev. Immunol.* 18 (2017) 212–219.
42. A. Dc, A. Dcs, Adoptive T cell cancer therapy, *Nat. Mater.* 17 (2018) 475–477.
43. A. Ribas, J.D. Wolchok, Cancer immunotherapy using checkpoint blockade, *Science*. 359 (2018) 1350–1355.
44. K.F. Bol, G. Schreibelt, W.R. Gerritsen, I.J.M. de Vries, C.G. Figdor, Dendritic Cell-Based Immunotherapy: State of the Art and Beyond., *Clin. Cancer Res.* 22 (2016) 1897–906.
45. S.H. Van Der Burg, R. Arens, F. Ossendorp, T. Van Hall, C.J.M. Melief, Vaccines for established cancer: Overcoming the challenges posed by immune evasion, *Nat. Rev. Cancer*. 16 (2016) 219–233.
46. L.H. Butterfield, Cancer vaccines., *BMJ*. 350 (2015) h988.
47. C.J.M. Melief, T. Van Hall, R. Arens, F. Ossendorp, S.H. Van Der Burg, Therapeutic cancer vaccines, *J. Clin. Invest.* 125 (2015) 3401–3412.
48. A.A. Wu, V. Drake, H.S. Huang, S.C. Chiu, L. Zheng, Reprogramming the tumor microenvironment: tumor-induced immunosuppressive factors paralyze T cells, *Oncoimmunology*. 4 (2015) 1–14.
49. R. Zappasodi, T. Merghoub, J.D. Wolchok, Emerging Concepts for Immune Checkpoint Blockade-Based Combination Therapies, *Cancer Cell*. 33 (2018) 581–598.
50. C. Schmidt, The benefits of immunotherapy combinations, *Nature*. 552 (2017) S67–S69.
51. S. Karaki, M. Anson, T. Tran, D. Giusti, C. Blanc, S. Oudard, E. Tartour, Is There Still Room for Cancer Vaccines at the Era of Checkpoint Inhibitors, *Vaccines*. 4 (2016) 37.
52. T.J. Vreeland, G.T. Clifton, G.S. Herbert, D.F. Hale, D.O. Jackson, J.S. Berry, G.E. Peoples, Gaining ground on a cure through synergy: combining checkpoint inhibitors with cancer vaccines, *Expert Rev. Clin. Immunol.* 12 (2016) 1347–1357.
53. J.L. Tanyi, S. Bobisse, E. Ophir, S. Tuyaerts, A. Roberti, R. Genolet, P. Baumgartner, B.J. Stevenson, C. Iseli, D. Dangaj, B. Czerniecki, A. Semilietof, J. Racle, A. Michel, I. Xenarios, C. Chiang, D.S. Monos, D.A. Torigian, H.L. Nisenbaum, O. Michielin, C.H. June, B.L. Levine, D.J. Powel, D. Gfeller, R. Mick, U. Dafni, V. Zoete, A. Harari, G. Coukos, L.E. Kandalaft, Personalized cancer vaccine effectively mobilizes antitumor T cell immunity in ovarian cancer, *Sci. Transl. Med.* 10 (2018) eaa05931.
54. J.J. Wallin, J.C. Bendell, R. Funke, M. Sznol, K. Korski, S. Jones, G. Hernandez, J. Mier, X. He, E.S. Hodi, M. Denker, V. Leveque, M. Cañamero, G. Babitski, H. Koeppen, J. Ziai, N. Sharma, E. Gaire, D.S. Chen, D. Waterkamp, P.S. Hegde, D.F.

- McDermott, Atezolizumab in combination with bevacizumab enhances antigen-specific T-cell migration in metastatic renal cell carcinoma, *Nat. Commun.* 7 (2016) 12624.
55. Y. Huang, J. Yuan, E. Righi, W.S. Kamoun, M. Ancukiewicz, J. Nezivar, M. Santosuosso, J.D. Martin, M.R. Martin, F. Vianello, P. Leblanc, L.L. Munn, P. Huang, D.G. Duda, D. Fukumura, R.K. Jain, M.C. Poznansky, Vascular normalizing doses of antiangiogenic treatment reprogram the immunosuppressive tumor microenvironment and enhance immunotherapy, *Proc. Natl. Acad. Sci.* 109 (2012) 17561–17566.
56. M. Noguchi, F. Moriya, N. Koga, S. Matsueda, T. Sasada, A. Yamada, T. Kakuma, K. Itoh, A randomized phase II clinical trial of personalized peptide vaccination with metronomic low-dose cyclophosphamide in patients with metastatic castration-resistant prostate cancer, *Cancer Immunol. Immunother.* 65 (2016) 151–160.
57. H. Akita, K. Kogure, R. Moriguchi, Y. Nakamura, T. Higashi, T. Nakamura, S. Serada, M. Fujimoto, T. Naka, S. Futaki, H. Harashima, Nanoparticles for ex vivo siRNA delivery to dendritic cells for cancer vaccines: Programmed endosomal escape and dissociation, *J. Control. Release.* 149 (2011) 58–64.
58. X.-T. Song, K. Evel-Kabler, L. Rollins, M. Aldrich, F. Gao, X.F. Huang, S.-Y. Chen, An Alternative and Effective HIV Vaccination Approach Based on Inhibition of Antigen Presentation Attenuators in Dendritic Cells, *PLoS Med.* 3 (2006) e11.

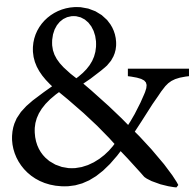
APPENDIX

Nederlandse Samenvatting

Acknowledgements

List of publications

Curriculum Vitae



In het afgelopen decennium hebben belangrijke ontwikkelingen in de werkingsmechanismen van coderende en niet-coderende ribonucleïnezuren (RNA) en de synthese van ribonucleotide analogen ervoor gezorgd dat RNA therapeutica een veelbelovend therapeutische entiteit zijn geworden voor de behandeling van een breed scala aan medische aandoeningen. Het gebruik van RNA als geneesmiddel geeft ons de mogelijkheid veel meer targets te bereiken dat tot nu toe mogelijk was met kleine moleculen en eiwitten. RNA therapeutica worden momenteel in verschillende klinische onderzoeken getest, bijvoorbeeld de toepassing van korte, interfererende RNAs (siRNA) voor de behandeling van nier- en leverstoornissen, boodschapper-RNA (mRNA) voor het bestrijden van kanker en recentelijk guide RNA (gRNA) voor het gericht sturen van Cas endonucleoasen naar specifieke genoomsequenties voor het initiëren van genmodificatie. Een belangrijk probleem in de ontwikkeling van RNA therapeutica is gerelateerd aan de inherente eigenschappen van het molecuul: niet gemodificeerd RNA is gevoelig voor afbraak van nucleasen, kan het immuunsysteem activeren en is uit zichzelf niet in staat om passief celmembranen te passeren. Daarom zijn dragersystemen die RNA therapeutica op de plaats van werking kunnen afleveren en helpen bij de intracellulaire afgifte van RNA zeer gewenst. Binnen het scala aan dragersystemen voor RNA zijn degenegebaseerd op synthetische polymeren van bijzonder belang vanwege hun hoge mate van chemische flexibiliteit en de mogelijkheid om verschillende functionaliteiten te integreren om specifieke membraanbarrières zoals hierboven genoemd te overwinnen. In dit proefschrift heb ik me gericht op het ontwikkelen van nieuwe en multifunctionele polymere dragersystemen voor verschillende therapeutische RNA-toepassingen waaronder de gerichte afgifte van siRNA aan tumorcellen, het gebruik van synthetisch, enkelstrengs RNA als adjuvans voor vaccins en tenslotte afgifte van mRNA coderend voor eiwitantigenen aan dendritische cellen voor immunotherapie van kanker.

In **hoofdstuk 1** wordt een inleiding gegeven over RNA therapeutica en RNA-afgiftesystemen. Dit hoofdstuk start met de beschrijving van de verschillende categorieën RNA therapeutica en vat kort de huidige klinische toepassingen van RNA-gebaseerde geneesmiddelen samen. Daarnaast worden de biologische barrières besproken die de therapeutische toepassing van RNA in de weg staan en worden afgiftesystemen voor RNA therapeutica, met in het bijzonder polymere afgiftesystemen, besproken. Tot slot wordt het principe van kankerimmunotherapie belicht en worden de voordelen van het gebruik van mRNA als kankervaccin en de noodzaak voor het gebruik van multifunctionele afgiftesystemen hiervoor benadrukt.

In **hoofdstuk 2** hebben we een reeks nieuwe RAFT-gesynthetiseerde poly(vinylbenzyltrimethyl-ammoniumchloride) (PVTC) homopolymeren en het afgeleide blokcopolymeer met poly(oligo (ethyleenglycol) methacrylaat) (POEGMA) getest. Deze polymeren bevatten quaternaire amines en hydrofobe benzyl groepen in de polymere keten die complexering van siRNA mogelijk maakt. Deze polymeren, wanneer gecomplexeerd met siRNA, vormden colloïdaal stabiele en kleine polyplexen met een gemiddelde grootte van 8 tot 25 nm. Studies op eierstokkankercellen met deze polyplexen lieten zien dat de polyplexen efficiënt door de cellen worden opgenomen en dat een siRNA gericht tegen het luciferase gen in deze cellen leidt tot functionele afgifte en remming van de luciferase expressie in deze cellen. De efficiëntie van functionele siRNA afgifte met deze polymeren is vergelijkbaar met dat van het

commercieel verkrijgbaar transfectiereagens Lipofectamine 2000. De geringe grootte en hoge stabiliteit van deze polyplexen in combinatie met zijn hoge transfectie-efficiëntie laat zien dat dit systeem mogelijk geschikt is voor de behandeling van solide tumoren, mede doordat kleinere afgiftesystemen doorgaans beter de tumorstroma kunnen binnendringen.

Hoofdstuk 3 beschrijft een cholesterol gestabiliseerd polymeer dat gefunctionaliseerd is met cRGD-peptiden voor de gerichte afgifte van siRNA aan glioblastoma cellen (GBM). Als eerste werd een copolymeer via RAFT-polymerisatie gesynthetiseerd dat bestaat uit N-(2-hydroxypropyl)-methacrylamide (HPMA) en N-acryloxysuccinimide (NAS) in random volgorde, gevolgd door radicaal-geïnduceerde modificatie met cholesterol voor stabilisatie. Vervolgens werden kationische aminen voor siRNA-complexatie en aziden voor modificatie van de polyplexen met targeting liganden geïntroduceerd. Incorporatie van hydrofobe cholesterolgroepen resulteerde in de vorming van stabiele siRNA polyplexen met een gemiddelde grootte van ~ 40 nm. Post-modificatie van de gevormde polyplexen met PEG-cRGD via kopervrije klikchemie leidde tot verbeterde cellulaire opname en verhoogde remming van de luciferase genexpressie in U87R-cellen. Bovendien toonde een *in vivo* pilot-onderzoek in gezonde, niet-tumor dragende C57BL/6 muizen aan dat dit PEG-cRGD polyplex-systeem na intraveneuze toediening goed werd verdragen door de muizen en geen acute toxiciteit liet zien.

In **hoofdstuk 4** wordt het ontwerp van een polymeer nanocomplex systeem beschreven voor de efficiënte afgifte van enkelstrengs RNA (PolyU, een ligand voor Toll-like receptor 7 en 8). Het beoogde doel is dat dit systeem als adjuvans dient voor het versterken van de immuunreactie tegen subunit vaccins gebaseerd op eiwit of peptide antigenen. Een copolymeer werd gesynthetiseerd met reactieve azido groepen en amines die aan de polymeerketen gekoppeld zijn via afbreekbare carbonaat bindingen. De polyplexen werden gevormd door een stapsgewijze procedure, te beginnen met de complexering van ssRNA en het kationische polymeer, gevolgd door post-PEGylering van de polyplexen door kopervrije chemie met behulp van PEG-bicyclononyne (BCN). Tenslotte werden de polyplexen via disulfidebindingen gefixeerd om hun stabiliteit te vergroten. The PEG modificatie kinetiek werd bestudeerd door middel van zeta-potentiaalmetingen, en fluorescentiecorrelatieanalyse (FCS). De gegenereerde bijna neutrale ssRNA nanocomplexen met een grootte van ~ 150 nm waren colloïdaal stabiel en in staat om RNA te beschermen tegen enzymatische afbraak. Er werd verder aangetoond dat deze deeltjes efficiënt door DC's werden opgenomen wat leidde tot DC maturatie. Een belangrijke bevinding was dat deze ssRNA-polyplexen in staat zijn na subcutane toediening de lymfeknopen te bereiken wat leidde tot efficiënte opname door DCs: 25-30% van de DC's in de lymfeknopen hadden polyplexen opgenomen. Wanneer deze polyplexen gelijktijdig werden toegediend met het modelantigeen ovalbumine (OVA), bleek de combinatie van OVA met ssRNA-polyplexen veel efficiënter in het induceren van CD8-cytotoxische T-cellen (CTL) in vergelijking met OVA en naakt ssRNA. Bovendien waren de IgG2c antilichaamtiteren tegen OVA >10 keer hoger met ssRNA-polyplexen in vergelijking met vrij ssRNA, wat aangeeft dat deze polyplexen in staat zijn een Th1 immuunreactie te induceren. Dit is een vereiste voor het induceren van robuuste cellulaire T cel reacties tegen kankercellen.

Gestimuleerd door de veelbelovende resultaten met betrekking tot de adjuvante eigenschappen van ssRNA-polyplexen beschreven in hoofdstuk 4, zijn we in **hoofdstuk 5** op zoek gegaan naar een manier om ssRNA (PolyU) en antigeen (OVA) samen in hetzelfde polymere nanodeeltje af te leveren. Anders dan de traditionele afgiftesystemen zoals PLGA en nanogelen waarin het antigeen en TLR-agonist beiden zijn ingekapseld in de kern van deze nanodeeltjes, stellen we in hoofdstuk 5 een alternatieve strategie voor om nanodeeltjes te bereiden gebaseerd op een laag-voor-laag bereidingsmethode. ssRNA werd eerst gecomplexeerd met twee klikbare kationische polymeren met respectievelijk BCN- en azidogroepen. Koper vrije klikchemie leidt na complexering tot een gestabiliseerd polymeer netwerk via covalente verbindingen tussen de twee polymeren. Vervolgens werd op deze polyplex kern BCN-gemodificeerde OVA en een geglycosyleerd polymeer (met mannose of galactose residuen) vastgezet d.m.v. klikchemie. Verder zijn disulfide groepen aanwezig in de polyplex-kern en buitenste laag om vrijgifte van RNA en antigeen onder gereduceerde condities (vergelijkbaar met de condities in het cytosol) mogelijk te maken wanneer de deeltjes eenmaal zijn opgenomen door de cellen. De kracht van dit vaccinafgiftesysteem ligt in de flexibiliteit waarmee de verschillende lagen op het polyplex kern kunnen worden “geklikt”, wat een veelzijdige aanpassing van het vaccin mogelijk maakt. De gevormde deeltjes lijken in termen van grootte en supramoleculaire organisatie op virussen en worden daarom virus-achtige nanopartikels (VNP) genoemd. Deze reductie-gevoelige VNP met een grootte van 200 nm en een negatieve oppervlaktelading (-14 mV) waren colloïdaal stabiel onder fysiologische condities. De immunogeniciteit van deze VNP-vaccins werd *in vitro* en *in vivo* getest. VNP gefunctionaliseerd met mannose residuen op het oppervlak (VNP-Man) vertoonden 5 maal hogere cellulaire opname door uit beenmerg opgewekte DCs in vergelijking tot gegalactosyleerde VNPs (VNP-Gal). Bovendien leidde opname van VNP-Man door DCs tot activatie van deze cellen en stimuleerde het kruispresentatie via MHC I. Vaccinatie van muizen met VNP-Man leidde tot sterke OVA-specifieke cytotoxische T-cel (CTL) responsen alsmede humorale immuunreacties. Samenvattend kan gesteld worden dat dit gelaagde polymeersysteem een veelbelovende modaliteit is voor het ontwikkelen van vaccins tegen ziekten waarbij zowel een sterke Th1/CTL respons en een antilichaamrespons vereist is voor adequate bescherming of therapie.

Helaas bleek dat de polyplexen die opgenomen werden door DCs in de lymfeklieren voornamelijk in het endo/lysosomale compartiment van deze cellen gevangen zaten, wat functionele afgifte van het mRNA in de weg stond. Om dit afgiftesysteem te kunnen gebruiken als mRNA-vaccin, hebben we in **hoofdstuk 6** de RNA-polyplexen gemodificeerd met verschillende membraanactieve peptiden via koppeling aan de PEG-ketens om zo vrijgifte van het mRNA uit de endosomen mogelijk te maken. De resultaten laten zien dat polyplexen die met het GALA-peptide (PPx-GALA) werden gedecoreerd, maar niet met de andere geteste peptiden, efficiënte mRNA transfectie van macrofagen en DCs gaven (25-50% van de cellen bracht EGFP tot expressie). De transfectie-efficiëntie met deze PPx-GALA is vergelijkbaar of hoger dan transfectie met commerciële lipofectamine en zonder cytotoxiciteit in de geteste concentratiereeks. Voor zover ons bekend is dit het hoogste DC-transfectieniveau dat tot dusverre is bereikt met negatief geladen gePEGylerde polymere afgiftesystemen. Vervolgens

werd cellulair opname en intracellulair transport van deze PPx-GALA nanodeeltjes bestudeerd. Hierbij werd duidelijk dat het GALA-peptide een dubbele functie heeft: het bindt actief asialzuur-getermineerde glycanen op DCs en medieert vervolgens vrijgifte van mRNA uit de endosomen naar het cytoplasma. Afgifte van mRNA coderend voor het OVA antigeen leidde tot OVA-specifieke activatie van cytotoxische T-cellen. Deze resultaten rechtvaardigen een verdere verkenning van PPx-GALA als vaccinplatform voor de ontwikkeling van gepersonaliseerde vaccins voor immunotherapie bij kanker.

| Acknowledgements

In September 16th 2013, it was a raining morning when I landed in Schipol airport and fantastically started to turn clear and sunny along my way to De Uithof campus in Utrecht. I still remember that how I started to explore the place where I will spend years to pursue my PhD degree with excitement and expectation. It is never easy to adapt to a totally new living style and culture, but nowadays I have get used to and even enjoyed them. Now, the PhD journal is coming to an end. Along the way, so many people have helped me and therefore it is the time to express my gratitude to all those people.

I would like to particularly thank my promoter Prof. Wim Hennink for giving me the opportunity to conduct my PhD at the Department of Pharmaceutics and for always trusting me and guiding me. I am impressed by your knowledge and dedication to the science. Your continuous support to build up cooperation with different research groups has broadened and deepened my research perspectives and I benefit a lot from that. Your understanding and patience during the last year is very important to me to finish the thesis. A lot of the time, your midnight emails about manuscript comments and scientific attitude to the details encouraged and inspired me.

Also, I have much to thank my co-promotor Dr. Enrico Mastrobattista for. In the last two years, you brought your wealth of knowledge which helped me to find out the solutions to overcome many challenges during my projects. Because of your patience and generous guidance, I slowly picked up scientific writing and managed to accomplish this thesis. Especially, thank you for your trust, constant supporting and warm encouraging during the difficult times. Of course I cannot forget Dr. René van Nostrum. As my daily supervisor during my first year, thank you for nicely guiding in the early stages of my PhD and the occasional conversation.

I would like to show my sincere gratitude to the great collaborators I had the privilege to work with. In particular, I would like to mention my great collaboration with Ghent University: Prof. Bruno De Geest, Dr. Stefaan De Koker and Dr. Ans De Beucklaer. I would like to thank you for all your constant help, support and for sharing your knowledge and ideas with me. Your inputs have decisively contributed to the success of my research project. Also thank Prof. Kevin Braeckmans and Dr. George Dakwar for the fully support with knowledge and equipment for fluorescence-labelled particles stability experiments. I would also like to thank Prof. Stergios Pispas from Greece, and Dr. Eduardo Ruiz-Hernandez, Prof. Annette T. Byrne, Dr. Kate Connor from Ireland for the fruitful collaborations with publications.

My special thanks to the master students, Eger and Rabab, part of their work has appeared in my thesis, and I am very grateful to have had such talented students help me to make this project a success.

None of my work would have been possible without the help of the excellent technicians in our groups. Mies, thank you for the generous help throughout the whole time, the beautiful and cheerful Friday afternoon song, and taking care of potted plants all the time. Jeop, thank you for TEM and of course always making sure the cell lab running smoothly. Roel, Feiko and Louis, thank you for the advices and maintaining lab clean and comfortable.



A huge amount of additional support also came from other great people in the Department. I own particular thanks to Nataliia who not only instructed me how to use Yokowaga and set up of cell experiments but also taught me the skill of processing images. In fact, I finished the very first paper here together with you. Your comments and kind words mean a lot to me! Sabrina, thank you for generous help with Luis' animal study in the first year. Also thank Roel from UMC for the help with MRI imaging of Gadolinium-chelated polymer, even though we did not publish the results of this part. Massi, always have nice chat with you and I will remember the time we spent together in Boston. Yvonne, thanks for encourage words and I wish you all the best. Special thanks to our secretary Barbara for arranging all the hospitality agreements, helping arrange meetings, extending Visa and contracts and many more. Eric, Lucia, Lies, Mahsa, Mazda, Negar, Leena, Carl, thank you for always be nice and helpful, I really enjoyed spending time with you during various activities.

The majority of my time has been spent in the synthesis lab, making a mess of my fumehood and any free space nearby. Thanks Neda for always allowing me to borrow your tips and materials. Marzieh, Mathew and Sjaak, thank you and I am always enjoy all the chat with you, no matter about the experiments or life. I would like to thank Luis, Hamid, Yang, Dandan, James, Yanna for their wise suggestions for my research projects.

In the first two years I have spent a lot grateful times with friends either in the lunch times, parties or travel together, thank you all and I always miss you: Andyhk, Luis, Maripaz, James, Rachel, Sima, Orn and Amr. I wish you all the best no matter where you are.

I would like to thank our PinPang and indoor soccer team for spent a lot joyful time together: Kung, Daiki, Feilong, Yong, Andhyk, Jeffery, Mohammad, Jan-Jaap, Enrico, Massi, Kamal, Hamid, Farshad, Jerry, Ali, Kamal, Nono, Khaled, Yudha, Mathew, Karina, Victor and Eko. The last football game and dinner afterward was great and it is a beautiful memory. Jerry and Andhyk, special thanks to you for taking the responsibility being my paranymphs.

I would like to thank our UIPS Chinese community, Yang, Qizhi, Weiluan, Dandan, Yinan, Feilong, Lemeng, Jibin, Haili, Yanna, Jerry, Linglei, Xiangjie, Yan, Mengshan and Boning. 很开心认识你们并一起工作。祝愿毕业了的师兄师姐们步步高升，大展宏图；师弟师妹们一切顺利，心想事成。挚友瑞学，陈晨，育茂，李梦，宏凯，纪元，郭勇，玉珑，张浩，杨欣，施杰，美玲，文静，作为到荷兰来认识的第一批朋友，也是相处相聚最多的，白驹过隙，四五年行来，有幸大家一起见证了各自的成长。感谢你们的美食和共度的美好时光，虽将相隔万里，情仍在意长存。祝愿你们前程似锦，幸福美满。富强，相处一年有余，感谢你在生活习惯上的的包容与谅解。知道你有鸿鹄之志，鲲鹏之愿，愿展翅冲九天！同时还有乌特勒支认识的其他朋友，付东龙，于光允，傅鸥，李靖，叶馨蔚，阿超，泽光，张正越，愈浩，雷志勇，刘金锋 … 博士的风雨路上有幸有你们相伴。以及乌特球队 (Utrecht United Football Club) 亲爱的球友和朋友们：曦晨，玉洁，桃子，志雄，天一，庆一，金地，小韦，郑强，Fish, Gary, 白哥，袁哥 等等，很开心认识你们，祝愿你们事事如意，事业有成！每周五的足球训练是苦闷的博士生活中的一丝闪亮，是宝贵的回忆。感谢陈斯毅队长对球队的极大贡献和对我生活上的关心和帮助。

非常感谢同济大学的林超老师和赵鹏老师，你们总是慷慨的给予我支持，在我迷茫时帮我指点方向，垂教之恩，重如山。感谢所有帮助过我的朋友，同学和老师，然篇幅所限，感激之言无法逐一具表，相会是缘，同行是乐，衷心祝愿你们万事安康。

我还要非常感谢哥哥嫂子以及姐姐们，在我求学期间一直照顾大家庭，孝敬父母。最后感谢老爸老妈一直以来的淳淳教诲，做我的坚强后盾，一定会不负众望。

Bo Lou

2018 June, Utrecht

| List of publications

Publications from this thesis:

B. Lou, N. Beztsinna, G. Mountrichas, J.B. van den Dikkenberg, S. Pispas, W.E. Hennink, Small nanosized poly(vinyl benzyl trimethylammonium chloride) based polyplexes for siRNA delivery, *Int. J. Pharm.* 525 (2017) 388–396. (Chapter 2)

B. Lou, K. Connor, K. Sweeney, I. Miller, A. O’Farrell, E. Ruiz-Hernandez, D. Murray, G.P. Duffy, A. Wolf, E. Mastrobattista, W.E. Hennink, A.T. Byrne, RGD-decorated cholesterol stabilized polyplexes for targeted siRNA delivery to Glioblastoma cells, Submitted for publication (2018) (Chapter 3)

B. Lou, A. De Beuckelaer, G.R. Dakwar, K. Remaut, J. Grooten, K. Braeckmans, B.G. De Geest, E. Mastrobattista, S. De Koker, W.E. Hennink, Post-PEGylated and crosslinked polymeric ssRNA nanocomplexes as adjuvants targeting lymph nodes with increased cytolytic T cell inducing properties, *J. Control. Release.* 284 (2018) 73–83. (Chapter 4)

B. Lou, A. De Beucklaer, E. Boonstra, D. Li, B.G. De Geest, S. De Koker, E. Mastrobattista, W. E. Hennink, Modular core-shell polymeric nanoparticles mimicking viral structures for vaccination, Submitted for publication (2018) (Chapter 5)

B. Lou, S. De Koker, C.Y.J. Lau, W.E. Hennink, E. Mastrobattista, mRNA polyplexes with post-conjugated GALA peptides efficiently target, transfect and activate antigen presenting cells. Submitted for publication (2018) (Chapter 6)

Other Selected Publications:

J. Guan, J. Sun, F. Sun, **B. Lou**, D. Zhang, V. Mashayekhi, N. Sadeghi, G. Storm, E. Mastrobattista, Z. He, Hypoxia-induced tumor cell resistance is overcome by synergistic GAPDH-siRNA and chemotherapy co-delivered by long-circulating and cationic-interior liposomes, *Nanoscale.* 9 (2017) 9190–9201.

D. Li, F. Sun, M. Bourajjaj, Y. Chen, E.H. Pieters, J. Chen, J.B. van den Dikkenberg, **B. Lou**, M.G.M. Camps, F. Ossendorp, W.E. Hennink, T. Vermonden, C.F. van Nostrum, Strong *in vivo* antitumor responses induced by an antigen immobilized in nanogels via reducible bonds, *Nanoscale.* 8 (2016) 19592–19604.

Y. Song, **B. Lou**, J. Cheng, P. Zhao, C. Lin, X. Wen, Redox-Responsive Amphipathic Dextran Nanomicelles for Solid Tumor Therapy, *J. Biomed. Nanotechnol.* 12 (2016) 2083–2096.

C. Lin, **B. Lou**, J. Zhao, R. Jin, P. Zhao, J. Li, J. Ren, Self-assembled micelles of PEG–poly(disulfide carbamate amine) copolymers for intracellular dual-responsive drug delivery, *J. Mater. Chem. B* 4 (2016) 902–909.

B. Zoetebier, A. Sohrabi, **B. Lou**, M.A. Hempenius, W.E. Hennink, G.J. Vancso, PEG stabilized DNA – poly(ferrocenylsilane) polyplexes for gene delivery, *Chem. Commun.* 52 (2016) 7707–7710.

Y. Song, **B. Lou**, P. Zhao, C. Lin, Multifunctional Disulfide-based cationic dextran conjugates for intravenous gene delivery targeting ovarian cancer cells, *Mol. Pharm.* 11 (2014) 2250–2261.

C. Lin, Y. Song, **B. Lou**, P. Zhao, Dextranation of bioreducible cationic polyamide for systemic gene delivery, in: *Biomed. Mater. Eng.*, (2014) 673–682.

L. Novo, L.Y. Rizzo, S.K. Golombek, G.R. Dakwar, **B. Lou**, K. Remaut, E. Mastrobattista, C.F. Van Nostrum, W. Jahnen-Dechent, F. Kiessling, K. Braeckmans, T. Lammers, W.E. Hennink, Decationized polyplexes as stable and safe carrier systems for improved biodistribution in systemic gene therapy, *J. Control. Release.* 195 (2014) 162–175.

R. Jin, **B. Lou**, C. Lin, Tyrosinase-mediated in situ forming hydrogels from biodegradable chondroitin sulfate-tyramine conjugates, *Polym. Int.* 62 (2013) 353–361.

| Curriculum Vitae

Bo Lou was born on the 13th of January 1989 in Nanyang City, Henan Province in China. During junior and senior high school period, he showed great interest in chemistry. In 2010, he received his Bachelor of Engineering degree from North China University of Water Resources and Electric Power (NCWU) in Zhengzhou. He was awarded national scholarships during his Bachelor's study and graduated with honors. In the same year, he pursued a Master's degree in Biomedical Engineering at Tongji University in Shanghai, where he involved in national project "Functional biodegradable polymers for gene delivery". During 2010-2013, a new type of bioreducible cationic polyurethane polymer was created in this project and showed highly efficient gene transfection, resulting in 3 papers and one patent production. Thereafter, he started his Ph.D. at Department of Pharmaceutics at Utrecht University, one of Europe's leading research groups. Here he studied the functional post-modification of polymeric mRNA nanoparticles for cancer immunotherapy. This thesis is the work from his Ph.D. under the supervision of Dr. E. Mastrobattista and Prof. W. E. Hennink.

